THE UNIVERSITY *of* EDINBURGH

Small Cell Lung Cancer and Cancer Stem Cell-Like Cells

Sana Sarvi

A thesis submitted for the degree of Doctor of Philosophy

University of Edinburgh

2014

Dedicated to my parents Ashraf and Hassan

Declaration

I hereby declare that this thesis has been composed solely by myself and has not been accepted in any previous candidature for a higher degree. All work presented in this thesis was, unless acknowledge, initiated and executed by myself. All sources in the text have been acknowledged by reference.

Sana Sarvi
May 2014

ABSTRACT

Small cell lung cancer (SCLC) is a highly aggressive malignancy with extreme mortality and morbidity. Although initially chemo- and radio-sensitive, almost inevitable recurrence and resistance occurs. SCLC patients often present with metastases, making surgery not feasible. Current therapies, rationally designed on underlying pathogenesis, produce *in vitro* results, however, these have failed to translate into satisfactory clinical outcomes. Recently, research into cancer stem cells (CSCs) has gained momentum and form an attractive target for novel therapies. Based on this concept, CSCs are the cause of neoplastic tissue development that are inherently resistant to chemotherapy, explaining why conventional therapies can shrink the tumour but are unable to eliminate the tumour completely, leading to eventual recurrence.

Here I demonstrate that SCLC H345 and H69 cell lines contain a subset of cells expressing CD133, a known CSC marker. CD133+ SCLC sub-population maintained their stem cell-like phenotype over a prolonged period of culture, differentiated in appropriate conditions and expressed the embryonic stem cell marker Oct-4 indicating their stem-like phenotype. Additionally, these cells displayed augmented clonogenic efficacy, were chemoresistant and tumorigenic *in vivo*, distinct from the CD133- cells. Thus, the SCLC CD133 expressing cells fulfil most criteria of CSC-like definition.

The molecular mechanisms associated with CD133+ SCLC chemoresistance and growth is unknown. Up-regulated Akt activity, a known promoter of resistance with survival advantage, was observed in CD133+ SCLC cells. Likewise, these cells demonstrated elevated expression of Bcl-2, an anti-apoptotic protein compared to their negative counterpart explaining CD133+ cell chemoresistance phenotype. Additionally, CD133+ cells revealed greater expression of neuropeptide receptors, gastrin releasing peptide (GRP) and V_{1A} receptors compared to the CD133- cells.

Addition of exogenous GRP and arginine vasopressin (AVP) to CD133+ SCLC cells promoted their clonogenic growth in semi-solid medium, illustrating for the first time neuropeptide dependent growth of these cells.

A novel peptide (peptide-1) was designed based on the known structure of the substance P analogues that have shown benefit in animal models and in early clinical trials. This compound inhibited the growth of SCLC cells in *in vitro* with improved potency and stability compared to previous analogues and reduced tumorigenicity *in vivo*. Interestingly, peptide-1 was more effective in CD133+ cells due to increased expression of neuropeptide receptors on these cells.

In conclusion, my results show that SCLC cells retain a sub-population of cells that demonstrate CSC-like phenotype. Preferential activation of Akt and Bcl-2 survival pathways and enhanced expression of neuropeptide receptors contribute to CD133+ SCLC chemoresistance and growth. Therefore, it can be proposed that CD133+ cells are the possible cause of SCLC development, treatment resistance and disease recurrence. Despite being chemoresistant, CD133+ cells demonstrated sensitivity to peptide-1. The identification of such new analogue that demonstrates efficacy towards resistant CD133+ SCLC cells is a very exciting step forward in the identification of a potential new therapy for resistant disease.

Acknowledgments

It would not have been possible to write this doctoral thesis without the help and support of the kind people around me, some of whom I particularly mention here.

First and foremost, I wish to thank my supervisor Dr. Alison Mackinnon for her support and patience throughout my PhD. Her advice and friendship was instrumental for the success of this work, for which I am eternally thankful. I would also like to thank Prof. Tariq Sethi and Prof. Christopher Gregory for their continued help and advice during the course of my PhD.

In addition, I would like to thank Edinburgh University for providing me with the Overseas Research Students Award Scheme (ORSAS) and University of Edinburgh Research Scholarship. These scholarships were a great help to my family and I for the continuation of my PhD.

I would like to acknowledge Prof. Mark Bradley and Dr. Nikolaos Avlonitis (School of Chemistry, University of Edinburgh) for the design of the Substance P analogues and the HPLC analysis.

I am grateful to the other members of the Sethi group, with special thanks to Dr. Brian McHugh for his excellent technical assistance, who told me that ‘PhD is the highest level of education, therefore it is not supposed to be easy, and only people who work hard and manage to overcome their disappointments succeed’, words which guided me though the difficult moments and led me to where I am today. Special thanks to Eleni Kouverianou, whose friendship and support will never be forgotten. I would also like to thank Sarah Farnworth, James Chalmers, Wei Wang and Kirsten Atkinson.

I am grateful to Mahshid Fardmehr, Shabnam Mojtaba, Ali Morvarid, Dean Gagnon and Joao Pedro Martin who supported me in writing, and incented me to strive towards my goal.

Many thanks to my mother Ashraf Jafari whose positive energy and immense emotional support has driven me forward and her strength and eternal love has been my initiative. I wish to thank my father Hassan Sarvi who has always supported me in the moments when there was no one to answer my queries. My fathers' faith in me and his encouragement in every step of my life led me to where I am today. My greatest wish is to make you both happy and proud and hope this PhD thesis has brought a smile to your faces.

Last, but no means least, I thank my brother, Ali Sarvi. My brother despite being miles away in the past 8 years has always been beside me whenever I have been in need. My brother is my soul mate and his presence has always given me the courage to face the most difficult steps in my life. His unequivocal support holds no bonds, for which I am eternally thankful.

Table of Contents

List of Figures

List of Tables

List of Abbreviations

aa	Amino acid
ABC	ATP-binding cassette
ABCG2	ATP-binding cassette superfamily G member 2
ALDH	Aldehyde dehydrogenase
ALDH1	Adehyde dehydrogenase 1
AML	Acute myeloid leukaemia
AMPS	Ammonium persulphate
AO	Acridine orange
ASCL1	Achaete-scute complex homolog-1
AT1,2	Alveolar type 1 and 2
AVP	Arginine vasopressin
BAA	BODIPY-aminoacetate
BAAA	BODIPY-aminoacetaldehyde
BADJ	Bronchoalveolar duct junction
BASC	Bronchoalveolar stem cells
BCA	Bicinchoninic acid
bFGF	basic fibroblast growth factor
BM	Brain metastasis
BRS-3	Bobesin receptor subtype-3
BSA	Bovine serum albumin
CAV	Cyclophosphamide, adriamycin (doxorubicin), and vincristine
CCSP	Clara cell specific protein
CGRP	Calcitonin gene related peptide
Chk1/2	Check point kinases 1/2
CHO	Chinese hamster ovary
CKs	Cytokeratins
CML	Chronic myeloid leukaemia
CR	Complete response
CSC	Cancer stem cell
CT	Computer tomography
DAB	Diaminobenzidine
DAG	Diacylglycerol
DAPI	4,6 diamidino-2-phenylindole
DEAB	Diethylaminobenzaldehyde
DMEM	Dulbecco's modified eagles media
DMSO	Dimethyl sulfoxide
DTT	Dithiothreitol
EB	Ethidium bromide
EB/AO	Ethidium bromide/acridine orange
ECL	Enhanced chemiluminescence
ECM	Extracellular matrix
ED	Extensive disease
EDTA	Ethylenediamineteraacetic acid
EGF	Epidermal growth factor
EMT	Epithelial–mesenchymal transition
EP	Etoposide and cisplatin

ERK	Extracellular signal regulated protein kinase
ESCs	Embryonic stem cells
FACS	Fluorescence-activated cell sorting
FCS	Foetal calf serum
FGF	Fibroblast growth factor
FHIT	Fragile histidine triad
FSC-A	Forward scatter-Area
FSC-W	Forward scatter-Width
FURA-2-AM	FURA-2-tetraacetoxymethylester AME
GM	Geometric mean
GMP	Granulocyte-macrophage progenitors
GPCR	G-protein coupled receptors
G-proteins	GTP binding proteins
GRP	Gastrin releasing peptide
GRPR	GRP receptor
Gy	Gray
HBE	Human bronchial epithelial
HBSS	Hanks balanced salt solution
HCC	Hepatocellular carcinoma
HEPES	4-(2-hydroxyethyl)-1-piperazineethanesulfonic acid
Hh	Hedgehog
HPLC	High performance liquid chromatography
HRP	Horseradish peroxidase
HSC	Hematopoietic stem cell
IGF-1	Insulin-like growth factor-1
IGF-1R	Insulin-like growth factor-1 receptor
IHC	Immunohistochemistry
IMF	Immunofluorescence
IP	Intra-peritoneal
IP3	Phosphatidylinositol 1, 4, 5-triphosphate
JNK	c-Jun N-terminal kinase
LD	Limited disease
LEMs	Lambert-Eaton myasthenic syndrome
MACS	Magnetic-activated cell sorting
MAPK	Mitogen activated protein kinase
Min	Minutes
MRI	Magnetic resonance imaging
MRP1,2	Multidrug resistance-associated protein1 and 2
MSCLC	Mouse SCLC
mTOR	Mammalian target of rapamycin
MTT	3-(4,5-dimethylthiazol-2yl)-2,5-diphenyl tetrazolium bromide
NB	Neuroblastoma
N-CAM	Neural cell adhesion molecule
NEB	Neuroendocrine bodies
NEB	Neuroepithelial body
NK	Natural killer
NMB-R	Neuromedian B receptor
NOD/SCID	Non-obese diabetic/severe combined immunodeficiency
NSCLC	Non-small cell lung cancer
ORR	Objective response rate

PBS	Phosphate buffered saline
PCI	Prophylactic cranial irradiation
PDGFR	Platelet-derived growth factor receptor
PEP	Paclitaxel, etoposide and cisplatin
PET	Positron Emission Tomography
PFA	Paraformaldehyde
PGP	P-glycoprotein (MDR1)
PI	Propidium iodide
PI3K	Phosphatidyl inositol-3 kinase
PKB/AKT	Protein kinase B
PKC	Protein kinase C
PKD	Protein kinase D
PLCβ	Phospholipase C-β
PNECs	Pulmonary neuroendocrine cells
PS	Performance status
Ptc	Patched
Q-PCR	Quantitative PCR
RA	Retinoic acid
Rb	Retinoblastoma
RPMI 1640	Rosewell Park Memorial Institute Medium 1640
RTK	Receptor tyrosine kinase
RT-PCR	Reverse transcription PCR
SCF	Stem cell factor
SCID	Severe combined immune deficient
SCLC	Small cell lung cancer
SDS	Sodium dodecyl sulphate
SDS-PAGE	Sodium dodecyl sulphate polyacrylamide gel electrophoresis
Sec	Seconds
SIADH	Syndrome of inappropriate antidiuretic hormone
SP	Substance P
SPC	Surfactant protein C
SSC	Side scatter
TA	Transit-amplifying
TBS	Tris-buffered saline
TEMED	Tetramethylethylenediamine
TGFβ-1	Transforming growth factor β-1
TM	Transmembrane domains
TNM	Tumour, node, metastases
TopoII	Topoisomerase II
TR	Thoracic irradiaton
TSA	Tyramide signal amplification
VALSG	Veterans' Administration Lung Study Group
VClara	Variant clara
VEGF	Vascular endothelial growth factor
Vol	Volume

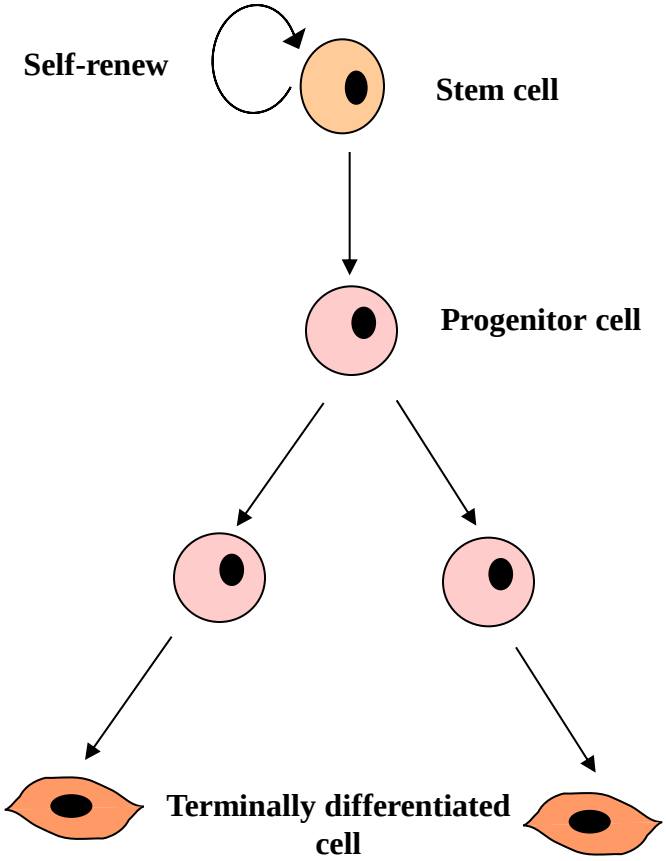

Figure 1: Stem cell hierarchy model
Stem cells via asymmetrical division can self-renew and generate progenitor cells. Progenitor cells have limited proliferation potential and ultimately divide into terminally differentiated cells.

Table 1: Prospective isolation of human cancer stem cells from solid tumours

Tumour type	CSC marker	% of tumour cells expressing CSC marker
Breast	CD44+ CD24-/low	11-35
Breast	ALDH1+	3-10
Brain	CD133	19-29
Brain	CD133	2-3
Colon	CD133	1.8-25
Colon	EpCAM+ CD44+	0.03-38
Lung	CD133	0.32-22
Melanoma	ABCB5	1.6-20
HCC	CD133	1-32

ALDH, aldehyde dehydrogenase; CSC, cancer stem cell; EpCAM, epithelial cell adhesion molecule, HCC, hepatocellular carcinoma. Data obtained from [73].

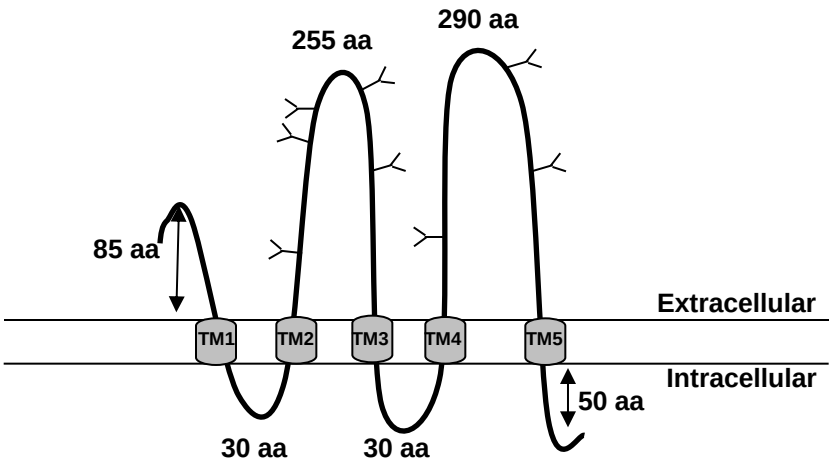

Figure 2: Membrane topology of CD133
CD133 is predicted to consist of an 85 aa N-terminal extracellular domain, five transmembrane domains (TM 1-5) with two large glycosylated extracellular loops containing 255 aa and 290 aa, and two small cytoplasmic loops, both containing 30 aa and an 50 aa C-terminal domain. Potential glycosylation sites are indicated as Y

Table 2: ALDH isoenzymes involved in stem cells and CSCs

ALDH isoenzyme	Function in stem cells and CSCs
ALDH1A1 ALDH1A2 ALDH1A3	Cellular protection against alkylating agnates Oxidize retinaldehyde to retinoic acids
ALDH2	Alcohol metabolism
ALDH3A1	Cellular protection against alkylating agnates
ALDH7A1	Regulation of cell cycle

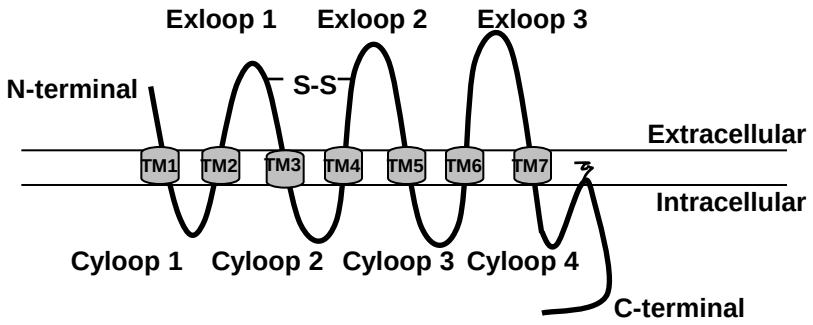

Figure 3A: Schematic representation of GPCR

GPCR receptor consists of a single polypeptide chain containing 7 hydrophobic α-halicase creating 7 TM (TM1-7) domains, three extracellular loops (Exloop) and four cytoplasmic loops (Cyloop). The receptor contains an extracellular N-terminal and an intracellular C-terminal.

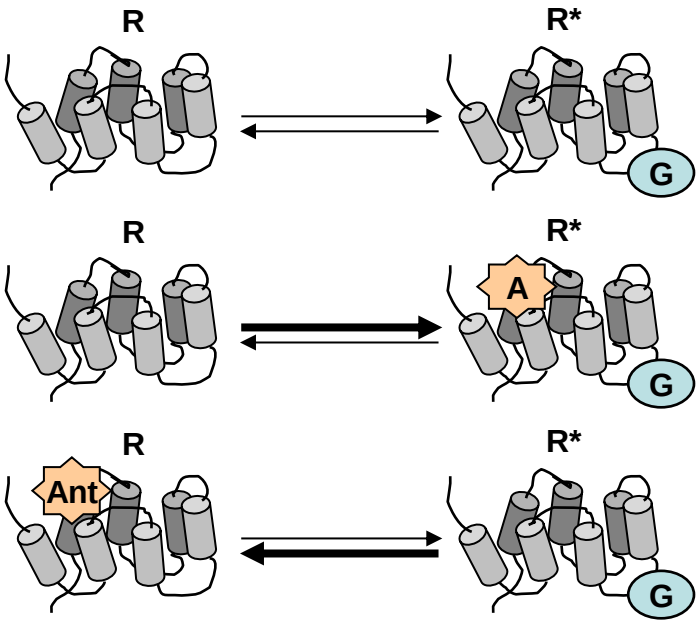

Figure 3B: Ternary complex model of GPCR activation

GPCRs exists in an equilibrium between active (R*) and inactive (R) state. Binding of an agonist (A) stabilises R* stimulating interaction with G-proteins (G) whereas binding of an antagonist (Ant) stabilises R, decreasing interaction with G.

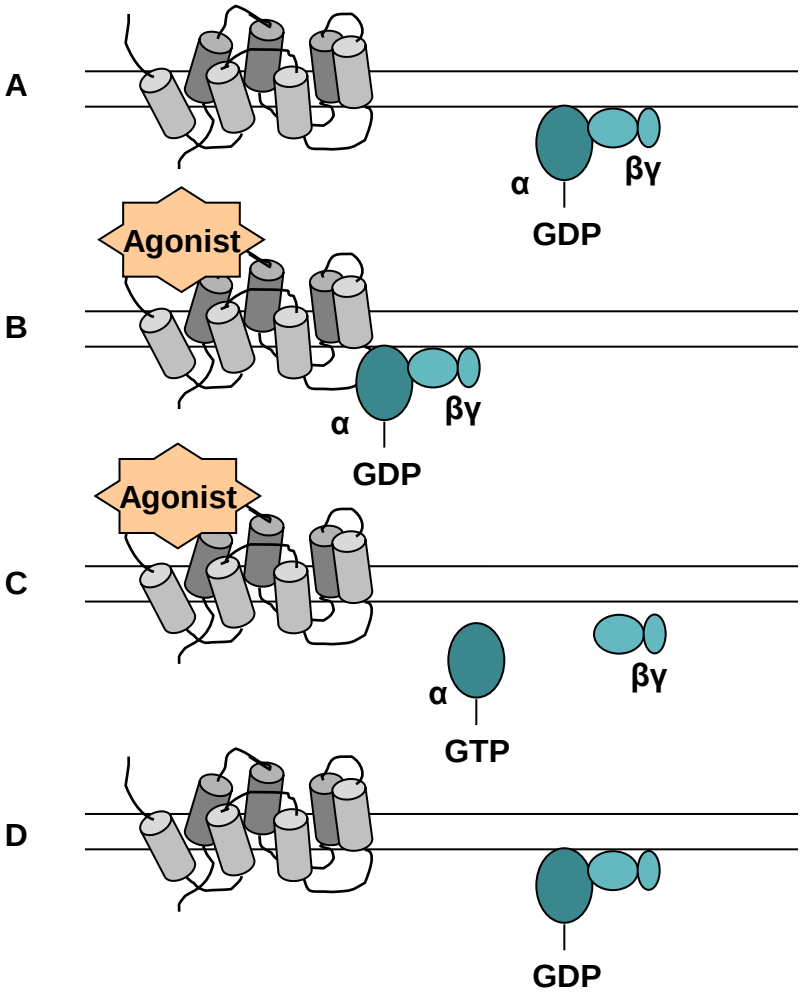

Figure 4: Schematic representation of the activation of G-proteins via activated GPCRs

(A) In the absence of agonist, the receptor favours no interaction with the G-proteins and the α-subunit contains bound GDP with α and βγ-subunit association. (B) Binding of an agonist induces GPCRs conformational changes exposing residues to G-protein, therefore promoting G-protein receptor coupling. (C) Binding of activated GPCRs to G-proteins triggers exchange of GTP for GDP with α and βγ subunit dissociation. (D) The intrinsic hydrolyte activity of α-subunit converts GTP to GDP and promotes re-association of the hetero trimer.

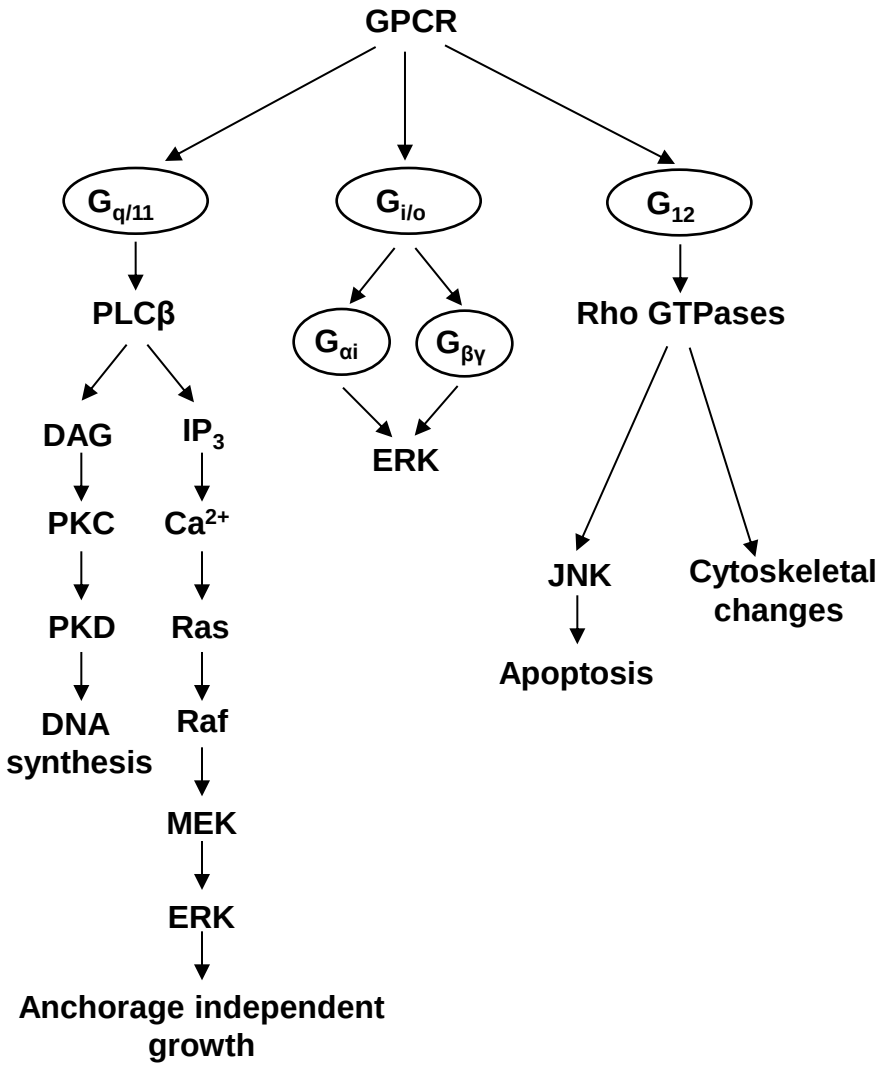

Figure 5: Neuropeptide analogue mediated signal transduction pathways

See text for details and abbreviations.

Table 3: Structure and the inhibitory affect of substance P analogues on the growth of H69 SCLC cells in liquid culture on day 12 (adapted from [303])

Substance P analogue	% of growth inhibition at 25 µM	
Arg-Pro-Lys-Pro-Gln-Gln-Phe-Phe-Gly-Leu-Met-NH2	0	(a)
Arg-DTrp-MePhe-DTrp-Leu-Met-NH2	30	(b)
DArg-DPro-Lys-Pro-DPhe-Gln-DTrp-Phe-DTrp-Leu-Leu-NH_2	55	(c)
DArg-DPro-Lys-Pro-DTrp-Gln-DTrp-Phe-DTrp-Leu-Leu-NH_2	92	(d)
DPro-Lys-Pro-DPhe-Gln-DTrp-Phe-DTrp-Leu-Gly-NH2	20	
Arg-DTrp-MePhe-DTrp-DLeu-Met-OH	16	
DPro-Lys-Pro-DTrp-Gln-DTrp-Phe-DTrp-Leu-Val-NH2	36	

(a) Substance P
(b) SP-G
(c) SP-D
(d) SP-A

Table 4: Growth inhibitory by SP-G (IC_{50}) in a panel of cell lines (adapted from [65]).

Cell lines	IC_{50} (µM)
H69 (SCLC)	10.5
H510 (SCLC)	29
W X330 (SCLC)	42
NX002 (NSCLC)	33.5
HT29 (Colorectal)	18
HRT18 (Colorectal)	37
HCT116 (Colorectal)	129
PEO4 (Ovarian)	31
PANC1 (Pancreatic)	58

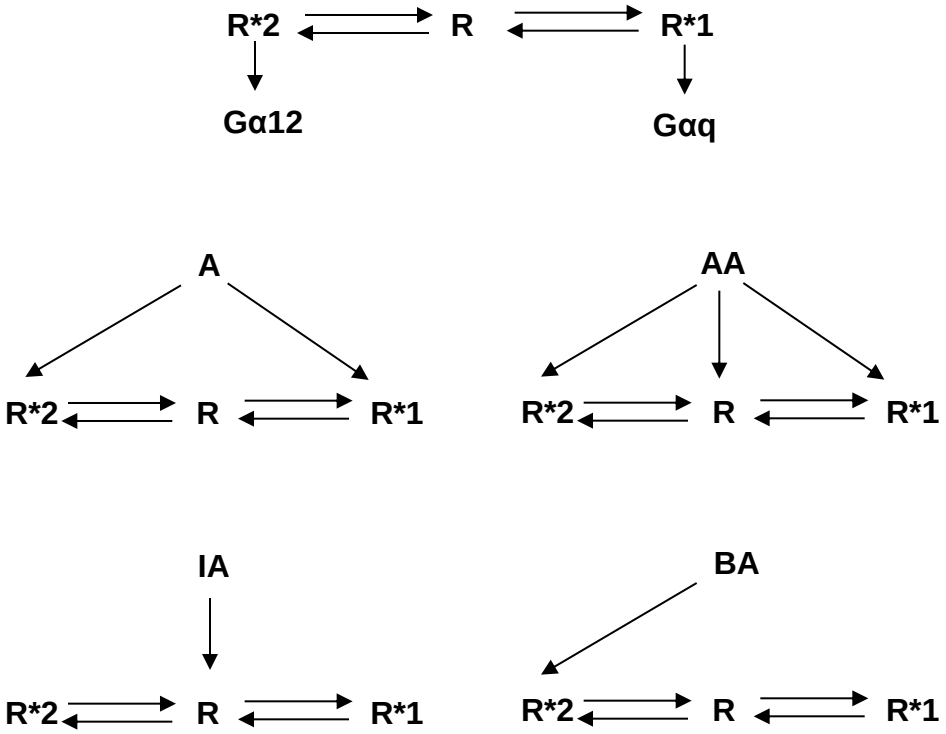

Figure 6: Biased agonist theory for receptor activation by neuropeptide antagonists

Adapted from [223]

A receptor is in an equilibrium of two or more active conformation states (R*1 and R*2) and one more energetically inactive state R. R*1, represents conformation state of GPCR that activates $G_{\alpha q}$ and R*2, represents conformation state of GPCR that activates $G_{\alpha 12}$. Upon binding of an agonist (A), both active state of the receptor is stabilised. An antagonist (AA) binds to all three states competing with the agonist. This interaction may or may not stabilise the active state. If the binding of the antagonist stabilises the active state of the receptor it is termed as partial agonist. Binding of an inverse agonist (IA) stabilises the inactive state of the receptor. A biased agonist (BA) preferentially binds to one of the active state and stabilises it, therefore activates one set of signal transduction events without activating others.

Table 5: Characteristics of H345 and H69 cell lines

Cell line	H345	H69
Sex	M	M
Prior Treatment	Chemotherapy	Chemotherapy
Source	PE	BM
Class	C	C
DDC u/mg	240	98
CK-BB μ/mg	2.2	5.8
NSE ng/mg	817	4075
BLI pmol/mg	1.7	4.7

Abbreviations: PE, pleural effusion; BM, bone marrow; C, classical; DDC, L-dopa decarboxylase (elevated > 1.0 u/mg; CK-BB, creatine kinase brain isoenzyme (elevated > 0.4 μg/mg); NSE, neurone specific enolase (elevated > 100 ng/mg); BLI, bombesin-like immunoreactivity (elevated > 0.1 pmol/mg).

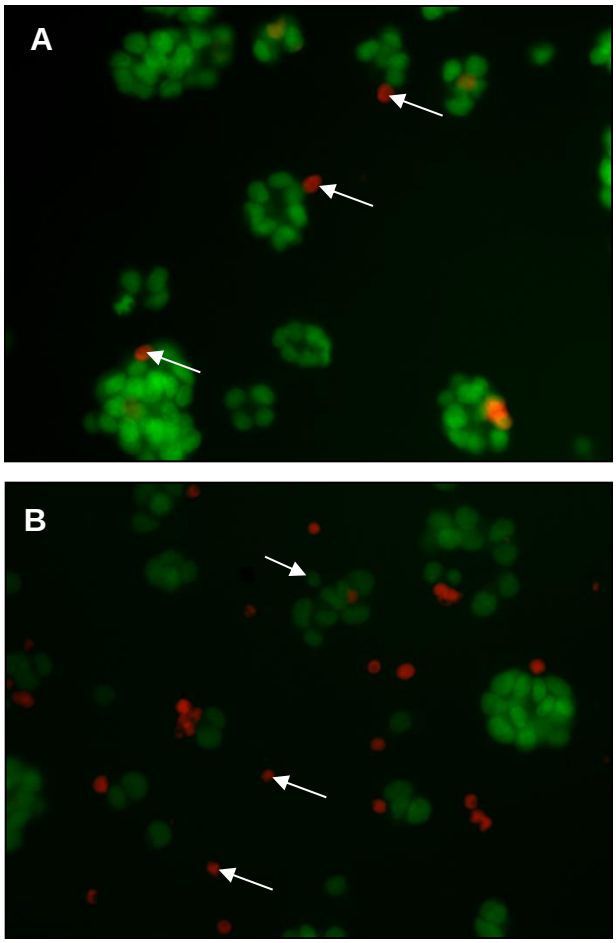

Figure 7: Representative images of H345 cells stained EB/AO for detection of apoptotic cells

(A) SCLC cells cultured in SITA medium for 72 hours. (B) SCLC cells cultured in SITA medium plus etoposide 100 μg/ml for 72 hours. 1μl of ethidium bromide (1mg/ml) and 1μl acridine orange (1mg/ml) was added to the wells, and the cells were viewed by fluorescent microscopy. Apoptotic cells are small and either green (early apoptosis) or orange (late apoptosis). (➔) represents apoptotic cell. Images were taken with 10× magnification.

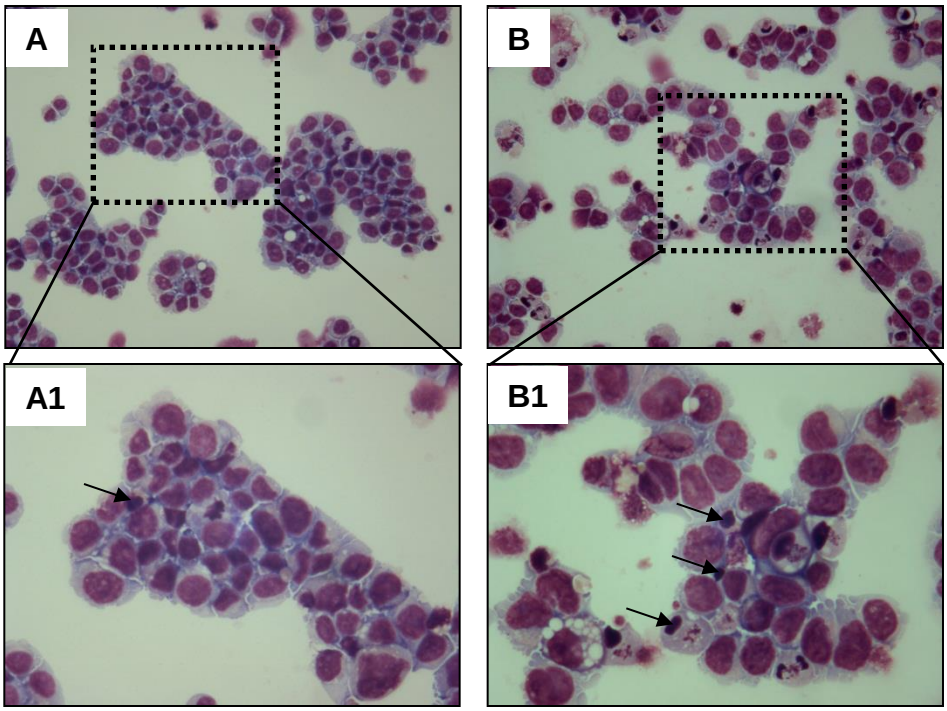

Figure 8: Representative images of H345 cells stained May-Grunwald-Giemsa for detection of apoptotic cells

(A and A1) SCLC cells cultured in SITA for 72 hours. (B and B1) SCLC cells cultured in SITA plus etoposide 100 μg/ml for 72 hours. Cells were cytocentrifuge onto glass cover slips, air dried, and fixed in methanol for 2 minutes and stained with May-Grunwald-Giemsa. Cell morphology was examined using light microscopy. Apoptotic cells were shrunken cells with dense nuclei. (➤) represents apoptotic cell. Images A and B were taken with 10× magnification and images A1 and A2 were taken with 20× magnification on light microscope.

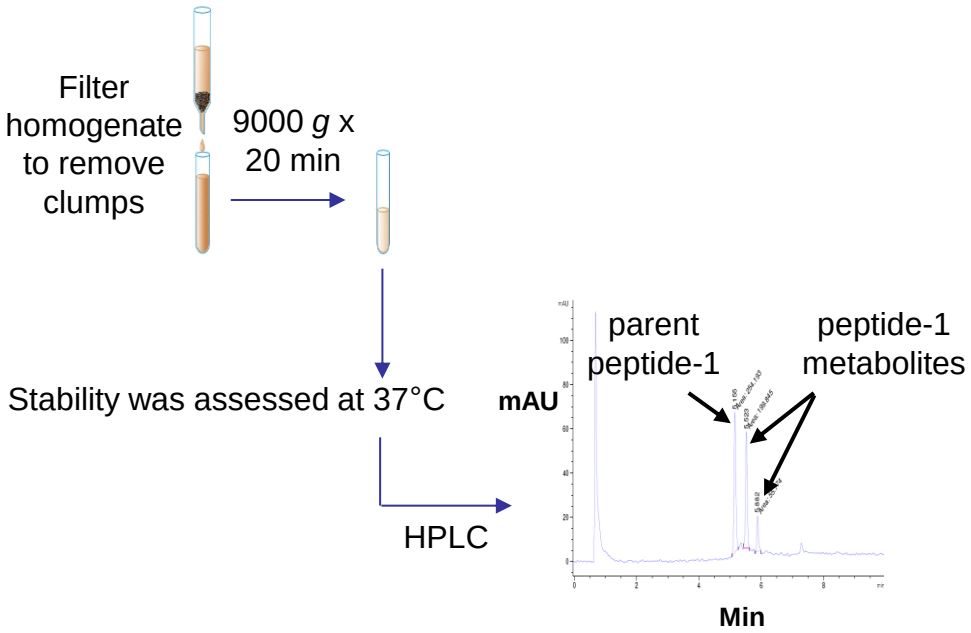

Figure 9: Schematic figure of S9 liver preparation
Livers from female C57BL/6 mice were removed and washed twice with cold potassium phosphate buffer 0.1 M. Liver tissue was homogenised using a glass Teflon homogeniser in the buffer to give a final homogenate consisting of 25% w/v tissue. Samples were spun at 9000 × g for 20 minutes at 4°C and the supernatant was stored on ice. The stability of SP-G and peptide-1 was assessed in the S9 liver preps at 37°C and data was analysed using HPLC. The HPLC presented is a representative figure, demonstrating the degradation of parent peptide-1 over time and generation of its metabolites.

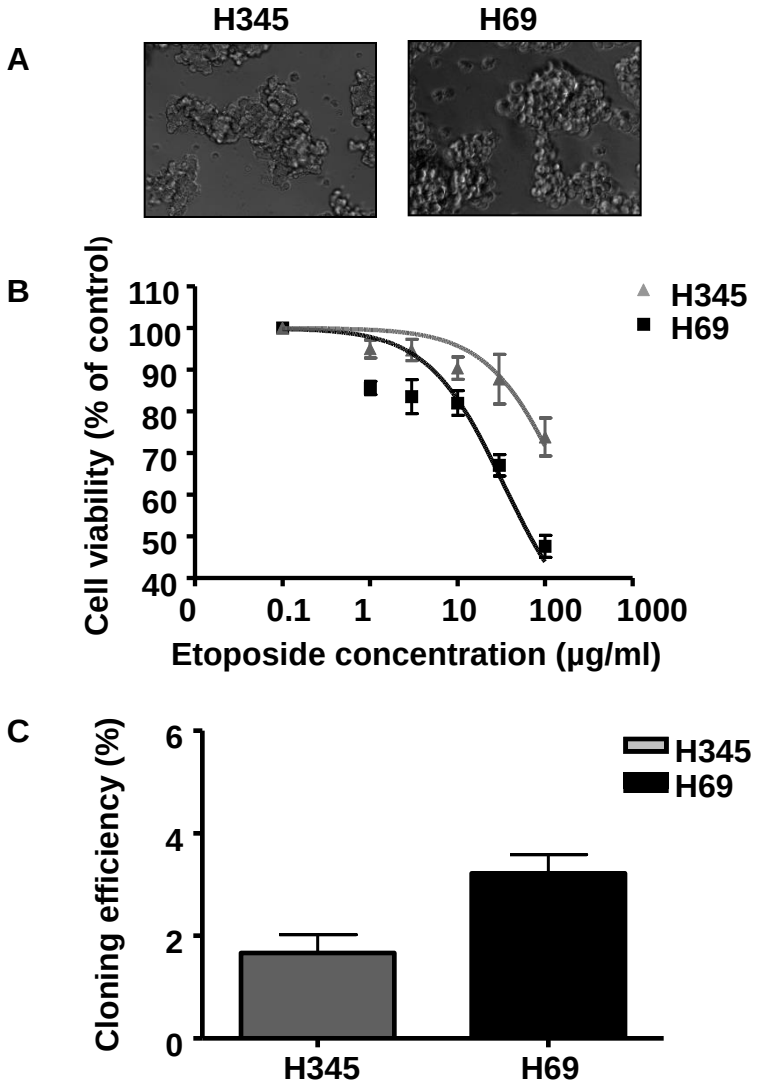

Figure 10: SCLC cell line characteristics

(A) SCLC cells grow as cellular aggregates in tissue culture. Images were taken with 20× magnification with light microscope. (B) H345 and H69 cells were treated with etoposide (1-100 µg/ml). After 72 hours, MTT was added and cell viability was determined. Data represents the mean ± SEM of three independent experiments performed in triplicates. (C) Cells were cultured in SITA medium containing 0.3 % agarose and were layered over a semi-solid base of 0.5% agarose. After 21 days colonies (>16 cells) were counted using light microscope. Results are expressed as percentage of number of cells seeded. Data represents the mean of three independent experiments ± SEM performed in duplicates.

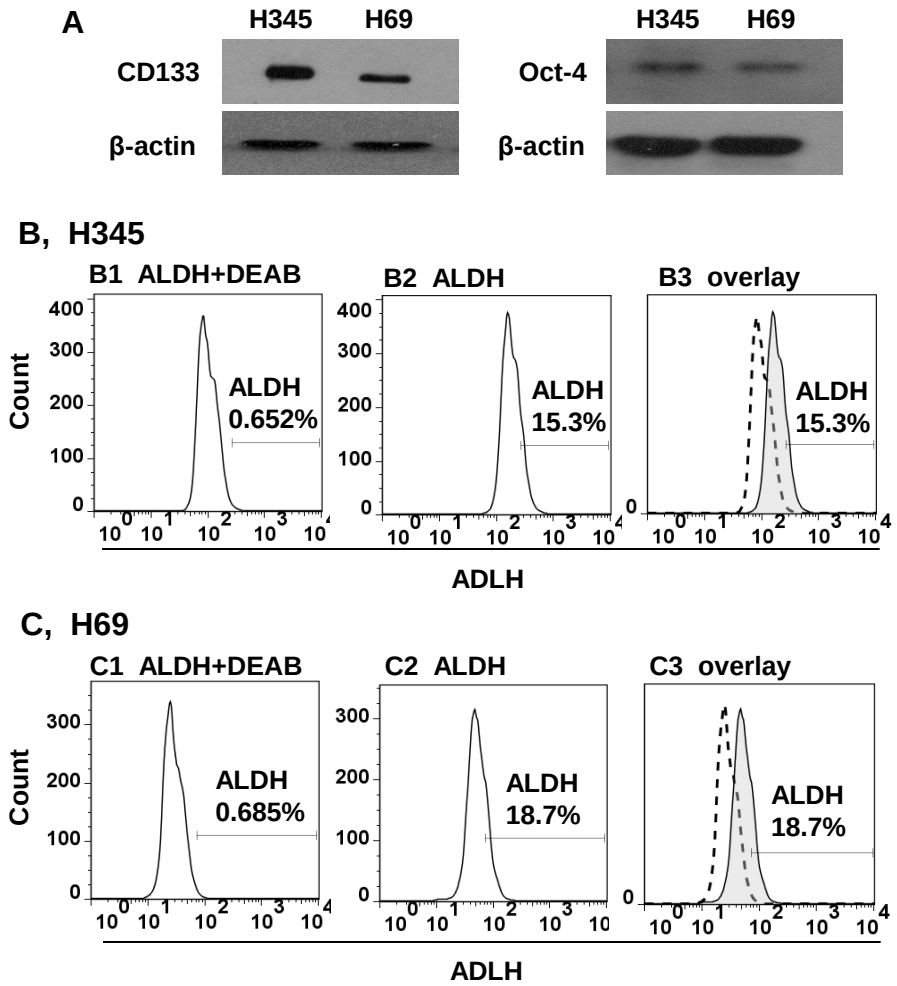

Figure 11: SCLC cell lines express stem cell markers

(A) Expression of CD133 and Oct-4 proteins demonstrated by western blot. A band of ~120 kDa and ~48 kDa represents CD133 and Oct-4 protein expression, respectively. β-actin was used as loading control. Images are representative of three independent experiments. (B and C) ALDH enzyme activity was measured by ALDEFLUOR® kit and data was analyzed by flow cytometry. See text for more details. Cells treated with DEAB were used as negative control and ALDH activity was calculated relative to negative control. B1 and C1, represents histograms of H345 and H69 cells stained with Aldefluor in the presence of DEAB, respectively. B2 and C2 represents histograms of H345 and H69 cells stained with Aldefluor in the absence of DEAB, respectively. B3 and C3 are overlay histograms of H345 and H69 cells in the presence (dashed histogram) and absence (grey histogram) of DEAB respectively. Data is representative of three independent experiments.

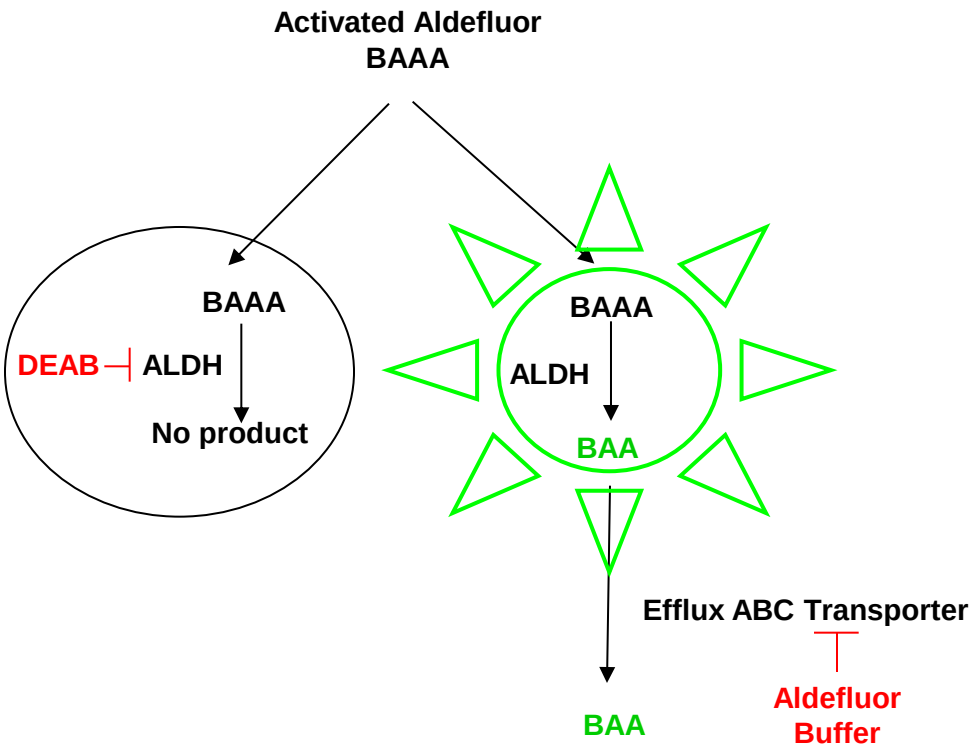

Figure 12: ALDEFLUOR assay schematic

ALDEFLUOR® is used to identify cells with elevated ALDH1 activity. The Fluorescent ALDH-substrate, BODIPY-aminoacetaldehyde (BAAA) freely diffuses into cells. In the presence of ALDH enzyme, BAAA converts to BODIPY-aminoacetate (BAA) which is negatively charged and is therefore, retained in the cells. Additionally the Aldefluor buffer provided with the kit also contains ABC transporter inhibitors further blocking BAA efflux from the cells.

The degree of fluorescent ALDH reaction produced directly correlated with the amount of ALDH activity. DEAB is an ALDH inhibitor, thus blocks the production of BAA in the presence of the ALDH enzyme.

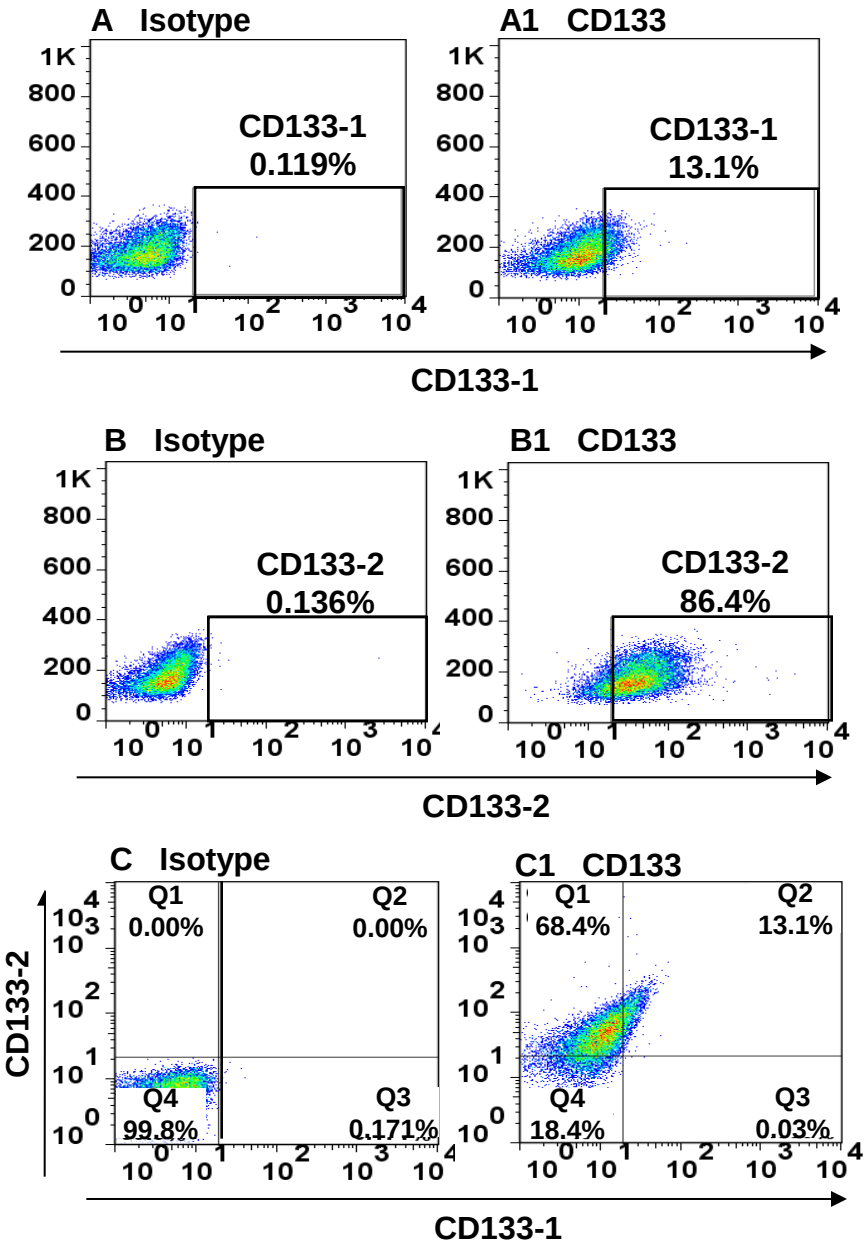

Figure 13: CD133-1 expressing H345 cells are positive for CD133-2 H345 cells were stained with monoclonal antibodies CD133-1-APC and/or CD133-2-PE. Cells stained with APC-conjugated and/or PE-conjugated isotype-matched mouse IgG were used as negative control. A1 demonstrates expression of CD133-1 according to its negative control, A. B1 displays expression of CD133-2 according to its negative control, B. C1 demonstrates co-expression of CD133-1 and CD133-2 on H345 according to its negative control, C. As shown, all H345 cells positive for CD133-1 are positive for CD133-2. Data is representative of three independent experiments.

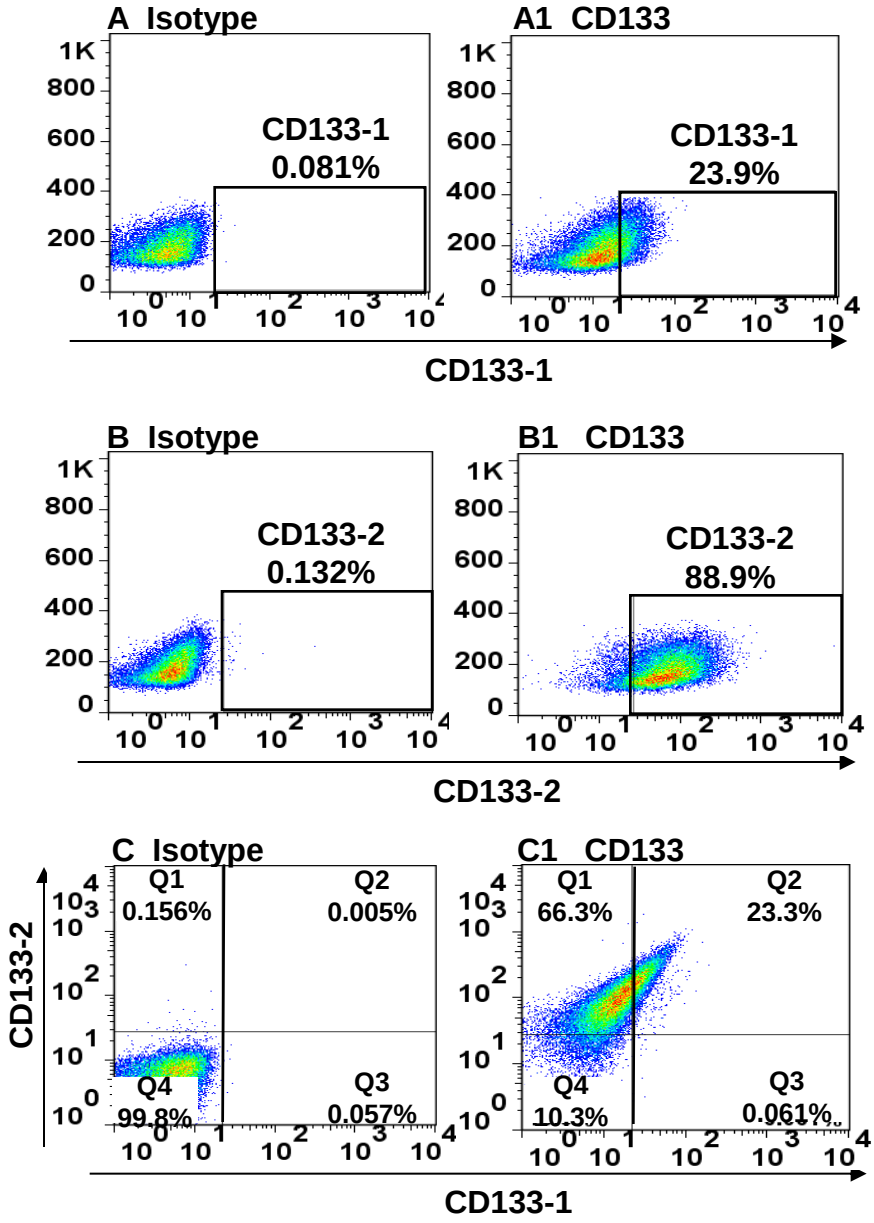

Figure 14: CD133-1 expressing H69 cells are positive for CD133-2
H69 cells were stained with monoclonal antibodies CD133-1-APC and/or CD133-2-PE. Cells stained with APC-conjugated and/or PE-conjugated isotype-matched mouse IgG were used as negative control. A1 demonstrates expression of CD133-1 according to its negative control, A. B1 displays expression of CD133-2 according to its negative control, B. C1 demonstrates co-expression of CD133-1 and CD133-2 on H69 according to its negative control, C. As shown, all H69 cells positive for CD133-1 are positive for CD133-2. Data is representative of three independent experiments.

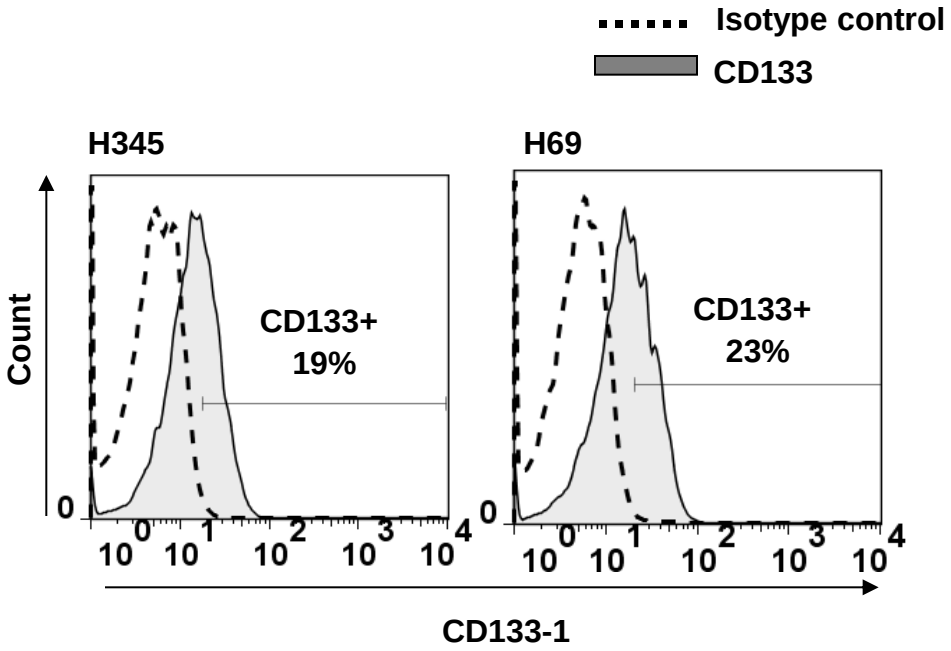

Figure 15: Flow cytometric analysis of CD133 expression on H345 and H69 cells

Cells were stained with CD133-1-APC monoclonal antibody and were analysed by flow cytometry. Cells stained with APC-conjugated, isotype-matched mouse IgG were used as isotype control. Percentage of CD133+ cells were calculated relative to isotype control. CD133 expression demonstrated a gaussian expression pattern on H345 and H69 cell lines. Data is representative of five independent experiments.

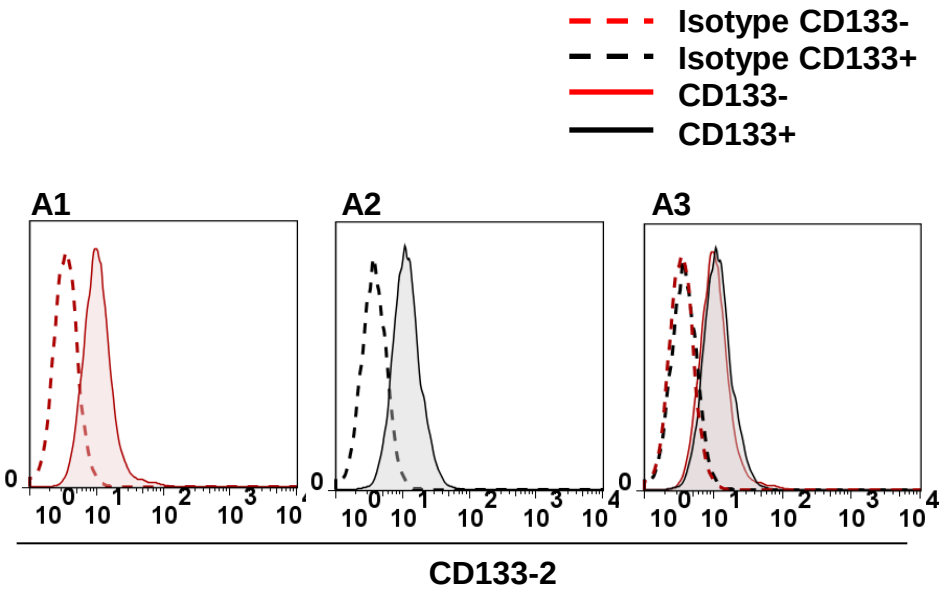

Figure 16: H345 CD133+ and CD133- cells isolated by MicroBeads kit demonstrated poor purity as analysed by flow cytometry

The purity of CD133+ and CD133- isolated cells using MicroBeads kit was analysed based on CD133-2 expression by flow cytometry. A1 represents CD133 expression on the negatively selected population. A2 represents CD133 expression on the positively selected population. A3 is an overlay histogram demonstrating CD133-2 expression on CD133+ and CD133- isolated populations with their respective isotype controls. As shown in the figure, no difference in the fluorescent intensity between the two populations could be observed, indicating CD133 MicroBead Kit did not select a pure populations. Data is representative of three independent experiments.

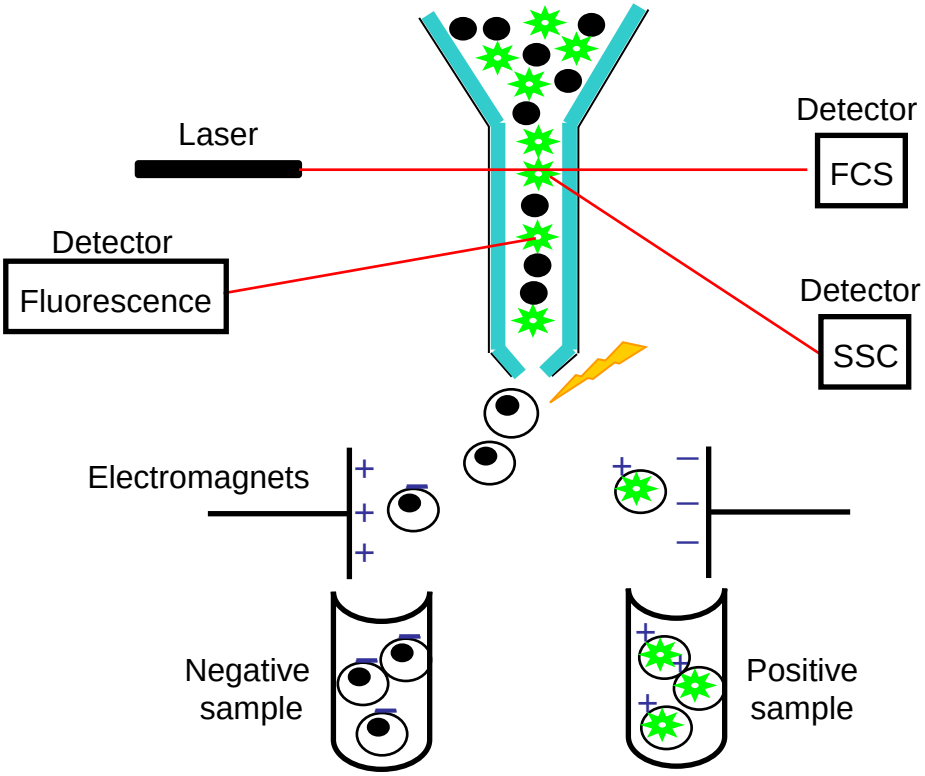

Figure 17: Schematic image of fluorescent activated cell sorting
Labelled cell suspension is directed into a thin stream of fluid which leads the cells to pass in a single file. The stream merges from a vibrating nozzle, breaking the stream into discrete droplets. A laser beam is directed at the stream and the scattered light and emitted fluorescence is captured by a number of detectors. The signals captured by the detectors are then processed by analysing the fluctuation in brightness at each detector which then allow to obtain various information regarding the cell of interest. If the signals from the detectors match the criteria set for size, shape and fluorescence, a positive or negative electrical charge is given to the fluidic stream. The stream of droplets is then directed through a pair of charged plates so that the charged droplets containing cells are deflected and collected.

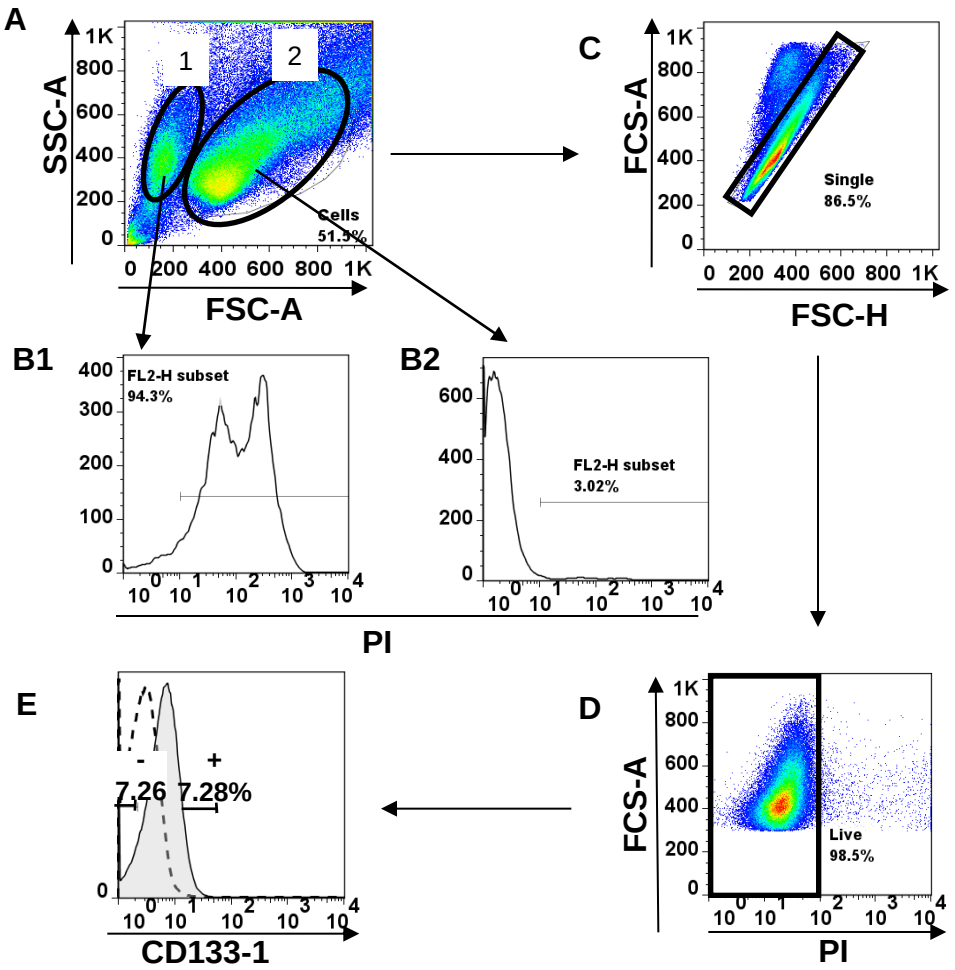

Figure 18: Fluorescent activated cell sorting in H345 cells
(A) Based on the forward and side scatter distribution of H345 cells, two populations were detected, population-1 and population-2. The viability of cells within the population-1 (B1) and -2 (B2) was evaluated based on PI exclusion. In contrast to population-1, most cells within population-2 were viable. (C) Single cells within the population-2 were selected by their Height (FSC-H) and FSC-Area (FSC-A) distribution. (D) After single cell selection within the population-2, viable cells within that population were gated based on PI exclusion. (E) demonstrates CD133 distribution on single, viable cells within population-2. Dashed histogram represents isotype control and gray histogram presents CD133 expression. Since CD133 exhibits a Gaussian expression pattern, the top ~7% of the cells with high expression of CD133 and the bottom ~7% of the cells with low/no CD133 expression were gated and subsequently isolated.

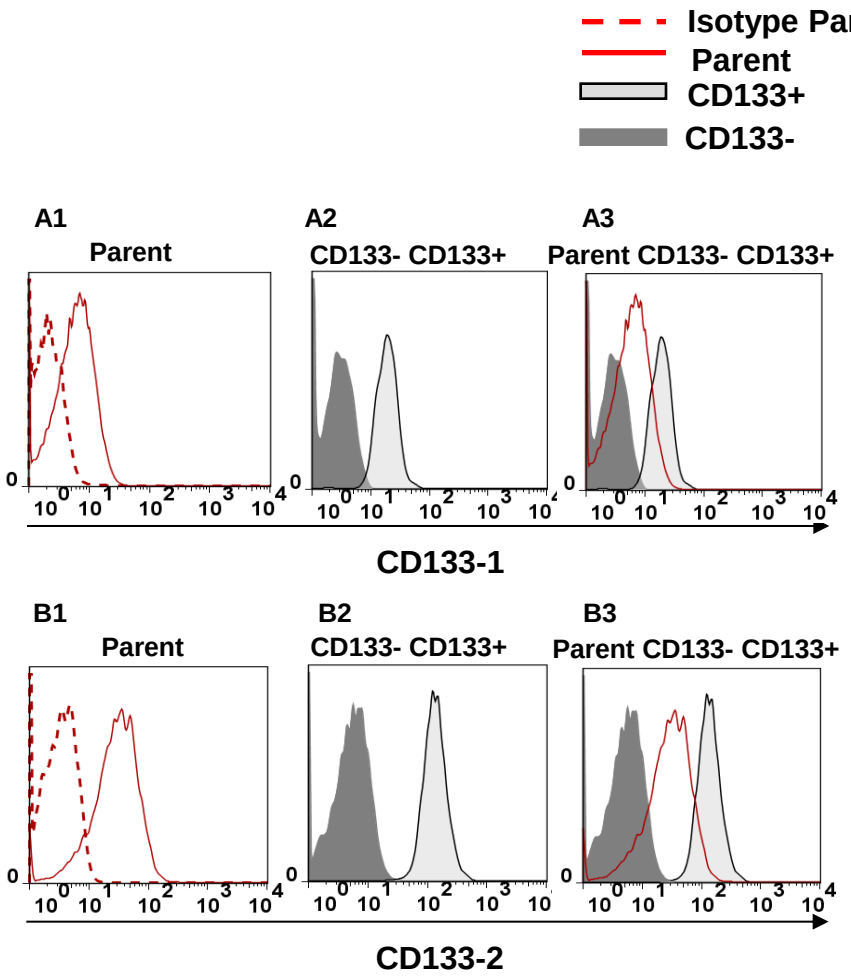

Figure 19: CD133+ and CD133- H345 cells isolated by fluorescent activated cell sorting are pure

A1 represents CD133-1 expression on the parent cells relative to isotype control. A2 is an overlay histogram of CD133-1 expression on CD133- and CD133+ cells. A3 is an overlay histogram of CD133-1 expression on the parent, CD133- and CD133+ cells. CD133+ cells exhibited the highest geometric mean (GM) while CD133- cells demonstrated the lowest GM indicating CD133+ cells have greater expression levels of CD133-1 compared to CD133- and parent cell, therefore pure and enriched isolation. B1 exhibits CD133-2 expression on the parent cells relative to isotype control. B2 is an overlay histogram of CD133-2 expression on CD133- and CD133+ populations. B3 is an overlay histogram of CD133-2 expression on the parent, CD133- and CD133+ cells. Likewise, isolated CD133+ cells demonstrated the highest GM in while CD133- showed the lowest GM, further supporting the purity of cell isolation. Data are representative of three independent experiments.

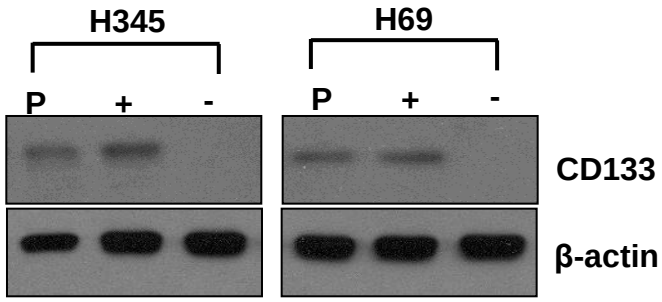

Figure 20: Purity of FACS sorted CD133+ and CD133- H345 cells was confirmed by western blot

The purity of sorted populations was analysed by CD133 protein levels in the sorted and parent cells by western blot. No band could be detected in CD133- isolated cells, whereas a band of ~120 kDa was representative of CD133 expression in the CD133+ isolated and parent cells confirming sort purity. β-actin was used as loading control. Images are representative of three independent experiments.

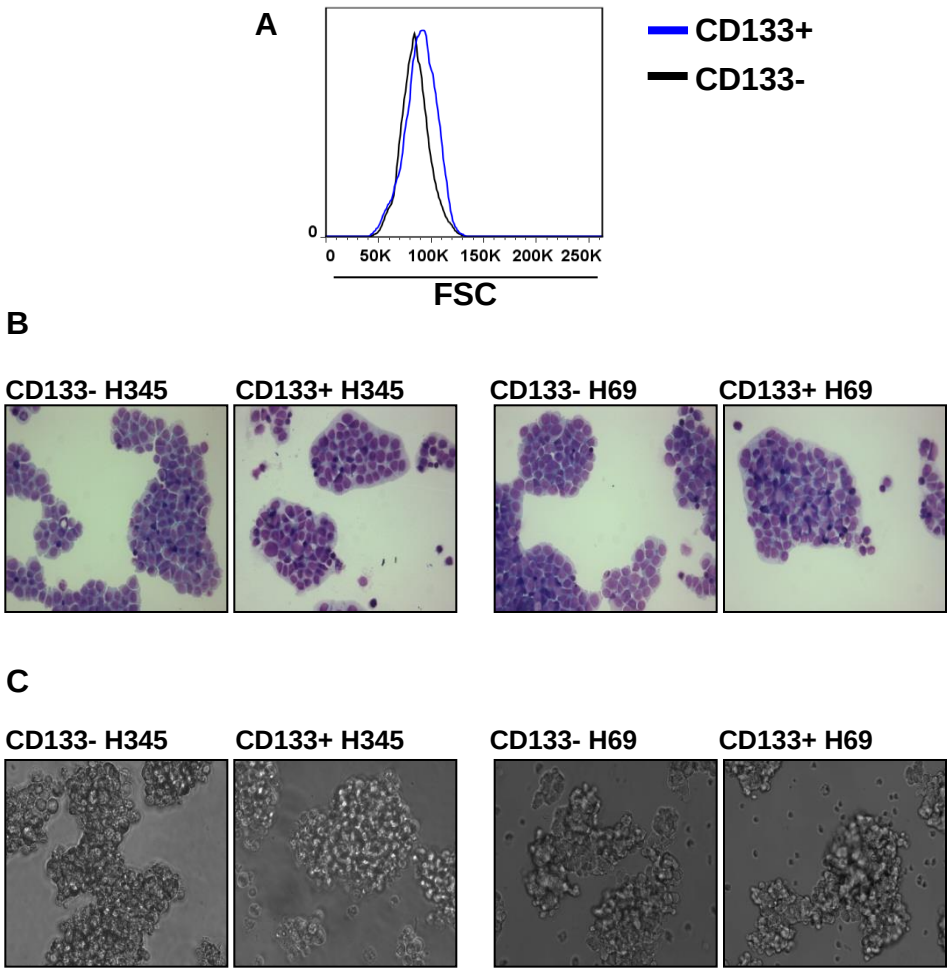

Figure 21: CD133+ and CD133- cells are similar in cellular size and illustrate similar tissue culture appearance

(A) The size of CD133+ and CD133- H345 cells were compared based on their Forward Scatter distribution (FSC) on flow cytometer. As shown, CD133+ and CD133- are similar in size. (B) Three days post-sorted cells cultured in SITA were cytocentrifuged onto glass cover slips and were stained with May-Grunwald-Giemsa. Isolated cells from both cell lines demonstrated similar morphology judged by light microscopy. (C) Tissue culture appearance of three days post-sorted cells cultured in SITA medium were observed under light microscopy. In both cell lines, CD133+ and CD133- cells grew as floating aggregates with no differences in the shape or size of the cellular clumps. Images were taken with 10× magnification.

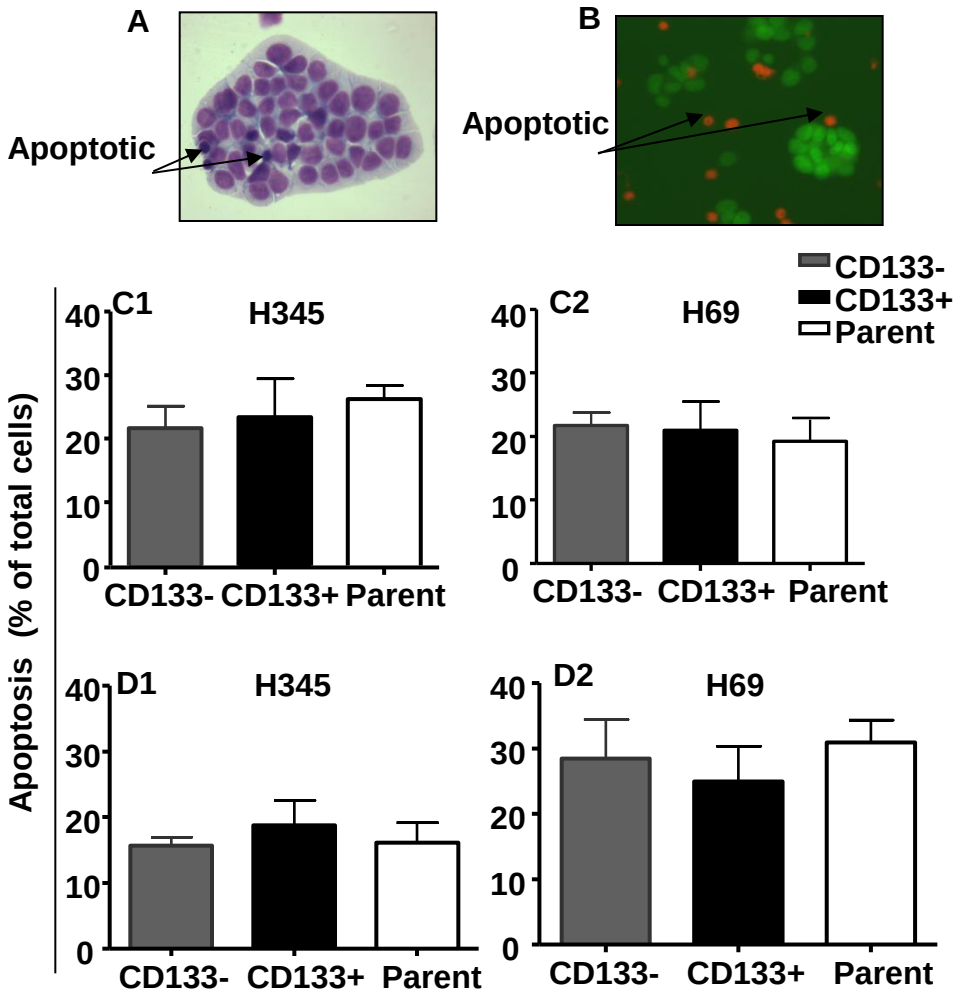

Figure 22: FACS does not effect the cell viability of isolated cells
The viability of sorted and unsorted H345 and H69 cells was measured by staining isolated cells with May-Grunwald-Giemsa and Ethidium bromide/acridine orange (EB/AO). A is a representative image of cells stained with May-Grunwald-Giemsa. Apoptotic cells appeared as shrunken cells with dense nuclei. B is a representative image of cells stained with EB/AO in which cells can be distinguished based on their nuclear morphology and fluorescence (viable cells, green nucleus, late apoptotic cells, shrunken cells with orange nucleus). No significant differences between the viability of sorted and parent H345 and H69 cells stained with either May-Grunwald-Giemsa (C1 and C2) or EB/AO (D1 and D2) could be detected. Data represents the mean of three independent experiments ± SEM.

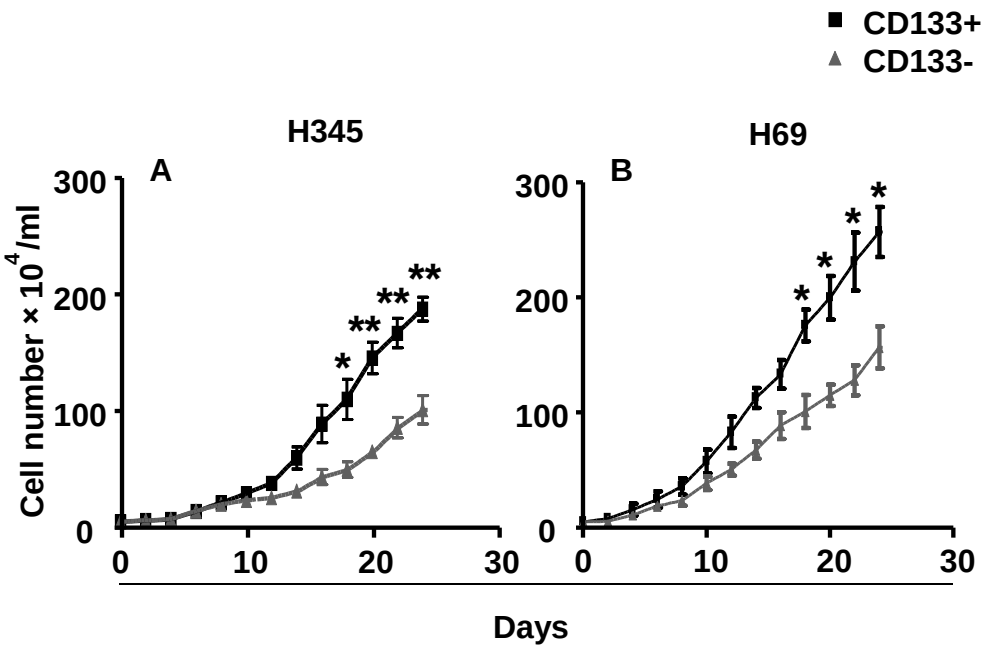

Figure 23: CD133+ are more proliferative than CD133- cells
Proliferation of sorted CD133+ and CD133- cells was evaluated by culturing 1×10^4 sorted cells/well in SITA medium and counting the viable cells by NucleoCounter NC-100 every two days over 24 days. In both H345 (A) and in H69 (B) cell lines, CD133+ cells were significantly more proliferative than CD133- cells. Data represents the mean ± SEM of three independent experiments performed in duplicates. (* $P<0.05$ and **, $P=0.005$)

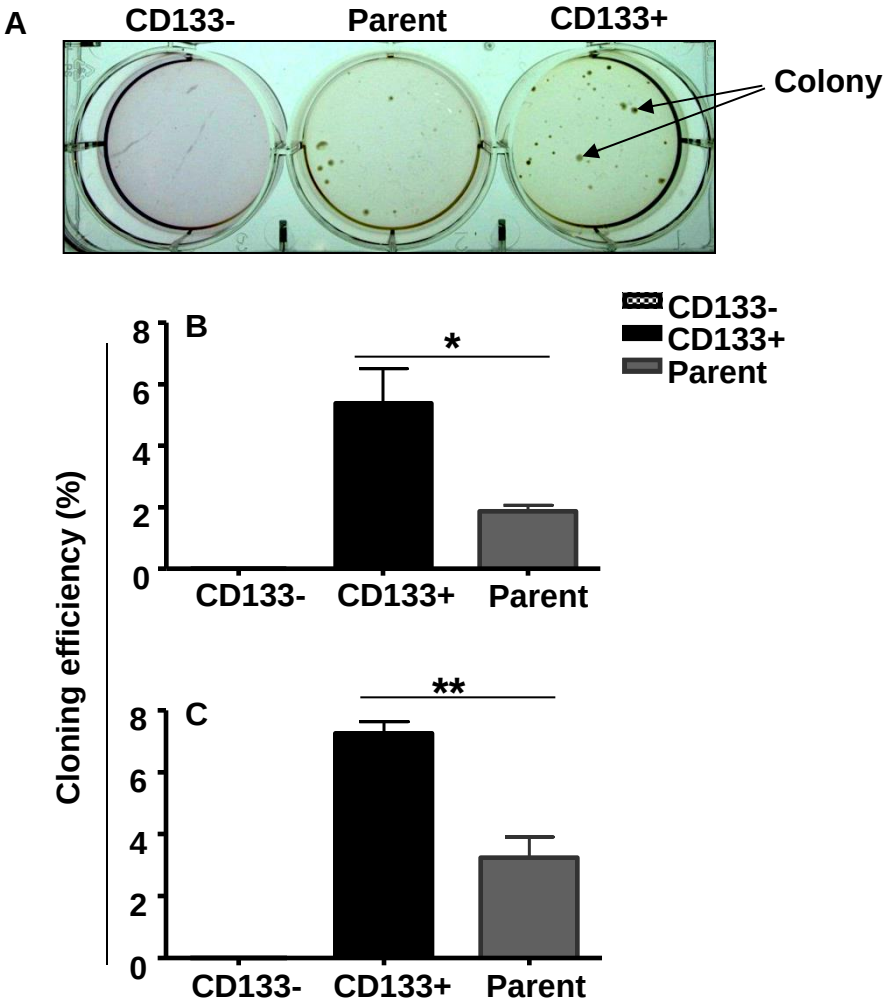

Figure 24: CD133+ cells are clonogenic

Cells were cultured in SITA medium containing 0.3% agarose and were layered on the same medium containing 0.5% agarose. Colonies (>16 cells) formed were scored after 21 days using standard light microscopy. Data is presented as percentage of the cells seeded (cloning efficiency). A, is a representative image of tissue culture dish containing CD133-, CD133+, and parent H345 cells in semi-solid medium after 21 days post-culturing. In contrast to the wells containing CD133+ and parent cells, no colonies within the well containing CD133- cells could be detected. In both H345 (B) and H69 (C) cells, CD133+ cells were more clonogenic than the CD133- and parent cells. Data represents the mean of three independent experiments ± SEM. (* P=0.04 and **, P=0.006).

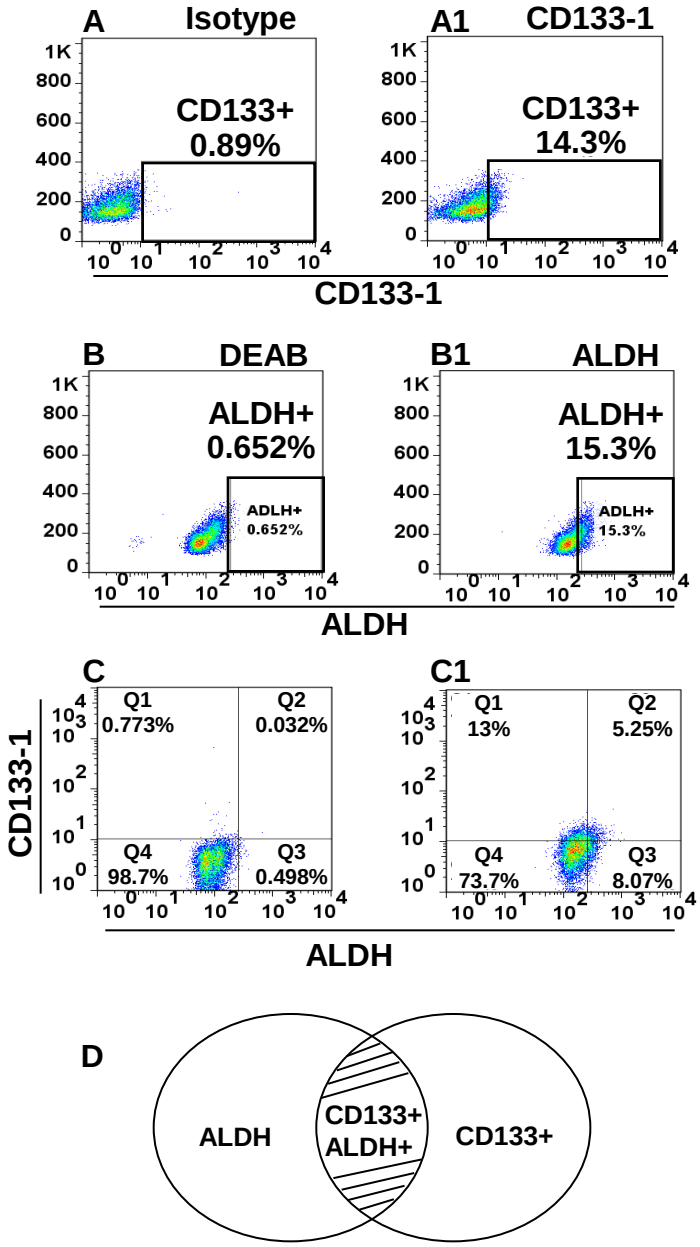

Figure 25: CD133+ cells are a heterogeneous population

To examine the heterogeneity within the CD133+ cells, H345 (unsorted) cells were evaluated for CD133-1 expression (A and A1), ALDH activity (B and B1), and co-expression of both markers (C and C1). Low percentage of cells co-expressing CD133 and ALDH indicates, CD133+ cells are a heterogeneous population of cells comprising of CD133+ ALDH+ and CD133+ ALDH- cells. Data is representative of three independent experiments. D, is a schematic illustration of heterogeneity within CD133+ cells.

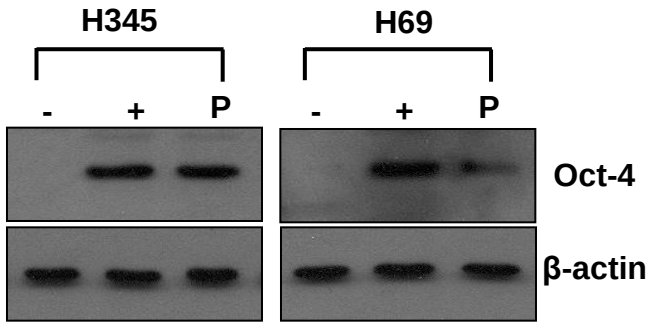

Figure 26: CD133+ cells express embryonic stem cell marker Oct-4
The presence of Oct-4 in the sorted and unsorted cells was examined by evaluating their protein levels by western blotting. A protein band of ~48 kDa in both CD133+ and parent cells indicated the presence of Oct-4 whereas no band could be detected in the CD133- cell lysates. β-actin was used as loading control. (-) represents CD133- cells, (+) represents CD133+ cells and (P) represents parent cells. Image is representative of three independent experiments.

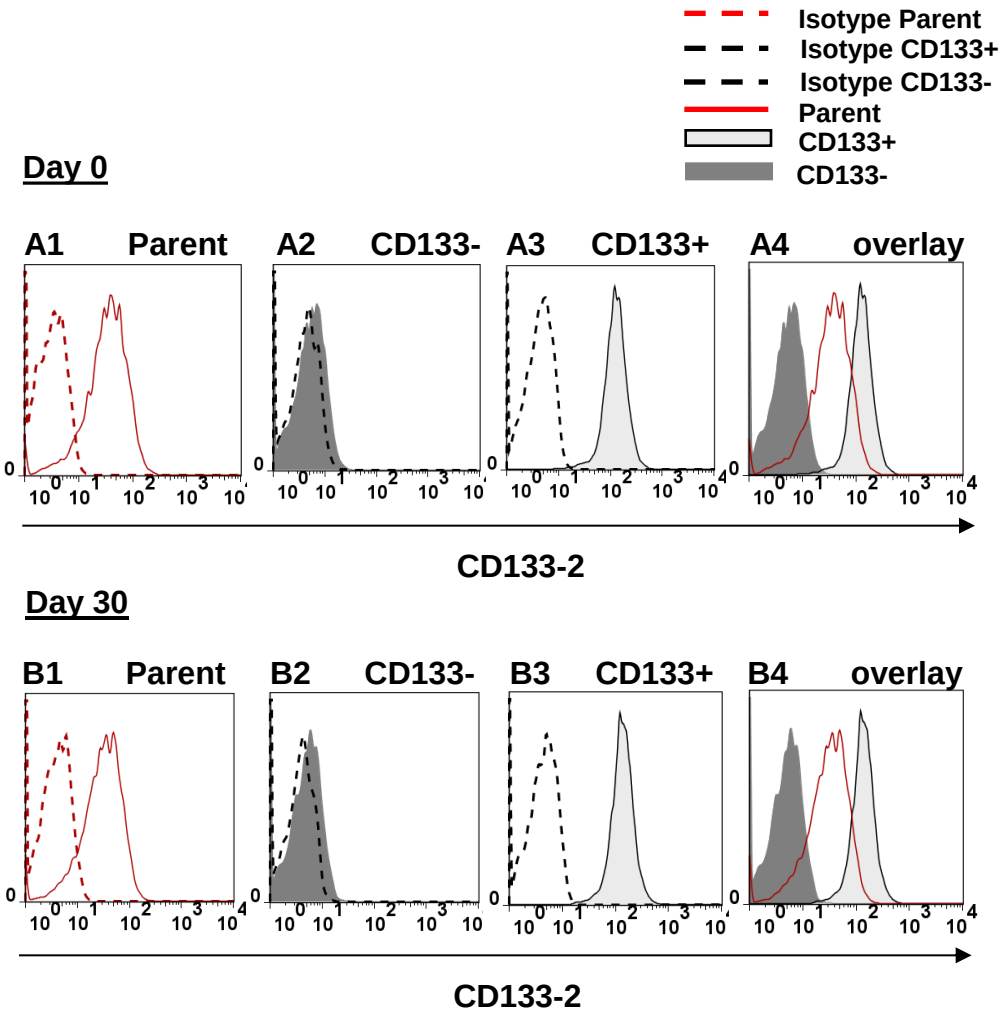

Figure 27: CD133+ cells maintain CD133 expression during prolonged periods of culturing

Sorted and unsorted H345 cells were cultured in serum-free SITA medium and the expression of CD133-2 was evaluated on day 0 (day when cells were cultured) and 30 days post-culture by flow cytometry. Data presented is a representative flow cytometry histogram showing the expression of CD133 on the parent (A1, day 0 and B1, day 30), CD133- (A2, day 0 and B2, day 30) and CD133+ cells (A3, day 0 and B3, day 30). In each histogram, CD133 expression was compared with its corresponding isotype control. Histograms A4 and B4 are overlay histograms of CD133-, CD133+ and parent cells on day 0 and on day 30 respectively. CD133+ cells demonstrated the highest GM compared to CD133- and parent cells on day 0 and day 30. Therefore, CD133+ were able to maintained the expression of the stem cell marker, CD133 during the prolonged periods of culturing. Data is representative of five independent experiments.

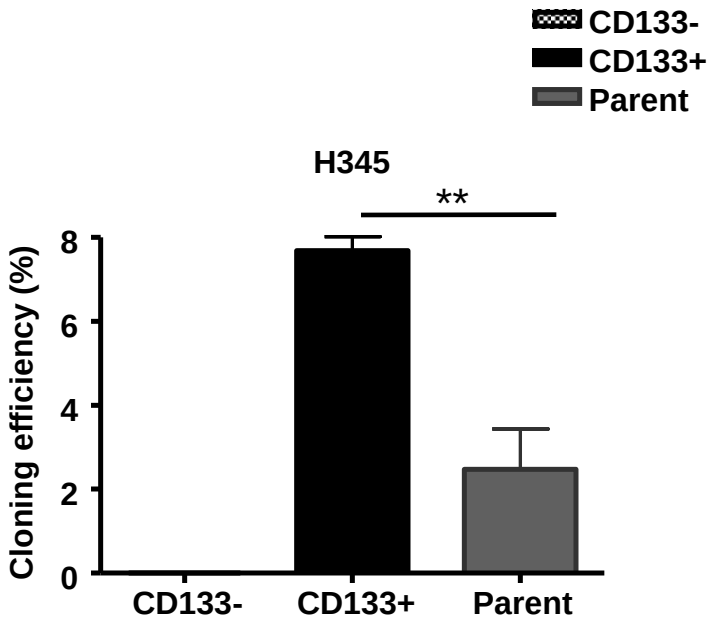

Figure 28: CD133+ cells maintain their high clonogenic potential over prolonged periods of culturing

To confirm CD133+ H345 cells retain their stem cell-like features over long periods of culturing, the clonogenicity of 30 days post-sorted CD133+, CD133-, and parent H345 cells was evaluated in semi-solid medium. Sorted cells were cultured for 30 days in SITA medium. After this period 10^4 cells were transferred into SITA medium containing 0.3% agarose and were layered on the same medium containing 0.5% agarose. SITA medium was used to inhibit possible cellular differentiation. Colonies were scored after 21 days using standard light microscopy. Data is presented as cloning efficiency. Despite long periods of culturing, CD133+ cells retained their clonogenic potential and were more clonogenic than CD133- and parent cells indicating that CD133+ cells are possibly capable of self-renewing. CD133- did not form colonies. Data represents the mean of five independent experiments ± SEM. (**, P=0.006)

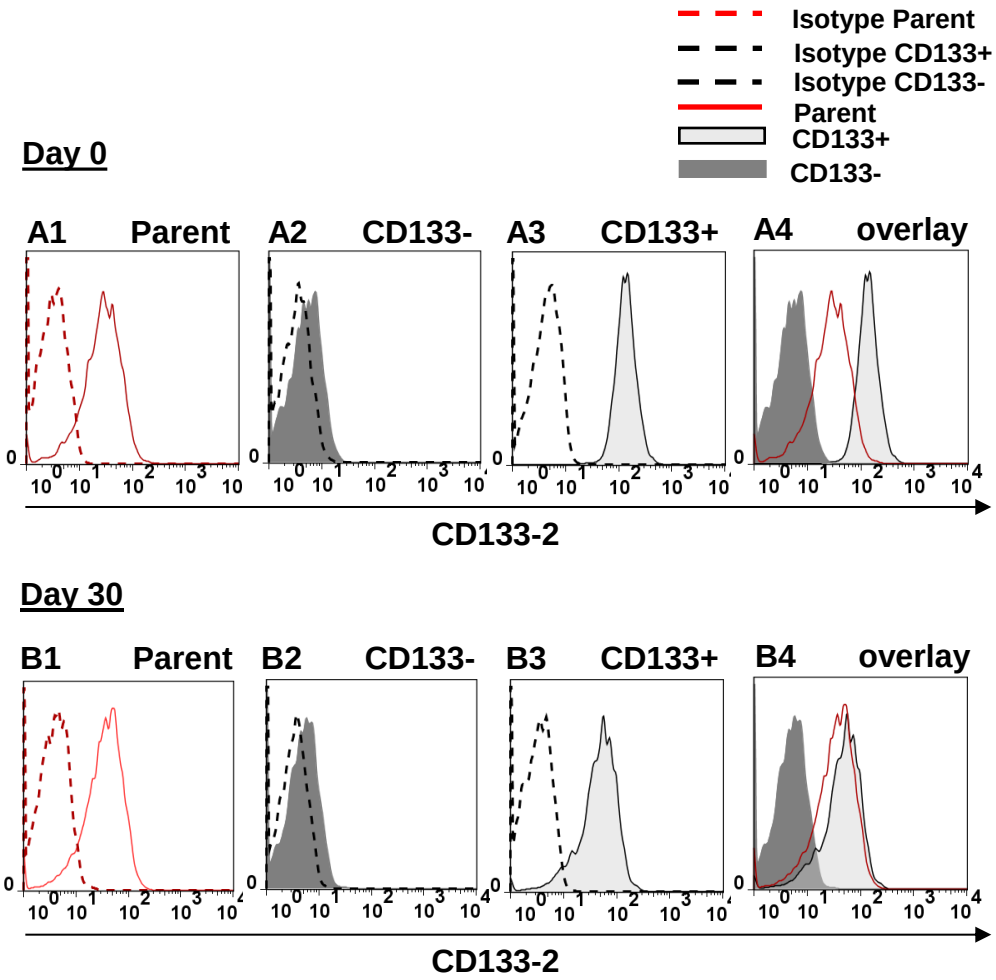

Figure 29: CD133+ cells differentiate in appropriate culture condition

Sorted H345 cells were cultured in serum containing medium (RPMI complete medium) and the expression of CD133 was evaluated on day 0 (day when cells were cultured) and 30 days post-culture by flow cytometry. Data presented is a representative flow cytometry histogram showing the expression of CD133 on the parent (A1, day 0 and B1, day 30), CD133- (A2, day 0 and B2, day 30) and CD133+ cells (A3, day 0 and B3, day 30). In each histogram, CD133 expression was compared with its corresponding isotype control. Histograms A4 and B4 are overlay histograms of CD133-, CD133+ and parent cells on day 0 and on day 30, respectively. In serum-containing medium CD133+ cells differentiated to generate a heterogeneous population similar to parent cells. Data is representative of five independent experiments.

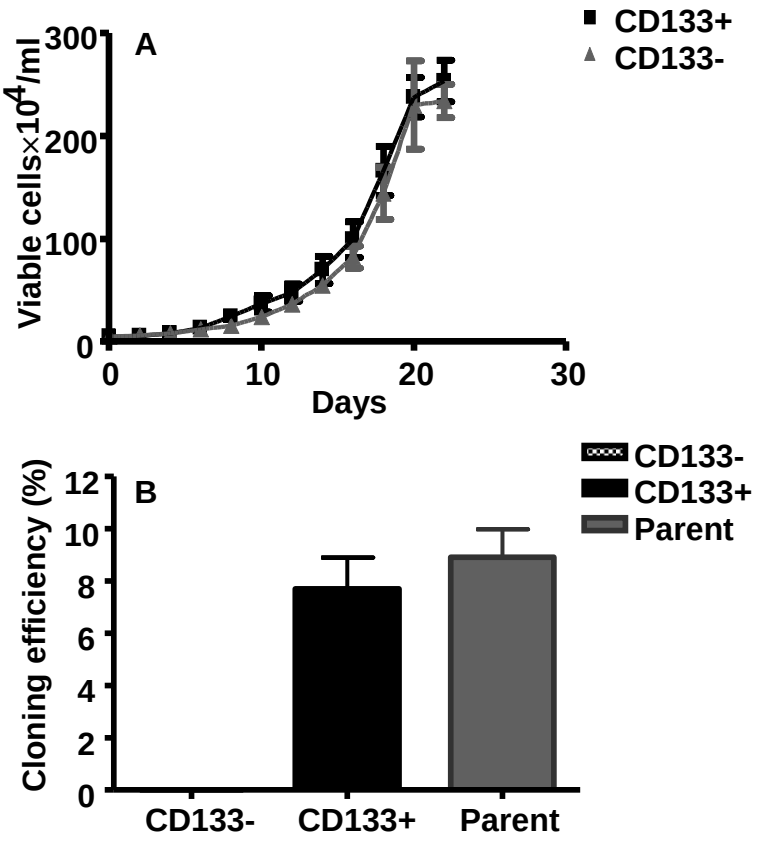

Figure 30: CD133+ cells on differentiation lose their stem cell-like phenotype

The proliferation and clonogenicity of differentiated CD133+ cells were evaluated in serum containing liquid culture and semi-solid medium respectively. (A) Sorted H345 cells were cultured in in RPMI complete medium for 30 days. After this period, 1×10^4 cells/well were transferred into fresh RPMI complete medium and the number of viable cells was counted every 2 days by NucleoCounter NC-100 over 24 days. Differentiated CD133+ cells grew at the same rate as the CD133- cells with no significant difference in their growth potentials. (B) 10^4 viable cells which were previously cultured for 30 days in RPMI complete medium were transferred into fresh differentiating medium containing 0.3% agarose and were layered on the same medium containing 0.5% agarose. Colonies were scored after 21 days using standard light microscopy. Data is presented as cloning efficiency. CD133+ differentiated cells demonstrated similar clonogenicity as the parent cells. Data represents the mean of five independent experiments ± SEM.

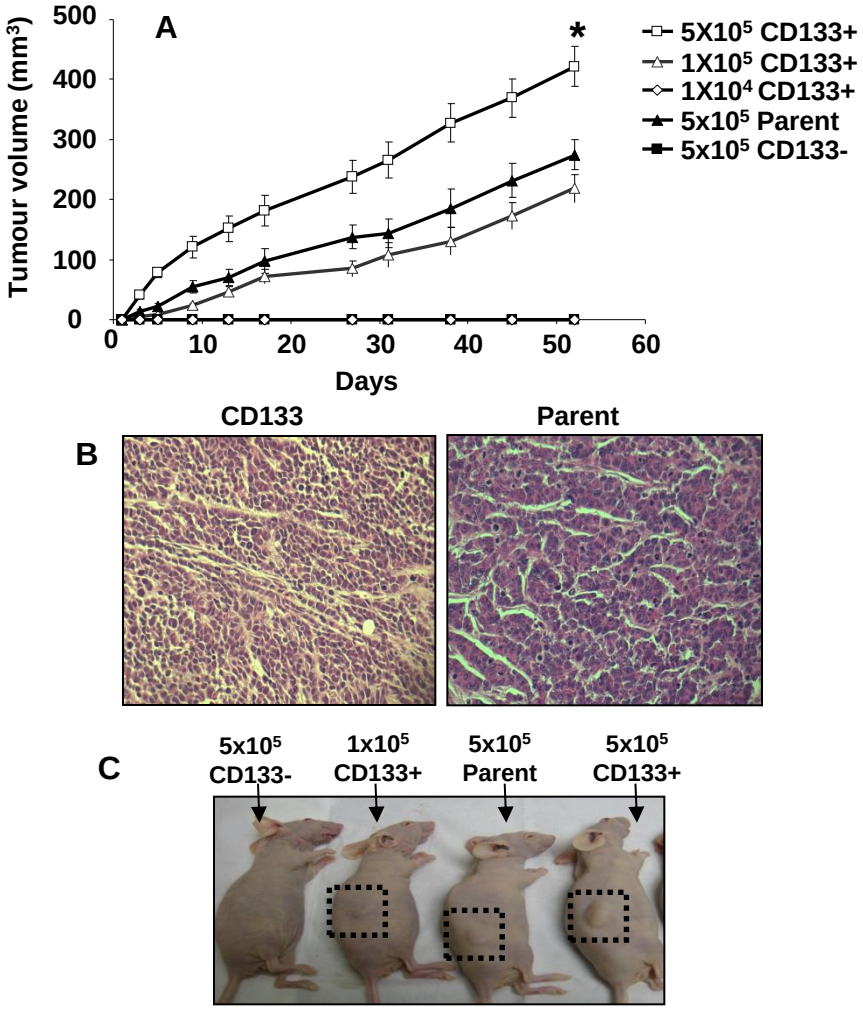

Figure 31: CD133+ cells are tumorigenic *in vivo*

Various cell numbers (5×10^5, 1×10^5, and 1×10^4) of sorted CD133+ and CD133- H345 cells in growth factor reduced Matrigel (1:1 volume of cells:Matrigel mixed at 4°C, total volume of 100 µl) were implanted subcutaneously in contralateral flanks of the *nude/nude* mice (n=4). Same numbers of unsorted H345 cells under the same conditions were implanted subcutaneously in the right flank of *nude/nude* mice (n=4). Tumour size was assessed with callipers every 3-4 days. (A) CD133+ cells were significantly more tumorigenic than CD133- and parent cells. B, is a representative H and E staining of sections taken from tumours developed from injecting CD133+ and parent cells. CD133+ cells consistently generated tumours with histological features closely resembling the tumours initiated by parent cells. Images were taken with 10× magnification. C, is a representative image of mice with subcutaneous implantation of CD133+, CD133- and parent cells. (*, $P<0.05$).

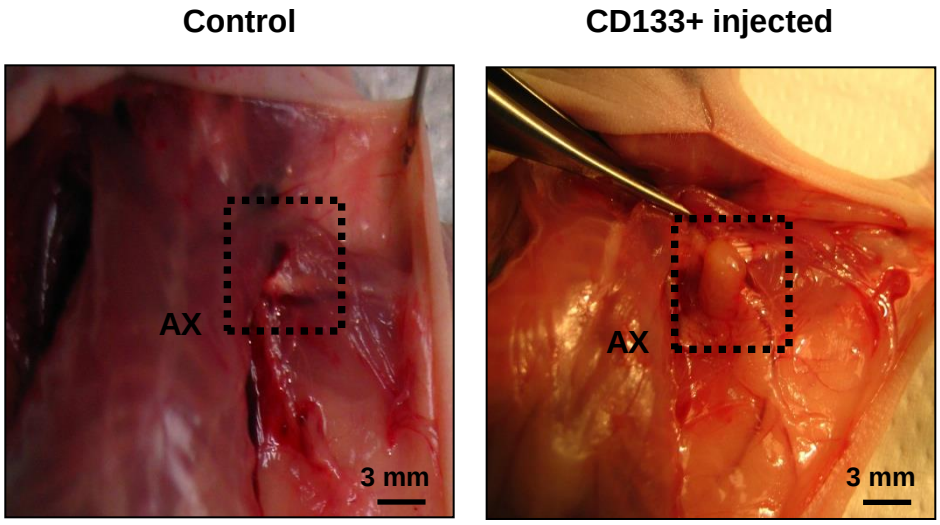

Figure 32: Mice injected with CD133+ cells exhibit enlarged inguinal and axillary lymph nodes

(A) Representative image of a control *nude/nude* mouse axillary (AX) lymph node. Mice lymph nodes are small and difficult to identify in physiological conditions. (B) Image of axillary lymph node in *nude/nude* mouse that was subject to CD133+ cell implantation.

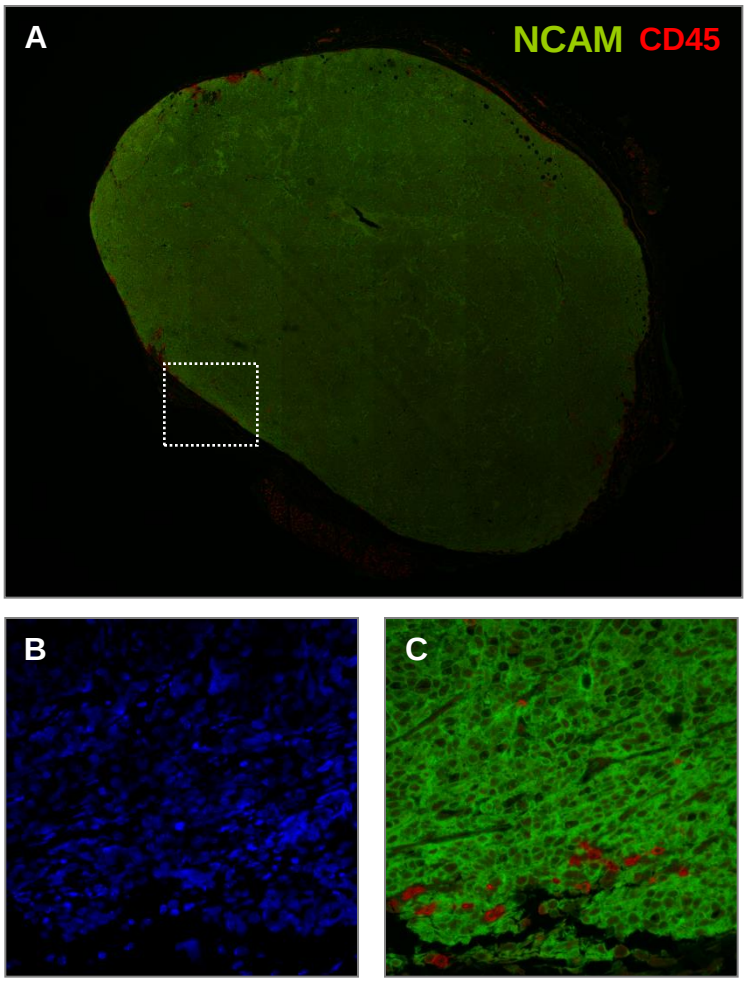

Figure 33: IHC staining of CD133+ primary tumour
Primary tumour (directly generated by implantation of CD133+ cells in mouse) was subject to IHC for detection of NCAM+ cells (representative of SCLC cells) and CD45+ cells (representative of mouse leukocyte cells). Sample was visualised using Tyramide signal amplification (TSA) plus fluorescent kit (NCAM, green; CD45, red) as described in materials and methods. DAPI (0.1 µg/ml) was added to stain the nuclei. Sections were mounted with PermaFluor Aqueous Mounting Medium. Samples were analysed by Confocal microscopy. (A) Almost all cells within the primary tumour were NCAM+. Some CD45+ NCAM- cells could be detected on the border of the tumour. Image was taken by 4× magnification. B, is a magnified image of the tumour region presenting DAPI staining. C, is a magnified image of the tumour region presenting CD45 and NCAM staining. B and C images were taken by 100× magnification.

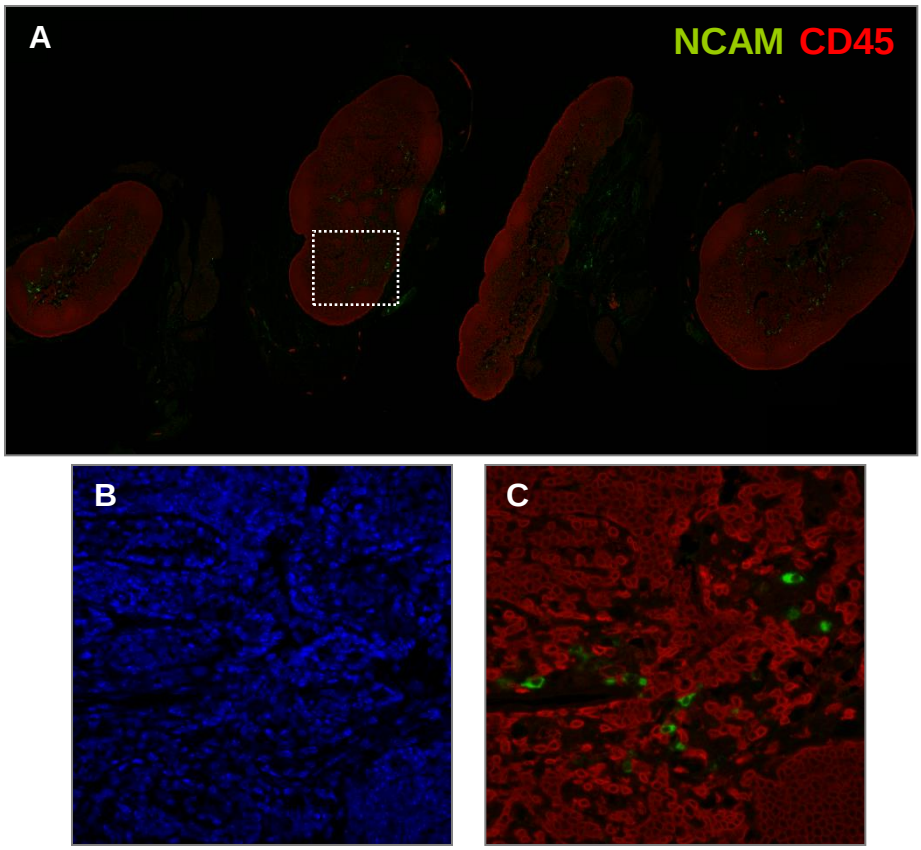

Figure 34: IHC staining of inguinal and axillary lymph nodes excised from *nude/nude* mouse with subcutaneous implantation of CD133+ cells

The four lymph nodes presented were excised from the inguinal and axillary regions of a mouse subject to CD133+ implantation. Lymph nodes were subject to IHC for detection of NCAM+ cells (representative of SCLC cells) and CD45+ cells (representative of mouse leukocyte cells). Sample was visualised using Tyramide signal amplification (TSA) plus fluorescent kit (NCAM, green; CD45, red) as described in materials and methods. DAPI (0.1 µg/ml) was added to stain the nuclei. Sections were mounted with PermaFluor Aqueous Mounting Medium. Samples were analysed by Confocal microscopy. (A) Almost all cells within the lymph nodes were CD45+. Few NCAM+ CD45- cells were also detected within all four lymph nodes. Image was taken by 4× magnification. B, is a magnified image of the lymph node region presenting DAPI staining. C, is a magnified image of the lymph node region presenting CD45 and NCAM staining. B and C images were taken by 100× magnification.

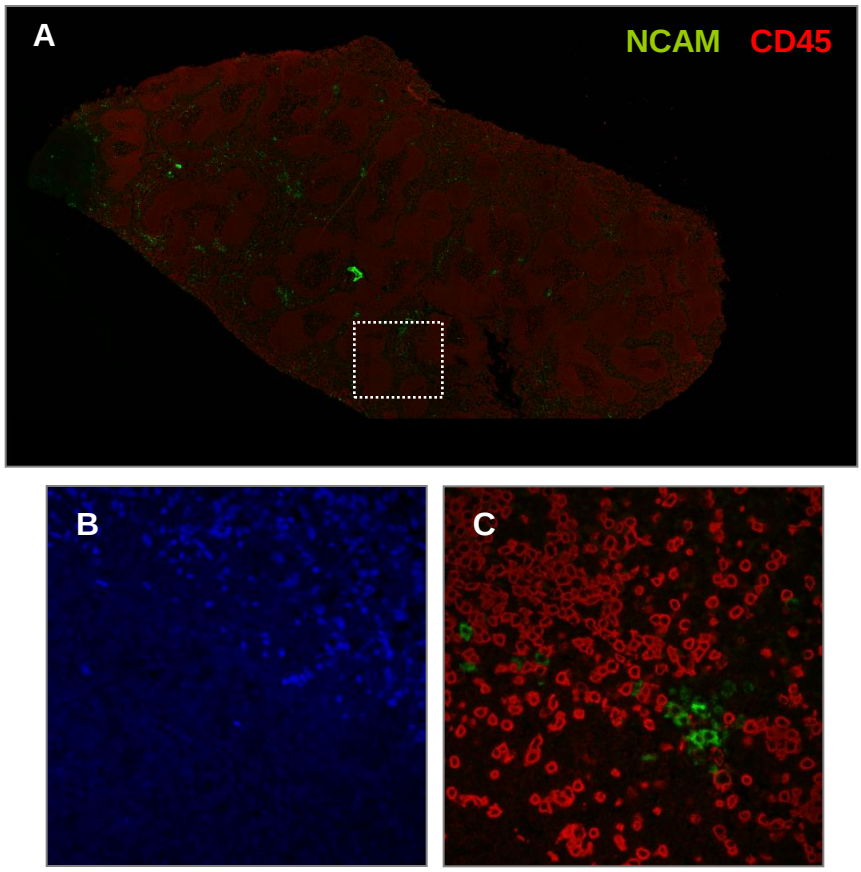

Figure 35: IHC staining of spleen from *nude/nude* mouse unexposed to human SCLC cells

Control *nude/nude* mouse spleen was subject to IHC for identification of NCAM+ cells (representative of SCLC cells) and CD45+ cells (representative of mouse leukocyte cells). Sample was visualised using Tyramide signal amplification (TSA) plus fluorescent kit (NCAM, green; CD45, red) as described in materials and methods. DAPI (0.1 µg/ml) was added to stain the nuclei. Sections were mounted with PermaFluor Aqueous Mounting Medium. Samples were analysed by Confocal microscopy. (A) Almost all cells within the spleen were CD45+. Some NCAM+ CD45- cells could be detected. Image was taken by 4× magnification. B, is a magnified image of the spleen region presenting DAPI staining. C, is a magnified image of the spleen region presenting CD45 and NCAM staining. B and C images were taken by 100× magnification.

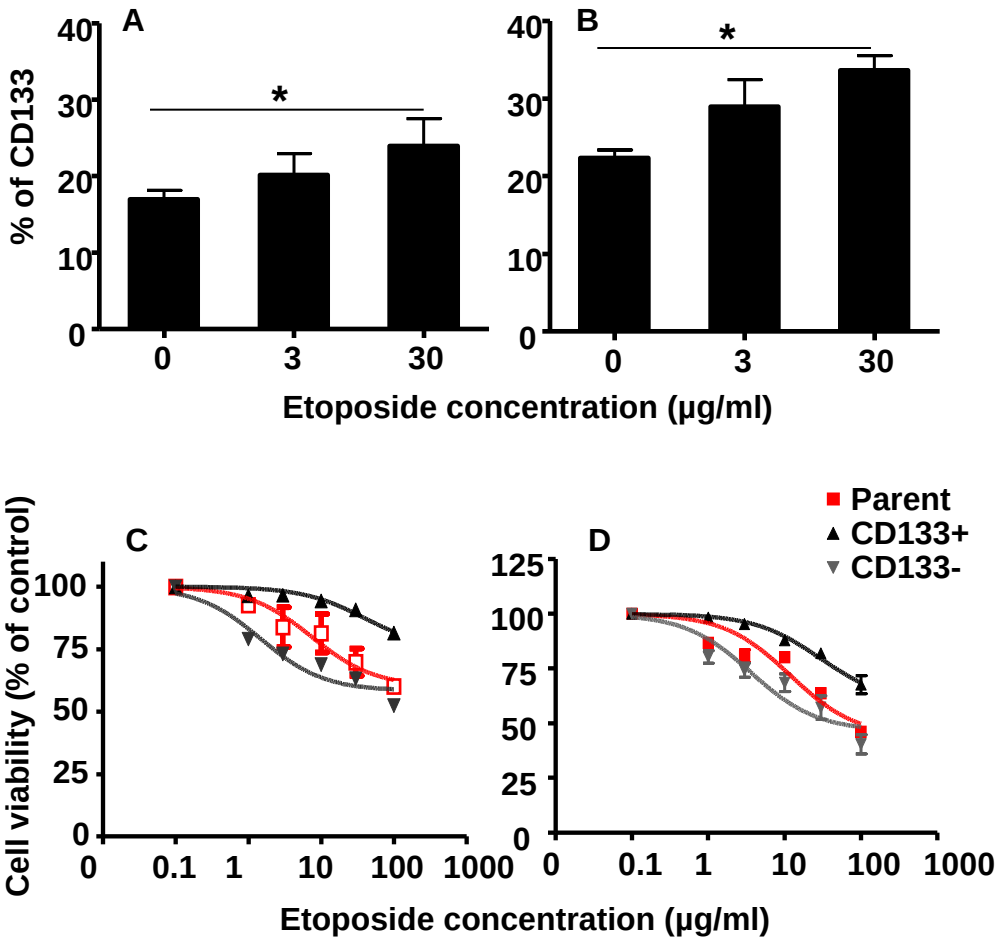

Figure 36: CD133+ cells are enriched by therapy due to their resistant phenotype

Unsorted (parent) H345 and H69 were treated with 3 or 30 µg/ml etoposide for 72 hours. After this period, the percentage of CD133+ cells was assessed by flow cytometry. Untreated cells were used as control. In both H345 (A) and H69 (B) cells, increasing concentration of etoposide was associated with greater enrichment of CD133+ cells. Data represents the mean of three independent experiments ± SEM. To confirm the resistant phenotype of CD133+ cells, cells were treated with increasing concentration (1-100 µg/ml) of etoposide and cell viability was determined after 72 hours by MTT assay. Untreated cells were used as control, and data is presented as percentage of control. In both H345 (C) and H69 (D) cells, CD133+ cells were most resistant to etoposide compared to CD133- and parent cells. Data represents the mean of three independent experiments ± SEM. (*, $P<0.05$)

Table 6: Percentage of CD133+ cells in SCLC cell lines following etoposide treatment

Cell type	Etoposide conc. (µg/ml)	CD133 %
H345	**0**	**16.97 ± 1.2**
	3	**20.18 ± 2.2**
	30	**26.31 ± 2.4**
H69	**0**	**22.34 ± 1**
	3	**28.98 ± 3.1**
	30	**35.78 ± 1.7**

Data represents the mean of three independent experiments ± SEM.

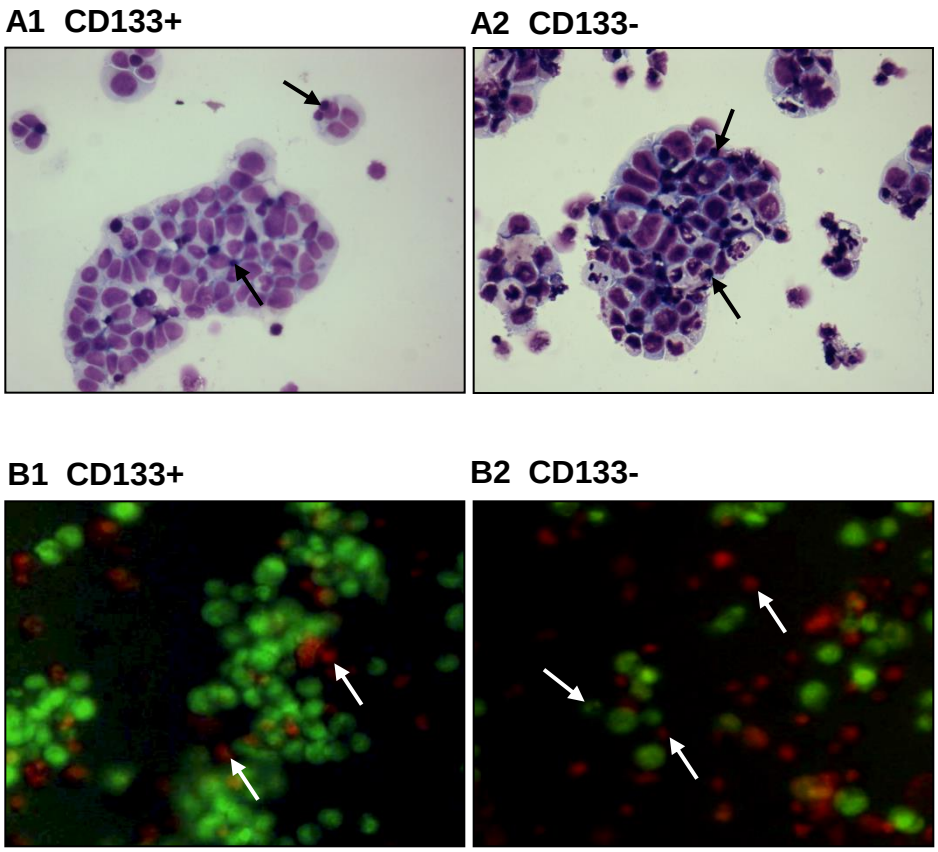

Figure 37: Representative images of CD133+ and CD133- H345 cells treated with etoposide and stained with May-Grunwald-Giemsa and EB/AO for detection of apoptotic cells

Sorted CD133+ and CD133- H345 cells were exposed to 30 µg/ml etoposide for 72 hours. After this period, the percentage of apoptosis by May-Grunwald-Giemsa and EB/AO staining method was calculated. A1 and A2 represent samples stained with May-Grunwald-Giemsa. Apoptotic cells appeared as shrunken cells with dense nuclei analysed by light microscopy. B1 and B2 represent samples stained with EB/AO in which apoptotic cells were shrunken cells with green nucleus (early apoptotic) or shrunken cells with orange nucleus (late apoptotic cells) analysed by fluorescent microscopy. In both staining method, CD133+ cells were significantly more resistant to etoposide treatment than CD133- cells. (➞) represents apoptotic cells. Images were taken with 20× magnification.

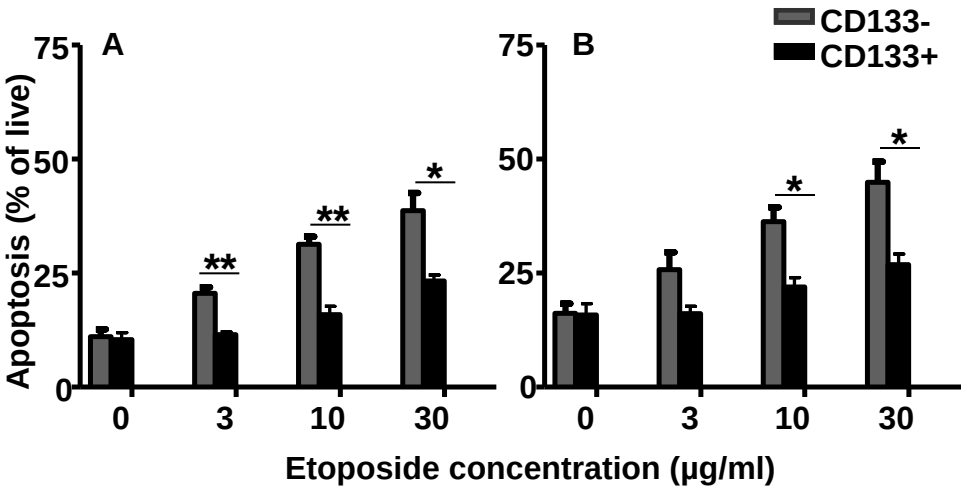

Figure 38: CD133+ H345 cells are resistant to apoptosis induced by etoposide

Sorted CD133+ and CD133- H345 cells were exposed to three different concentrations of etoposide (3, 10, and 30 µg/ml) for 72 hours. After this period, the percentage of apoptosis by May-Grunwald-Giemsa and EB/AO staining was calculated. In both May-Grunwald-Giemsa (A) or EB/AO staining (B), CD133+ cells were significantly more resistant to etoposide treatment than CD133- cells. Data represents the mean of three independent experiments ± SEM. (*, $P<0.05$, and **, $P<0.005$).

Table 7A: Percentage of apoptosis induced by etoposide in CD133+ and CD133- H345 cells measured by May-Grunwald-Giemsa staining

Cell type	Etoposide conc. (µg/ml)	Apoptosis %
CD133+	**0**	**10.37 ± 1.6**
	3	**12.48 ± 0.6**
	10	**15.94 ± 1.77**
	30	**23.3 ± 1.3**
CD133-	**0**	**11.1 ± 1.57**
	3	**20.52 ± 1.36**
	10	**31.3 ± 1.66**
	30	**38.63 ± 2.9**

Data represents the mean of three independent experiments ± SEM.

Table 7B: Percentage of apoptosis induced by etoposide in CD133+ and CD133- H345 cells measured by EB/AO staining

Cell type	Etoposide conc. (µg/ml)	Apoptosis %
CD133+	**0**	**15.76 ± 2.54**
	3	**17.11 ± 1.59**
	10	**21.96 ± 2**
	30	**26.86 ± 2.3**
CD133-	**0**	**16.13 ± 2.17**
	3	**27.77 ± 2.72**
	10	**36.29 ± 3.07**
	30	**45.9 ± 3.47**

Data represents the mean of three independent experiments ± SEM.

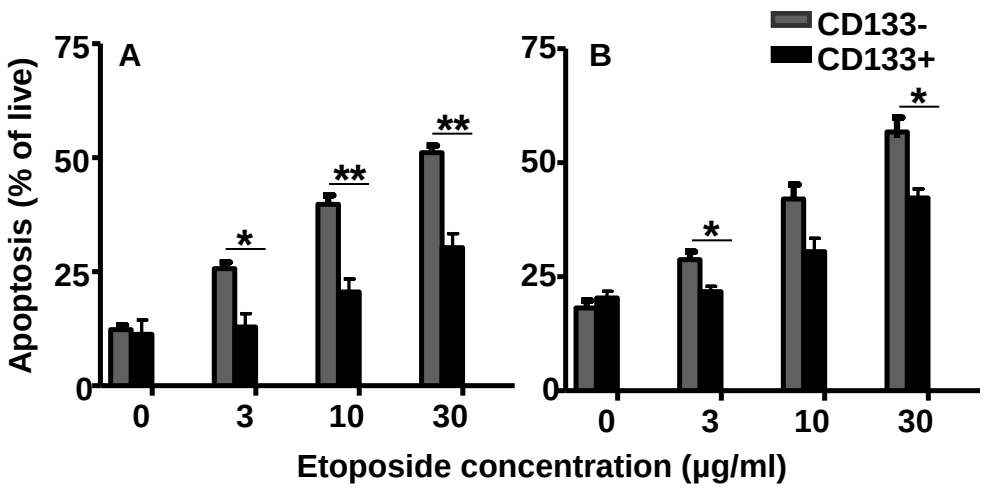

Figure 39: CD133+ H69 cells are resistant to apoptosis induced by etoposide

Sorted CD133+ and CD133- H69 cells were exposed to three different concentrations of etoposide (3, 10, and 30 µg/ml) for 72 hours. After this period, the percentage of apoptosis by May-Grunwald-Giemsa and EB/AO staining was calculated. In both May-Grunwald-Giemsa (A) or EB/AO staining (B), CD133+ cells were significantly more resistant to etoposide treatment than CD133- cells. Data represents the mean of three independent experiments ± SEM. (*, $P<0.05$, and **, $P<0.005$).

Table 8A: Percentage of apoptosis induced by etoposide in CD133+ and CD133- H69 cells measured by May-Grunwald-Giemsa staining

Cell type	Etoposide conc. (µg/ml)	Apoptosis %
CD133+	0	12.31 ± 2.11
	3	12.91 ± 2.89
	10	20.56 ± 2.82
	30	30.25 ± 3.07
CD133-	0	12.28 ± 0.99
	3	25.26 ± 1.38
	10	39.75 ± 1.94
	30	52.09 ± 1.56

Data represents the mean of three independent experiments ± SEM.

Table 8B: Percentage of apoptosis induced by etoposide in CD133+ and CD133- H69 cells measured by EB/AO staining

Cell type	Etoposide conc. (µg/ml)	Apoptosis %
CD133+	0	20.32 ± 1.42
	3	21.74 ± 1.17
	10	30.46 ± 2.96
	30	42.28 ± 3.26
CD133-	0	18.18 ± 1.58
	3	28.8 ± 1.73
	10	42.02 ± 3.14
	30	58.72 ± 3.48

Data represents the mean of three independent experiments ± SEM.

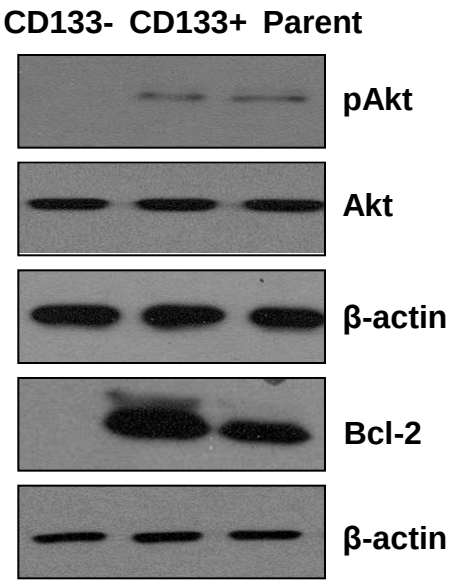

Figure 40: CD133+ are resistant to apoptosis due to preferential expression of proteins involved in survival pathways

Endogenous expression of activated Akt (phosphorylated at Ser473), or Bcl-2 proteins were evaluated in CD133+, CD133- and parent H345 cell lysates by western blotting. CD133+ cells demonstrated significantly elevated levels of $pAkt^{Ser473}$and Bcl-2 compared to CD133- cells. Elevated expression of phosphoserine-specific Akt in CD133+ H345 cells was not a result of an increase in total Akt protein levels. β-actin was used as a control for equal loading. Data is representative of three independent experiments.

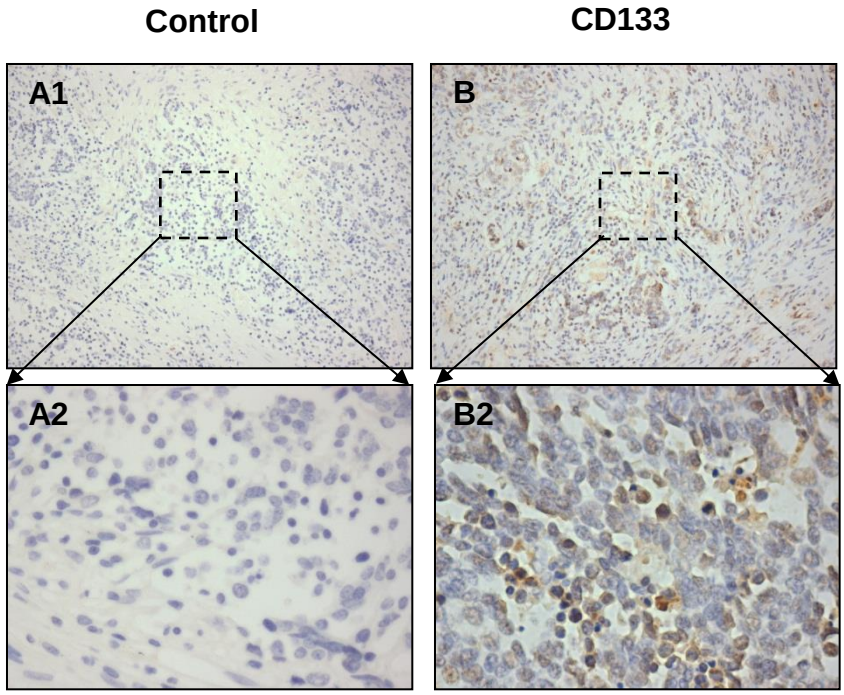

Figure 41: Human SCLC tissue sections retain high levels of CD133+ cells

The expression of CD133 was evaluated in primary SCLC tissues by IHC. IHC was performed using a DAKO Envision kit (for more detail see materials and methods). CD133 antibody was diluted 1:100 in antibody diluent. Sections were labelled with biotinylated donkey anti-rabbit IgG (H+L) secondary antibody (diluted 1:200 in antibody diluent) and were counterstained with Mayers haematoxylin. In each experiment, negative controls of secondary antibody only was used. A1 and A2 are negative controls (A2 is a magnified image of a region within A1). B1 and B2 are images of a SCLC section stained with CD133 (B2 is a magnified image of a region within B1). High levels of CD133 expression was detected in SCLC biopsy samples judged by light microscopy. Images are representative of three independent experiments. A1 and B1 are images taken with 5× magnification and A2 and B2 are images taken with 32× magnification.

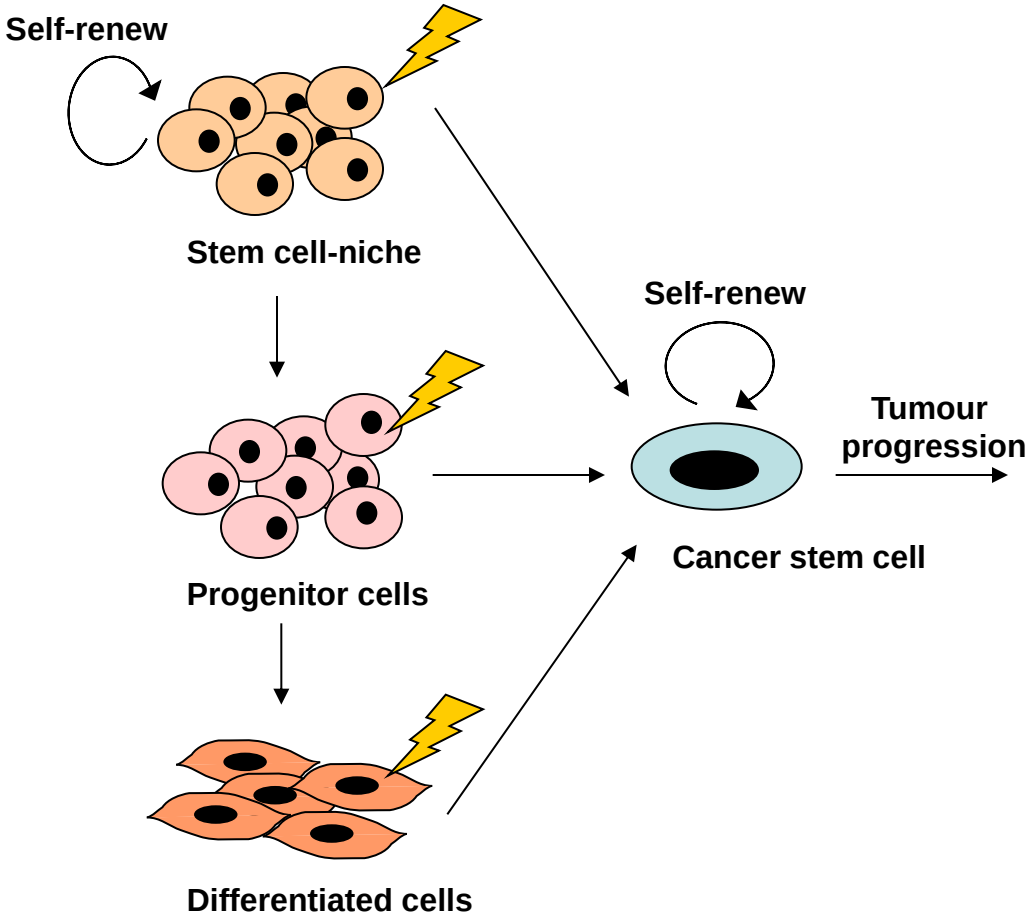

Figure 42: Schematic illustration of origin of cancer stem cells

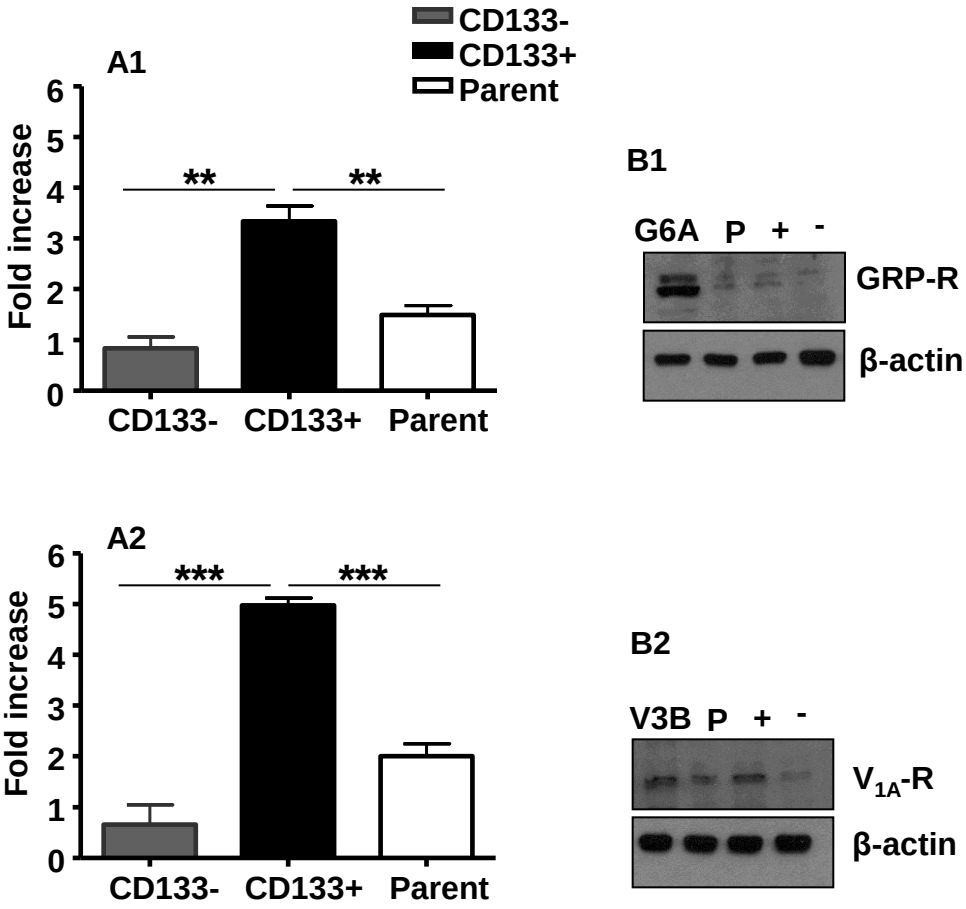

Figure 43: CD133+ cells express higher levels of neuropeptide receptors compared to the CD133- cells

(A1) mRNA encoding GRP-R in H345 cells or (A2) mRNA encoding V_{1A}-R in H69 cells was measured by quantitative q-PCR. 18s mRNA was used as internal control. Graphs show fold increase relative to external calibrator which was a pool of experimental cDNA. In both cell lines, CD133+ cells expressed significantly higher levels of GRP-R or V_{1A}-R compared to CD133- and parent populations. Results represent the mean ± SEM of five independent experiments. (B1) Protein levels of GRP-R in H345 cells or (B2) V_{1A}-R in H69 cells was evaluated by western blotting. Lysates of G6A cells (GRP-R expressing CHO cells), and V3B cells (V_{1A}-R expressing CHO cells) were used as positive control. β-actin was used as loading control. Results represent five independent experiments. (**, P<0.005, and ***, P=0.0005).

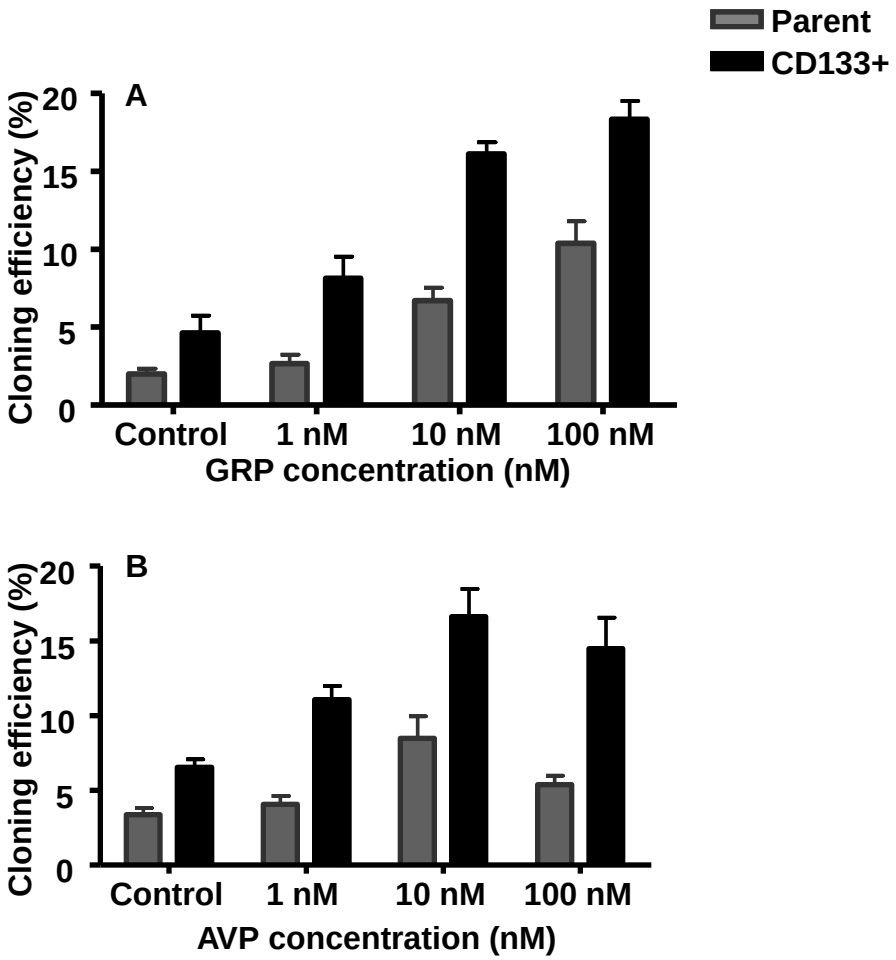

Figure 44: Exogenous neuropeptides enhance the colony formation of CD133+ cells

The effect of exogenously added neuropeptide on the clonogenicity of CD133+ and parent cells was evaluated by seeding cells in semi-solid SITA medium in the presence/absence of GRP or AVP. The number of colonies was evaluated after 21 days using a light microscope. (A) Addition of GRP enhanced clonogenicity in a dose-dependent manner in both CD133+ and parent H345 cells. However, the affect of this neuorpeptide on the clonogenicity of CD133+ cells was significantly enhanced. (B) AVP enhanced the colony formation of both CD133+ and parent H69 cells, however, its affect on the clonogenicity of CD133+ H69 cells was significantly higher. Results represent the mean ± SEM of three independent experiments.

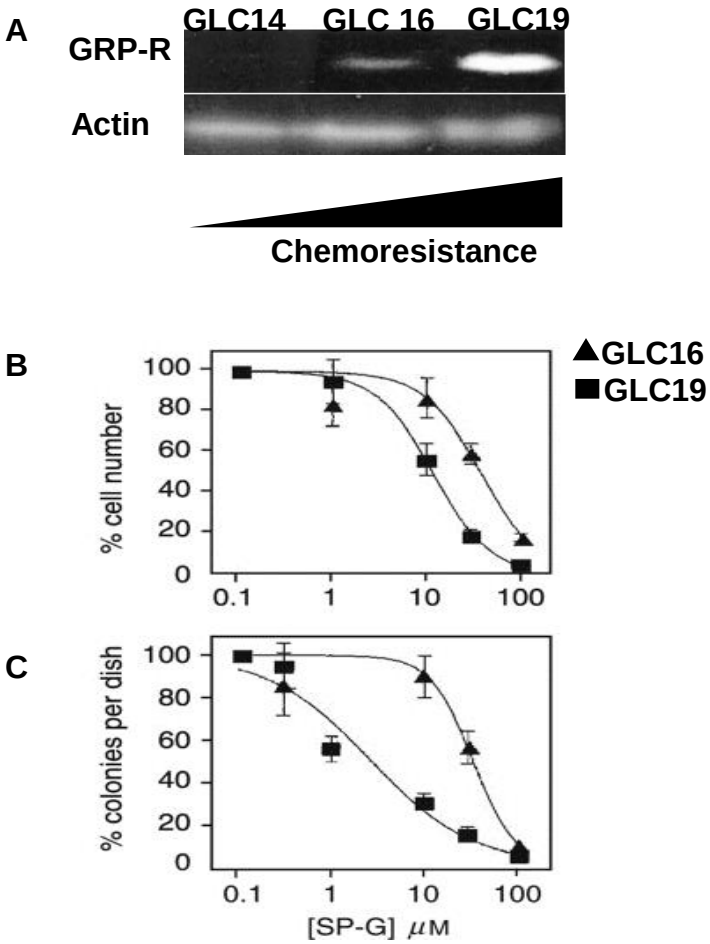

Figure 45: SP-G is more effective in chemoresistant cells
Figure taken from [65]
(A) mRNA encoding GRP-R in three human SCLC cell lines, GCL14, 16 and 19 was evaluated by semi-quantitative RT-PCR. β-actin mRNA levels was used as internal control. Increased mRNA levels of GRP-R was in line with progression of resistant phenotype in the SCLC cell lines. (B) The inhibitory effect of SP-G on the cell growth of GLC16 and GLC19 was evaluated by culturing cells in SITA medium in the presence or absence of SP-G. SP-G was a more effective inhibitor of cell growth in GLC19 cells than GLC16 cells. (C) The inhibitory effect of SP-G on colony forming ability of GLC16 and GLC19 cells was evaluated by plating cells in SITA medium containing 0.3% agarose in the presence or absence of SP-G layered on a base of 0.5% agarose in culture medium. After 21 days, number of colonies formed were counted using light microscopy. SP-G was more potent inhibitor of colony formation in GLC19 cells than GLC16 cells. Each point represents the mean ± SEM of five independent experiments.

Table 9: IC_{50} values in µM of H345 and H69 cells treated with substance-P analogues

Substance-P analogues	H69	H345
SP-G Arg-DTrp-MePhe-DTrp-Leu-Met-NH2	15.53 ± 1.99	11.87 ± 1.04
Peptide 1 DArg-Pro-Lys-Pro-DTrp-Gln-DTrp-Phe-DTrp-DLeu-Leu	4.96 ± 0.64	3.06 ± 0.411
Peptide 2 DArg-Pro-Lys-Pro-DTrp-Gln-DTrp-Phe-DTrp-Leu-GABA	>100	>100
Peptide-3 DArg-Pro-Lys-Pro-DTrp-Gln-DTrp-Phe-DTrp-Leu-Gly	>100	>100
Peptide 4 DArg-Pro-Lys-Pro-DTrp-Gln-DTrp-Phe-DTrp-Leu-1,2 Ethylenediamine	>100	>100
Peptide 5 Arg-DTrp-NMePhe-DTrp-DLeu-Met	46.63 ± 2.63	44.34 ± 3.29
Peptide 6 Arg-DTrp-NMePhe-DTrp-Leu-GABA	>100	>100
Peptide 7 Arg-DTrp-NMePhe-DTrp-Leu-Gly	>100	>100
Peptide 8 Arg-DTrp-NMePhe-DTrp-Leu-1,2 Ethylenediamine	>100	>100

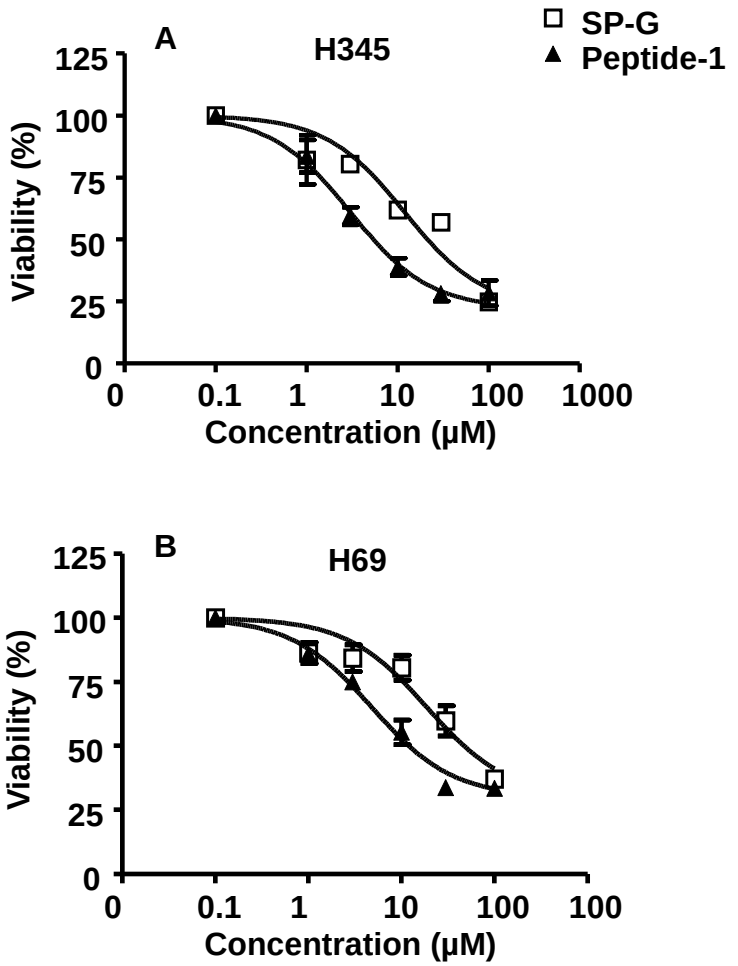

Figure 46: Peptide-1 is a more potent inhibitor of cell viability than SPG

H345 and H69 cells were cultured in SITA medium in the presence or absence of SP-G or peptide-1 (1-100 μM). After 72 hours MTT was added and cell viability was assessed. Untreated cells were used as control. Data is presented as percentage of control. (A) In H345 cells and (B) in H69 cells, peptide-1 was significantly more potent in inhibiting SCLC cell viability than SP-G Results represent the mean ± SEM of three independent experiments.

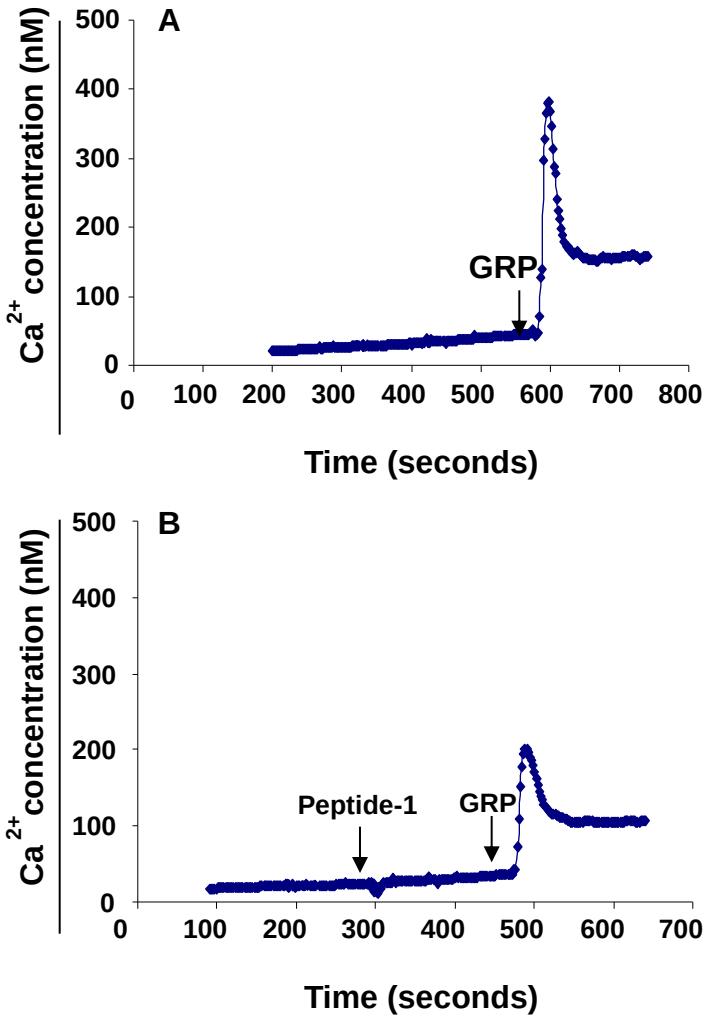

Figure 47: Representative tracing of intracellular calcium mobilisation

(A) Represents tracing of intracellular calcium mobilisation in G6A cells exposed to 10 nM GRP. (B) Represents tracing of calcium mobilisation in G6A cells treated with 0.3 µM peptide-1 and 10 nM GRP.

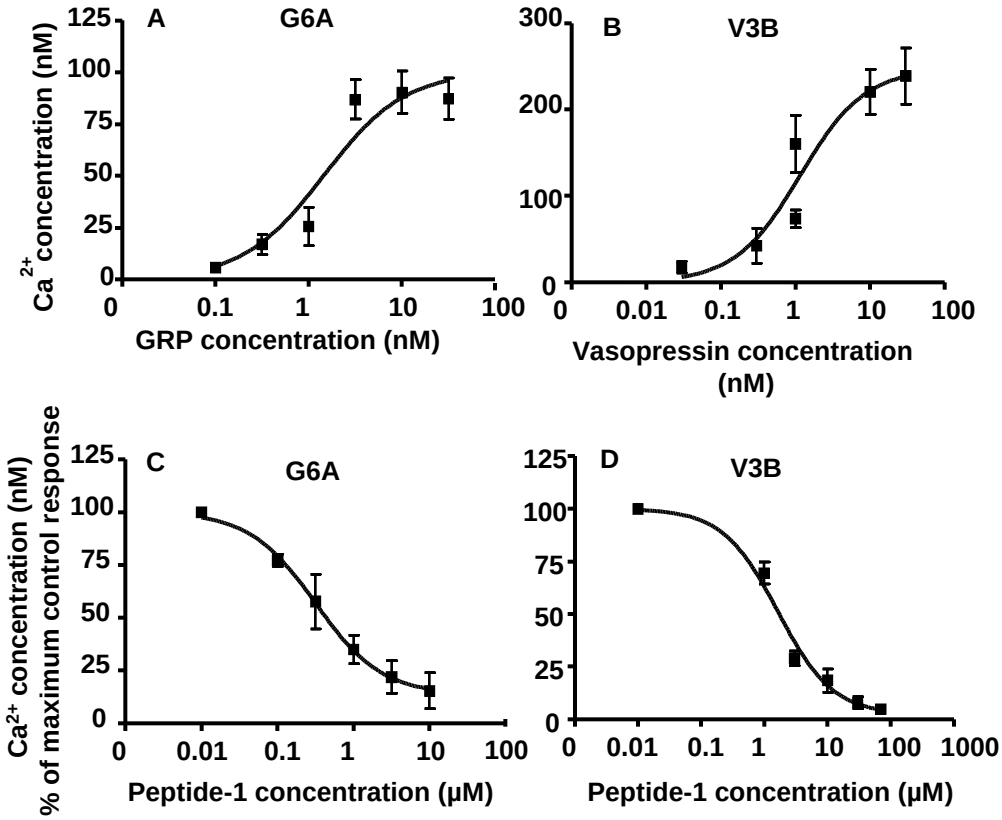

Figure 48: Peptide-1 inhibits $[Ca^{2+}]_i$ mobilisation stimulated by neuropeptides

Quiescent G6A (GRP-R expressing CHO cells) and V3B (V_{1A}-R expressing CHO cells) were incubated with FURA-2AM for 20 min at 37°C and ratiometric fluorescence was monitored at 37°C. Intracellular calcium mobilisation was observed in a dose-dependent manner in (A) G6A exposed to GRP and (B) V3B cells exposed to AVP. The inhibitory affect of peptide-1 on $[Ca^{2+}]_i$ mobilisation induced by neuropeptides, was evaluated initially by pre-treating the samples with various concentrations of peptide-1 (1-100 µM) for 2 minutes at 37°C before adding 10 nM GRP for G6A cells or AVP for V3B cells. Peptide-1 inhibited $[Ca^{2+}]_i$ stimulated by GRP in G6A (C) and by AVP in V3B cells (D). Results represent the mean ±SEM of five experiments.

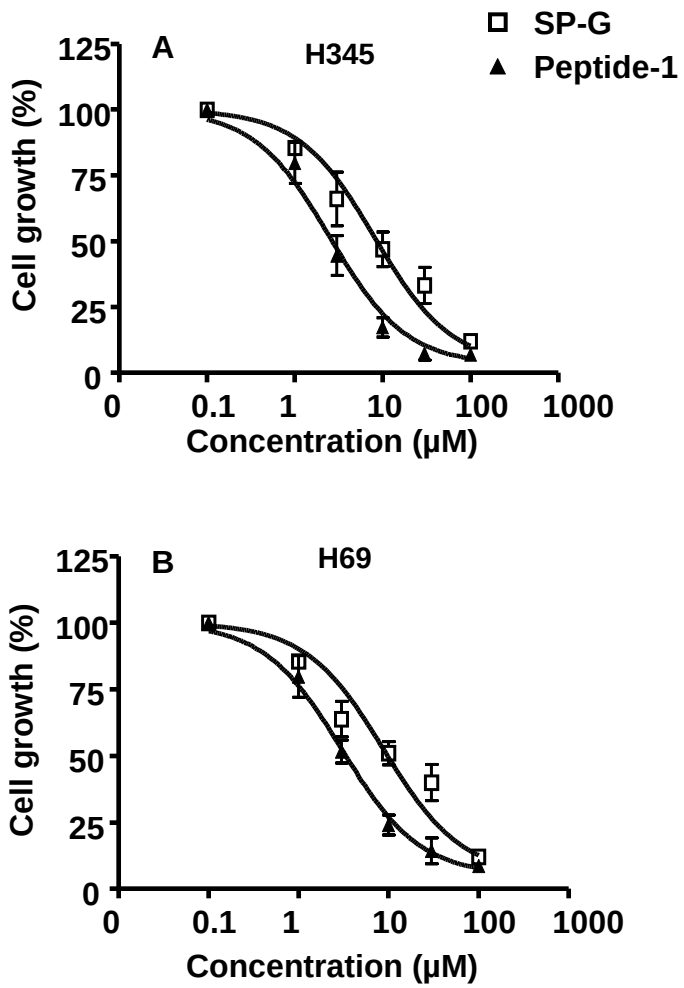

Figure 49: Peptide-1 is a more potent inhibitor of cellular growth than SP-G

H345 and H69 cell proliferation was evaluated in SITA medium in the presence of 1-100 μM concentration of SP-G or peptide-1. Cell number was evaluated by counting cells using the NucleoCounter for 24 days. Untreated cells were used as control and data is presented as percentage of control on day 24. (A) In H345 cells as well as (B) in H69 cells, peptide-1 was more potent inhibitor of cellular proliferation than SP-G. Each point represents the mean ± SEM of three independent experiments performed in duplicates.

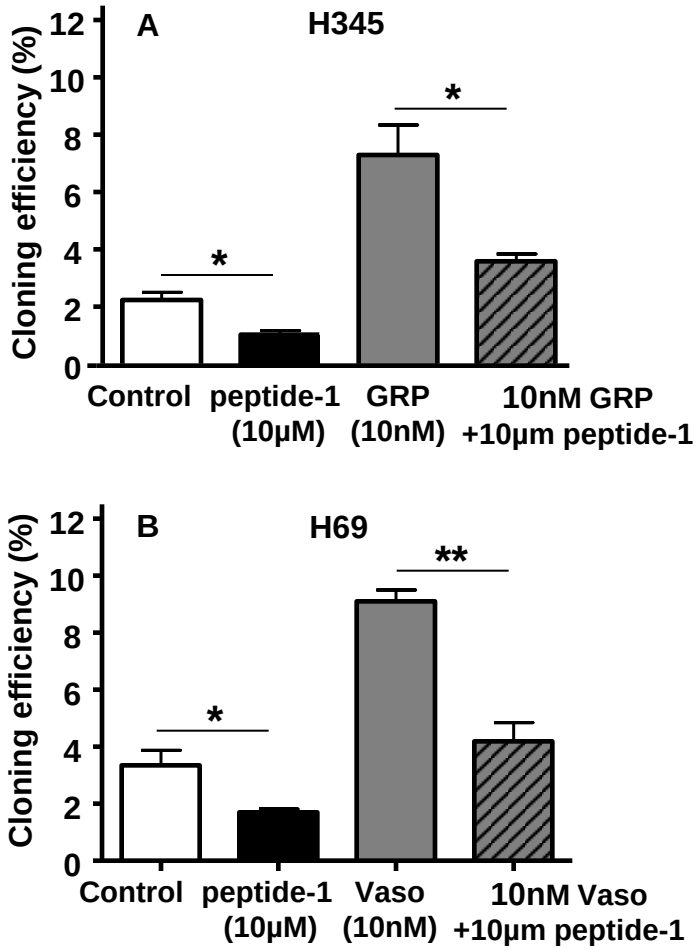

Figure 50: Peptide-1 inhibits basal and neuropeptide stimulated colony formation

Cells were cultured in SITA medium containing 0.3% agarose in the presence or absence of 10 nM GRP or AVP and/or 10 μM peptide-1 or combination of neuropeptide and peptide-1 were cultured over solid SITA medium with 0.5% agarose. After 21 days colonies of >16 cells were counted under microscope. (A) In H345 cells as well as (B) in H69 cells, peptide-1 inhibited the basal and neuropeptide stimulated clonal growth of SCLC cells in semi-solid medium. The data represent the mean ± SEM of three independent experiments performed in duplicate. (*, $P<0.05$, and **, $P<0.005$)

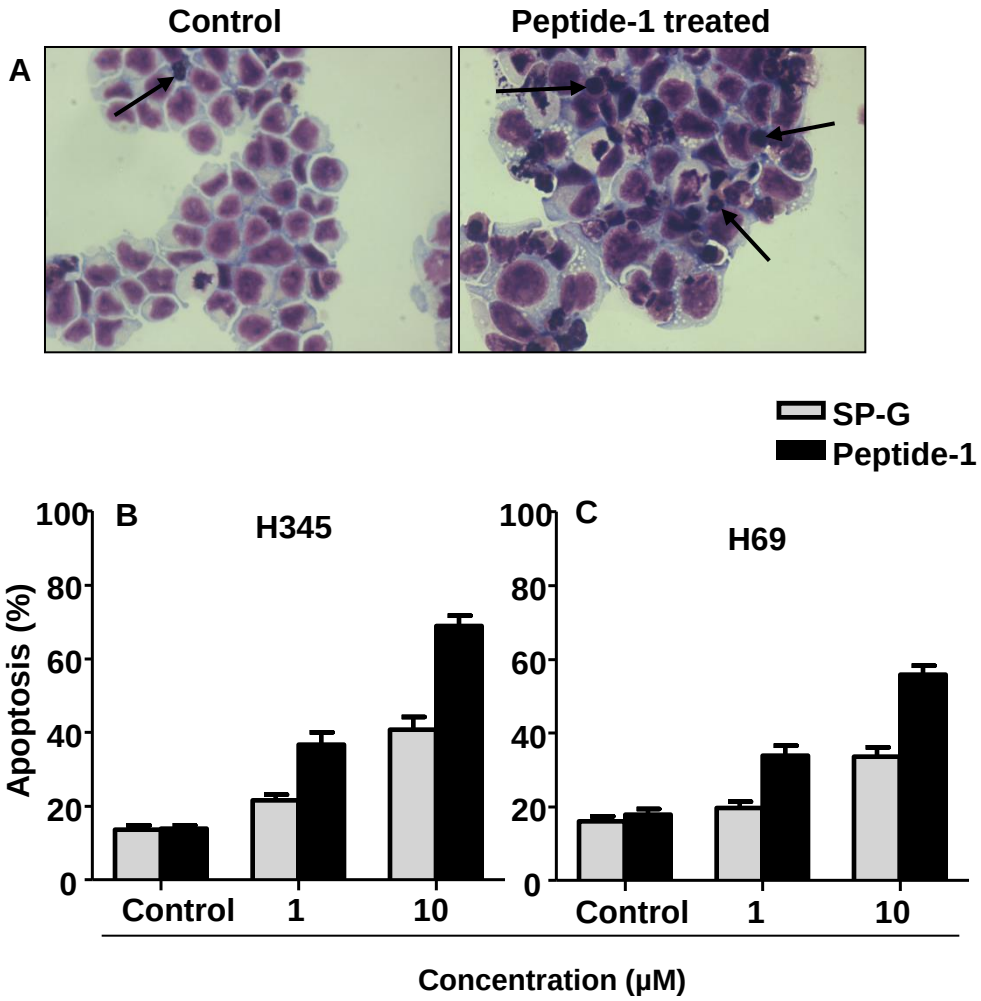

Figure 51: Peptide-1 is a more potent inducer of apoptosis than SP-G
H345 and H69 cells cultured in SITA medium were treated with two different concentrations of SP-G or peptide-1 (1 µM and 10 µM) for 72 hours. After this period, apoptosis was determined by cytocentrifuging cells onto glass cover slips and staining with May-Grunwald-Giemsa. Images were taken with 40× magnification. (A) Representative image of control and 10µM peptide-1 treated H345 cells. Apoptotic cells appeared as shrunken cells with dense nuclei and are presented by (→). (B) In H345 cells and (C) in H69 cells, peptide-1 induced apoptosis and its effect was significantly greater than SP-G. Untreated cells were used as control. The data represent the mean ± SEM of four independent experiments performed in duplicate.

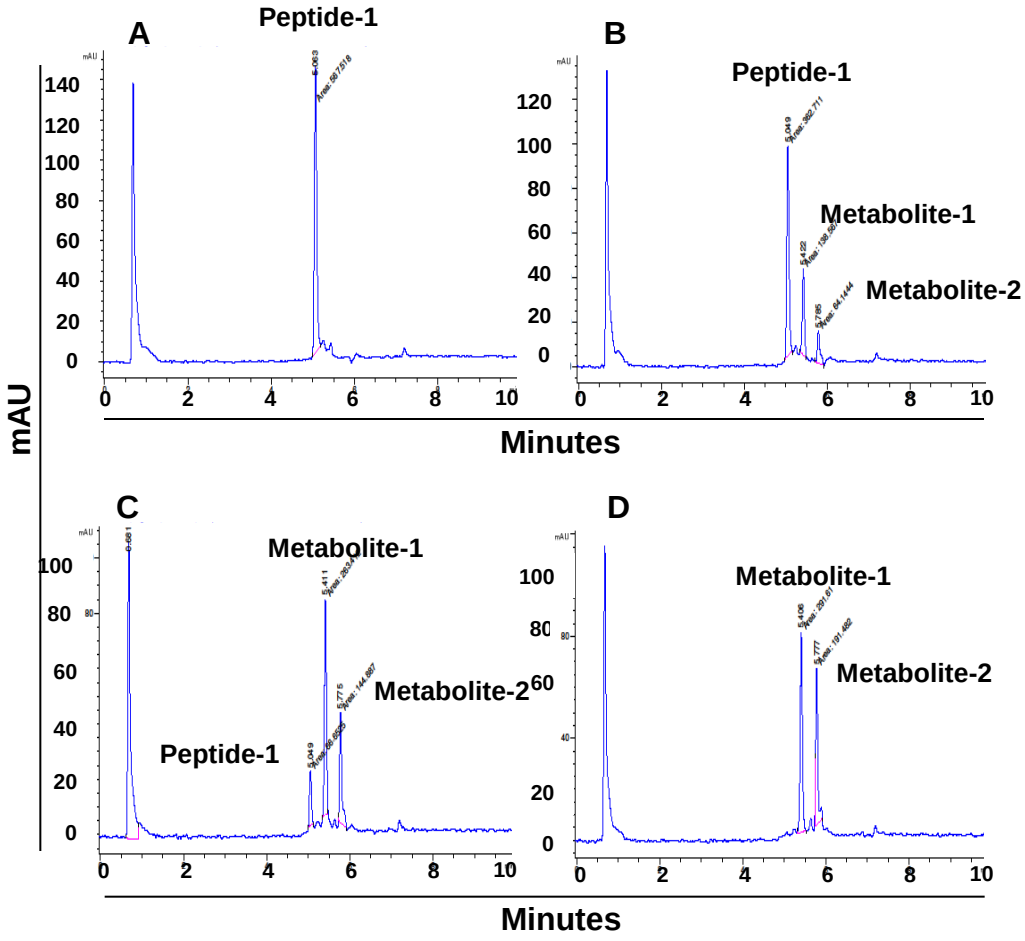

Figure 52: Representative image of a HPLC tracing

(A) Represents the presence of peptide-1 at time point 0 (the time which immediately after addition of peptide-1 to S9 liver preparation an aliquot of sample was removed for HPLC analysis). (B), (C), and (D) traces demonstrate the degradation of peptide-1 and production of metabolites 1 and 2 after 20, 80 and 130 minutes exposure to S9 liver preparation.

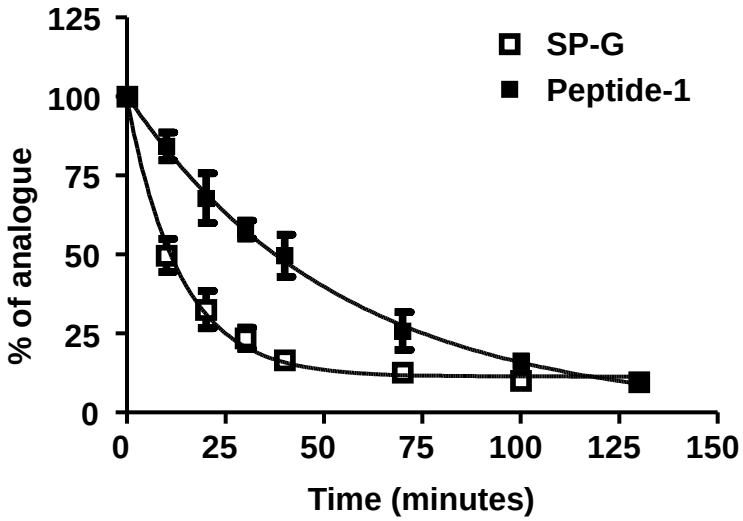

Figure 53: Peptide-1 is more stable than SP-G
The stability of SP-G and peptide-1 (0.1 mg/ml) was evaluated in mouse S9 liver preparation. Samples were incubated at 37°C for 130 minutes and aliquots were removed at appropriate time points for HPLC analysis. The figure indicates the percentage of non-metabolised SP-G and peptide-1 present in the sample with time. Peptide-1 was approximately four times more stable than SP-G. Each point represents the mean ± SEM of three independent experiments.

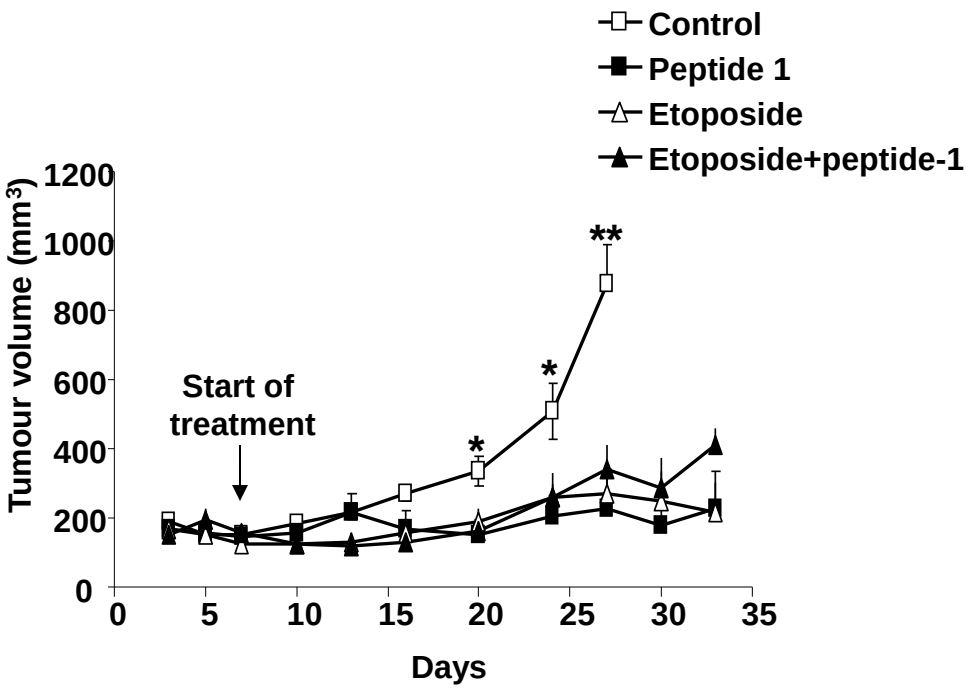

Figure 54: Peptide-1 significantly inhibits H345 growth *in vivo*
15×10^6 H345 cells suspended in growth factor reduced Matrigel (1:1 vol of cells : Matrigel mixed at 4°C, total volume of 100 µl) were implanted subcutaneously in the right flank of *nude*/*nude* mice. H345 xenografts were palpable 3 days post injection. Treatment started on day 7 and animals were treated once a day for 5 consecutive days. Peptide-1 was dissolved in sterile distilled H_2O and was administered by subcutaneous injection at 25 mg/kg. Etoposide was dissolved in sterile distilled H_2O and was administered by subcutaneous injection at 15 mg/kg. Controls received the same dose schedule of vehicle (H_2O). As shown in figure, peptide-1 administered alone profoundly reduced growth of SCLC xenograft and was as efficacious as etoposide alone. Each point represents the mean ± SEM of six animals. (*, $P<0.05$, and **, $P<0.005$).

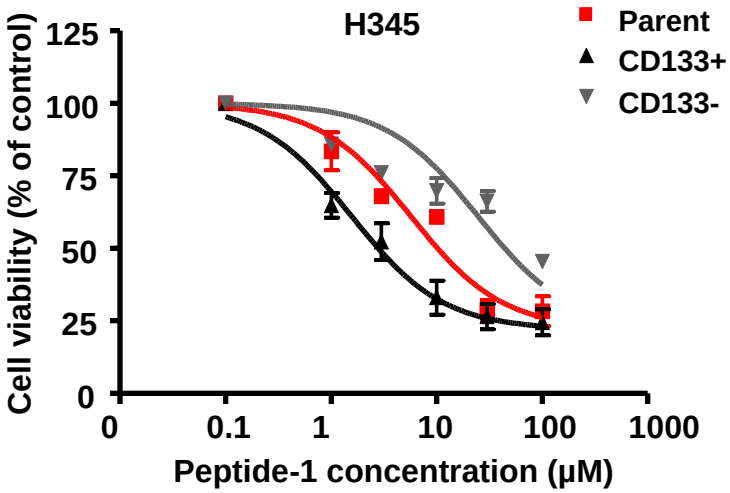

Figure 55: Peptide-1 is more potent in CD133+ cells than in CD133- cells

Sorted H345 cells and unsorted parent cells were treated with different concentrations of peptide-1 (1-100 µM) for 72 hours and cytotoxicity was evaluated by MTT assay. CD133+ H345 cells were more sensitive to peptide-1 than CD133- and parent cells. Each point represents the mean ± SEM of three independent experiments performed in triplicates.

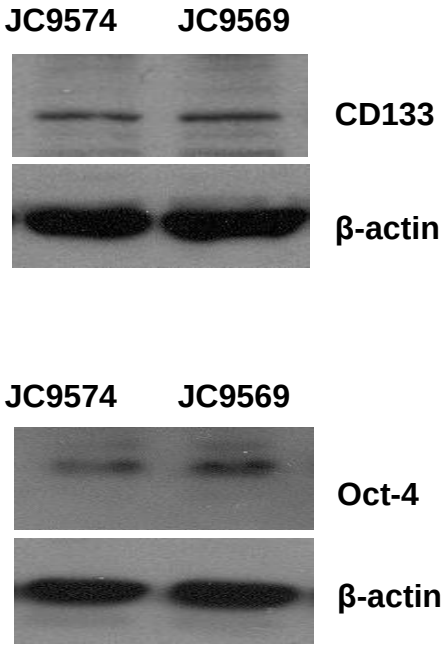

Figure 56: Mouse SCLC cell lines express CD133 and Oct-4
The presence of CD133 and Oct-4 in JC9574 and JC9569 cell lysates were examined by evaluating their protein levels by western blotting. A band of ~120 kDa and a band of ~48 kDa in both cell lines were indicative of presence of CD133 and Oct-4 proteins in these cell lines. β-actin was used as loading control. Image is representative of three independent experiments.

CHAPTER 1:
Introduction

Lung cancer is a lethal malignancy with high tendency for relapse. It is histologically classified into two main groups of small cell lung cancer (SCLC) and non small cell lung cancer (NSCLC) [1]. The classification has important implication for clinical management and prognosis. NSCLC accounts for about 80% of lung cancers in the UK which have comparatively better prognosis than SCLC. NSCLC include adenocarcinoma (30%-40%), squamous cell carcinoma (25%-35%) and large cell carcinoma (10%) [2, 3].

Long term exposure to tobacco smoke is the principle cause of lung cancer, in particular SCLC. SCLC accounts for 15-20% of all lung cancers and over two thirds of patients on presentation have metastasis [4, 5]. Resection is rarely an effective treatment strategy for SCLC and although initially chemo-radio-sensitive, recurrence and resistance is almost inevitable [6, 7]. Thus, overall prognosis is unsatisfactory with a 5-year survival rate less than 5%. These figures have unfortunately not improved significantly in the past two decades despite advances in diagnosis and treatment [8]. Therefore, urgent research focus on SCLC is required for development of novel and more effective therapies.

1.1 Epidemiology

Lung cancer is the most frequently encountered malignancy in the world, accounting for 1 in every 8 new cancer cases [9]. In the United Kingdome (UK), pulmonary cancer is the second most common malignancy in men accounting for 14% of all new cancer cases in male and the third most common cancer in women accounting for more than 11% of all new cancer cases in females [10]. A decline in SCLC incidence (11%-13%) world wide including UK over the past few decades has been addressed [2, 3]. This may be due to increase abstinence from smoking, change to low tar filter cigarettes, and possibly by the revision of the pathological classification

where by a few SCLCs are now classified as NSCLCs with neuroendocrine features [11, 12].

Lung cancer is rarely seen before the age of 40 and most SCLC cases diagnosed are above 65 years old. The disease is more common in men than women. However, the male/female ratio has declined in the past fifty years from 6:1 to approximately 7:5 due to increase in smoking habits in women [3].

Smoking is the main risk factor for lung cancer with SCLC having the clearest association with tobacco consumption. More than 95% of SCLC cases are attributable to tobacco smoking [13]. Therefore, the future trends in lung cancer, and particularly SCLC, will be shaped by the increase in female smokers and the higher prevalence of tobacco use in lower socio-economic groups [14]. Other risk factors include atmospheric pollution, industrial exposure to carcinogens and chronic lung disease [15]. Unfortunately, it is clear that SCLC will continue to be a significant health burden for the foreseeable future.

1.2 Genetic alteration associated with SCLC

SCLC early lesions are rare making access to sequence of genetic alteration that leads to disease development unclear. Commonly encountered chromosomal abnormality is, deletion of the short arm of chromosome 3 (3p) at distinct areas (3p(14-25)) [16, 17]. Deletion of this region is observed in 90% of SCLC cases and is mostly loci for tumour suppressor genes including, *RASSF1A*, *FUS1*, and Fragile histidine triad (*FHIT*). Other common chromosomal aberrations include loss of 5q, 13q, and 17p [18]. The latter two are loci with tumour suppressor genes *Rb* and *p53* and deletion or inactivating mutations are observed in 90% of SCLCs. Gain of 1p, 2p, 3q, 5p, 8q and 19p which encode oncogenes including, Myc and K-ras are also commonly detected [19, 20]. Despite numerous studies, the contribution of each genetic alteration promoting SCLC is unknown.

1.3 Clinical features, diagnosis and staging of SCLC

1.3.1 Clinical features

SCLC is the most aggressive form of lung cancer [21]. In addition to cachexia, symptoms can be due to local growth of tumour (persistent cough, obstructive pneumonia, hemoptysis), and involvement of adjacent structures (superior vena cava obstruction syndrome, hoarseness, dysphagia). Extrathoracic metastasis to bone (19%-38%), liver (17%-34%), adrenal glands (10%-17%) and brain (up to 14%) may present with features of the involved organ [22]. Mediastinal and metastatic complications are frequently encountered.

Several paraneoplastic syndromes are associated with SCLC. These are broadly divided into endocrine and neurological syndromes [23]. Endocrine syndromes associated with SCLC include, hyponatraemia seen in syndrome of inappropriate antidiuretic hormone (SIADH) [24, 25] due to ectopic release of arginine vasopressin (AVP) and Cushing's syndrome (hypercortisolism) which is associated with release of adrenocorticotropic hormone or corticotropin releasing factor [25, 26]. The best described neurological syndromes associated with SCLC is Lambert-Eaton myasthenic syndrome (LEMs) observed in 50-60% of SCLC patients and features proximal muscle weakness and autonomic dysfunction with significant serum levels of autoantibodies against P/Q-type voltage-gated calcium channels [26].

1.3.2 Diagnosis

Radiological findings usually demonstrate SCLC as tumours with hilar (84%) or mediastinal (92%) lymphadenopathy [22]. Computer tomography (CT) of the chest and upper abdomen determines intra-thoracic and distal organ involvement. Magnetic resonance imaging (MRI) of the brain and radionuclide bone scan additionally searches for possible metastasis. MRI is usually utilised to resolve ambiguous CT findings [27, 28].

Diagnosis of SCLC is primarily based on histopathology of samples obtained by bronchoscopy or percutaneous needle aspiration/core biopsies. Typically, SCLC tumour cells are small, round or spindle shaped with scant cytoplasm and minimal or absent nucleoli. High mitotic count and large areas of necrosis are frequently observed [21]. In addition to tumour cell morphology, immunohistochemical stains are often helpful in the diagnosis of SCLC using markers including chromogranin, CD56/Neural cell adhesion molecule (NCAM) and synaptophysin [21, 22].

1.3.3 Staging

SCLC is classified as either limited disease (LD) or extensive disease (ED) as recommended by the Veterans' Administration Lung Study Group (VALSG) [25]. LD stage is defined for tumours confined to one hemi-thorax (including ipsilateral supraclavicular lymph nodes) that can be encompassed within a tolerable radiation field. ED spreads beyond these boundaries including bilateral pulmonary lesion, malignant pericardial and pleural effusion and extrathoracic involvement where radiation required would be too large with toxicity [25, 29]. Tumour, node, metastases (TNM) staging, a fundamental system for classification of NSCLC, requires accurate surgical lymph node and secondary sampling, making most patients with SCLC inappropriate candidates [30]. Accurate staging is fundamental to select an appropriate treatment for individual patients.

1.4 Treatment of SCLC

SCLC usually presents as inoperable centrally located lung lesions with loco-regional and distant metastasis. Thus, chemo-radiation forms the cornerstone for its management [31, 32].

1.4.1 Chemotherapy

SCLCs show initial chemo-sensitivity to cytotoxic agents. In the 1970's, monotherapy with cyclophosphamide [33], other alkylating agents, and platinum based treatments were replaced by combination of multiple therapies [30].

Combination regimes achieved a response rate of 57% as against 12% with monotherapy. Likewise, the survival curve for combination regimes was significantly higher (P=0.012) [34].

Over the last 30 years, the standard first line therapy for SCLC has comprised of etoposide with a platinum-based drug administered in 4-6 cycles. Etoposide plus cisplatin (EP) is active in both LD and ED SCLC with 85% objective response rates (ORR) and 50%-60% complete response (CR) in LD SCLC, and 50%-60% ORR and 7%-10% CR in ED SCLC [35-37]. Despite initial sensitivity to first-line chemotherapy, 80% of LD SCLC patients and almost all ED SCLC patients relapse making them candidates for second-line treatment [38].

1.4.2 Second-line therapy

Efficiency of second-line chemotherapy in SCLC patients is lower with objective response rate of 18-24% however it can significantly provide prolongation of survival [39]. Response to second-line therapy is influenced by physical status (PS), disease stage and relapsed or refractory disease. Disease relapse after 3 months of completion of first-line therapy is considered chemosensitive disease. Relapse in less than 3 months or limited or no response to first-line therapy is described as chemoresistant disease [40]. 25% response is observed in chemosensitive as against 10% in chemoresistant group. For relapse after 6 months, a repeat of the initial regime instead of monotherapy is applied [41]. Agents used as second-line therapy for SCLC include, topotecan and irinotecan which are camptothecin derivatives and topoisomerase I inhibitors [39, 42-44], paclitaxel, a cell cycle inhibitor by stabilising microtubules [45, 46], and amrubicin, a topoisomerase II inhibitor [47, 48].

Although some promising results have been obtained for SCLC treatment, however, a gain of only a few months in survival have been achieved and SCLC remains an incurable disease. Thus, the need for novel, more effective therapeutics with minimal toxicity is urgently required.

1.4.3 Radiotherapy

SCLC cells are initially highly radio-sensitive. Since the 1990's, combination of chemotherapy and radiotherapy has been considered as standard therapy for SCLC confined to one hemithorax [49, 50]. Chemoradiation schedules include concurrent, sequential, or alternating therapy [51]. Concurrent approach shortened duration of treatment and increased overall survival rate with improved 2-, 3-, and 5-year survival rates by 54.4%, 29.8% and 23.7%, respectively [52]. Optimal dose of thoracic irradiation (TR) TR is debatable with some favouring dose intensification. In a randomised phase II trial, twice daily TR at a dose of 45 Gray (Gy) concurrent with EP improved 5-year overall survival rates and is currently considered as standard therapy in LD SCLC [53].

TR is not yet been considered as a standard therapy in ED SCLC. Although, in a randomised study by Jeremic et al. [54], TR as consolidation treatment for ED SCLC showed promising results with a 5 year survival rate of 9%, the data obtained was from a single study and requires confirmation [54].

1.4.4 Prophylactic cranial irradiation

Brain metastasis (BM) is common in SCLC patients. Half of LD SCLC in complete remission after standard chemotherapy regimes will develop brain metastasis [55] making prophylactic cranial irradiation (PCI) mandatory. A meta-analysis of 987 SCLC patients in complete remission showed at three years, a 25.3% decreased incidence of BM and ~5% improvement in survival with the addition of PCI [56]. Currently, the standard doses used is 24-30 Gy, administered over 8-10 fractions.

PCI offers convincing results in ED SCLC. PCI in ED SCLC reduced BM at 1 year by 26% and increased 1 year survival rate by 27% in PCI group versus 13% in control group [57]. PCI is now considered as a standard therapy in ED patients with complete or partial response to chemotherapy.

Despite years of research in the field of chemo-radiation, dramatic initial response was often followed by recurrence and resistance. Thus, a shift in therapeutic approach is needed. With better understanding of SCLC, several molecular targets have been identified in various preclinical studies.

1.4.5 Novel targeted therapies in SCLC

Targeted therapies have been rationally designed on current analysis of SCLC biology. Therapies used to target apoptosis resistance, unrestrained growth, and drug efflux in SCLC will be described in the following section.

1.4.5.1 Inhibitors of cell survival pathways

Circumventing apoptosis underpins cancer cell survival and promotes chemo- and radio-resistance. Bcl-2, a central regulator of apoptosis, is over-expressed in 80% of SCLC and serves as a promising target for SCLC therapy [58]. Small molecule inhibitors of Bcl-2 family proteins (ABT-737 and ABT-263) have been developed for SCLC treatment [59, 60]. ABT-263 has recently entered clinical trials, posing as a promising agent for the treatment of SCLC.

PI3K/AKT/mTOR pathways are critical for SCLC cell survival [61]. Both temsirolimus and everolimus have been used as mTOR inhibitors in ED SCLC patients. However, in phase II clinical trials, these agents did not show improved median survival [62, 63].

1.4.5.2 Growth and proliferation pathway inhibitors

Multiple neuropeptides via autocrine and paracrine loops fuel unrestrained SCLC cell proliferation. Synthetic peptide analogues such as SP-G [Arg^{6},D-$Trp^{7,9}$,$N^{me}Phe^{8}$]-substance-P (6-11) function as broad spectrum antagonist, inhibiting SCLC growth *in vitro* and in nude mice xenograft models [64]. Interestingly, SP-G has proven to be more effective in chemoresistant cells suggesting its implication in recurrent and resistant SCLCs [65]. SP-G has completed a phase I clinical trial with

minimal toxicity at therapeutic plasma concentrations [66]. Neuropeptide antagonists and their implication in SCLC treatment will be detailed in section 1.6.6.

SCLC cells express a range of RTKs which also regulate SCLC growth and proliferation. High expression of c-Kit and its ligand, SCF, has been associated with SCLC pathogenesis [67]. Imatinib is a broad spectrum RTK inhibitor [67]. The efficiency of imatinib as a monotherapy or in combination with chemotherapy, tested in two phase II clinical trials for relapsed SCLC patients, demonstrated poor efficiency [68, 69].

1.4.5.3 Inhibition of efflux pump

Active efflux pumps that expel cytotoxic agents are logical targets for chemo-sensitisation. However, biricodar that blocks the action of efflux pump P-gp and MDRP when combined with chemotherapy produced poor response along with significant toxicity which resulted in early termination of the trail [70].

Despite advances in unveiling pathogenesis of SCLC, so far the methods to circumvent resistance have not been successful in clinical practice. These failures could possibly result from treating tumour mass but failing to eliminate a sub-population within the tumour that may trigger relapse and resistance. In this regard, cancer stem cells (CSCs) may be particularly relevant in SCLC.

1.5 Cancer stem cells

Cancer cells exhibit broad spectrum of heterogeneity in their cellular morphology and functional properties. Evidences indicate that cells within tumour lesion may differ in their proliferation index, therapeutic response and tumorigenicity [71]. Southam was the first to demonstrate tumour cell heterogeneity [72]. Tumour cell heterogeneity may be due to the presence of cancer stem cells (CSCs) within the neoplasm, a sub-population of cells with similar characteristics to normal stem cells (reviewed in [73]). Stem cells are specialised cells found in multicellular organs.

They have the potential to self-renew as well as to differentiate, thus replenishing adult tissue. Self-renewal is defined as the ability to undergo unlimited cycles of cell division while still maintaining its undifferentiated state. The classical stem cell hierarchy model is illustrated in Figure 1. Transformed stem cells are the suggested origin of CSCs.

Figure 1

Evidence of CSC was initially observed in myeloid leukaemia where in only a small subset of cells (0.01%-1% of the total population) initiated the disease when transplanted into severe combined immune deficient (SCID) mice [74]. Numerous studies support the existence of CSCs in various malignancies including solid tumours [75-78] such as lung cancer [79]. These cells are chemoresistant [80-82] and their presence in clinical specimens is associated with poor survival [83-85]. Based on these observations, it has been proposed that conventional therapies target tumour bulk, sparing the chemoresistant CSCs. The surviving cells, with their stem cell-like phenotype, are speculated to regenerate the tumour leading to disease recurrence. Thus, identification and characterization of CSCs may improve strategies for better clinical outcomes.

1.5.1 Origin of lung cancer stem cells

In lung cancer, it is debatable whether lung CSCs arise from lung stem cells that have acquired oncogenic mutations or from differentiated lung cells that have acquired mutations including re-programming with acquisition of stem cell-like properties. In this section the presence of stem cells in adult lung tissue and the role of stem and more differentiated cells in pulmonary epithelial repair and lung cancer development will be described.

1.5.1.1 Lung stem cells

It has become increasingly accepted that in adult organisms, stem cell populations exist and serve to maintain tissue homeostasis. Presence of stem cells have been well characterised in organs with fast cell turnover including, skin, hematopoietic system, and the small intestine where a classic model of a stem cell hierarchy is observed [86, 87].

In contrast, the cell turnover rate is significantly slower in the lung. However, in stress conditions such as lung injury, increased pulmonary cell proliferation is observed. Along the respiratory system, stem cells as well as differentiated pulmonary epithelial cells are involved in tissue maintenance and repair [88].

Giangreco et al. [89] proposed that in normal lungs, after mild to moderate pulmonary injury, tissue repair is undertaken by resident pulmonary progenitor cell activation. However, with extensive pulmonary injury, respiratory stem cells are mobilised. Thus, the classic stem cell hierarchical model has to be redefined in the lung [86, 90]. Injury models that mimic lung damage inflicted by environmental conditions or infectious disease are most frequently employed to elicit repair programmes by surviving stem/progenitor cells.

1.5.1.2 Lung epithelial injury and stem/progenitor cell repair

Adult lung is a complex organ that features major differences in its cell composition from proximal to distal axis. The proximal lung contains ciliated and Clara-like cells. A few sub-mucosal glands present in this region contain mucous-producing cells. The more distal lung is composed of Clara cells and neuroendocrine cells. The distal pulmonary system is organised into a complex system of alveoli and the epithelium consists of, alveolar type 1 (AT1) and 2 (AT2) cells. The origin of the progenitor cells present in the proximal region of the lung is different from those of the distal lung. The function of different pools of lung progenitor cells is restricted to their regional specificities in both proximal and distal airway during lung development and repair (reviewed in [91]).

Injury models project the properties of stem/progenitor cells in lung repair. The most common injury model is treatment of mice with naphthalene to ablate Clara cells [92, 93]. After naphthalene injury, Clara cell repopulation depends on the region of the lung. In the proximal airway, basal cells function as stem cells replenishing the Clara cells [94]. This was evident by genetic lineage labelling approach in mouse with inducible Cre-recombinase controlled by a cytokeratin K14 promoter that is selectively active in basal cells. The $K14^{+}$ featuring basal cells were able to self-renew and reconstitute both Clara and ciliated cells upon injury, displaying stem cell characteristics [94].

In the distal airway system, after naphthalene injury, Clara cells are restored by a rare population of naphthalene resistant Clara cells known as variant Clara (vClara) cells [95] [96]. Clusters of vClara cells are localised in specialised niches including neuroendocrine bodies (NEB) in the bronchi/bronchioles or at the broncho-alveolar duct junctions (BADJs) [95, 97]. NEB associated vClara cell express Clara cell marker CC10 also known as CCSP, CCA, or secretoglobin Scgb1a1 and appear to function as stem cells after pulmonary injury.

Kim et al, 2005 [98] demonstrated that vClara cells that reside at the BADJ exhibit stem cell phenotype. These cells, termed bronchoalveolar stem cells (BASCs), co-express both the alveolar type II cell marker, surfactant protein-C (SPC), and the Clara cell marker, CC10 and are positive for CD34, a somatic stem cell marker. $Sca1^{+}/CD34^{+}/CD45^{-}/Pecam^{-}$ isolated BASCs expanded in culture and gave rise to cells that expressed markers for Clara and alveolar cells *in vitro*. Although BASCs self-renewal and differentiation potential *in vivo* has not be proven, recent cell-tracing studies have suggested that these cells are involved in the maintenance and repair of the proximal pulmonary system, but not the alveolar epithelium [89, 99]. Therefore, both lung progenitors and stem cells repair pulmonary tissue injury. However, it needs to be noted that both vClara cells and BASCs differ from classical stem cells as they express proteins that are present in fully differentiated lung cells [96].

1.5.1.3 Lung cancer stem cells in mouse

BASC as the origin of adenocarcinoma has been addressed in several mouse models. Kras mutation is commonly observed in NSCLC [100]. Thus, transgenic mice expressing activation variants of Kras, (for example Kras-G12D), serve as an ideal tool for lung CSC study. The importance of BASCs as the cell of origin in Kras-G12D induced adenocarcinoma has been pointed out in several studies that showed: (1) In these transgenic mice, an outgrowth of BASCs was observed which was associated with atypical adenomous hyperplasia, a precursor lung adenocarcinoma lesion [98, 101], (2) The transgenic BASCs were highly proliferative and multipotent

in colony assay, (3) Exposure of these transgenic mice to naphthalene enhanced tumour growth (~11 fold) compared to control animals [98, 101]. In line with these observations, Ventura et al, 2007 [102], demonstrated that inducible p38 knockout mice were more prone to Kras-G12D induced adenocarcinoma. P38 positively regulates differentiation and inhibits the proliferation of BASCs. Therefore, based on the above data it can be suggested that transformed BASCs are the CSCs leading to adenocarcinoma development. However, to support this concept the ability of transformed BASCs to develop tumours during serial transplantation in mice is necessary.

Unipotent progenitors PNEC, subject to oncogenic mutations are suggested forerunners of SCLC. Both PNECs and SCLC are co-located at the midlevel bronchioles and express similar neuroendocrine markers including calcitonin-gene related peptide (CGRP) and NCAM [103, 104]. Mutations in the tumour suppressor genes, retinoblastoma (*Rb*) and *p53* are common genetic abnormality associated with SCLC [105]. Mouse models with Rb depletion and p53 knockout, formed SCLC-like hyperplastic foci that corresponded to NEB microenvironment. More recently, using an inducible lung-specific Rb knockout strategy, PNEC hyperplasia was exclusively observed despite Rb deficiency in other cell types along the lung [106]. Conditional inactivation of both Rb and p53 in mouse lung epithelial cells resulted in pulmonary neoplasm with striking similarities to human SCLC [103]. Importantly, these tumours gave rise to extrapulmonary metastasis closely resembling its human counterpart. Despite wide spread conditional mutation along the respiratory tree, only PNECs responded. These observations imply the crucial role of transformed PNECs cells in SCLC tumorigenesis.

Evidence that common signalling pathways are activated in NEB associated PNECs and SCLC cells further emphasises PNECs as SCLC cells of origin. Hedgehog (Hh) signalling, an embryonic pathway essential for lung development, is elevated in NEB during lung repair, while elevated expression of Patched (Ptc) Hh receptor in PNECs is observed during pulmonary repair [107]. Similarly, Hh activation with increased sonic hedghog (Shh) receptor and ligand is observed in SCLC [107]. Inhibition of

Shh ligand activity in SCLC cell lines using monoclonal antibodies was associated with inhibition of SCLC growth *in vitro* [108]. Likewise, Notch signalling involved in NEB growth and SCLC progression is indicative of common signalling pathways [109]. Concluding, co-location of PNEC and SCLC along the airway system, similar neuroendocrine phenotype and signalling pathways, makes transformed PNECs putative SCLC CSC candidates.

1.5.2 Cancer stem cell markers

The identification of reliable markers for the study and isolation of cancer stem cells has been the main challenge facing researchers in this area, but a number of candidates have been hypothesised such as CD133, expression of drug efflux pumps and, enhanced aldehyde dehydrogenase (ALDH) enzyme activity. Table 1 summarises key markers employed for isolation of prospective CSCs in solid tumours. It is apparent that common markers, in particular CD133, have been used to detect CSCs in diverse solid tumours. To be noted, none of these markers are exclusively expressed by the CSCs, indicating the need for more specific or the use of combination of markers. In this section I will be focusing on CD133, ALDH and Oct-4 as CSC markers in various malignancies including lung carcinoma.

table 1

1.5.2.1 CD133

CD133 (prominin-1 in mice), a cholesterol-binding protein, in humans was initially detected in hematopoietic stem and progenitor cells [110]. The protein is selectively associated with plasma membrane protrusions and due to this intrinsic preference, it inherits the name 'prominin' (from the Latin word *prominere*, to be prominent) [111, 112]. Glycosylated form of CD133 epitopes select for stem and CSCs. Most commonly used antibodies for detection of glycosylated epitopes of CD133 antigen include, monoclonal CD133-1-APC (clone AC131) antibody which recognises eptiope-1 of the CD133 antigen, and monoclonal CD133-2-PE (clone AC141) antibody that detects epitope-2 of the same antigen [110, 113, 114]. Both antibodies are commercially available from Miltenyi Biotec, Germany. Although CD133-2 has been used for isolation of hematopoietic stem cells (HSC), due to cross reactivity of the antibody with cytokeratin-18 [115], it is not commonly employed for CSC selection.

CD133 expression is detected in several stem cells [116, 117] and CSCs [76-79]. The prognostic value of CD133 expression has been documented in various malignancies [85, 118] [119-121], making this marker a valuable tool to develop future therapies towards identifying CSCs. The development of such therapies would require clearer understanding of the characteristics and molecular mechanisms that regulate the behaviour of CD133 expressing cells.

1.5.2.1.1 CD133 structure

The *Prominin-1* gene is located on chromosome 4 (locus p15.33) in humans and on chromosome 5 (locus 5B3) in mice. The genomic organisation in both species is similar consisting of 37 (human) and 34 (mice) exons spanning approximately 160 kb. In human it is under control of five alternative promoters [122]. Mouse and human prominin-1 share approximately 60% homology. To date several spliced variants affecting the open reading frame have been identified in mice and in human several of which exhibit distinct C-terminal domains explaining the diverse cytoplasmic protein interactions [122].

Human Prominin-1 (CD133) consists of 865 amino acids (aa) with a predicted molecular weight of 95 kDa and apparent molecular mass of 120 kDa due to glycosylation [114]. CD133 displays a membrane topology consisting of an 85 aa N-terminal extracellular domain, five transmembrane domains with two large extracellular loops, and an 50 aa C-terminal domain (Figure 2). Analysis of this protein has revealed eight potential N-glycosylation sites: five on the first extracellular loop and three on the second, conserved cysteine-rich region located in the transition of the first transmembrane domain and the first cytoplasmic loop and leucine zipper-like motifs in the extracellular loops. This unique protein does not share sequence homology to other known proteins, making it challenging to resolve its biological role [114].

Figure 2

1.5.2.1.2 CD133 function

The function of CD133 is not fully understood. Numerous studies indicate the stem cell-like phenotype of CD133 expressing cells. Hematopoietic stem cells (HSC) expressing CD133 were multipotent when compared with CD34+/CD133- cells [123]. During self-renewing of HSCs via asymmetric cell division, CD133 was transferred to daughter cells with stem cell phenotype [124]. Similar observations were made in lung cancer cells. DNA co-segregation is a mechanism by which the cellular components are divided asymmetrically during mitosis in intestinal, muscle and neural cells. Interestingly, Pine et al., [125] showed during asymmetric division in lung cancer cell lines and primary tissues, CD133 co-segregated with the template DNA, while the differentiation markers such as prosurfactant protein-C and pan-cytokeratins were transferred to the more differentiated cells. The above data imply that CD133 expression may be associated with stem cell phenotype.

Differentiation of neuroepithelial cells to neuron-generating progenitors upon neurogenesis is associated with budding of CD133-containing membrane particles known as prominosomes [126]. Release of prominosomes from differentiating stem cells could be a mechanism of intracellular communication and/or removal of proteins that regulate stem cell phenotype, further emphasizing the possible role of CD133 in maintaining the "stemness" of a cell. In line with these observations, stable knockdown of CD133 by lentivirus mediated shRNA in neuroblastoma cells was associated with loss of anchorage independent colony formation and *in vivo* tumorigenicity in contrast to wild type cells [127], characteristic of CSCs. Although CD133 expression appears critical for stem cell-like phenotype, it is at present not possible to draw solid conclusions on the molecular function of CD133 in stem and CSCs.

1.5.2.1.3 CD133, somatic stem and progenitor cell marker

The human HSCs were initially identified as CD34+ cells. However, recently CD133 has attracted greater attention as an alternative maker for HSC. CD133 expressing CD34+ HSCs regenerated the entire immune system in NOD/SCID mice in contrast

to CD34+ CD133- sub-population [128]. Additionally, CD133+ cells ably differentiated into endothelial and neuronal cells and myoblasts in specific culture conditions [117, 129, 130], underlining the plasticity of the CD133+ cells in comparison to the CD34+ cells. Large-scale immunomagnetic selection of CD133+ HSCs from healthy mobilised adult donors has allowed enrichment of sufficient numbers of cells for transplantation [116]. In a study by Koehl, et al, [131] engraftment of CD133 selected autologous progenitor cells (2.5×10^6 cells/kg) in a pediatric patient with meningeal relapse of CD34+ CD133- Precursor B-Cell Lymphoblastic Leukemia-Lymphoma led to complete remission. Thus, these data emphasise the essential role of CD133 in selection of HSC.

CD133 is also an ideal marker for selection of somatic stem cells/progenitors in adult tissues including kidneys, muscle, skin and prostate [117, 132-134]. CD133+ cells from adult human kidneys were capable of self-renewal and differentiation into epithelial or endothelial cells, both *ex-vivo* and *in vivo*. Interestingly, in SCID mice with glycerol-induced tubulonecrosis, CD133+ cells contributed to the renal tissue regeneration [132]. Likewise, CD133 identified a rare population (~1%) of progenitors located in the basal layer of human prostate. These cells possessed high proliferative potential *in vitro* and when engrafted in immunocompromised mice, reconstitute prostatic-like acini [134].

1.5.2.1.4 CD133, cancer stem cell marker

The expression of CD133 has been addressed in various malignancies including brain, lung, prostate and colon carcinomas [76, 78, 79, 135]. CD133 expression is proven to select for self-renewing with differentiation potential, chemoresistant and tumorigenic cells. Characterising these aggressive cells could possibly allow explaining the tumour initiation and chemoresistance after therapy. In this section I will provide data regarding the role of CD133 expression in tumorigenesis, chemoresistance and prognosis of colorectal, brain, hepatocellular carcinoma, and lung cancers.

1.5.2.1.4.1 Colorectal cancer

The presence of colon CSCs was first described in 2007 [136]. In contrast to CD133- cells, injection of CD133+ cells under the renal capsule of NOD/SCID mice resulted in generation of tumours retaining their parental tumour morphology even after serial transplantation in mice [136]. Similar observations were made by Ricci-Vitiani et al., [77] where 3000 CD133+ cells engrafted successfully in mice while 10^5 CD133- were not tumorigenic. Differentiation of CD133+ cells in the presence of serum was associated with loss of CD133 expression and tumorigenicity *in vivo* [77]. In HT29 colorectal cancer cell line, CD133+ selected the chemoresistant population. CD133 knockdown enhanced sensitivity to staurosporine and reduced cell motility [137]. The importance of CD133 as marker in colorectal cancer has also been clinically proven. Higher CD133 expression levels (≥55%) in 104 stage IIIB colon cancers, strongly suggested lower 5-year survival rates [138]. These data demonstrate that CD133 expression identifies the stem cell-like, chemoresistant colorectal CSCs and the association of its expression with poorer prognosis in colon cancer patients implies its contribution in tumour progression.

1.5.2.1.4.2 Brain cancer stem cells

CD133+ glioma cells exhibit tumorigenity in mice. Culturing dissociated tumour samples of 14 pediatric patients with brain tumours led to formation of neurospheres similar to normal neural stem cells which expressed CD133. Injection of 100 CD133+ cells into NOD/SCID mice produced tumours with exact phenocopies of the original tumour, where as 10,000 CD133- cells were not tumorigenic *in vivo* [78]. In addition to the tumour initiating potential, CD133+ glioma cells were also more resistant to radiotherapy than the CD133- population and were enriched after exposure to radiation [139]. CD133 expression was assessed in a cohort of 95 glioma samples where the frequencies of CD133+ cells correlated with tumour grade [120]. Therefore, CD133 serves as an ideal marker to detect the aggressive, chemoresistant brain cancer cells.

1.5.2.1.4.3 CD133 and hepatocellular carcinoma (HCC)

Various studies have demonstrated the importance of CD133 as HCC CSCs marker. Sorted CD133+ cells had higher cloning efficiency and proliferation *in vitro* and significantly more tumorigenicity *in vivo* [140-142]. HCC CD133+ cells expressed Oct-4 and Nanog in contrast to CD133- cells, further confirming that CD133 selects for stem cell-like cells in HCC [140]. Exposure of HCC tumours to doxorubicin and fluorouracil *in vivo* resulted in the enrichment of CD133+ cells in a dose-dependent manner [141] indicating, conventional chemotherapy is ineffective and increase doses and cycles of therapy only add to the toxicity. Clinical significance of CD133 expression in HCC has also been addressed. Analysis of 63 HCC tissue specimens revealed increased CD133 expression correlated with increased tumour grade and advance stage, indicating poor prognosis [143].

1.5.2.1.4.4 CD133 and lung cancer stem cells

The presence of a stem cell-like sub-population in SCLC and NSCLC specimens was addressed in 1980's by Carney et al., [144]. Since then, various studies have successfully isolated chemoresistant, stem cell-like lung pulmonary from primary tissue and cell lines [79, 145, 146]. Eramo and colleagues in 2008 [79], demonstrated that CD133+ lung cells expanded in growth factor containing serum-free cultures as self-renewing tumour spheres and differentiated into CD133- in the presence of serum. These cells were highly tumorigenic *in vivo* and generated tumours that mimic the histology of the primary tumour. Co-expression of embryonic stem cells markers such as Oct-4 and Nanog, further confirmed the stem cell nature of CD133-expressing cells. Thus, *in vitro* and *in vivo* studies suggest CD133+ cells as putative lung CSCs that initiate and propagate the malignant neoplasm.

Lung cancer CD133+ cells are resistant to most conventional chemotherapy, emphasising the urgent need of alternative therapies [79, 84]. In vitro treatment of NSCLC cells with cisplatin resulted in enrichment of CD133+ sub-population both after acute cytotoxic exposure and in cells with stable cisplatin-resistant phenotype [84]. Likewise, treatment of lung cancer cell lines with doxorubicin, cisplatin, or

etoposide enriched CSCs which expressed CD133 [82]. The exact mechanism of lung cancer CD133+ chemoresistance is unknown. Understanding underlying mechanisms of chemoresistance is critical for an appropriate approach.

The importance of CD133 as a marker for predicting chemo-response and disease prognosis has also been addressed by several studies. The expression of CD133 was associated with shorter progression-free survival in NSCLC candidates treated with platinum-based regimens [79, 84]. A recent study assessed the value of CD133 expression and its association with disease recurrence in 117 samples from patients with stage I adenocarcinoma. Patients expressing higher CD133 had greater risk of recurrence than those with low CD133 expression; 5-year disease-free survival rate was 77.2% versus 95.1% (P=0.004) [118]. In another study, the association of CSC marker expression with overall survival rate in 50 NSCLC candidates undergoing induction chemo-radiotherapy was evaluated. These patients had received docetaxel and cisplatin concurrently with thoracic radiation followed by surgery. Patients positive for CD133 and ALDH exhibited worse 5-year overall survival rate than patients with both CD133 and ALDH negative expression (44.9% versus 90.0%, respectively) [85].

These findings infer that, CD133 expression identifies the stem cell-like, tumorigenic, chemoresistance cells and is a valuable prognostic marker for lung cancer.

1.5.2.2 Aldehyde Dehydrogenase

Certain isoenzymes of aldehyde dehydrogenase (ALDH) superfamily are shown to be creditable for selection of CSCs. Antibodies are commercially available for detection of ALDH enzymes however, most studies have used ALDEFLUOR® kit for identification of ALDH+ cells.

1.5.2.2.1 The Human Aldehyde Dehydrogenase superfamily

Human ALDH represents a superfamily currently consisting of 19 genes, sub-divided in 11 families and 4 sub-families, which differ in their chromosomal locations [147, 148]. At sub-cellular levels, ALDH enzymes can be found in the nucleus, cytosol, mitochondria and endoplasmic reticulum and have wide tissue distribution [147, 148]. These cognate proteins are NAD $(P)^+$-dependent enzymes involved in converting aldehydes into weak acids, a reaction associated with resistance to alkylating chemotherapeutic agents in CSCs [147-149]. Sub-family of ALDH enzyme catalyse the final and irreversible step in the conversion of retinol to retinoic acid, essential for embryogenesis [150]. From the ALDH super-family, those involved in stem cells as well as CSCs are shown in Table 2. ALDH1 is commonly used as a marker for stem cells and CSCs and will be discussed in the following section.

table 2

1.5.2.2.2 ALDH in CSCs

The ALDH activity has been employed as a functional marker to identify and isolate CSCs in various malignancies including breast, prostate, colon as well as lung cancers (reviewed in [151]). In breast cancer, 500 ALDH+ cells were tumorigenic in nude mice whereas the same number of ALDH- cells and even higher (50,000) were not sufficient to generate tumours in animals [83]. In lung cancer cell lines, ALDH+ cells were clonogenic, tumorigenic and resistant to the chemotherapeutic agents commonly used as first-line therapy [152]. The importance of ALDH as a marker has also been clinically demonstrated. In a study of 303 NSCLC candidates, expression of ALDH1 in early-stage lung cancer was associated with poor prognosis [152].

ALDH1A1 and ALDH3A1 expression, due to their intrinsic ability to oxidise alkylating agents to weak acids, have been associated with chemoresistance [151]. Knock-down of ALDH1A1 and ALDH3A1 by siRNA in NSCLC resulted in loss of clonogenecity and increase sensitivity to 4-hydroperoxycyclophosphamide (4-HC) [153]. Treatment of acute myeloid leukemia cell line resistant to cyclophosphamide with ALDH1 inhibitor, DEAB, restored sensitivity to 4-HC [154]. Therefore, targeting ALDH1 could be a strategy for re-sensitising chemoresistant disease.

These data indicate that ALDH1 can be used as a marker for identifying and isolating CSCs from malignancies.

1.5.2.3 Oct-4

Oct-4 or octomer binding transcription factor 4 is a protein of the POU domain family. Expression is restricted to pluripotent cells with decrease in levels on cell differentiation and loss of pluripotency [155]. The protein is a key regulator of self-renewal and differentiation in embryonic stem (ES) cells. Oct-4 has been shown to increase the malignant potentials of ES cells in a dose dependent manner, indicative of possible oncogenic role [156]. Oct-4 transcripts have been consistently detected in embryonic carcinoma cells, testicular germ cells tumours, seminomas and bladder cancers [157, 158].

With regards to CSCs, the expression of this gene correlates with tumorigenesis, with particular emphasis on tumour recurrence and treatment resistance [157]. Its expression in mammary CSCs suggested self-renewal and tumorigenesis [159]. Likewise, Chen et. al., [158] demonstrated that Oct-4 maintained the stem-like properties of lung cancer CD133+ cells. Knockdown of Oc-4 in CD133+ cells was associated with differentiation of these cells to CD133- cells accompanied by loss of clonogenicity *in vitro* and tumorigenicity *in vivo*. Additionally, Oct-4 knockdown significantly sensitised cells to anti-cancer therapy including chemotherapy, radiotherapy or combined treatment. In the same study the author demonstrated that increased incidences of Oct-4 expression positively correlated with advanced stage of lung cancer. Thus, Oct-4 may serve as an important marker for CSCs.

1.5.3 Targeting CSCs

Conventional therapeutic approaches eradicate cells that form tumour bulk but spare the CSC sub-population. These surviving cells with stem cell-like phenotype are the proposed cause of tumour recurrence or relapse after therapy. Targeting CSCs may lead to improvement in long-term outcomes.

Embryonic signalling pathways such as Wnt, Notch and Hedgehog signalling involved in self-renewal, proliferation and differentiation of normal stem cells, are also active in CSCs. Novel drugs have been designed that specifically target CSCs in glioblastoma, multiple myeloma, and leukaemia [160-163]. These studies demonstrate reduction in CSC population, inhibition of sphere formation, proliferation and colony formation, indicating the pivotal role of these pathways in CSC stemness. Clinical trials using agents against Wnt (PRI-724), Notch (RO4929097, BMS-906024, MK0752), and Hedgehog pathways (GDC-0449, PF-04449913, BMS-833923, IPI-926, TAK-441) have begun, however their effects on the CSCs in patients remains to be assessed [164].

As mentioned earlier, CSCs are resistant to conventional chemotherapy. Sensitisation of these aggressive cells to treatment is also a promising strategy. Levina et al., [165]

demonstrated that lung CSC growth is mediated by autocrine loop that activates the c-Kit receptors. Blocking c-Kit by imatinib (Gleevec) combined with cisplatin was sufficient to increase sensitivity, thereby inhibiting tumour cell growth [165]. Similarly inhibiting interleukin 4, which increases the chemoresistance of colon CSCs via autocrine and paracrine signalling, was associated with chemosensitivity [166].

Differentiation of CSCs results in loss of stemness. Recently, the novel compound salinomycin, by induction of epithelial cell differentiation in breast CSCs, inhibited *in vitro* and *in vivo* growth [167]. Likewise, treatment of multiple myeloma cells with interferon-alpha, a pleotropic cytokine, induced terminal differentiation of the CSCs with loss of cellular proliferation and clonogenic growth [168]. These data provide the rationale for clinical differentiation therapy for the treatment of resistant cancers.

In summary, if CSCs are the principle cause of treatment resistance and cancer relapse, targeted strategies against these aggressive cells in combination with conventional treatment would be a promising avenue. This would not only eradicate most non-tumorigenic cells within the tumours but also eliminate the root cells considered as the source of malignancy. SCLCs are neuroendocrine tumours with extensive neuropeptide network which through autocrine and paracrine signalling fuel SCLC growth and are associated with their chemoresistance [65, 169-171]. Primary findings have demonstrated the involvement of expression of neuropeptide receptor in expansion of the brain CSCs *in vitro* [172]. Similar findings in SCLC putative CSCs may be speculated. Below, the role of neuropeptides in SCLC growth and the effect of neuropeptide antagonists as treatment for SCLC will be described.

1.6 Neuropeptides

The regulation of cellular growth and proliferation is essential for various physiological processes including embryogenesis, development and tissue repair. Cancerous cells escape the regulatory signals from their environment and acquire independence from mitogenic controls. For example, various malignancies produce

growth factors such as neuropeptides that trigger unrestrained growth via autocrine (receptors present on the same cell) or paracrine signalling (receptors on adjacent cells) [171]. This is illustrated by the observation that, in contrast to normal tissue cells, cancer cells can proliferate in serum free medium [169]. These cells can evade physiological growth controls by alerting the number or the structure of growth receptors and by changes in the activity of post-receptor signalling pathways [65, 171].

Small regulatory peptides or neuropeptides are structurally diverse group of hormones and neurotransmitters. In the nervous system, they serve as neurotransmitters, while in the peripheral neuroendocrine cells they act systematically as circulating hormones and locally via autocrine and paracrine loops [170]. Expression of neuropeptides and their receptors have been implicated in several diseases including inflammatory and cardiovascular diseases and malignancies such as breast, prostate, colon, pancreatic, renal, gastric carcinoma and SCLC [173]. In SCLC, neuropeptides are the principle driving force that promotes SCLC cell growth *in vivo* and *in vitro* [169]. Neuropeptides that act as growth factors include, bombesin/gastrin-releasing peptide (GRP), vasopressin, neurotensin, bradykanin, cholecyctokinin, and galanin [64, 169]. Modulating neuropeptide induced signalling may serve as a promising strategy for treatment of malignancies with neuroendocrine phenotype.

1.6.1 G-protein coupled receptors

Neuropeptides exert cell proliferation by binding to surface receptors known as G-protein coupled receptors (GPCRs). The GPCRs are the largest group of integral membrane proteins involved in signal transduction. These receptors bind to, and transduce signals via heterotrimetic GTP binding proteins (G-proteins). GPCRs possess 7 membrane spanning α-helices referred to as transmembrane domains (TM) 1-7 in addition to extracellular amino termini and cytoplasmic carboxyl termini (Figure 3A) [174]. Sequence homology among the GPCRs is mainly observed in the 7 TM regions. A single conserved cysteine residue on the first two extracellular

loops is believed to form a disulphate bond which maintains the active form of the protein. Proline residues located in TM 4, 5, 6, and 7 are suggested to be essential for formation of binding pocket. Ligand binds to GPCRs via receptor binding pocket which is created by its three dimensional arrangement within the plasma membrane [174, 175].

GPCRs in the absence of ligand are maintained in an inactive conformation by stabilising intramolecular interactions. Receptor interaction with ligand leads to release of these constrains causing the key sequences of GPCRs to be exposed to various G-proteins. There are several theories explaining GPCRs activation. The ternary complex model, the most widely accepted theory, explains the active /inactive state of GPCR (Figure 3B) [176]. Inactive 'R' state indicates no reaction with G-proteins, whereas active 'R*' state indicates G-protein activation with subsequent signalling. In the absence of neuropeptide ligand, basal receptor activity is determined by the equilibrium between R and R*. Agonist binds to and stabilises R*, promoting interaction with G-proteins, whereas antagonist binds to and stabilises R, attenuating G-protein interaction.

Figure 3

Altered GPCR signalling has been documented in several cancers making these receptors the largest class of drug discovery targets (reviewed in [177]). A single GPCR can activate more than one G-protein, thus it is possible to design selective pathway antagonist which inactivate a selective subset of responses triggered by the receptor. Such ligand-dependence theoretically offers a completely new dimension to ligand-induced receptor signal control in that they have the potential to allow beneficial signalling to continue while blocking signalling due to pathology. This is useful in cancers which demonstrate inappropriate GPCR signalling due to elevated receptor expression or mutations causing constitutive activity leading to cellular proliferation and transformation [177].

1.6.2 G-proteins

G-proteins are a large family of highly homogenous heterotrimeric proteins that comprises of α, β, and γ subunits. At least 18 different human Gα exists which are divided into 4 families based upon sequence similarity: $G_{\alpha s}$, $G_{\alpha i}/G_{\alpha o}$, $G_{\alpha q}/G_{\alpha 11}$, and $G_{\alpha 12}/G_{\alpha 13}$ [178]. Similarly, at least five G_{β} types and 11 Gγ types are present. Members of the G-proteins can stimulate multiple down-stream pathways [178]. The $G_{\alpha s}$ family of the G-protein stimulate adenylate cyclase, resulting in increase in the intracellular cAMP concentration. The G-proteins of the $G_{\alpha i}/G_{\alpha o}$ family are ubiquitously expressed and G_i proteins are identified as inhibitory regulators of various types of adenylyl cyclases. In addition, recently G_i proteins are demonstrated to be activators of mitogen activated protein kinase (MAPK) and tyrosine kinase pathways. The G-proteins of the $G_{\alpha q}/G_{\alpha 11}$ family are also ubiquitously expressed and couple receptors to β-isoforms of phospholipase C. Indirect studies indicated $G_{\alpha 12}/G_{\alpha 13}$ role in activation of phospholipase A_2 and c-jun NH2-terminal kinase. In addition to α-subunit of the G_i proteins, dissociated βγ-complex from the α-subunit can also mediate multiple effectors including regulation of ion channels, specific isoforms of adenylyl cyclase and phospholipase C, as well as of phosphoinositide-3-kinase isoforms [179, 180].

Transfer of signals from activated receptor to effectors, requires G-proteins to undergo an active-inactive cycle (Figure 4). In basal state, the α-subunit contains bound GDP with α and βγ-subunit association. Binding of activated GPCRs to G-proteins triggers exchange of GTP for GDP with α and βγ subunit dissociation. Thus, two potential pathways, the α-GTP and the βγ-subunit are generated for downstream signalling. The intrinsic hydrolyte activity of α-subunit finally converts GTP to GDP with return of G-protein to its inactive state [179, 181].

Despite the importance of G-proteins in regulation of cell growth, some G-proteins can induce cellular transformation. Various G-protein α-subunits due to GTPase inactivating mutations lead to cellular transformation by protein constitutive activity [182]. Constitutive activity of members of α-subunit has been detected in human cancers such as, activated $G_{\alpha s}$ in 30% of thyroid adenomas, active mutant of $G_{\alpha i}$ in adrenal cortical tumours as well as in human ovarian sex cord stromal tumours [183], and activated $G_{\alpha 12}$ as an oncogene present in soft tissue sarcoma [184]. Despite transforming mutations of $G_{\alpha q}/G_{\alpha 11}$ has not been detected in human tumours, activated $G_{\alpha q}/G_{11}$ leads to transformation of fibroblasts.

Figure 4

1.6.3 Bombesin/GRP and its receptors

Bombesin, a 14-amino acid bioactive peptide, was initially isolated from frog skin [185]. GRP, a mammalian homologue, consists of 27 amino acids and is closely related to bombesin [186]. The GRP gene is located on chromosome 18 at 18q21 [186]. It functions as a neuro-transmitter as well as an intestinal, adrenal and pituitary hormone [187]. In lungs, GRP is a potent mitogen for both normal bronchial epithelial and malignant SCLC cells [188-190]. Studies on Swiss 3T3 cells have shown that this neuropeptide stimulates colony formation in semi-solid medium and can induce DNA synthesis and cellular proliferation.

Three structurally and pharmacologically distinct bombesin receptors have been identified which belong to the super-family of GPCRs. These include the GRP-R, neuromedin B receptor (NMB-R) and bombesin receptor subtype-3 (BRS-3) that display different affinity for ligand GRP and NMB. These receptors are expressed in an overlapping subset of human lung cancer cell lines [191].

1.6.4 Vasopressin and its receptors

Arginine vasopressin (AVP) is a cyclic nonapeptide and its expression is mainly restricted to the hypothalamus in physiological conditions [192]. Two main types of vasopressin receptors have been identified, V_1 and V_2 receptor [192]. V_1 receptor, sub-divided into V_{1a} and V_{1b}, is involved in multiple physiological processes including vasoconstriction, liver glycogenolysis and various brain functions. V_2 receptor expression is mainly identified in the renal system, and its activation is associated with reabsorption of H_2O [193].

V_1 receptors via activation of inositol phosphate turnover regulate vascular and hepatic functions stimulated by AVP. V_2 receptors couple to adenylate cyclase and regulate antidiuretic responses. Like bombesin/GRP, in Swiss 3T3 cells, AVP results in Ca^{2+} mobilisation and PKC production mediated by G-protein linked transduction pathway leading to cellular proliferation in liquid culture and increased clonogenicity in semi-solid medium (reviewed in [170]).

1.6.5 Neuropeptide mediated signal transduction

Neuropeptides, including GRP and vasopressin are principle mitogenic stimuli for SCLC cells which activate the heterotrimeric G-proteins, namely $G_q/_{11}$, $G_i/_o$, and G_{12} (Figure 5) [194]. Predominantly, receptors couple to G_q to elicit phospholipase C-β (PLCβ) activation with subsequent production of diacylglycerol (DAG) and phosphatidylinositol 1, 4, 5-triposphate (IP_3), triggering protein kinase C (PKC) activation and Ca^{2+} mobilisation, respectively [195, 196]. The resultant Ca^{2+} induced extracellular signal regulated kinase (ERK) activation is essential for the anchorage-independent phenotype and SCLC proliferation [197]. PKC activation by neuropeptides is involved in cell cycle regulation through Ras/Raf/ERK cascade in several cell types. Additionally, neuropeptide activated PKC results in activation of protein kinase D (PKD), a novel kinase cascade downstream of PKC. In Swiss 3T3 cells, neuropeptide activated PKC with subsequent PKD activation leads to DNA synthesis and cell proliferation raising the possibility of the PKC/PKD pathway in SCLC growth [198].

These peptides also activate G_i and G_{12} (Figure 5). Receptors coupled to G_i family regulate cellular proliferation through both αi and βγ subunits. The βγ subunits via direct stimulation of PI3K activate the Ras/Raf/MEK/ERK cascade. ERK activation can be mediated by $G_{\alpha i}$ subunit independent of βγ subunits and PI3K Ras activation [199]. Therefore, ERK activation via G_i protein is by both α and βγ subunits. Neuropeptide receptors couple to G_{12} to elicit activation of Rho family of small GTPase which are involved in the regulation of cytoskeleton and contribute to C-Jun N-terminal Kinase (JNK) cascade activation [200]. Activation of $G_{12/13}$ proteins in SCLC cell is associated with maintenance of cellular morphology but does not have any impact in SCLC proliferation. Rho family by regulating the dynamics of cytoskeleton, have a significant role in metastasis (Figure 5).

Figure 5

1.6.6 Neuropeptides and SCLC

SCLC cells express and secrete various neuropeptides that mediate uncontrolled growth of the malignancy [169, 201]. The concept was supported by colony assay in which multiple neuropeptides stimulated clonal growth of SCLC cell lines in serum-free semi-solid medium. In this section the effects of GRP and vasopressin on SCLC cell growth will be discussed.

1.6.6.1 Gastrin releasing peptide and SCLC

GRP regulates growth of normal human bronchial epithelium as well as SCLC cells [188, 189]. In the embryonic lung, expression of bombesin is associated with branching morphogenesis which could be blocked by bombesin inhibitor, [Leu^{13} –psi (CH_2N_2) Leu^{14}]-bombesin [188]. In the adult lung, GRP is secreted by lung neuroendocrine cells as a response to change in lung oxygen levels as observed in lung diseases including chronic obstructive airway diseases which causes reduced lung oxygenation [202]. Elevation in GRP secretion in adult lung is associated with lung neuroendocrine hyperplasia and increased expression of GRP has been documented in smokers [203].

GRP stimulates SCLC growth *in vitro* and *in vivo*. Treatment of 10 SCLC cell lines with GRP increased colony formation up to 150-fold in 9/10 cell lines [204]. In another study, addition of GRP was associated with increased DNA synthesis in SCLC cell lines [205]. The mitogenic effect of this neuropeptide was also confirmed *in vivo*. Treatment of NCI-H69 xenograft with GRP three times daily IP injections, increased tumour growth by 77% when compared with untreated controls [206].

1.6.6.2 Vasopressin and SCLC

Vasopressin is mitogen for SCLC. Both vasopressin and its receptor expression in SCLC indicate that the neuropeptide is an autocrine growth factor for the malignancy enhancing transcription, cell proliferation and augmenting cell survival [64, 171]. 67% of SCLCs show immunoreactivity to AVP [207]. All three receptors of

vasopressin, namely V_{1a}, V_{1b}, and V_2 are present in SCLC cells [208]. The expression of AVP and its receptor serve as a diagnostic tool to differentiate SCLC from NSCLC which are devoid of the hormone and its receptors [209]. The ectopic expression produces clinical syndrome known as SIADH, as seen in SCLC patients [24]. Targeting this growth factor could benefit SCLC patients.

1.6.7 Blocking growth factor action as a therapy for neuroendocrine cancers

Current chemotherapeutic agents target rapidly dividing malignant cells. However, normal tissue cells are also exposed to cytotoxic insults, producing adverse effects. Targeting neuropeptide autocrine and paracrine loops in SCLC and other neuroendocrine cancers by neutralising ligand or inhibiting its interaction with its receptors are promising interventional strategies that would block mitogenic effects on neoplastic cells.

Several groups have designed specific bombesin antagonist aimed at inhibiting its mitogenic effect on cancer cells. Bombesin monoclonal antibody, 2A11, was used to retard SCLC cell growth *in vitro* and in nude mice xenografts [190]. The antibody entered phase I clinical trial with no limiting toxicity [210]. However, antibodies may be antigenic, are costly to manufacture and its large size makes tissue penetration ineffective compared to small peptide drugs. Alternatively, peptide receptor antagonists such as [Leu^{13}-*psi* (CH_2NH) Leu^{14}] bombesin that readily inhibited Ca^{2+} mobilisation and clonal growth in Swiss 3T3 cells was introduced [211]. However, these receptor antagonists are effective in malignancies selectively expressing bombesin receptors and are expected to have poor clinical outcome in cancers with multi-neuropeptide receptor expression including SCLC. This necessitated the introduction of broad spectrum Substance P analogues that are able to block binding and biological activities of multiple neuropeptide loops.

1.6.7.1 Broad spectrum neuropeptide antagonists as novel SCLC therapy

Substance P (SP) is an 11-amino acid neuropeptide (Arg-Pro-Lys-Pro-Gln-Gln-Phe-Phe-Gly-Leu-Met-NH_2) that functions as neurotransmitters and neuromodulators [212]. Synthetic analogues of SP proved to be antagonists of various SP mediated cellular effects as well as other neuropeptide activities. Some of these analogues are shown in table (Table 3). In SCLC cells, SP analogues inhibited $[Ca^{2+}]_i$ mobilisation stimulated by multiple neuropeptides including bombesin, vasopressin, bradykinin, gastrin, galanin, cholecystokinin, and neurotensin [64, 213, 214]. Based on this characteristic these peptide antagonists were termed as ‘broad spectrum antagonists’.

Table 3

Set backs encountered with SP analogues are their relatively low potency (μM range). Additionally, easy inactivation of antagonists by serum peptidases makes systemic delivery difficult and often impossible. Thus, chemical modifications for augmentation of affinity and stability have been suggested. Victor Hruby et al., [215] demonstrated improved stability with D-amino acid substitution. Substitution of glutamine in position 5 by D-phenylalanine (DPhe) in a SP analogue spantide (DArg-DPro-Lys-Pro-Gln-Gln-DTrp-Phe-DTrp-Leu-Leu-NH_2) resulted in 5-10 fold increased potency to inhibit neuropeptide mediated growth of the new analogue, DArg-DPro-Lys-Pro-DPhe-Gln-DTrp-Phe-DTrp-Leu-Leu-NH_2 (SP-D). Additionally, the replacement of position 5 DPhe by D-tryptophan (DTrp) in SP-D produced even greater inhibitory potency of the new analogue, DArg-DPro-Lys-Pro-DTrp-Gln-DTrp-Phe-DTrp-Leu-Leu-NH_2 (SP-A) [216, 217].

SP-G (Arg ^{6}-DTrp ^{7,9}-N^{me} Phe^{8}) substance P (6-11) is a broad spectrum neuropeptide antagonist. It functions as an antagonist to multiple neuropeptide mitogens including GRP, vasopressin, bradykinin, and endothelin [213, 218]. This analogue inhibited the growth of SCLC cell lines in liquid and semi-solid media with IC_{50} values of approximately 20 μM [213, 214]. SP-G has also demonstrated dramatic inhibitory effect on SCLC cell cloning efficiency in the absence of exogenously added neuropeptide (basal colony formation) [219]. The knowledge that SP-G inhibits basal and stimulated clonal growth of SCLC cells regardless of positivity for bombesin receptors strongly suggest that, it could be a more effective anticancer drug than ligand specific growth factor antagonists.

In addition to *in vitro* inhibitory effect, SP-G effectively inhibited *in vivo* growth of SCLC H69 and WX322 cells [220]. Peri-tumoral administration 45 mg kg^{-1} day^{1-} produced complete inhibition with effects extending beyond the period of administration. Intra-peritoneal (IP) injections of 45 mg kg^{-1} day^{1-} for 7 days likewise produced significant growth inhibition in WX322 xenograft [220]. The growth inhibitory effect of SP-G has been shown to be at least partly due to apoptosis. In SCLC cell lines, this analogue has proven to induce apoptosis at similar concentrations that causes growth inhibition [221].

SP-G inhibited growth of various other neuroendocrine tumours including colorectal, pancreatic and ovarian cancers [65]. The growth inhibitory effects of SP-G (IC_{50}) in a panel of cell lines are demonstrated in Table 4. According to unpublished data from my laboratory, SP-G retarded the tumour growth of colorectal cancer cell lines, HT29 and ovarian cancer cell line, PE04 *in vivo* indicating the analogue could additionally be utilised for other malignancies with neuroendocrine secretion.

table 4

The exact mechanism by which these analogues induce their cytotoxic effect is subject to considerable debate. SP analogues can reversibly inhibit the binding of multiple neuropeptides to their receptor subsequently retarding signalling pathways stimulated by these growth factors. This observation suggested that SP analogues function as competitive antagonists of ligand binding. However, even in the presence of high concentrations of exogenous neuropeptides, the growth inhibitory and pro-apoptotic effect of SP analogues are not reversible indicating these analogues function via a mechanism distinct from or in addition to competitive neuropeptide antagonism [221]. One theory is that SP analogues may also insert cell membrane and induce their cytotoxic effect by directly modulating G-proteins [222]. However, this concept was rejected in a study produced by Seckl and Rozengurt, 1996 [217]. [D-Arg^{1}, D-Phe^{5}, D-Trp^{7,9}, Leu^{11}] substance P, abolishes the signal transduction produced by both bombesin and vasopressin. A truncated version of this analogue, [D-Arg^{1}, D-Phe^{5}, D-Trp^{7,9}] demonstrated inhibitory effect against vasopressin but was ineffective against bombesin suggesting that SP analogues induce their effect at receptor level.

Multiple studies have recently demonstrated that SP analogues function in a more complex manner than data documented previously. Jarpe et al., [223] demonstrated that SP-D, similar to neuropeptides, via G_{12} activate JNK thus, demonstrating agonist activity. However, in contrast to neuropeptides, SP-D via G_q inhibited Ca^{2+} mobilisation demonstrating antagonist activity. Similar observation was made in my laboratory. SP-D administered to block bombesin stimulated Ca^{2+} release via G_q protein, additionally caused sustained activation of JNK and ERK [224]. Likewise, at V_{1A} vasopressin receptor, SP-G via G_i led to sustained activation of ERK alongside G_q inhibition [225]. Thus, SP analogues are able to activate and inactivate different arms of signal transduction pathways at single receptors. Based on these observations the terminology of “biased agonism” was proposed to define SP analogue mechanism of action (Figure 6) [223]. Based on this theory, SP analogues preferentially stabilise R*2 than R*1. Discordant signalling induced by sustained activation of JNK and ERK along inhibition of $[Ca^{2+}]_i$ mobilisation is the proposed cause of induction of apoptosis and inhibition of tumour growth upon SP analogue exposure.

Figure 6

The most exciting property of SP-G is that it is more effective in resistant disease [65, 171, 226]. Waters et al, [65] demonstrated that chemoresistance in SCLC cell lines was associated with increase expression of neuropeptide receptors. This was evaluated by quantifying the expression levels of GRP-R by semi-quantitative RT–PCR in three human SCLC cell lines (GLC14, 16 and 19) established from the same patient during longitudinal follow-up [227, 228]. During therapy, the patients' tumour progressively changed from chemosensitive to resistant. GLC14 was established before treatment, GLC16 was derived from tumour recurrence after chemotherapy and GLC19 was derived from tumour recurrence after chemo- and radio-therapy. Increase expression of GRP-R on the drug resistant cells was subsequently associated with enhanced responsiveness to SP-G. Treatment with SP-G inhibited the growth and the cloning efficiency of GLC14, 16 and 19, but the analogue was most efficient in the GLC19 cell line (IC_{50} for the GLC14, 16 and 19 SCLC cells was 25, 25 and 15 μM, respectively, for liquid culture, and 25, 25 and 5 μM, respectively, for cloning efficiency) [65]. Similarly, in ovarian, colorectal and pancreatic cancer cell lines, sensitivity to SP-G positively correlated to the expression of GRP-R expression in these cell lines [65]. Moreover, transfection of GRP-R into rat-1A fibroblast significantly increased their sensitivity to SP-G [65]. Thus, targeting resilient malignant cells with SP-G and other novel analogues may opened a new horizon for cancer management.

SP-G has completed a phase I clinical trial where in patients on consent received 6 hour infusion of the peptide every three weeks for up to 12 cycles [66]. Pharmacokinetic analysis of patient plasma demonstrated that the mean plasma concentration at maximum dose was 40 μM, well within the range for *in vitro* growth inhibition. No dose limiting toxicity was observed. This analogue did not enter phase II clinical trail due to its major set back with *in vivo* rapid degradation. Plasma concentration of the antagonist was brief on discontinuation of the drug [66]. Such short exposure of an agent cumulates into unsatisfactory therapeutic outcomes. Rapid antagonist clearance implicates larger doses. Thus, continuous protracted infusions were required making therapy not feasible.

Together these data suggest that the post-chemotherapy, clinically aggressive, resilient SCLCs might display a more extensive network of neuropeptide regulation. On the other hand, SP-G may be more beneficial in chemoresistant disease and can sensitise SCLC to chemotherapy. With the concept of CSCs, the pathogenesis of SCLC should be revised. These cells are the proposed cause of chemoresistance in cancer. Thus, targeting resilient malignant cells with analogues similar to SP-G but with higher stability could opened a new horizon for cancer management.

1.7 HYPOTHESIS

Despite advances in chemotherapy and radiotherapy regimes there has been little impact on the long-term survival in SCLC patients. The presence of CSCs which are stem cell-like cells with chemoresistant and tumorigenic potentials are the possible explanation for therapy resistance and tumour recurrence observed in these patients, emphasising the urgent need of alternative therapies. Based on the findings in my laboratory, resistance in SCLC cells is associated with increased expression of neuropeptide receptor expression and subsequent enhanced sensitivity to neuropeptide analogues. Therefore, it is hypothesised that SCLC CSCs express higher levels of neuropeptide receptors making these chemoresistant aggressive cells more susceptible to neuropeptide antagonist.

1.8 AIMS

With the background described in the introduction the aims of this PhD were:

A. Identify and characterise SCLC CSCs
B. Investigate the expression of neuropeptide receptors on the CSCs
C. Design more stable and potent neuropeptide antagonist for the eradication of the CSC population

CHAPTER 2:
Materials and Methods

2.1 Chemotherapeutic reagents

Etoposide was purchased from Sigma-Aldrich, UK. In collaboration with Professor Mark Bradley (Department of Chemistry, Kings Building, Edinburgh) a series of analogues were synthesised based on the structure of SP-G and SP-A. The eight analogues are listed below:

1) DArg-Pro-Lys-Pro-DTrp-Gln-DTrp-Phe-DTrp-DLeu-Leu
2) DArg-Pro-Lys-Pro-DTrp-Gln-DTrp-Phe-DTrp-Leu-GABA
3) DArg-Pro-Lys-Pro-DTrp-Gln-DTrp-Phe-DTrp-Leu-Gly
4) DArg-Pro-Lys-Pro-DTrp-Gln-DTrp-Phe-DTrp-Leu-1,2 Ethylenediamine
5) Arg-DTrp-NMePhe-DTrp-DLeu-Met
6) Arg-DTrp-NMePhe-DTrp-Leu-GABA
7) Arg-DTrp-NMePhe-DTrp-Leu-Gly
8) Arg-DTrp-NMePhe-DTrp-Leu-1,2 Ethylenediamine

2.2 Antibodies

2.2.1 Antibodies used for flow cytometry

Mouse monoclonal anti-human CD133-1, APC conjugated (clone AC133), anti-human CD133-2, PE conjugated (clone AC141), monoclonal anti-mouse IgG1, APC conjugated, and monoclonal anti-mouse IgG1, PE conjugated were from Miltenyi Biotec, Germany.

2.2.2 Antibodies used for western Blotting

Rabbit monoclonal anti-βactin was from Sigma-Aldrich, UK. Mouse monoclonal anti-human CD133-1 (W6B3C1) was purchased from Miltenyi Biotec, Germany. Goat polyclonal anti-human Oct-3/4 (C-20) was from Santa Cruz Biotechnology, USA. Rabbit monoclonal anti-Protein Kinase B (Akt/PKB) [pS^{473}] (193H12) antibody was from Cell Signalling, USA. Mouse monoclonal anti-Bcl-2 (Ab-1) was

from Merck Millipore, Germany. Rabbit polyclonal anti-gastrin-releasing peptide receptor, GRP-R was from Fisher scientific, USA. Rabbit polyclonal anti-vasopressin receptor, V_{1A}-R was from Enzo Life Sciences, UK.

2.2.3 Antibodies used for IHC

Rabbit polyclonal anti-human CD133 (ab16518) was from Abcam, UK. Biotinylated donkey anti-rabbit IgG (H+L) was from Vector laboratories, USA. Rabbit monoclonal anti-human NCAM (clone EP2567Y) was from Epitomics, USA. Rat monoclonal anti-mouse CD45 (clone 30-F11) was from BD Biosciences, USA.

2.3 Tissue culture reagents and cell lines

Tissue culture plates (6- and 96-well plates) were purchased from Life Technologies, UK. 20 µM pore size nylon gauze was from BD Biosciences, USA. Tissue culture reagents Rosewell Park Memorial Institute Medium 1640 (RPMI 1640), Dulbecco's Modified Eagles Media (DMEM), Phosphate buffered saline (PBS) without Ca^{2+} and Mg^{2+}, Hanks balanced salt solution (HBSS) with/without calcium and L-glutamine, penicillin/streptomycin, and trypsin were from PAA, Austria. Foetal Calf Serum (FCS) was from Biosera, UK. Insulin-Transferrin-Sodium Selenite (SIT) media supplement, soya bean trypsin inhibitor, Bovine Serum Albumin (BSA) and Agarose were from Sigma-Aldrich, UK.

Small cell lung cancer cell lines (SCLC), NCI-H69 and NCI-H345 were obtained from American Type Tissue Culture Collection, USA. Table 5 demonstrates the characteristics of cell lines used. Cells were maintained in RPMI 1640 supplemented with 10% (v/v) heat-inactivated FCS (heat-inactivated at 57ºC for 1h), 5 µg/ml L-glutamine, 50 U/ml penicillin and 50 µg/ml streptomycin (complete medium). For experimental purposes and sorted CD133+, CD133- cells were washed twice in PBS without Ca^{2+} and Mg^{2+} and were re-suspended in RPMI 1640 supplemented with, SIT media supplement consisting of, 30 nM selenium, 5 µg/ml insulin, 10 µg/ml transferrin and 0.25 % (w/v) BSA (SITA medium). SCLC cells were maintained in suspension at 1-3 × 10^6 cells/ml and were passaged into fresh medium twice a week.

G6A-CHO and V_{1A}-CHO cells are CHO-K1 cells expressing with full-length human GRP-receptor or human V_{1A}-receptor, respectively by Mackinnon et al., 2005 [171] Both cell lines were maintained in DMEM supplemented with 10% (v/v) heat-inactivated FBS, 5 μg/ml L-glutamine, 50 U/ml penicillin and 50 μg/ml streptomycin, 1% non-essential amino acids and 400 μg/ml G418-sulphate (DMEM complete medium). Cell lines were maintained at 10-80% confluence and passaged twice a week by treatment with trypsin (0.1%). For experimental purposes, cells were washed twice in PBS without Ca^{2+} and Mg^{2+} and were resuspended in DMEM supplemented with 5 μg/ml L-glutamine, 50 U/ml penicillin and 50 μg/ml streptomycin and 1% non-essential amino acids, and 0.1% FCS (DMEM quiescent medium).

All cells were maintained in a humidified atmosphere of 5% CO2 at 37ºC and were passaged twice a week as required.

Table 5

2.4 Liquid growth assay

SCLC cells were centrifuged at 300 × g for 5 minutes, washed twice in PBS and re-suspended in SITA or complete medium. Cells were gently disaggregated by 3 × passes through a p1000 pipette and then filtered through a 20 µm pore size nylon gauze. Cell viability and number was evaluated using NucleoCounter NC-100 (ChemoMetec, Denmark) based on the manufacturer's instruction. In brief, samples were treated with equal volumes of NucleoCounter reagent A100 (lysis/disaggregation buffer) and reagent B (stabilising buffer) which causes disruption of plasma membrane of all cells, permitting access of propidium iodide (PI) to cell nucleus, and therefore allowing determination of total number of cells within the sample. The number of non-viable cells was determined in parallel samples suspended in reagent B only. Viable cell number was calculated as total cell number minus non-viable cell number. Cells were plated at a density of 1×10^4 cells/well, in the presence or absence of mediators in triplicate in flat bottom 96-well plates. Cell number was determined every 2 days for a period of 24 days using the NucleoCounter NC-100. Prior to counting cell clumps were disaggregated by passing the cell suspension gently 3 times through p1000 pipette.

2.5 MTT Assay

MTT assay is a colorimetric method to determine cell viability. Yellow MTT (3-(4,5-dimethylthiazol-2yl)-2,5-diphenyl tetrazolium bromide) is reduced to purple formazan in the mitochondria of living cells, allowing measurement of the cytotoxic affect of chemotherapeutic agents on cell viability. Dimethyl sulfoxide (DMSO) (Sigma-Aldrich, UK) is added to dissolve the insoluble purple formazan product into a coloured solution, the absorbance of which can be measured at λ570 nm on a spectrophotometer. Viable cells at density of 5×10^4 cells/well were re-suspended in SITA medium and cultured in 96-well round-bottom plates. Cells were exposed to a series of concentrations of SP-G or neuropeptide analogues from 1 µM to 100 µM or etoposide from 1 µg/ml to 100 µg/ml and were incubated in 5% CO_2 at 37°C. After 72 hours, 1:10 dilution of 4 mg/ml MTT (Sigma-Aldrich, UK) solution in PBS was

added to each well (0.4 mg/ml final concentration) and samples were further incubated for 4 hours at 37°C. Plates were centrifuged at 300 × g for 5 minutes and supernatant was replaced by DMSO. The purple solution was transferred to a 96-well flat-bottom plate and absorbance was determined. Viability is expressed as a percentage of control.

2.6 Western blot

2.6.1 Cell lysis and assessment of protein concentration

Cells were washed once in PBS, lysed with appropriate volume of lysis buffer at 4°C for 25 minutes at 4°C. Lysates were cleared by centrifugation at 13000 rpm for 10 minutes at 4°C. Whole cell lysates were normalised for protein concentration using bicinchoninic acid (BCA) protein assay reagent according to the manufacturer's instructions (Pierce, USA). BCA protein assay is a two-step method with an initial biuret reaction where cupric ion reduces to cuprous ion followed by the chelation of BCA with the cuprous ion, resulting in purple colour that can be measured by spectrophotometry. Normalised whole cell lysates were solubilised in 4 × sodium dodecyl sulphate polyacrylamide gel electrophoresis (SDS-PAGE) sample buffer at 95°C for 5 minutes. Samples were analysed immediately or stored at -20°C for future analysis.

2.6.2 SDS-PAGE and western blotting

Buffer ingredients are explained in detailed in sections 2.6.3. Equal amount of cell extract (20-80 µg/lane) were loaded onto 10-12 % SDS-PAGE gels using a vertical electrophoresis tank Bio-Rad Mini Protean® II system (Bio-Rad, USA). Samples were electrophoresed at 150 V for 1-2 hours using electrophoresis buffer. Proteins were transferred onto Hybond C nitrocellulose (GE Healthcare Life Sciences, UK) membrane in an ice-cold transfer buffer at 100 V for 60 minutes. Equal protein loading was confirmed by incubating blots for 5 minutes in 1% Ponceau S (AMS Biotechnology, UK). Non-specific binding sites were blocked by incubating the membrane with 5% non-fat dried milk powder or 5% BSA in Tris-buffered saline

(TBS)-Tween 20 (0.1%) overnight at 4°C. Membranes were probed with appropriate antibodies diluted in blocking buffer, overnight at 4ºC. Membranes were washed 3 × 5 minutes in TBS-Tween before incubating for 1 hour at room temperature (20-25 °C) with species-appropriate horseradish peroxidase (HRP) conjugated secondary antibody (diluted 1:2000 in blocking buffer). Membranes were further washed in TBS-tween 20 (3 × 5 minute washes) and the immunoreactive bands were identified using enhanced chemiluminescence (ECL) (GE Healthcare Life Sciences, UK) as per manufacturer's instructions. ECL is a high resolution, non-radioactive method of detecting specific immobilised antigens that are conjugated (directly or indirectly) to HRP labelled antibodies. Membranes were then exposed to Kodak Medical X-ray film, which was then developed using a Konica SRX-101A film processor.

2.6.3 Buffers

Lysis buffer

HEPES, PH7.4	25 mM
NaCl	0.3 M
MgCl2	1.5 mM
Ethylenediaminetetraacetic acid (EDTA)	0.2 mM
Triton X-100	0.5% (v/v)
Sodium orthovanadate	1 mM
Dithiothreitol (DTT)	0.5 mM

One Complete™ protease inhibitor tablet (Roche, UK) was added per 50 ml of lysis buffer.

4 × SDS-PAGE sample buffer

Tris-HCl	50 mM
SDS	2% (v/v)
Glycerol	10% (v/v)
Bromophenol blue	0.1% (v/v)
β-mercaptoethanol (PH, 6.8)	10% (v/v)

SDS polyacrylamide gels

Stacking gel:

Tris base (pH 6.8)	0.125 M
SDS	0.1% (v/v)
Acrylamide solution	4.5% (v/v)
Ammonium persulphate	0.1% (v/v)
TEMED	0.02% (v/v)

Separating gel:	
Tris base (pH 8.8)	0.375 M
SDS	0.1% (v/v)
Acrylamide solution	10-12% (v/v)
Ammonium persulphate	0.1% (v/v)
TEMED	0.02% (v/v)

1 × Gel electrophoresis running buffer	
Tris base	50 mM
Glycine	250 mM
SDS	0.1% (v/v)

Blotting buffer	
Glycine	210 mM
Tris base	24.7 mM
Methanol	20% (v/v)

TBS-Tween 20 wash buffer	
Tris HCl (pH 7.4)	20 mM
NaCl	150 mM
Tween-20	0.1% (v/v)

2.7 Clonogenic assay

SCLC cells were centrifuged at 300 × g for 5 minutes, washed twice in PBS and re-suspended in SITA or complete medium. Cells were gently disaggregated by 3 × passes through a p1000 pipette and then filtered through a 20 µm pore size nylon gauze. Single cell suspension was judged by light microscopy. 10^4 viable cells counted using the NucleoCounter NC-100, were suspended in SITA or complete medium containing 0.3% low melting point SeaKem agarose in the presence or absence of mediators, and layered over a solid base of 0.5% agarose in SITA or complete media, in 35 mm plastic tissue culture dishes. The cultures were incubated at a humidified atmosphere of 5% CO_2 at 37ºC for 21 days. Colonies (>16 cells) were counted by light microscope. Colonies of at least 10 different random fields were counted for each well. Clonogenic efficiency is presented as the percentage of the cells seeded forming colonies and is calculated as below:

Step 1:

Average of number of colonies counted × Area of the dish in which cells were seeded
= Total number of colonies

Step 2:

(Total number of colonies / The number of cells seeded) ×100
= cloning efficiency

2.8 Flow cytometry

Cells were centrifuged at 300 × g for 5 minutes, washed twice in PBS and re-suspended in MACS buffer (PBS without Ca^{2+} and Mg^{2+}, 0.5% BSA, and 2 mM EDTA, pH 7.2). Cells were gently disaggregated by 3 time passes through a p1000 pipette and then filtered through a 20 µm pore size nylon gauze. Single cell suspension was judged by light microscopy. 10^6 viable cells were counted using a NucleoCounter NC-100 (ChemoMetec, Denmark) and were added to polystyrene FACS tubes (Becton Dickinson, UK). Cells were re-centrifuged at 300 × g for 5 minutes and re-suspended in MACS buffer with FCR blocking reagent (1:50 dilution, Miltenyi Biotec, Germany) and CD133-1-APC or CD133-2-PE antibodies (1:100 dilution) or mouse IgG1-APC or IgG1-PE isotype control (1:100 dilution). Samples were incubated at 4°C for 10 minutes and subsequently washed with MACS buffer at 300 × g for 10 minutes and re-suspended in the same buffer. Until analysis, all samples were kept on ice. Samples were analysed on FACSCalibur or LSRFortessa (BD Biosciences, USA) with Diva option. Data was analysed using FlowJo software (Tree Star Inc., USA). Dead cells were excluded from the analysis using 0.1 µg/ml 4,6 diamidino-2-phenylindole (DAPI) or propidium iodide (PI) at 1µg/ml.

2.8.1 Flow sorting

Cells were stained for CD133 as described above with minor modifications. After CD133 staining, cells were re-suspended in RPMI 1640 supplemented with 5 µg/ml L-glutamine, 50 U/ml penicillin and 0.1 % BSA. Addition of BSA was required to maintain cell viability during sorting. Before cell sorting samples were filtered again

through a 20 µm pore size nylon gauze. Approximately 10^8 cells were prepared per sort. Samples were loaded on the machine in 3 ml volumes. This was the optimal volume for maintaining cell flow throughout the cell sorting. Cells were sorted with a 100 µM nozzle on a FACSVantage (BD Biosciences, USA).

2.8.2 MicroBeads isolation

CD133 MicroBead Kit (Miltenyi Biotec, Germany) was used to isolate CD133+ and CD133- SCLC cells. The procedure of cell isolation is as described my manufacturer's protocol. In brief, cells were centrifuged at 300 × g for 5 minutes, washed twice in PBS and re-suspended in MACS buffer (PBS without Ca^{2+} and Mg^{2+}, 0.5% BSA, and 2 mM EDTA, pH 7.2). Cells were gently disaggregated by 3 time passes through a p1000 pipette and then filtered through a 20 µm pore size nylon gauze. Single cell suspension was judged by light microscopy. 10^8 viable cells were counted using a NucleoCounter NC-100 and were added to polystyrene FACS tubes (Becton Dickinson, UK). Samples were incubated with CD133 MicroBeads (magnetic nanoparticles coated with CD133 antibody provided by the kit) for 30 minutes at 4°C and washed with 2 ml of MACS buffer at 300 × g for 10 minutes and re-suspended in 500 µl MACS buffer. For magnetic sorting MS MACS column (Miltenyi Biotec, Germany) with MiniMACS separator (Miltenyi Biotec, Germany) was used. The column was placed on the separator and was rinsed with 500 µl of buffer. Cell suspension was applied to the column and flow-through (containing unlabelled cells, CD133- cells) was collected. The column was washed 3 × with 500 µl of buffer and the flow-through was discarded. To collect the CD133 labelled cells, the column was removed from the separator and 1 ml of buffer was added to the column was immediately flushed out by firmly pushing the plunger into the column. To increase the purity of CD133+ cells, samples were run over a second MS column and the magnetic separation procedure was repeated as described above.

2.8.3 Flow sorting and MicroBeads isolation purity check

The purity of the sorted populations was checked by evaluating the expression of CD133 antigen via the presence of its epitope-1 and epitope-2. CD133-1-APC antibody binds to epitope-1 and CD133-2-PE antibody binds to epitope-2 of this antigen. Cell sorting was performed using CD133-1-APC antibody. To evaluate the purity of sorted cells based on epitope-1 of CD133 antigen, an aliquot of the sorted cells was re-run on the same machine used for cell sorting (FACSVantage). Analysing the expression of sorted cells based on the presence of CD133-1 epitope (an epitope of CD133 antigen initially used for cell sorting) was carried out to determine whether the sorted cells would appear in the gates that they were initially selected, therefore confirming the purity of isolation.

The purity of sorted cells (by Flow sorting or MicroBeads) was also confirmed via the presence of epitope-2 of CD133 antigen. An aliquot of the sorted cells were stained by CD133-2-PE antibody (as described in section 2.8) and were analysed on the flow cytometry. Evaluating the presence of CD133 antigen via a second epitope could further confirm that sorted cells are pure.

2.9 ALDH and ALDH, CD133-1-APC double staining

To identify cells with high aldehyde dehydrogenase 1 (ALDH1) enzymatic activity, ALDEFLUOR® kit (Stem cell Technologies, UK) was used. The protocol was based on the manufacturer's instructions. In brief, H345 and H69 (1×10^6 cells/ml) were centrifuged at 300 × g for 5 minutes and were washed once in PBS. Cells were then re-suspended in Aldefluor assay buffer containing fluorescent ALDH-substrate, BODIPY-aminoacetaldehyde (BAAA) at 1 µmol per 1×10^6 cells/ml, and incubated in the dark for 30 minutes at 37°C. BAAA in the presence of ALDH enzyme is converted to fluorescent BODIPY-aminoacetate (BAA) which is negatively charged thus, live cells retain the product causing the cell to fluorescence. CSCs are identified by flow cytometry as cells with higher fluorescence due to higher levels of ALDH. ALDH activity was measured by LSRFortessa (BD Biosciences, USA). As a

negative control, an aliquot of samples were treated with ALDH inhibitor, diethylaminobenzaldehyde (DEAB) at a concentration of 50 mM.

For double staining SCLC cells with ALDH and CD133-1-APC, samples were initially labelled for ALDH activity and subsequently CD133 expression. The staining procedure for ALDH activity and CD133 expression was as described above. However, after labelling cells with CD133 antibody, samples were re-suspended and washed with Aldefluor buffer containing 0.5% BSA instead of MACS buffer. This was based on the knowledge that the Aldefluor assay buffer contains specific inhibitors necessary to maintain Aldefluor reaction products inside the cell, allowing detection of ALDH+ population. Samples labelled with mouse IgG1-APC, DEAB, and double stained with mouse IgG1-APC and DEAB were used as negative controls.

2.10 Self-renewal (maintaining stem cell-like phenotype) and differentiation

The self-renewing potential of CD133-expressing cells was evaluated based on the ability of these cells to retain the expression of the stem cell marker CD133 after 30 days of culturing in SITA medium. CD133+ and CD133- H345 sorted cells and parent (unsorted) cells were immediately transferred into SITA medium, a well characterised serum-free medium appropriate for SCLC *in vitro* growth. Cells were cultured in SITA medium for 30 days and were maintained in suspension at 1-3 × 10^6 cells/ml and were passaged into fresh medium twice a week. 30 days post-culturing, 1 × 10^6 viable cells were stained with CD133-2-PE and the expression of CD133 (epitope-2 of this antigen) was analysed by flow cytometry (for details of CD133 staining see section 2.8).

The self-renewing potential of cells was also assessed by the ability of CD133+ cells to maintain their colony forming ability after long periods in culture. Therefore, 10^4 viable cells cultured for 30 days in SITA medium were transferred into semi-solid SITA medium (for details of colony assay see section 2.7). After 21 days the cloning efficiency was determined using light microscopy.

To assess the differentiation potential, H345 sorted and unsorted parent cells were immediately plated in RPMI 1640 complete medium (serum-containing medium) for 30 days and were maintained in suspension at 1-3 × 10^6 cells/ml and were passaged into fresh medium twice a week. After this period, 1 × 10^6 viable cells were stained with CD133-2-PE and the expression of CD133 was analysed by flow cytometry.

Additionally, to confirm differentiation, the colony forming ability and liquid growth potential of the sorted populations cultured in serum containing media was evaluated. For colony assay, 10^4 viable cells maintained in serum-containing medium for 30 days were transferred into semi-solid RPMI 1640 complete medium (for details of colony assay see section 2.7). After 21 days the cloning efficiency was determined using light microscopy. For liquid growth, cultured cells for prolong period in serum containing medium were transferred in fresh RPMI 1640 complete medium at a density of 1 × 10^4 cells/well. Cell number was determined every 2 days using NucleoCounter NC-100 (ChemoMetec, Denmark) over 24 days (for details of liquid growth assay see section 2.4).

2.11 Assessment of apoptosis

2.11.1 Ethidium bromide/acridine orange staining

SCLC cells were plated into 96-well plates at a density of 1 × 10^4 cells/well in SITA medium containing test compounds and apoptosis was assessed after 72 hours exposure by the addition of 1μl of ethidium bromide (EB) (1mg/ml) and 1μl of acridine orange (AO) (1mg/ml) (Sigma-Aldrich, UK). Samples were mixed gently and after 2 minutes the percentage of apoptotic cells were determined by fluorescent microscopy (Olympus BH2 fluorescence microscope). The assay is based on the loss of plasma membrane integrity during cell death. The cationic dye, AO, can cross the plasma membrane of viable and apoptotic cells, which when intercalated with DNA can be excited and emits green fluorescence. Conversely, EB is unable to penetrate the intact cell membrane of viable and early apoptotic cells. With apoptosis membrane permeability increases and apoptotic cells stain with both EB and AO.

However, EB has higher intensity emission and on binding to DNA emits orange fluorescence on excitation, therefore, apoptotic cells appear orange. Viable cells and cells at different stages of apoptosis can be identified based on their fluorescence and their morphology (Figure 7);

Healthy viable cells:	Green nucleus
Early apoptotic cells:	Shrunken cells with green nucleus
Late apoptotic cells:	Shrunken cells with orange nucleus
Necrotic cells:	Swollen cells with orange nucleus

Figure 7

2.11.2 Morphological assessment

Apoptosis was also assessed based on the morphology of cells. Cells were cytocentrifuged at 300 × g for 3 minutes onto glass slides using a Cytospin 3 (Shandon, USA). Slides were then air dried, fixed in methanol for 2 minutes and stained with May-Grunwald-Giemsa. Cell morphology was examined using an Olympus BH2 microscope. Apoptotic cells were shrunken cells with dense nuclei (Figure 8).

Figure 8

2.12 SCLC Xenograft

All animal studies were performed on six week old female CD1 *nude/nude* mice (Harland, UK) which were maintained in 12 hours light/12 hour dark cycles with free access to food and water. All procedures were performed in accordance with Home Office guidelines [Animals (Scientific procedures) Act 1986].

2.12.1 Peptide-1 *in vivo* efficiency

15×10^6 H345 cells suspended in growth factor reduced Matrigel (1:1 volume of cells:Matrigel mixed at 4°C, total volume of 100 µl) were implanted subcutaneously in the right flank of *nude/nude* mice. Tumours were palpable 3 days post-injection. Drug exposure was initiated on day 7 and was continued once daily for 5 consecutive days. Peptide-1 was dissolved in sterile distilled H_2O and administered by subcutaneous injection at a dose of 25 mg/kg. Etoposide dissolved in sterile distilled H_2O and was administered by subcutaneous injection at 15 mg/kg. Controls received the same dose schedule of vehicle (H_2O). Tumours were measured using callipers every 3-4 days for a total of 33 days. Tumour volume was calculated as below:

$$\text{Volume} = (\text{Length})^2 \times \text{Width}/2$$

2.12.2 CD133+ tumorigenicity

Various cell numbers of sorted CD133+ and CD133- H345 cells (5×10^5, 1×10^5, and 1×10^4) in growth factor reduced Matrigel (BD Biosciences, USA) (1:1 volume of cells:Matrigel mixed at 4°C, total volume of 100 µl) were implanted subcutaneously in contralateral flanks of *nude/nude* mice (4 animals per condition). Same numbers of unsorted parent H345 cells with the same method of preparation were implanted subcutaneously into the right flank of *nude/nude* mice (4 animals per condition). Tumour size was assessed with callipers every 3-4 days.

2.13 Immunohistochemistry

Immunohistochemistry (IHC) can detect and visualise antigens at cellular levels by using primary and secondary antibodies to indirectly identify antigens in paraffin-embedded or frozen tissue sections. Formalin-fixed, paraffin-embedded SCLC resection specimens were de-waxed in xylene (Fisher Scientific, UK) for 10 minutes and were rehydrated through graded ethanol (100% → 90% → 70%, 20 seconds each) and rinsed in water. Tissue sections were then heated in 740 ml distilled water plus 7.5 ml antigen retrieval solution (Vector Laboratories, USA) which is based on a citric acid formula using a 750W microwave oven for 15 minutes at maximum power. Sections were cooled in running tap water for 15 minutes. Endogenous peroxidase activity was blocked in 3% hydrogen peroxide (VWR international, UK) (v/v in distilled water) for 15 minutes, rinsed once with TBS. After non-specific binding was blocked using serum free protein block and avidin/biotin blocking kit (Vector Laboratories, USA), the sections were incubated with the primary antibody, CD133 (diluted to 1:100 in antibody diluent, DAKO, UK) overnight at 4°C. After 3 × 5 minutes washes with TBS, sections were labelled with biotinylated donkey anti-rabbit IgG (H+L) secondary antibody (diluted 1:200 in antibody diluent) for 30 minutes at room temperature. Slides were rinsed 3 × 5 minutes with TBS and incubated with 3 drops of avidin:biotinylated enzyme complex (ABC) (Vector Laboratories, USA) per slide for 30 minutes at room temperature and washed × 3 with TBS. Diaminobenzidine (DAB) (DAKO, UK) solution prepared with substrate as per manufacturers instructions was applied for 5 minutes at room temperature. Slides were rinsed × 3 in TBS, counterstained for 30 seconds with Mayers haematoxylin (Thermo Shandon, UK) and 30 seconds in Scotts tap water (83 mM $MgSO_4$, 7.1 mM $NaHCO_3$ in tap water), dehydrated through graded ethanol (70% → 90% → 100%), and cleared in xylene. Slides were mounted using Pertex mounting solution (CellPath Hemel Hempstead, UK). In each experiment, negative controls of secondary antibody only were performed. Images were acquired using a Leica DM LB light microscope, Leica DC 300 digital camera and Leica IM50 software.

For staining sections with CD45 and NCAM antibodies, IHC was performed using ImmPRESS™ system (Vectore Laboratories, USA) which is based on the method of polymerizing enzymes and attaching these polymers to antibodies. The advantage of this system is it provides high signal intensity with minimal background staining in IHC. In this study, ImmPRESS™ anti-rat Ig reagent was used for staining sections with CD45 antibody raised in rat, and ImmPRESS™ anti-Rabbit Ig reagent was used for staining sections with NCAM antibody raised in rabbit. The ImmPRESS™ anti-rat Ig, and anti-rabbit Ig reagents contain a "micropolymer" of an active peroxidase coupled to affinity-purifies anti-rat IgG (H+L) secondary antibody and affinity-purifies anti-rabbit IgG (H+L) secondary antibody, respectively. The method used was performed as manufacturers' protocol. In brief, formalin-fixed, paraffin-embedded SCLC resection specimens were de-waxed in xylene for 10 minutes and were rehydrated through graded ethanol (100% → 90% → 70%, 20 seconds each) and rinsed in water. Antigen retrieval was performed by boiling samples in 10 mM citrate (pH 6.0) for 5 minutes. Sections were cooled in running tap water for 15 minutes. Endogenous peroxidase activity was blocked in 3% hydrogen peroxide (v/v in distilled water) for 15 minutes and subsequently rinsed once with TBS. Non-specific binding was blocked with 3 drops of ready to use (2.5%) goat serum or horse serum provided by the kit for 30 minutes at room temperature (20-25°C) and rinsed once for 5 minutes in TBS. Both CD45 and NCAM antibodies were diluted 1:500 in blocking serum and incubated overnight. After washing samples 3 × 5 minutes in TBS, sections were incubated with 1 drop of appropriate ImmPRESS reagent for 30 minutes in room temperature and washed again for 3 × 5 minutes with TBS.

To amplify the signal of interest, samples were treated with Tyramide Signal Amplification (TSA) plus Cyanine-3 kit (PerkinElmer, USA) for CD45 stained sections or TSA plus Fluorescein kit (PerkinElmer, USA) for NCAM stained sections. CD45 and NCAM stained samples were treated with 1:50 dilution of the appropriate TSA plus amplification reagent for 10 minutes in the dark at room temperature. Sections were then washed 3 × 5 minutes with TBS, in the last wash DAPI at a concentration of 0.1 µg/ml was added to stain the nuclei. Sections were

mounted with PermaFluor Aqueous Mounting Medium (ThermoFisher Scientific, USA). Cells were analysed using Confocal microscopy (Zeiss Axiovert 100M, UK)

2.14 Quantitative PCR (q-PCR)

2.14.1 RNA extraction

RNA was prepared from, 2×10^6 H345 and H69 cells using the RNeasy Mini Kit and QIAshredder columns (Qiagen, Netherlands) according to the manufacturer's instruction. RNA concentrations, purity and quality of the samples were determined using the NanoDrop 1000 spectrophotometer (Thermo Scientific, USA) and RNA was stored at -80°C until further use.

2.14.2 DNase treatment of RNA

DNase treatment of RNA was performed in a sterile eppendorf by adding 2 µl RQ1 RNase (Promega, USA) and 2 µl 10 × reaction buffer (Promega, USA) to 2 µg RNA, made up to final volume of 20 µl with nuclease-free H_20 ($_{NF}H_2O$). Samples were incubated for 30 minutes at 37°C and the reaction was terminated by adding 2 µl RQ1 DNase stop solution (Promega, USA) and incubated at 65°C for 10 minutes. 'Clean' RNA was stored at -80°C until further use.

2.14.3 Real-Time Reverse Transcription-PCR (Real-Time RT-PCR)

Clean RNA samples were reverse transcribed to cDNA using TaqMan® reverse transcription reagents (Applied Biosystems, USA). The following volumes were used per RT-PCR reaction:

1x Reaction mix:		Conditions:	
10 × TaqMan RT buffer	4 µl	25°C	10 min
25 µM $Mgcl_2$	8.8 µl	48°C	40 min
dNTP	8 µl	95°C	5 min
Random Hexamers	2 µl	4°C	hold
RNase inhibitor	0.8 µl		
Multiscribe reverse transcriptase	1 µl		
RNA	15.4 µl		
Total Volume	40 µl		

The RT-PCR reaction was performed in a PTC-100 programmable thermal controller (MJ Research Inc., Canada). Samples were stored at -20°C.

2.14.4 Quantitative PCR

Every experiment was carried out under sterile conditions using filter tips and sterile $_{NF}H_2O$. The expression levels of GRP-R and V_{1A}-R in the isolated cells were quantified using the TaqMan® gene expression assay kit (Applied Biosystems, USA). 18S rRNA primer probe mix was purchased from (Applied Biosystems, USA) and was used as internal control. Volumes used per PCR reaction were,

1x Reaction mix:

TaqMan mastermix (Applied Biosystems)	12.5 µl
18S Probe (primer/probe)	1.25 µl
TaqMan® gene expression assay (5x)	5 µl
$_{NF}H_20$	3.75 µl

Each reaction was prepared in triplicates containing 2.5 µl cDNA or $_{NF}H_2O$, giving a total volume of 25 µl, and transferred to Micro Amp Optical 96-well reaction plates. The q-PCR reaction was carried out in a 7500 fast Real-Time PCR system (Applied Biosystems, USA) and data was analysed using the System detection software (7500 fast system SDS software) using the 2-ΔΔct calculation method (Applied Biosystems, USA). Gene expression is shown as fold increase as compared to an external calibrator which was a pool of experimental cDNA. Water only was used as

a negative control since these primer/probe kits did not amplify genomic DNA and would only detect gene expression.

2.15 Liver S9 preparation

Liver S9 fractions are sub-cellular fractions most frequently used to measure drug metabolism. It is defined as the supernatant fraction usually obtained from the liver homogenate following centrifugation at 9000 × g for 20 minutes in appropriate solutions. S9 fraction is rich in drug-metabolizing enzymes including the cytochromes P450, flavin monooxygenases, and UDP glucuronyl transferases [232, 233]. Livers from female C57BL/6 mice were removed and washed twice with cold potassium phosphate buffer 0.1 M (50 mM KCl, 5 mM EDTA, pH ~7.4). Liver tissue was homogenised using a glass Teflon homogeniser in phosphate buffer to give a final homogenate consisting of 25 % w/v tissue (Figure 9). Samples were centrifuged at 9000 × g for 20 minutes at 4°C and the supernatant was stored on ice. Protein concentration was determined using BCA protein assay reagent (Pierce, USA).

The metabolism of SP-G and peptide-1 was studied by adding the drugs at a final concentration of 0.1 mg/ml into 2 ml of incubation mixture containing the S9 liver prep (equivalent to 4 mg of protein) and PBS. Reactions were incubated at 37°C with a continuous gentle shake. In order to stop the reactions, at appropriate time points, 100 µl of the incubation mixture was removed and added to 200 µl of eluting buffer (methanol:1M ammonium acetate (90:10 v/v)) followed by vigorous vortexing. Samples were then centrifuged at 1300 × g for 3 minutes and the supernatant was frozen at -80°C until analysed by High Performance Liquid Chromatography (HPLC).

Figure 9

2.16 HPLC

HPLC analysis was kindly conducted by Doctor Nikolaos Avlonitis in Professor Mark Bradley's laboratory, Institute of Chemistry, Edinburgh University. HPLC was carried out on liquid chromatograph consisting of a Model 500 solvent delivery system, a Model 680 controller, a Wisp autosampler (all from Waters, UK), a Model 5100A coulochem electrochemical detector with pre-colum Model 5020 guard cell and a twin electrode (D1 and D2) Model 5011 high sensitivity analytical cell (ESA inc). The stationary phase was μ-Bondpack C18 packed in a 30 cm x 3.9 mm I.D. stainless steel column (Waters, UK) and the mobile phase consisted of 0.15% TFA in 10 mM ammonium acetate (PH 2.75)-acetonitrile: 60:40 (v/v).

2.17 Determination of intracellular Ca^{2+} concentration

Intracellular calcium concentration was measured using Fura-2 (Invitrogen, UK), a UV-excited chemical indicator. Fura-2 was chosen for the Ca^{2+} studies based on its features including, the ability to exhibit high fluorescence which allows measurements at intracellular concentrations, low Ca^{2+} affinity, and favourable spectral properties, including shift in absorption upon binding to Ca^{2+}. Additionally, Fura-2 allows ratiometric measurements by computing the ratio of the fluorescence at two wavelengths thus, considerably reducing the effects of photobleaching, leakage of dye, and uneven dye loading, as well as problems associated with measuring Ca^{2+} in cells of unequal thickness [234, 235].

G6A and V3B cells were grown to 50-70% confluence in DMEM complete medium, washed twice with PBS and quiesced overnight in DMEM quiescent medium (for details of culture medium used see section 2.3). Cells were then trypsinised, and to subsequently inhibit the affect of trypsin 1mg/ml soya bean trypsin inhibitor was added to the cell suspension. Cells were centrifuged at 300 × g for 5 min and the cell pellets were re-suspended in hanks buffered salt solution (HBSS) without calcium at 5×10^6 cells/ml and were transferred into 2 ml eppendorf. 1μM FURA-2-tetraacetoxymethylester AME (FURA-2-AM) (Merck Millipore, Germany) was

added and samples were incubated at 37°C for 20 minutes. The cell suspension was centrifuged at 300 × g for 5 minutes and re-suspended in 2 ml of HBSS with calcium, transferred to a cuvette and stirred continuously at 37°C. Fluorescence was recorded in a Model F2000 fluorescence spectrophotometer (Hitachi, Japan). Alternate dual wavelength excitation at 380 nm and 410 nm allowed ratiometric analysis of bound and unbound FURA-2AM when measured at 505 nm. Intracellular Ca^{2+} concentration was calculated according to the equation:

$$[Ca^{2+}] = K(F-F_{min})/(F_{max}-F),$$

F is the ratio of the unknown sample, F_{max} is the ratio after the addition of 0.1% triton X-100 causing cell membrane fracturing therefore release of all intracellular calcium, and F_{min} is the ratio after Ca^{2+} chelation with 10 mM EGTA. K is the dissociation constant for Fura-2, which is 224 nM.

2.18 Statistical analysis

Results are reported as pooled data from a series of separate experiments and presented as mean ± standard error mean (SEM). Statistical significance was mainly analysed by two-tailed Student's *t* test and in the other cases by two-way analysis of variance (ANOVA) (Prism Software). Statistical significance was assigned to data returning a P value of less than 0.05.

CHAPTER 3:
Human SCLC cell lines are clonogenic and chemoresistant and a sub-population of these cells express stem cell markers which can be isolated by fluorescent activated cell sorting

3.1 Introduction

Rapid growth, highly invasive and metastatic potentials and almost inevitable recurrence despite initial chemo- and radiosensitivity has made SCLC one of the most challenging diseases to cure. Despite a multitude of studies in unveiling the pathogenesis of resistance in SCLC, so far methods to circumvent resistance have not been successful in clinical practice. The presence of chemoresistant cells with a stem cell-like phenotype known as cancer stem cells (CSCs) is the proposed cause of treatment resistance in cancer patients with tumour recurrence after therapy. Thus, novel interventional strategies based on CSC elimination should be designed.

An accurate detection and pure isolation of CSCs is essential for their characterisation. Lung CSC identification is commonly based on the expression of surface proteins such CD133 and cellular characteristics including high ALDH enzyme activity and the ability to form tumour spheres [79, 236]. CD133 is one of the most commonly used markers for lung CSC detection [79, 84, 118, 158, 236, 237]. Cells expressing CD133 are chemoresistant, tumorigenic and exhibit stem cell-like features such as the expression of Oct-4, and the ability to self-renew and differentiate [79, 82, 158]. Common methods for isolation of CSCs include magnetic-activated cell sorting (MACS®), fluorescent-activated cell sorting (FACS) and selection of tumour spheres. FACS has been routinely used for the study of CSCs. This method enables simultaneous multi-parametric analysis of physical and/or chemical characteristic of viable cells with high performance and accuracy as well as isolation of cells of interest on the basis of specific marker expression or functional characteristics [238].

As SCLC tumours are rarely resected and fresh specimens are often inaccessible, in the present study two human SCLC cell lines, H345 and H69 were utilised and the

expression of CD133, Oct-4 and ALDH activity was evaluated. To characterise prospective SCLC CSCs, two methods of isolation were used, MACS and FACS. If the presence of a CSC sub-population within tumours is the proposed cause of tumour resistance to therapy and recurrence, therefore, characterisation of such cells within SCLC could be a possible explanation for the aggressive phenotype of this disease.

3.2 Results

3.2.1 Human SCLC cell lines, H345 and H69 are chemoresistant and clonogenic

Human SCLC cell lines, H345 and H69 were established from patients who had relapsed after initial therapy. Both cell lines were derived from metastatic sites - H345 cells from bone marrow and H69 cells from pleural effusion [239]. As shown previously [239], these cells grow in suspension as cellular aggregates (Figure 10A), indicative of their anchorage-independent growth and subsequently their possible tumorigenic and metastatic potentials *in vivo*. The sensitivity of the cells to chemotherapy was assessed by MTT assay (Figure 10B). H345 and H69 cells were treated with etoposide, the most commonly used chemotherapeutic agent for SCLC treatment, and cytotoxity was determined after 72 hours. Results are expressed as percentage of untreated cells and the potency. Even high doses of 100 µg/ml of etoposide were relatively insufficient to inhibit 50% of the H345 and H69 cell viability (Figure 10B). This confirmed the chemoresistant phenotype of both SCLC cells and correlated with the knowledge that these cells were isolated from patients who were already resistant to chemotherapy.

Colony assay reflects the ability of a single cell to survive anchorage-independent growth and its stem cell-like feature to undergo unlimited division [144, 240, 241]. This assay is the gold standard *in vitro* method that reflects the tumorigenic potential of cells *in vivo* [241, 242]. In this study, a colony was defined to consist of >16 cells. The cloning efficiency of H345 and H69 was 1.8 ± 0.25% and 3.23 ± 0.36%, respectively (Figure 10C). Despite the ability of these cells to form colonies in the

semi-solid medium, not all cells cultured were clonogenic indicative of cellular heterogeneity within the SCLC cells.

Figure 10

3.2.2 H345 and H69 SCLC cell lines express stem cell markers

The protein levels of CSC markers CD133 and Oct-4 were examined in H345 and H69 cell lines by western blotting. A band of ~120 kDa and ~48 kDa were representative of presence of CD133 and Oct-4 proteins, respectively (Figure 11A). β-actin, a housekeeping gene and a major component of the cytoskeleton was used as a loading control [243]. Therefore, the human SCLC cells retain a population of cells expressing stem cells markers.

Increased ALDH enzyme activity has proven to be a reliable marker for the selection of CSCs [151, 236]. The 'gold standard' of studying the activity of ALDH is using the commercial reagent ALDEFLUOR® (STEMCELL™ technologies, Canada) which allows the assessment of functional activity of ALDH1 in viable cells (Figure 12). In this method, the uncharged ADLFLUOR substrate, BODIPY aminoacetaldehyde (BAAA) in viable cells is taken up by passive diffusion. In the presence of ALDH, specifically ALDH1, BAAA is converted to negatively-charged BODIPY-aminoacetate (BAA^-). BAA^- is fluorescent and is retained inside the cell due to its negative charge in addition to the presence of ABC-transporter inhibitors in the assay buffer which inhibits compound efflux, causing the cells with high ALDH activity (ALDH+) to become highly fluorescent. Using appropriate sorting gates (review section 3.2.4 for selection of gates for flow cytometry analyses) the ALDH+ can be identified and isolated by flow cytometry. Diethylaminobenzaldehyde (DEAB), and ALDH inhibitor was used as a negative control. In the present study 16.3 ± 0.23% of H345 cells (Figure 11B1-B3) and 19.56 ± 0.5% of H69 cells (Figure 11C1-C3) had high ALDH activity. The gates were chosen relative to DEAB samples.

Figure 11

Figure 12

3.2.3 H345 and H69 SCLC cell lines express CD133

CD133 is the most commonly used CSC marker and has consistently selected the stem cell-like, chemoresistant and tumorigenic lung cancer cells [79, 82, 84, 118, 158, 237, 244]. Therefore, CD133 expression was chosen as a maker to identify and isolated putative SCLC CSCs. Two monoclonal antibodies, CD133-1-APC (clone AC131) and CD133-2-PE (clone AC141), commercially available from Miltenyi Biotec, Germany, have been commonly used for the detection of CD133 expressing cells. CD133-1-APC binds to glycosylated epitope-1 of the CD133 antigen and CD133-2-PE binds to glycosylated epitope-2 of this antigen. Due to the cross reactivity of the CD133-2-PE antibody with cytokeratin-18 [115], in the present study, CD133-1-APC was utilised for the identification of CD133 expressing SCLC cells and CD133-2-PE antibody was used to confirm the purity of cells isolated based on the epitope-1.

To confirm all cells positive for CD133 epitope-1 are also positive for CD133 epitope-2, H345 and H69 were double stained with CD133-1-APC and CD133-2-PE. Cells stained with APC-conjugated or PE-conjugated isotype-matched mouse IgG were used as negative controls (isotype control). The gate for the isotype control was chosen so that the value in the gate would be >1% for the isotype control. As shown in Figure 13A-A1, 13.1% of H345 cells were positive for epitope-1 and as shown in Figure 13B-B1, 86.4% of H345 cells were positive for epitope-2. Higher percentage of cells expressing epitope-2 could be associated with cross-reactivity of the monoclonal antibody. Interestingly, when analysing cells co-stained with both antibodies (Figure 13C-C1), 13.1% of H345 cells were double positive (note the similarity in the percentage between cells positive for eptiope-1 and cells double positive for epitope-1 and -2, both show ~13% positivity), 68.4% of cells were epitope-2+ and very low levels were epitope-1+ (0.03%), indicating that most cells expressing the CD133 epitope-1 also express CD133 epitope-2, but not all epitope-2+ cells are epitope-1+.

Similar observation was made in H69 cells (Figure 14). In these cells, 23.9% of cells were epitope-1+ (Figure 14A-A1) and 88.9% of cells were epitope-2+ (Figure 14B-B1). When co-staining H69 cells for both antibodies (Figure 14C-C1), 23.3% of cells were double positive for both epitopes whereas very few epitope-1+ cells did not express the CD133 epitope-2 (0.061%) indicating almost all epitope-1+ cells also express the CD133 epitope-2. These data indicate that epitope-1 of the CD133 antigen is ideal for selection of cells expressing CD133. Therefore, in this study the presence of CD133 antigen will be evaluated based on the presence of its epitope-1 using CD133-1-APC antibody. Positivity of CD133 expressing cells will be confirmed using CD133-2-PE which detects epitope-2 of the antigen. In this thesis, cells expressing the CD133 epitope-1 will be termed as CD133-1 cells and cells expressing epitope-2 will be termed as CD133-2. To be noted, despite the primary selection of cells has been based on CD133-1-APC antibody and CD133-2-PE antibody has been utilised for the confirmation of CD133 expression post cell sorting, in order to discard the possibility that CD133-2 positivity is a consequence of cross-reactivity with cytokeratine-18, in future experiments using CD133-2-PE antibody should be repeated using the CD133-1-APC antibody.

Figure 15, is a representative histogram of CD133-1 expression on H345 and H69 cells. In H345 cells 18 ± 1.24% and in H69 cells 22 ± 1.76% of the population was CD133+, relative to isotype control. The expression pattern of CD133 was continuous rather than showing discrete positive and negative populations. This data is consistent with previous observations where a gaussian rather than a bimodal pattern of CD133 expression was detected in SCLC cell lines [79, 80, 236] .

Figure 13

Figure 14

Figure 15

3.2.4 Fluorescent activated cell sorting produces pure isolation of CD133+ and CD133- cells

CD133+ and CD133- H345 cells were isolated by the MACS® method using the CD133 MicroBead Kit (Miltenyi Biotec, Germany). This kit is designed for the positive selection of CD133+ cells (for more details see materials and methods). The principle of the MACS® separation is that cells positive for the CD133 antigen are magnetically labelled with CD133 MicroBeads (magnetic nanoparticles coated with CD133 antibody). The cell suspension is then loaded on to the appropriate MACS® Column which is placed onto the MACS Separator unit that contains a magnetic field. The magnetically labelled CD133+ cells will be trapped in the column and the unlabelled cells will run through, thereby, positively selecting for the CD133+ population. The positive population can be retained by removing the column from the magnetic field and flushing the column with 1 ml of buffer. To increase the purity of the isolated population, both cell fractions, the positively selected and the negatively selected cells, were passed over a second column. The purity of the isolated cells was evaluated by flow cytometry, by staining cells with CD133-2-PE (recommended by the protocol) to determine the efficiency of the separation (Figure 16). To compare the expression levels of CD133-2 between the isolated populations, Geometric mean (GM) value was calculated. No difference in GM values of CD133- (Figure 16A1) and CD133+ (Figure 16A2) selected populations could be observed, indicating CD133 MicroBead Kit did not select a pure populations. Therefore, CD133 MicroBeads was not suitable for isolation of CD133 expressing cells in human SCLC cell lines.

Figure 16

FACS is the most common method for selection of CSCs [78-80]. In the present study, this method allowed isolation of cells of interest based on the expression of CD133-1. In brief, a cell suspension labelled with APC conjugated CD133-1 is directed into a thin stream of fluid forcing cells to pass in single file (Figure 17). The stream of fluid by passing through a vibrating nozzle breaks into droplets. Some of these droplets may contain single cells. A laser beam is directed at the stream just before it breaks up into droplets. When a labelled cell passes through the laser beam, it emits light. The scattered light and the emitted fluorescence is captured by a number of detectors including detectors in line with the axis of the light beam (forward scatter, FSC), perpendiculars to axis of the beam (side scatter, SSC) and the fluorescence detectors. The intensity of FSC correlates with the size of cells and the intensity of SSC depends on the shape and intracellular complexity of the cells. If the signals from the detectors match the criteria set for size, shape and fluorescence, a positive or negative electrical charge is given to the fluidic stream. The droplets then pass through a pair of charged plates so that the charged droplets are deflected and collected.

Figure 17

The populations of interest are chosen based on selecting specific gates. A gate in flow cytometry is a set of chosen boundaries that serve to select the population of interest from the total cell population. Before gating on the CD133+ and CD133- populations, single and viable cells were selected from the total population. The presence of cell clumps within samples could reduce the purity of the cell sorting. For example, if a positive event were measured at the same time as a negative event in a cell clump, both would be selected and isolated because the software considers it as a single positive event. On the other hand, dead cells could bind non-specifically to the antibody causing false-positive results. Therefore, it is important to exclude the cell clumps and dead cells. Populations of interest were initially selected based on their FSC and SSC and viability judged by propidium iodide (PI) exclusion (Figure 18A, B1, and B2). PI is membrane impermeant and generally excluded from viable cells. Population-2 contained the majority of the viable cells (PI positive 4.48 ± 0.81%) (Figure 18B2) whereas most cells within the population-1 were dead (PI positive 94.54 ± 0.76%) or debris (particles smaller than cells) (Figure 18B1). Debris can be excluded based on their low FSC and SSC and dead cells can be excluded by their lower FSC and higher SSC compared to the living cells in addition to their response to PI. To increase the accuracy during the cell selection, cells within population-2 were gated on their FSC- Height (FSC-H) and FSC-Area (FSC-A) distribution to select on the single cells (Figure 18C). Using FSC-H allows measurement of how long a particle takes to traverse the laser beam. Cell clumps and doublets tend to become orientated lengthways while travelling the stream of fluid therefore, can be excluded on the basis of their pulse Height [245]. This was followed by selecting on the viable cells within the single cell gate (Figure 18D) based on their PI intensity. Since CD133 exhibits a gaussian expression pattern, the top ~7% of the cells with high expression of CD133 and the bottom ~7% of the cells with low/no CD133 expression (based on the isotype control distribution) were gated and subsequently sorted (Figure 18E).

Figure 18

To confirm a successful isolation, the purity of the sorted cells was evaluated based on the expression of CD133-1. Re-analysing sorted cells based on CD133-1 expression (an epitope of CD133 initially selected for cell sorting) would allow evaluating if the sorted populations would re-appear in the same gates as they were initially selected. Figure 19A1-3 illustrates CD133-1 levels on H345 parent (unsorted) cells (Figure 19A1), overlay histogram of CD133+ and CD133- H345 cells (Figure 19A2), and overlay histogram of all three populations (Figure 19A3). To compare the fluorescence on each population, GM was calculated. This permits comparison of the amount of antibody binding to the CD133 expressing cells; higher GM would correlate with higher CD133 expression. The GM of CD133+ was 22.40 ± 2.37, the GM of CD133- cells was 2.36 ± 0.32, and the GM of parent cells was 8.98 ± 1.51. These values indicate that CD133+ cells are the most fluorescent cells and based on the sorting layouts, the two population of CD133+ and CD133- are distinct with CD133+ cells having significantly higher levels of this antigen (P=0.0012). The overlay histogram of 19A3 demonstrates that compared to parent cells, CD133+ population is enriched for cells with CD133 antigen and are therefore located at the top arm of parent population where the CD133+ gate for sorting was chosen, whereas CD133- population contains cells with no CD133 antigen expression and are therefore located at the lower arm of the parent cells where the CD133- gate for sorting was selected. This data indicates that cell sorting by FACS produced pure isolations.

Purity of the sorted cells was further analysed using CD133-2-PE antibody that recognises the epitope-2 of the CD133 antigen (Figure 19B1-B3). As demonstrated earlier, Figures 13 and 14, SCLC cells positive for CD133-1 are also positive for CD133-2. Therefore assessing the presence of CD133 antigen via its epitope-2 could further confirm the purity of the isolated populations. Sorted cells were immediately stained with the CD133-2-PE antibody and were analysed by flow cytometry. To compare the intensity of fluorescence on each population, GM was calculated. The GM in the CD133+, CD133-, and parent cells were 125 ± 3.6, 3.03 ± 0.62, and 25.09 ± 1.68, respectively. Therefore, CD133-1+ cells are enriched in cells positive for

CD133-2 and its expression is higher than that of CD133- and parent cells further indicating the purity of sorted cells.

Figure 19

The purity of sorted populations was further analysed by the CD133 protein levels in the sorted cells (Figure 20). This was to rule out the possibility that the cell selection was based on non-specific staining. CD133 is 95 kDa in length however, in line with previous data documented [110], this protein was detected at approximately at 120 kDa by western blot due to glycosylation of the protein in both CD133+ and parent cells. No protein expression in the CD133- population could be detected. β-actin was used as a loading control.

Figure 20

To confirm that selection of CD133+ and CD133- was not associated with their cellular size (bigger cells would have higher levels of CD133 antigen compared to smaller cells) but was associated with the levels of CD133 expression, the size of sorted CD133+ cells was compared with that of CD133- cells by flow cytometry and standard microscopy. Figure 21A is representative histogram illustrating the FSC distribution of CD133+ and CD133- H345 cells. As shown, no significant differences in cellular size between the sorted populations could be observed indicating that CD133+ and CD133- are similar in their size. This was further confirmed by microscopically evaluating the appearance of the sorted cells (Figure 21B). Three days post sorting cells cultured in SITA medium were cytocentrifuged onto glass cover slips and stained with May-Grunwald-Giemsa, to visualise the cells as well as distinguish viable from dead cells. As illustrated in Figure 21B, in both cell lines, CD133+ and CD133- populations exhibited similar morphology. Additionally, the tissue culture appearance of the sorted population was evaluated by observing the three days post-sorted cells cultured in SITA medium under standard microscopy (Figure 21C). Similar to parent cells (unsorted cells), in both H345 and H69 cells, CD133- and CD133+ grew as floating aggregates with no differences in the shape or size of the cellular clumps. These observations indicate that CD133+ and CD133- cells share similar morphology and that isolation of these cells using FACS is solely associated with differences in the expression levels of CD133 on these cells.

Figure 21

To confirm that the process of cell sorting does not effect cell viability, the percentage of apoptosis in CD133-, CD133+ and parent cells, 5 days post-sorting was evaluated by May-Grunwald-Giemsa and ethidium bromide/acridine orange (EB/AO) staining. Apoptotic cells in May-Grunwald-Giemsa staining appeared as shrunken cells with dense nuclei (Figure 22A). All three cell populations exhibited a similar percentage of apoptosis (Figure 22C1 and C2). In EB/AO staining, cells were stained with the fluorescent dyes and viability was judged based on nuclear morphology and fluorescence. Viable cells (green nucleus), apoptotic cells (early apoptotic, shrunken cells with green nucleus and late apoptotic cells, shrunken cells with orange nucleus) and necrotic cells (swollen cells with orange nucleus) were distinguished (Figure 22B). Figure 22D1 and D2 illustrates no significant differences in the percentage of apoptosis between the three populations. Therefore, the process of cells sorting does not affect the viability of sorted populations.

Figure 22

3.3 Discussion

The results in this chapter demonstrated that the two human SCLC cells lines, H345 and H69, were chemoresistant and clonogenic in culture and contained a population of cells which expressed CSC makers including CD133, Oct-4 and ALDH. CD133+ H345 and H69 cells could be isolated by FACS with high purity.

H345 and H69 were established from patients who had relapsed after initial therapy. In line with their clinical chemoresistant characteristic, H345 and H69 cells were resistant to etoposide *in vitro* and even a high dose of 100 μg/ml was relatively insufficient to eradicate 50% of these cells. Previously, findings in my laboratory showed β1-integrin mediated SCLC cell interaction with extra cellular matrix (ECM) components leads to activation of PI3K which inhibits etoposide-induced caspase-3 activation and therefore inhibits apoptosis [246]. Chemoresistance can also be a result of increased expression of anti-apoptotic proteins such as Bcl-2, increased expression of cell surface efflux pumps such as P-gp and/or reduced topoisomerase II activity [247-250].

In addition to the molecular mechanism associated with treatment resistance, multiple studies have documented the presence of CD133+ cells as the cause of cancer chemoresistance [79, 82, 84, 141]. CD133+ cells, due to their resistant phenotype, escape therapeutic insults and are instead enriched after chemotherapy. SCLC cell lines used in this study were derived from relapsed patients. The presence of CSCs was confirmed by the expression of CD133, Oct-4 and ALDH in H345 and H69 cells. Therefore, it can be proposed that increased resistance to etoposide observed in both cell lines could be associated with enrichment of the drug resistant CSCs. To confirm this concept, it would be essential to evaluate the percentage of CSCs in cell lines derived from SCLC patients before and after treatment.

Anchorage-independent proliferation is an essential hall-mark of tumour cells with colony forming ability *in vitro* and metastatic potential *in vivo* [240, 241]. As demonstrated, both cell lines not only grew as anchorage-independent aggregates in

liquid culture, but also formed colonies in semi-solid medium, reflecting their ability to escape anoikis. Despite the fundamental biological role of PI3K activation in cellular development, growth and survival, activation of this pathway protects malignant cells against anoikis therefore, promoting tumour cell migration and metastasis [251, 252]. Previously, in my laboratory, Moore, et al., [231] demonstrated that constitutive activation of PI3K pathway which results in high levels of basal PKB and p70s6k activity is the underlying molecular explanation of anchorage-independent growth in SCLC cells.

Interestingly, in the present study, not all cells cultured in the semi-solid medium were clonogenic indicating tumour cell functional heterogeneity. Based on the CSC theory, not all the cells within a neoplasm are clonogenic and tumorigenic and only a subset of cells with stem cell-like phenotype propagate tumour development, metastasis and treatment resistance [74]. This observation further triggered the speculation that the colony forming ability observed in the H345 and H69 cells was due to the presence of CSC population within these cells. To evaluate this concept, it was necessary to isolate the putative SCLC CSCs and non-CSCs and compare the clonogenicity between the two populations.

Expression of stem cell markers, CD133, Oct-4 and ALDH has been associated with the presence of CSCs in malignancies [79, 152, 157, 158]. Although CD133 expression in lung cancer selects for chemoresistant and aggressive cells, its contribution to the fundamental properties of CSCs is not fully understood. In CD133-knock down experiments by Takenobu et al., [127] it was demonstrated that CD133 expression inhibits neuroblastoma cell differentiation and accelerates their cell proliferation and anchorage-independent growth and tumour formation *in vivo*. Additionally, treatment of colorectal tumour cell lines with the CD133 monoclonal antibody 6B6, which directly targets human CD133 antigen, inhibited their proliferation [253]. These data demonstrate the biological function of CD133 and the importance of this molecule in regulating the undifferentiated state and growth of CSCs. The importance of CD133+ cells in pulmonary cancer patients has also been clinically documented [85]. Fifty NSCLC patients undergoing concurrent chemo-

radiotherapy with docetaxel, cisplatin and thoracic radiation followed by surgery were examined. Using IHC to evaluate the expression of CD133 and ALDH1 in patient's specimens, the expression of these markers was associated with poor prognosis in NSCLC patients. Similarly, the CD133 expression on lung cancer cells predicts shorter progression-free survival of candidates treated with platinum-based regimens [84]. Although, to my knowledge, no study has directly evaluated the relation of CD133 expression with SCLC patient prognosis, however, multiple *in vitro* studies performed on SCLC cells from primary tumours and cell lines have illustrated the importance of this marker in selecting cells with an aggressive, chemoresistant and tumorigenic phenotype [79, 82, 158]. Therefore, identifying and characterising cells positive for CD133 could be a valuable tool for developing more effective treatments for SCLC.

High ALDH activity is associated with CSCs in lung cancer [146, 152, 153]. ALDH enzyme plays a pivotal role in mediating resistance to alkylating drugs in CSCs by recycling aldehydes [151]. Additionally, ALDH1 by regulating the production of retinoic acid (RA) plays a central role in stem cell differentiation [150]. Similar to CD133, the expression of ALDH in lung cancer patients has a prognostic impact [254] making it a valuable marker for detection of CSC in SCLC.

Oct-4 is a well-known stem cell and CSC marker [155, 157, 158, 255]. Targeted disruption of Oct-4 in mice developed embryos which were not pluripotent and were restricted to differentiate [255]. Thus, Oct-4 has been proposed as the main regulator of cell fate to be pluripotent or to be differentiated. In lung cancer, Oct-4 expression maintained the stem cell phenotype of CD133+ cells [158] making this transcription factor useful for identification of CSCs in SCLC.

Based on the above data, CD133, Oct-4, and ALDH were selected as markers for detection of prospective SCLC CSCs. CD133 and Oct-4 protein expression in both SCLC cell lines was detected by western blot and the ALDH enzyme activity was confirmed by flow cytometry. CD133, the most commonly used marker, that consistently identifies the chemoresistant, clonogenic and tumorigenic CSCs [77-79,

84, 127], was selected for the identification of putative SCLC CSCs. Oct-4 is not an ideal marker for the isolation of these aggressive cells since Oct-4 is an intracellular protein and isolation of CSCs based on this marker would require cellular permeabilisation which consequently would compromise the cell viability. Therefore, Oct-4 was used to confirm the stem cell phenotype of the isolated cells. Despite ALDH enzyme activity selects for CSCs, in the present study it was not used as a CSC marker. However, in future it would be interesting to evaluate the characteristics of SCLC cells positive for ALDH activity and compare its characteristics with SCLC cells positive for CD133 antigen.

In the present study, 18 ± 1.24% of H345 and 22 ± 1.76% of H69 cells were CD133+. However, the CSCs theory states CSCs to be a 'rare' fraction of cells residing within the tumour bulk. The generality of the CSC hypothesis merits some discussion since the frequency of CSCs appears to be highly variable between cancers of the same type [73]. In the study by Eramo et al., [79] 0.33-22% of lung cancer cells were CSCs. Variation in CSC frequency was explained by the differences in cancer subtypes (SCLC and NSCLC). Consistent with previous observations, it can be presumed that different cancers will exhibit variable functional differences as a result of specific oncogenic pathway activity within a known tumour, manipulating the CSC frequency [256]. Additionally, chemotherapy enriches the CSC population [80, 257]. In breast cancer patients after primary systemic therapy an increase in the proportion of CSCs was observed [258]. Both H345 and H69 cells are derived from post-chemotherapy patients, therefore, high percentage of CD133+ cells could be associated with enrichment of this population after therapy. However, it is essential to point out that the fundamental concept underlying the CSC hypothesis is not associated with the absolute CSC frequency; instead, CSC hypothesis emphasises that the basis for the functional heterogeneity within tumours is the result of the presence of a sub-population of cells with tumour initiating capacity whereas the rest of the tumour cells are devoid of it.

CD133 distribution followed a gaussian rather than a bimodal pattern. Similar diffuse CD133 expression pattern has been observed in various other cancers [80, 111, 236,

259]. This observation is essential for the future studies in this thesis when categorising cells into CD133+ and CD133- cells (see below).

Characterisation of CSCs essentially requires accurate identification and isolation of these cells. Various methods are employed for the selection of CD133+ cells. However, a successful selection of population of interest can only be confirmed by evaluating the purity of the isolated cells. In this study two methods were used for the isolation of CD133+ cells, MACS and FACS. Post-sort purity was examined by the expression of CD133 antigen and its protein levels in the sorted populations. Based on the flow cytometry analysis, isolation of SCLC cell by the CD133 MicroBead Kit did not produce a pure selection due to technical issues. SCLC cells grow as cell aggregates. Thus, experimental studies would require the disruption of the cell clumps. This was achieved by mechanical force (gentle pipetting) accompanied by straining the cell suspension through a cell strainer. Although the majority of cells obtained were single cells, complete disruption of cell clumps was not possible whilst maintaining high viability. Presence of cell clumps could reduce the purity of the isolated cells using the CD133 MicroBead Kit. In this method, CD133+ cells are selected by binding of the positive cells to the magnetic MicroBeads and subsequent entrapment in the magnetic field. If the cell of interest is attached to a cell clump, the total cell clump would be selected as a positive cell. On the other hand, if a positive cell is surrounded by negative cells, it could hamper the positive cell entrapment. Additionally, the presence of dead cells could also cause impure selection as dead cells may bind non-specifically to MACS MicroBeads. Due to SCLC cell characteristics, approximately 20% of the cells are found dead in culture. A similar observation was made in a study by Clement et. al.,[260] in which, in contrast to pure isolation and enrichment of CD133 population using FACS, non-specific binding was observed using the CD133 MicroBead in gliomas. In addition to the technical issues involving the CD133 MicroBead Kit, as demonstrated, CD133 exhibits a gaussian rather than a distinct positive and negative distribution. Therefore, it would not be possible to select on what we consider as CD133high (CD133+) and CD133low (CD133-) cells. Therefore, the CD133 MicroBead Kit was not suitable for isolation of prospective SCLC CSCs.

Fluorescent activated cell sorting proved ideal for the isolation of the population of interest in the SCLC cell lines. This was confirmed by analysing the purity of sorted population. In contrast to the MACS method, by selecting specific flow cytometry gates it was possible to exclude cell clumps and dead cells which significantly contributed to sort purity. Additionally, by comparing the distribution of CD133 expression with the isotype control, it was possible to selectively isolate cells with higher or lower expression of this antigen. Thus, the method was selected for isolation of CD133+ cells for further analysis in the present study.

Despite the data in this chapter demonstrates that SCLC cells retain cells expressing CSC markers, it is essential to assess these cells for their CSC-like characteristics. CD133 was selected as the most ideal marker for the characterisation of prospective SCLC CSCs. Evaluation of the clonogenic, chemoresistance and tumorigenic features of CD133+ SCLC cells would allow us to judge if these cells could be the possible explanation for SCLC development and chemoresistance.

CHAPTER 4:
CD133+ cells are proliferative, clonogenic cells with stem cell-like phenotype and are chemoresistant *in vitro* and tumorigenic *in vivo*

4.1 Introduction

The presence of stem cell-like cells within tumours is the suggested underlying cause of tumour initiation, propagation, resistance and recurrence (reviewed in [73, 261, 262]). CD133, the most well known marker for CSCs of the epithelial origin [263], was selected to identify the aggressive SCLC sub-population in the present study. Characterisation of CD133+ cells in SCLC and dissection of molecular mechanism underpinning their chemoresistance could contribute to novel effective intervention.

CD133+ cells demonstrated higher proliferation compared to the CD133- population as seen in glioblastoma, lung cancer and hepatocellular carcinoma (HCC) [80, 118, 264]. Increased proliferation of CD133+ cells has been associated with aggressive phenotype. In samples taken from 44 glioblastoma candidates who had undergone complete or partial tumorectomy with adjuvant radiotherapy and temozolomide (an alkylating agent) treatment, CD133+ cells displayed high Ki-67 activity. Ki-67 is a nuclear protein and can be detected in all active phases of the cell cycle. Co-expression of both markers was a poor prognostic factor [264]. Similar observations were made in 177 samples from patients with stage I lung adenocarcinomas. In these candidates, CD133 expression was an independent prognostic marker and its combination with proliferating activity (Ki-67 expression) demonstrated a prognostic value to predict postoperative recurrence in lung cancer patients. Ma et al., [80] demonstrated CD133+ cells were significantly more proliferative in serum-free medium compared to its negative counterparts. Active proliferation in these cells may be a result of expression of various growth factors and their cognate receptors promoting expansion through autocrine and paracrine signalling [82, 169]. A better understanding of its growth profile and the underlying mechanism of the putative SCLC CSCs would permit designing more effective drugs that target these aggressive cells.

Self-renewal and differentiation are the two main characteristics of CSCs. Through self-renewal, these cells form new stem cell-like cells with identical ability to proliferate indefinitely without maturing whereas by differentiation, they generate a heterogeneous population of cells with a more mature phenotype and limited proliferative ability. A gold standard method to reflect CSC self-renewal and differentiation potentials is serial transplantation in recipient animals [79]. The stem cell-like features of CSCs can also be evaluated by their ability to form tumour spheres in liquid cultures and colonies in semi-solid medium in serum-free conditions. In these assays, a single CSC is able to proliferate indefinitely and generate a cellular mass without losing their stem cell-like potential. In pulmonary malignancies, CD133 selects for cells which are able to self-renew and differentiate [79] indicating the utility of CD133 as a CSC marker.

It is unknown if CD133 expression directly regulates a cell's stem-like phenotype. However, multiple studies suggest the importance of CD133 expression on stem cells and CSCs. During Hematopoietic stem cell (HSC) self-renewal via asymmetric cell division, CD133 was transferred to daughter cells with a stem cell phenotype [124]. Similarly, a small fraction of lung cancer cells asymmetrically divided its template DNA. Interestingly, CD133 expression was preferentially enriched in the stem-like daughter cells, whereas the differentiation markers such as pro-surfactant protein-C and pan-cytokeratins were transferred to the more differentiated daughter cells [125]. Stable knockdown of CD133 by shRNA in neuroblastoma cells was associated with the loss of anchorage-independent colony formation and tumour development *in vivo* in contrast to wild type cells [127]. The association of CD133 expression with the immature phenotype was further supported in differentiation studies. Differentiation of lung cancer CD133+ cells *in vitro* led to loss of CD133 expression and gain of differentiation markers, loss of unlimited proliferation and the ability to form lung cancer spheres *in vitro* and tumorigenicity *in vivo* [79]. Therefore, although the function is unknown, CD133 is preferentially expressed on stem cells and CSCs.

Embryonic signalling pathways critical for maintenance of the stem cell phenotype is also active in CSCs. Oct-4 is a key regulator of self-renewal and pluripotency of

embryonic stem cells (ESCs) [155, 265]. In addition to mouse pulmonary stem cells, the expression of this transcription factor has also been documented in human lung cancer and is associated with its stem cell-like phenotype [158]. Chen et. al., 2008 [158] demonstrated that the expression of Oct-4 was transcriptionally and translationally up-regulated in CD133+ lung CSCs. Knock-down of Oct-4 expression using siRNA in the CD133+ cells, inhibited sphere formation and further facilitated differentiation with loss of CD133 expression [158]. The self-renewal and differentiation potential of CD133+ SCLC cells and the mechanisms associated with these phenotypes in SCLC have not yet been fully documented.

CSCs, based on their aggressive and their stem cell phenotype, are the suggested cause of tumour development and metastasis. In contrast to non-CSCs, low numbers of CSCs are sufficient to generate tumours. In pulmonary cancer, 10^4 lung cancer CD133+ cells readily generated tumour xenografts in immune-compromised mice, whereas 5×10^4 CD133- cells did not develop tumours [79]. In breast cancer, 100 CSCs were tumorigenic in mice where as tens of thousands of non-CSCs failed to generate tumours [75]. These data demonstrate the pivotal role of CSCs in tumour initiation making the study of CSC even more intriguing.

In addition to their tumour initiation potential, CSCs confer resistance to classical therapeutic approaches. Instead, these therapies enrich CSC population by preferentially eliminating differentiated cancer cells [141, 266]. Some of the mechanisms associated with this resistance include efficient DNA repair, increased expression of membrane transporters with efflux of cytotoxic agent and resistance to apoptosis [139, 267] [80]. Resistance to apoptosis may be achieved by overamplifying antiapoptotic proteins by CSCs allowing these cells to escape the cytotoxic insults of treatments. This was demonstrated in hepatocellular carcinoma (HCC) wherein chemoresistant CD133+ cells exhibited preferential activation of survival pathways Akt/PKB and Bcl-2 [80]. Yet, despite a multitude of studies, the specific signalling pathways and mechanisms as to how CD133 CSCs are able to evade conventional therapies in SCLC remains largely unknown.

In this chapter I will examine the growth profile, stem cell nature, tumour initiating and chemoresistant phenotype of CD133+ SCLC cells. Despite multiple studies in the field of CSC, this will be the first to characterise mechanisms associated with CD133 SCLC chemoresistance. Characterising SCLC CSCs could be a great step towards effective management.

4.2 Results

4.2.1 SCLC CD133+ cells are proliferative *in vitro*

Previous studies have shown that CSCs are more proliferative compared to non-CSCs cells [78-80, 264]. The growth rates of CD133+ and CD133- in H345 and H69 cells were evaluated by sorting the populations as described in chapter 3 and immediately seeding 1×10^4 sorted cells/well in SITA medium and counting the viable cells every two days over a period of 24 days. SITA medium (RPMI 1640 supplemented with, SIT media supplement consisting of, 30 nM selenium, 5 µg/ml insulin, 10 µg/ml transferrin and 0.25% (w/v) BSA) is a serum-free medium ideal for SCLC growth in liquid culture [268]. Serum-free medium was selected since serum in culture induces cellular differentiation of stem-like cells [79, 269]. Cell number was evaluated using the NucleoCounter NC-100 (ChemoMetec, Denmark). The CD133+ and CD133- H345 and H69 cells grow as cellular aggregates. Despite disaggregation of cells prior to cell count, residual cell aggregates could increase errors. NucleoCounter allows accurate counting of viable cells by analysing the light emitted from PI-positive dead cells. As shown in Figure 23A, in H345 cells, no significant difference in the growth rate between the two populations could be observed until day 16. From day 18 onwards, CD133+ H345 cells were significantly more proliferative than CD133- population (P=0.03). By the end of the study, day 24, cell numbers of CD133+ were approximately twice than that of CD133- cells (CD133+ cells, $1.88 \pm 0.10 \times 10^6$ cells/well and CD133- cells, $1.00 \pm 0.12 \times 10^6$ cells/well, P=0.005).

Similarly, in H69 cells, until day 16 no significant difference between CD133+ and CD133- cells was observed (Figure 23B). From day 18 onwards, CD133+ H69 cells were significantly more proliferative than the CD133- cells (on day 18, P=0.01). On day 24, CD133+ cell number had reached $2.57 \times 10^6 \pm 21.61$ cells/well compared to CD133- cells which numbered $1.48 \times 10^6 \pm 18.22$ cells/well. In this cell line, CD133+ cells were 1.74 times more proliferative than CD133- cells P=0.02.

Figure 23

4.2.2 CD133+ cells are clonogenic *in vitro*

Clonogenic assays reflect the stem cell features of a single cell that is resistant to anoikis and is able to generate a clonal population [144, 240]. Post-sorted cells, cultured in SITA medium containing 0.3% agarose, were layered on the same medium with 0.5% agarose. The low percentage of agarose promotes 3 dimensional cell growth in semi-solid medium. SITA medium was used to inhibit possible cellular differentiation. Colonies were scored after 21 days by standard light microscopy. Number of colonies per dish was presented as percentage of the cells seeded and is defined as cloning efficiency.

In H345 cells, the CD133- population despite being proloferative in liquid culture did not form any colonies in semi-solid medium. Lack of growth of CD133- cells in semi-solid medium could possibly be due to the nature of the clonogenic assay. In this assay cells are cultured as single cells in the semi-solid medium, limiting cell-cell interaction, allowing only cells with stem cell nature and clonogenic potential to surivive and generate colonies. Whereas, in liquid growth assays, the floating H345 and H69 cells can directly interact with their adjacent cells providing appropriate growth signals via autorcine and paracrine signallings.

Both CD133+ and parent cells were clonogenic with CD133+ cells demonstrating 2.9 times (P=0.04) more clonogenicity than the parent cells (Figure 24B). The cloning efficiency of the CD133+ cells was 5.30 ± 1.12% compared to 1.91 ± 0.17% in the unsorted cells. On gross observation, colonies formed by CD133+ or parent cells were similar in their morphology. Figure 24A illustrates the clonogenic ability of CD133-, CD133+, and parent H345 cells in a tissue culture dish. As illustrated, the pink colour of the semi-solid medium containing the non-clonogenic CD133- cells was indicative of lack of cellular growth in culture. In contrast, colonies can be detected in tissue culture-well containing CD133+ and parent cells. The number of colonies formed by CD133+ cells was greater than that formed by parent cells.

Similar observations were made in H69 cells (Figure 24C). CD133- cells were unable to form colonies whereas both CD133+ (7.90 ± 0.3%) and parent (3.25 ± 0.6%) cells were clonogenic with CD133+ cells exhibiting greater colony forming ability than parent population (*P*=0.006). Colonies formed by both CD133+ and parent cells had similar morphology. In conclusion, supporting the CSC hypothesis, in both H345 and H69 cells, CD133+ cells were significantly more clonogenic than CD133- cells. The clonogenic efficiency of the CD133+ cells was also significantly greater than the parent population indicating that the parent cells contain a population of cells with stem cell-like phenotype, however the CD133+ population are enriched for these aggressive cells.

Figure 24

Despite high clonogenic efficiency of CD133+ cells, not all CD133+ cells cultured in the semi-solid medium formed colonies. Therefore, CD133 expressing cells could be a heterogeneous population of cells. Similar observation was made by Eramo et al., [79] where in only 5-30% of lung cancer spheres were capable of self-renewing. In the present study this hypothesis was assessed by double staining unsorted cells with CD133-1-APC and ALDH to evaluate the number of cells co-expressing both stem cells markers. As shown in Figure 25, 18 ± 1.01% of H345 cells were CD133+ (Figure 25A and A1) and 16 ± 0.78% of cells were ALDH+ (Figure 25B and B1), however, only 5.8 ± 0.86% of cells were positive for both markers (Figure 25C and C1). Thus, despite similarity in the expression of CD133 antigen, not all CD133+ cells share similar phenotype.

Figure 25

4.2.3 CD133+ cells express the embryonic stem cell marker, Oct-4, and maintain their stem cell-like phenotype over long periods in culture

The presence of Oct-4 in the sorted and unsorted cells was evaluated based on the protein levels using western blotting. As shown in Figure 26, a protein band of ~48 kDa in both CD133+ and parent cells represented the presence of Oct-4 in these cell lines whereas no band could be detected in the CD133- cell lysates. β-actin was used as loading control. Oct-4, the master switch during differentiation, is essential for maintaining the stem cell-like phenotype [255]. Thus, it can be concluded that, in contrast to CD133- cells, CD133+ subset are immature cells. Oct-4 protein expression in the parent cell lysates could be associated with the presence of CD133+ sub-population.

Figure 26

CSCs are considered self-renewing cells based on their ability to grow for extended periods of time without losing their phenotype [78, 79]. CD133+ and CD133- H345 cell line were cultured in serum-free SITA medium for 30 days. After this period, the expression of the stem cell marker, CD133, and the clonogenic potential of these cells was evaluated. If CD133+ cells retain stem cell-like nature, prolonged period of culturing should not affect its stem cell-like potentials such as its clonogenicity.

Initially, CD133 expression was evaluated on post-sorted cells cultured for 30 days in SITA. The expression of CD133 on sorted cells on day 30 was compared with that of cells on day 0 (the day of cell isolation). Geometric mean (GM) was used to calculate changes in CD133 expression on day 0 and 30. Figure 27 is representative flow cytometry histograms showing the expression of CD133 on the parent cells (A1, day 0 and B1, day 30), CD133- (A2, day 0 and B2 day 30) and CD133+ (A3, day 0 and B3 day 30). CD133 expression was compared with its corresponding negative control (isotype control). Histograms A4 and B4 are overlay histograms of CD133-, CD133+ and parent cells on day 0 and on day 30, respectively.

The GM of CD133+ cells did not significantly change over the period of 30 days (A3, GM on day 0 was, 121.35 ± 1.45 and B3, GM on day 30 was, 128.10 ± 1.21), indicating that despite a long period of culturing, CD133+ cells retained the CD133 expression in SITA medium. CD133- cells are not capable of self-renewing therefore, as expected, the GM of CD133- cells remained unaltered (A2, GM on day 0 was, 4.35 ± 1.02 and B2, GM on day 30 was, 4.01 ± 1.63). The difference in the CD133 expression between CD133+, CD133-, and parent cells was more apparent on the overlay histograms (A4, day 0 and B4, day 30). As demonstrated, on day 0, CD133+ cells displayed the highest GM for CD133 expression (121.35 ± 1.45) compared to its negative counterpart (4.35 ± 1.02) and the parent cells (32.7 ± 2.86). Similarly, on day 30, CD133+ cells displayed the highest GM of CD133 expression (128.10 ± 1.21) compared to its negative counterpart (4.01 ± 1.63) and the parent populations (30.97 ± 1.32). Therefore, CD133+ cells were able to proliferate for prolonged periods of time in serum-free culture without losing the expression of its stem cell marker. This data additionally indicates that SITA medium can be

employed for the expansion of SCLC CSC-like cells which is essential finding for their characterisation *in vitro*.

Figure 27

To further confirm CD133+ H345 cells retained their stem cell-like features over prolonged periods of culture, clonogenicity of 30 days post-sorted CD133+, CD133-, and parent cells was evaluated. Eramo et al. 2008 [79], demonstrated that CD133+ cells isolated from primary lung cancer tissues were able to maintain their stem cell phenotype in culture and reproduced the original tumour *in vivo*. In the present study, the stem cell-like phenotype of the cultured CD133+ cells was examined based on their colony forming potential *in vitro*. As shown in Figure 28, despite CD133+ cells being cultured in serum-free medium for 1 month, they still retained their aggressive phenotype and were able to form colonies with a cloning efficiency of 7.49 ± 0.21%. CD133- cells do not retain stem cell-like phenotype and therefore did not form colonies in the semi-solid cultures and within 3-5 days post-culturing most of the cells appeared apoptotic. Parent cells were clonogenic with efficiency of 2.18 ± 1.05%. Parent cells comprises of both CD133+ and CD133- cells therefore, it was expected that these cells would form colonies. However, the cloning efficiency of CD133+ cells were 3.43 times (P=0.006) greater than that of the parent cells. Based on these data, CD133+ cells not only retained the expression of their surface marker over extended periods of *in vitro* culturing, but also maintained their aggressive phenotype suggesting the possible self-renewing ability of these cells. To confirm self-renewing potential of CD133+ cells, serial transplantation of CD133+ cells in animal models would be necessary.

Figure 28

4.2.4 CD133+ cells upon differentiation lose their CD133 expression and stem cell-like characteristics

CSCs along with their self-renewal phenotype are able to differentiate to generate cells that make up the bulk of the tumour. Presence of serum in culture medium can induce differentiation [269]. The differentiation potential of CD133+ H345 cells was evaluated by culturing isolated cells for 30 days in serum containing medium (RPMI 1640 supplemented with 10% (v/v) heat-inactivated FCS, 5 µg/ml L-glutamine, 50 U/ml penicillin and 50 µg/ml streptomycin) (RPMI complete medium) and analysing changes in the expression levels of CD133 on the day 30. Figure 29 is representative flow cytometry histograms showing the expression of CD133 on the parent cells (A1, days 0, and B1 day 30), CD133- (A2, day 0, and B2, day 30) and CD133+ cells (A3, day 0, and B3 day 30). CD133 expression was compared with its corresponding negative control (isotype control). Histograms A4 and B4 are overlay figures of CD133-, CD133+ and parent cells on day 0 and day 30, respectively.

The GM of CD133- did not significantly change over time (A2, GM on day 0 was, 4.21 ± 0.61 and B2, GM on day 30 was, 4.72± 0.23) indicating that they were unable to generate different progeny of cells and remained a negative population. On the other hand, a significant reduction in the GM of CD133+ cells from day 0 (130.04 ± 1.5) compared to day 30 (53.72 ± 0.94) was observed (P<0.0001). Comparing the GM of CD133+ cells with parent population on day 0, CD133+ cells were significantly more fluorescent than parent cells (A3, GM of CD133+ cells on day 0 was, 130.04 ± 1.5, and A1, GM of parent cells on day 0 was, 30.10 ± 1.4, P<0.0001). However, on day 30, despite significant difference between the GM of CD133+ and parent cells (B3, GM of CD133+ cells on day 30 was, 53.72 ± 0.94, and B1, GM of parent cells on day 30 was, 36.13 ± 1.4, P=0.009), the GM of CD133+ cells more closely resembled the parent cells than CD133- population, indicating that in the presence of serum, CD133+ cells differentiate and generate a mixed progeny similar to parent population. To further confirm differentiation potential of CD133+ cells in serum, loss of Oct-4 expression and gain of differentiation marker should be evaluated.

Figure 29

Loss of CD133 expression upon CD133+ differentiation is associated with loss of stemness [77, 79]. As shown above, culturing CD133+ cells in serum containing medium for 30 days was associated with differentiation of CD133+ cells and generation of a mixed progeny. To further evaluate the effect of this culturing method on the functional properties of differentiated CD133+ cells, liquid growth profile and the clonogenic potential of these cells were assessed. The 30 days post-sorted CD133+ and CD133- cells (1×10^4 cells/well) were cultured in fresh RPMI complete medium and the number of viable cells was counted every 2 days by NucleoCounter NC-100 (ChemoMetec, Denmark) over 24 days. In contrast to high proliferation of CD133+ cells compared to CD133- cells observed when cultured in serum-free SITA medium (Figure 23A), H345 CD133+ cells grown in serum containing medium grew at the same rate as the CD133- cells with no significant difference in their growth potential (Figure 30A). This observation indicated that in the presence of serum, CD133+ cells differentiate which was associated with loss of their high proliferation phenotype. This was in line with previous documented data that CSCs cultured in serum-containing medium lose their high proliferation potential [79].

The clonogenic potential of 30 days post-sorted CD133+, CD133- H345 and unsorted parent cells was evaluated in serum-containing semi-solid medium. CD133- cells in the presence of serum were still unable to form colonies which further emphasised on their non-CSC phenotype (Figure 30B). In contrast, both CD133+ cells and parent cells generated colonies with cloning efficiencies of 7.72 ± 1.26% and 8.93 ± 1.08%, respectively. No significant differences between the cloning efficiency of the CD133+ and parent populations was observed. Therefore, in line with data shown in Figure 29, in the presence of serum, CD133+ cells differentiated to generate a mixed progeny similar to the parent cells thus, exhibited a colony forming ability similar to the parent population (Figure 30B). To further support this observation, the tumorigenicity of differentiated CD133+ cells should be assessed *in vivo*.

Figure 30

4.2.5 CD133+ cells are tumorigenic *in vivo* and reproduce the parent tumour

The tumour initiation ability of the H345 CD133+ cells was evaluated by subcutaneous injection of various numbers of isolated CD133+ and CD133- and parent cells (5×10^5, 1×10^5, and 1×10^4) mixed with growth factor reduced matrigel (1:1 volume of cells:Matrigel mixed at 4°C, total volume of 100 µl) in *nude/nude* mice. Implantation of 1×10^4 CD133+ did not form tumours. However, injection of 1×10^5 CD133+ cells consistently resulted in the growth of tumour xenografts (Figure 31A) with histological features closely resembling the tumours initiated by parent cells (unsorted cells) as shown by hematoxylin and eosin staining (Figure 31B). However, the same number of CD133- or parent cells did not form tumours in *nude/nude* mice. At least 5×10^5 unsorted cells were required to form tumours yet, the tumours formed by 5×10^5 parent cells were significantly smaller than the same number of cells injected by CD133+ cells (tumour volume of CD133+ on day 52 was, 421.73 ± 33.30 mm^3, and tumour volume of parent cells on day 52 was, 274.41 ± 24.46 mm^3, P=0.031). No tumours could be detected in animals injected with CD133- cells. Figure 31C is representative of tumour generated in mice implanted with CD133-, CD133+ or parent cells. Therefore, in contrast to CD133- cells, CD133+ cells were tumorigenic and low numbers of these aggressive cells were sufficient to generate a tumour. Based on this observation it can be proposed that CD133+ cells are the possible cause of tumour initiation in SCLC patients.

Figure 31

4.2.6 Metastatic ability of CD133+ cells was evaluated

A growing body of evidence suggest that cancer metastasis occurs due to migration of CSCs to distant organs [270, 271] [272]. In patients with SCLC, cells initially metastasise to regional followed by distal lymph nodes. Haematogenous spread include bone, liver, adrenal glands, and brain [22]. High rate of cancer metastasis in SCLC patients is one of the main causes of poor survival rates. Therefore, identifying the underlying cause of SCLC metastasis could be essential to improve survival.

The *nude/nude* mice injected with CD133+ cells showed an enlargement of inguinal and axillary lymph nodes. Mice lymph nodes were initially impalpable. One month after CD133+ SCLC implantation, animal inguinal and axillary lymph nodes were obvious on inspection and palpable (Figure 32). Initially, swelling of the ipsilateral inguinal and axillary lymph nodes was detected and over time contralateral lymph nodes were also enlarged. On day 52 (last day of experiment) axillary and inguinal lymph nodes were measured by calliper. The size of the ipsilateral lymph nodes was larger (inguinal lymph node, 120.12 ± 15.87 mm^3 and axillary lymph node, 100.60 ± 14 mm^3) but not significantly different from the contralateral lymph nodes (inguinal lymph node, 98.52 ± 16.63 mm^3 and axillary lymph node, 90.31 ± 18.01 mm^3). Therefore, SCLC metastasis to the lymph nodes was speculated.

Mouse lymph nodes were subject to IHC for detection of the SCLC marker, neural cell adhesion molecule (NCAM), for pathological confirmation of metastasis. NCAM, a cell-cell adhesion molecule, is detected in almost all SCLC cells [273]. Samples were double-stained with CD45, a marker widely expressed on murine leucocytes, to distinguish human from murine cells. Primary tumours (tumour generated at the site of injection) of the animals that had enlarged lymph nodes were used as a positive control for NCAM and spleen of an untreated mouse (not exposed to human SCLC cells) was used as a negative control. NCAM (green) was detected on the surface of all cells of the primary tumour (Figure 33). This was expected since the tumour was generated from H345 CD133+ cells. Interestingly, infiltrating

CD45+ cells (red) was observed on the surface of the tumour (Figure 33). As expected, almost all of the four lymph nodes, garrisons of immune cells, extracted from axillary and inguinal regions, were positive for CD45 (Figure 34). A few NCAM+ CD45- cells were detected in the four lymph nodes extracted from animals injected with CD133+ cells. Presence of NCAM+ cells could be indicative of SCLC metastasis to lymph nodes. However, similar observations were made in mouse spleen which was used as negative control (Figure 35) where most cells were CD45+ however few NCAM+ CD45- cells were detected. Spleen utilised in this study was obtained from animals which were not exposed to human SCLC cells therefore, the NCAM+ cells could not have been SCLC cells. Thus, based on these observations it could not be concluded that lymphadenopathy in animals subjected to CD133+ SCLC cell implantation was due to metastasis.

Figure 32

Figure 33

34

35

4.2.7 CD133+ cells confer resistance to conventional chemotherapeutic agent

CD133 expressing cells are the proposed chemoresistant cells and cytotoxic agents instead enrich this population by eradicating CD133 non-expressing cells. To evaluate this concept in SCLC cells, unsorted (parent) H345 and H69 cells were treated with two different concentrations of etoposide (3 and 30 µg/ml). The percentage of CD133+ cells was assessed after 72 hours by analysing CD133-1 expression levels on treated cells by flow cytometry. Untreated cells were used as control. Although both cell lines demonstrated a dose-dependent decrease in the total number of viable cells, a significant increase in the percentage of CD133+ cells was observed in H345 (P=0.043, ANOVA) (Figure 36A) and H69 cells (P=0.039, ANOVA) (Figure 36B) suggesting that etoposide was not only ineffective against CD133+ cells but instead enriched this population (Table 6).

To confirm that CD133+ cells are chemoresistant, the effect of etoposide on the cell viability of H345 and H69 sorted and parent cells was assessed. Both SCLC cell lines have been obtained from patients that had originally undergone a period of chemotherapy and are therefore relatively resistant to etoposide in culture. Sensitivity to etoposide was assessed by MTT assay 72 hours after treatment. As shown in Figure 36C, in H345 cell line, all three populations demonstrated resistance to etoposide and it was not possible to calculate the IC_{50} values since etoposide was not potent and effective enough to inhibit 50% of cell viability. Among the three populations, resistance to etoposide was more apparent in CD133+ cells. Similar observation was made in H69 cells, in which all three populations demonstrated resistance to etoposide however, this resistance was more apparent in CD133+ population (Figure 36D). Therefore, based on this data, CD133 selects for the most chemoresistant cells within SCLC cell lines.

Figure 36

table 6

4.2.8 CD133+ cells are resistant to apoptosis due to preferential expression of the anti-apoptotic Akt/PKB and Bcl-2 proteins

Evasion of programmed cell death is one of the hallmarks of cancers (reviewed in [274]). Most cytotoxic agents primarily act by triggering apoptosis. Thus, resistance to apoptosis could be a possible mechanism supporting SCLC CSCs survival against cytotoxic insults. To evaluate this concept, sorted populations were subject to three different concentrations of etoposide (3, 10, and 30 µg/ml) and after 72 hours, the percentage of apoptosis using EB/AO and the May-Grunwald-Giemsa staining was calculated. Figure 37 is representative images of May-Grunwald-Giemsa (Figure 37A1-A2) and EB/AO (Figure 37B1-B2) staining in CD133+ and CD133- H345 cells treated with etoposide 30 µg/ml for 72 hours. In H345 cells, CD133+ and CD133- cells responded to etoposide in a dose-dependent manner. However, as demonstrated using May-Grunwald-Giemsa staining (Figure 38A), in contrast to CD133+ cells, CD133- cells were significantly more sensitive to treatment (at 3 µM, P=0.004, at 10 µM, P=0.004, at 30 µM, P=0.02) (Table 7A). This data was further supported using EB/AO staining in which CD133- cells were more sensitive to etoposide than CD133+ cells (at 3 µM, not significant, at 10 µM, P=0.02, at 30 µM, P=0.02) (Figure 38B, Table 7B).

Figure 37

Figure 38

table 7

Similar observations were made in H69 cells; the CD133- cells were significantly more responsive to etoposide than CD133+ cells confirmed by staining samples with May-Grunwald-Giemsa (at 3 µM, *P*=0.02, at 10 µM, *P*=0.004, at 30 µM, *P*=0.003) (Figure 39A, Table 8A) and EB/AO (at 3 µM, *P*=0.03, at 10 µM, not significant, at 30 µM, *P*=0.02) (Figure 39B, Table 8B). Note that, in both cell lines, the percentage of apoptosis in untreated CD133+ and CD133- are very similar. Therefore, CD133+ cells do not respond to etoposide due to resistance to apoptosis.

Figure 39

table 8

While most studies have proven the chemoresistance phenotype of CSCs, the exact mechanisms which enable survival of CD133+ SCLC cells are unclear. Deregulation in the Akt/PKB pathway and members of the Bcl-2 survival family in cancer cells have been studied extensively and play a provital anti-apoptotic role in various malignancies [275, 276]. To address the mechanism by which CD133+ SCLC cells confer resistance to etoposide, both CD133- and CD133+ cells were probed by western blot for endogenous expression of proteins involved in Akt/PKB and Bcl-2 survival signalling pathways. CD133+ cells isolated from H345 cell lines, compared to matched CD133- counterparts, displayed a higher expression of active Akt (phosphorylated at Serine 473) and Bcl-2, indicating that this pathway may contribute to the resistance to apoptosis in CD133+ (Figure 40). Total Akt protein levels were assessed at the same time to confirm that increased expression of phosphorylated Akt in the CD133+ cells was not due to increased in total Akt levels. β-Actin was used as control for equal loading.

Figure 40

4.2.9 Human SCLC tissue samples retain high levels of CD133+ cells

The expression of CD133 was evaluated in primary human SCLC tissues by IHC. It was unknown if samples were taken from patients who were previously exposed to chemotherapy treatment. IHC was performed using a DAKO Envision kit (see chapter 2 for more details). Rabbit polyclonal anti-human CD133 (ab16518, Abcam) was used for IHC. Figure 41 is representative of a tissue sample taken from a SCLC patient. High CD133 staining could be observed in the samples. Based on this observation, it could be suggested that the tissue sample was taken from a patient who had been previously undergone therapy, however due to lack of information regarding the background of the patient such conclusion could not be made.

Figure 41

4.3 Discussion

Data gathered from this chapter demonstrated that the SCLC CD133+ sub-population comprises of aggressive cells with augmented proliferative and clonogenic capacity *in vitro* and significantly increased tumour initiation potential *in vivo*. These cells exhibited similar characteristics to normal stem cells including Oct-4 expression, the ability to maintain their stem cell-like characteristics over prolonged periods of culturing and differentiate in appropriate conditions. On differentiation, the CD133+ cells lost CD133 expression and their enhanced growth potential in liquid and semi-solid medium, and retained a phenotype similar to parent cell line, a population of both CD133+ and CD133- cells. Treatment of unsorted SCLC cell lines (H345 and H69) with etoposide significantly enriched the CD133+ sub-population, illustrating the chemoresistant phenotype of CD133+ cells. The enriched CD133+ cells from SCLC cell lines survived chemotherapy relative to unsorted cells and CD133- cells. The study for the first time demonstrated that chemoresistance in these cells was associated with preferential expression of anti-apoptotic Bcl-2 and activated Akt proteins known to support cell survival. Therefore, based on these observations, it can be concluded that CD133+ cells within SCLC cells are the possible explanation for tumour development and treatment resistance.

In line with previous observations [80], SCLC CD133+ cells exhibited significantly greater proliferation in serum-free medium compared to the CD133- cells. Contributing factors promoting CSC growth may be attributed to over expression of growth factors by the CSCs. In 2008, Levina et al., [82] demonstrated higher expression of various cytokines, chemokines, angiogenic and growth factors including IL6 (CXCL6), IL8 (CXCL8), bFGF, VEGF, HGF, PDGF-BB, G-CSF, and SCGF-β in CSCs than non-CSCs in lung cancer cell lines. These cells also expressed higher levels of VEGFR1, FGFR2, CXCR1, and CXCR4 receptors compared to the non-CSC sub-population. The author concluded that the growth factors produced by CSCs through autocrine and paracrine signalling promote CSC proliferation, tumour progression and metastasis. Likewise, increased expression of C-kit and its ligand stem cell factor (SCF) on NSCLC CSCs has been proposed to be associated with

their proliferation [165]. Proliferation of these cells was inhibited by SCF-neutralising antibodies or by imatinib, an inhibitor of c-kit. The significant role of growth factors on CSC proliferation makes these pathways interesting for targeting CSCs. Multiple Ca^{2+} mobilising-neuropeptide through autocrine and paracrine growth loops mediate SCLC growth and proliferation [169]. The mechanism propelling extensive growth of SCLC CD133+ cells is unknown. It would be interesting to evaluate the expression of neuropeptide receptors on these cells underlying their enhanced proliferation.

Contradictory data suggest CSCs as quiescent cells. The CD24+ ovarian CSCs were slow proliferative than the tumour bulk cells suggesting their quiescent phenotype [277]. In breast cancer cell lines, CD44+/CD24−/ESA+ cells were also quiescent compared to the tumour bulk [278]. The quiescent phenotype of the CSCs is supported by the concept that tissue stem cells may be the origin of CSCs, thus they share similar characteristics. Low proliferation of stem cells is a protection mechanism to prevent exhausting stem cell proliferative ability and to limit accumulation of mutation during frequent cell divisions [279]. However, quiescence is not a dogma for stem cells. Slow-cycling LRCs (label-retaining cells**)** at the +4 position at the base of the colon crypt are suggested intestine stem cells. These crypt based cells are maintained in low number of approximately 4-6 cells that divide once a week. However, upon irradiation, these stem cells evaded radiation induced apoptosis and demonstrated high proliferation with regeneration of the damaged crypt [280]. Similar observations were made by Kim et al. 2008, [98] in lung where in bronchoalveolar stem cells (BACS), generally quiescent, actively proliferated in response to bronchiolar and alveolar injury.

Tissue stem cells reside in specific areas known as niche which along with the neighbouring differentiated cells that secrete and generate a rich microenvironment of extracellular matrix and other factors, regulate stem cell quiescence and un-differentiated state [281]. The importance of these specialised areas in regulating stem cell activity can be explained in an experiment where the fate of embryonic stem cells (ESCs) was monitored upon implantation into mice. ESCs isolated from

blastocyst-stage mouse embryo, when forced in an environment other than their niche *in vivo* these cells can turn into an undesirable differentiated multicellular mass. For example, ESC once subcutaneously injected into nude mice led to the formation of uncontrolled multicellular tumour mass. In contrast, injection of the same stem cells into mouse blastocyst, an environment similar to their native niche, resumed normal stem cell behaviour and contributed to the development of healthy offspring [281]. Data suggest that CSCs also exist in a similar niche, dubbed "CSC niche" which regulates their growth, self-renewal and un-differentiation state (reviewed in [282, 283]). Conclusively, stem cells and CSCs located in their niche are generally quiescent however their quiescent status depends on the signals that they receive from the environment such as signals during tissue injury. Previous data from my laboratory shows that SCLC cell lines produce and secrete various components of extracellular matrix (ECM) [230, 231, 284]. The generated ECM protects these cells from cytotoxic insults induced by etoposide and promotes SCLC cellular growth. Therefore, it can be proposed that ECM can serve as CD133+ SCLC cell niche and that the growth promoting signals from the interaction of these cells with ECM components as well as signals from the environment, such as those from the tissue culture medium could possibly explain the increased proliferation of these cells in culture.

CSCs are characterised as the clonogenic cells within the tumour bulk. Colony assay evaluates the ability of a single cell to survive anchorage-independent growth and its stem cell-like nature to generate a cellular progeny. The present study demonstrated that CD133+ cells were significantly clonogenic in SITA medium as against the non-clonogenic CD133- cells, thus, representing the aggressive, stem cell-like sub-population of SCLC cells. Increased expression of growth factors on lung CSCs not only promotes their liquid growth but also is associated with enhanced colony formation [82, 165]. Expression of neuropeptides and their receptors as the known regulators of SCLC growth and proliferation through autocrine and paracrine signals. Waters et al., [65] demonstrated that chemoresistant, aggressive SCLC cell line, GLC19 expresses higher levels of neuropeptide receptors compared to chemosensitive SCLC cell line, GLC14. Therefore, based on the above data is can be

speculated that increased clonogenecity observed in CD133+ SCLC cells is regulated by the enhanced expression of the neuropeptides and their receptors (for more details see chapter 5).

The expression of CD133 has been another factor proposed as mediator of anchorage-independent growth of CSCs. Tumour sphere formation and the anchorage-independent growth of Neuroblastoma (NB) CSCs was maintained by CD133-related activation of PI3K/AKT pathways [127]. Concluding, in the present study, higher CD133 expression of sorted cells, by activating the down stream survival signals may have also been associated with their survival and growth in the semi-solid medium. In the present study, parent cells also formed colonies. Parent cells contain CD133+ and CD133- cells and colony formation can be attributed to CD133+ sub-population. Extensive colony forming ability of CD133+ cells compared to the parent population could be explained by lower frequency of the CD133+ cells in the parent population. Interestingly, the colonies formed by the CD133+ and parent cells were similar in shape and size. The observation further supports the notion that clonogenic cells within the parent population are the CD133+ cells.

Interestingly, despite high clonogenic efficiency, not all CD133+ cells formed colonies in the semi-solid medium suggesting heterogeneity within the CD133+ population. Similarly, Eramo et al (2008), [79] documented that the number of self-renewing cells within cancer spheres ranged from 5-30% as measured by colony assay and not all CD133+ cells were CSCs. Therefore, to further confirm heterogeneity within the SCLC CD133+ cells, sorted population were stained with an additional stem cells marker, ALDH, in search of cells co-expressing both markers. As shown in Figure 25, only 5.8 ± 0.86% of the population was positive for both markers. Taken together, it may be suggested that SCLC CD133+ cells contain a subset of cells with similar phenotype but different potentials necessitating the use of novel markers or combination of markers to select highly enriched CSC-like cells. Heterogeneity in CD133+ fraction has likewise been documented in NSCLC. Cisplatin treatment of xenografts of primary NSCLC tumours from patients resulted

in remarkable enrichment of the CD133+ cell fraction in the residual tumours. However, within the CD133+ fraction the CD133+ ABCG2 and CD133+ CXCR4 sub-population selectively displayed a clear enrichment after treatment [84]. Mammary CSCs are enriched in both CD133+ CD24-/low population and ALDH+ sub-fractions. However, co-expression of CD133+/CD24-/low/ALDH+, despite low overlap of the two populations (0, 1-1.2%), selected highly aggressive cells *in vitro* and *in vivo* [75, 83]. Therefore, based on the above data, despite CD133 expression in the SCLC cells selected the aggressive and chemoresistant cells, identifying makers which would isolate a more purified population of CSC-like cells could further aid us to better understand these aggressive cells.

CSCs can proliferate indefinitely in appropriate serum-free cultures without losing their stem cell-like nature including clonogenecity and tumorigenicity, indicative of their self-renewing potential [77-79]. Thus, it was hypothesised that H345 CD133+ cells would exhibit similar stem cell-like characteristics in appropriate conditions. In line with data from other malignancies, CD133+ cells cultured in serum-free SITA medium retained CD133 expression in culture without losing clonogenicity in semi-solid medium. In the presence of serum most H345 CD133+ cells lost CD133 expression and generated a population with heterogeneous levels of CD133 expression resembling the parent (unsorted) cells. This was accompanied by loss of high proliferation in serum containing liquid culture and attenuated enhanced clonogenic ability in semi-solid medium. Likewise, Eramo et al., [79] demonstrated differentiation of lung CSCs in the presence of serum was associated with loss of CD133 expression, gain of differentiation marker including cytokeratins (CKs), and inability to grow indefinitely *in vitro* and form tumours *in vivo*. Data in this section indicate that SCLC CD133+ cells are the stem cell-like population that can be maintained and expanded as undifferentiated cells in SITA medium. However, to confirm the self-renewing potential of CD133+ SCLC cells it is necessary to evaluate their tumorigenicity upon serial transplantation.

Signalling pathways including Sonic hedgehog, Wnt and Notch that regulate tissue stem cell self-renewal and fate are common in CSCs (Reviewed in [285, 286]). For

example, NSCLC CSCs have elevated Notch pathway transcript expression. Suppression of this pathway by either gamma-secretase inhibitor or stable expression of shRNA against *NOTCH3* resulted in significant decrease in CSCs population, reduction in tumour cell proliferation and clonogenicity [287]. In glioma CD133+ cells, Hedgehog signalling regulates their "stemness" genes and their self-renewal. Lentiviral-mediated silencing of this pathway resulted in the differentiation of the CD133+ cells and abolished their tumorigenic potential *in vivo* [288]. Therefore, tissue stem cells and CSCs share similar pathways associated with their self-renewal and fate. In the present study it has been shown that CD133+ cells express the embryonic stem cell marker, Oct-4 similar to that of mouse pulmonary stem/progenitor cells [79]. This observation indicated the stem cell nature of SCLC CD133+ cells, further suggesting the role of this sub-population in SCLC development in patients. Based on such similarities between tissue stem cells and CSCs, it is tempting to conclude that CSCs are generated from stem cells which already posses a favourable background. However, as documented by Clarke et al. (2006) [289], it is now widely accepted that CSCs may also develop from more differentiated cells that have acquired reprogramming hits and therefore regained the stem cell phenotype (Figure 42). Better understanding of these pathways could guide us to target cells with self-renewing potential and possibly inhibit further cancer progression in patients.

Figure 42

A hallmark of CSCs is tumour initiation potential in recipient animals with the hypothesis being that neoplastic growth can be initiated by low counts of cells that possess stem cell-like phenotype and growth advantage. As expected clonogenic CD133+ cells exhibited enhanced tumorigenesis potential in immune-compromised mice compared to the CD133- and parent subset. Counts as low as 1×10^5 CD133+ cells subcutaneously implanted in nude mice consistently resulted in the growth of tumour xenografts whereas the same number of CD133- cells or even higher cell number were devoid of tumorigenesis (Figure 31). CD133+ cell xenografts had histological features closely resembling the tumours initiated by the parent cells. These results further supported that CD133+ cells are the tumour initiating undifferentiated cells and that small numbers of these cells are sufficient to generate a progeny with cellular heterogeneity similar to that generated by the parent population. Non-clonogenic CD133- cells were not tumorigenic *in vivo* as observed within the duration of the experiment. This further emphasised that CD133- cells are not the tumour initiating cells, unable to survive anchorage-independent growth and devoid of stem-cell like phenotype. Enriched CSC population within the CD133+ population was additionally demonstrated when comparing the tumorigenic potential of CD133+ cells with that of parent cells. Although parent cells were also tumorigenic in the immune-compromised animals, at least 5 fold higher cell number compared to CD133+ population was required for tumour development. Additionally, tumours formed by parent cells were significantly smaller than the neoplasm generated by CD133+ cells when the same number of parent cells as CD133+ cells (5×10^5) was implanted. Thus, the *in vivo* tumorigenic assay indicates CD133+ population are tumour initiation cells in the SCLC cell lines.

According to the established CSC theory, a single CSC should be sufficient to develop tumour xenografts. However, at least 1×10^5 CD133+ cells were required for tumour initiation in the immune-compromised mice. The conflicting observation is in line with the data obtained from colony assay which demonstrated that not all SCLC CD133+ were able to form colonies in semi-solid medium. The presence of heterogeneity within the CD133+ SCLC (Figure 25) could be a possible explanation for high number of CD133+ cells required for tumour initiation. In addition, human

cell engraftment in xenotransplant models is limited by the presence of the recipient immune system and its environment. The *nude/nude* mice utilised in the present study are immune-deficient athymic animals that lack T cells but produce B cells and natural killer (NK) cells. Highly immune-compromised mice such as non-obese diabetic/severe combined immunodeficiency (NOD/SCID) mice deficient in both T and B cells with impaired natural killer cells would be more suitable for these studies. The importance of the strain of the mice used can be exemplified in the study conducted by Quintana and colleagues where in the NOD/SCID$^{Il2rg-/-}$, NOD/SCID strain lacking the interleukin-2 receptor gamma, ably generated melanoma tumours from a single human melanoma cell seeding [290]. Another reason could also be associated with the length of the study. It could be that if animals were left longer (several months), even lower numbers of CD133+ cells would form a tumour. Thus, further purification of CSCs, the use of appropriate mouse strain, and a longer study period could result in more successful graft uptake with lower CSCs numbers.

Tumour cell dissemination and metastasis is a relatively early event in SCLC. Loco-regional and subsequently distant lymph node involvement include epsilateral intrapulmonary, hilar and mediasternal nodes, contralateral nodes, and extrathoracic scalene and supraclavicular lymph nodes [291]. Distant metastases, generally hematogenous, include bone, liver, adrenal glands, and brain. About 18-24% of SCLCs at initial diagnosis and 50% of SCLCs during course of disease have CNS metastasis [292, 293]. Cancer metastasis is associated with loss of epithelial characteristics of the cancer cells and acquisition of migratory phenotype. The process referred to as the epithelial to mesenchymal transition (EMT), is an essential event in metastasis [294]. In line with this observation, EMT in the self-renewing lung neuroendocrine cells led to acquisition of an invasive and metastatic phenotype [295]. Interestingly, metastatic cancer cells recapitulated the organisation of their primary tumours. The presence of migratory CSC is the proposed explanation for such observations. The induction of EMT by transforming growth factor β-1 (TGFβ-1) enhanced NSCLC CD133+ population with enforced ability to form sphere and initiate tumours in NOD/SCID mice [296]. In pancreatic carcinoma, CD133+ CXCR4+ CSCs cells were identified in the invasive front of pancreatic tumours.

Depletion of this population abrogated the metastatic phenotype of the pancreatic tumours suggesting the importance of CSCs in cancer metastasis [297].

Animals injected with CD133+ cells in the present study presented with lymph node enlargement. In SCLC patients, metastasis to lymph nodes is often clinically observed. Therefore, based on the above data it was hypothesised that lymph node enlargement observed in animals was associated with CD133+ cell metastasis. Mouse lymph nodes are normally small and usually impalpable. Presenting lymph node enlargement could be a result of inflammation or metastasis. Inflammatory reactions usually subside after a few days. However, 52 days after subcutaneous implantation of SCLC CD133+ cells, episilateral and contralateral lymph nodes showed considerable enlargement suggestive of metastasis. Epislateral lymph nodes were slightly larger than contralateral nodes indicating sequential seeding of metastatic cells.

In the present study, enlarged axillary and inguinal lymph nodes were subject to IHC for histological confirmation. Prospective metastatic SCLC cells were subjected to NCAM evaluation, a cell adhesion molecule widely expressed on all SCLC cells contributing to its invasive behaviour [273, 295]. NCAM, a transmembrane glycoprotein, expressed during embryonic development and in adult tissues on neural cells, is a marker for cells of neuroendocrine origin [273]. Primary tumour (generated by injecting SCLC CD133+ cells) was used as positive control and mouse spleen never exposed to human SCLC was used a negative control. Sections were double stained with CD45 antibody. CD45 selects mouse leucocyte cells, and since lymph nodes are enriched in these cells, it was essential to distinguish these cells from prospective human SCLC cells.

Few NCAM+ CD45- cells in all four enlarged lymph nodes excised from the mice exposed to CD133+ SCLC cells were detected. However, few NCAM+ CD45- cells were also identified in mouse spleen used as negative control. NCAM a well-known maker for SCLC cells is also associated with NK cells. The *nude/nude* mice employed in this study, lack T cells but can produce B cells and NK cells. However,

the NCAM+ cells within the lymph nodes and the spleen were not NK cells, since they were not positive for CD45 antigen. SCLC cells express a range of neuropeptides and their corresponding receptors including gastrin releasing peptide (GRP) and its receptor GRP-R and vasopressin and its receptor, V_{1A}. It would be interesting to evaluate the expression of these receptors as a marker for possible SCLC metastasis to lymph nodes.

CSCs are chemoresistant cells. Supporting the CSCs hypothesis and in line with data observed in HCC and glioblastoma [80, 139, 141], 3 days after *in vitro* exposure of unsorted H345 and H69 cells to etoposide, the percentage of CD133+ cells significantly increased as the concentration of etoposide increased. The result suggests that in contrast to eradicated CD133- cells within SCLC cell lines, CD133+ cells were enriched on etoposide treatment. To further support the resistant phenotype of CD133+ cells, sorted population were subject to etoposide and after 72 hours the percentage of survival was evaluated by MTT assay. CD133+ cells in comparison to the CD133- cells exhibited a profound resistant to etoposide. The inhibitory effect of etoposide was not influenced by the growth rate ability of the two populations. As show in Figure 23, the growth of CD133+ and CD133- cells were similar on the day 3, the time when MTT cell viability assay was conducted. It was only around day 18 when the growth rate of the both population significantly changed. Parent cells that contained both CD133+ and CD133- population, moderately responded to etoposide compared to the sorted populations. These data provide direct evidence that chemotherapeutic agents eradicate the bulk of the tumour but leave behind CSCs unaffected with resultant chemotherapeutic failure.

Resistance to etoposide may be due to resistance to apoptotic. Therefore, apoptosis induced by etoposide on sorted population of H345 and H69 cells was evaluated after 72 hours exposure. As indicated by EB/AO and the May-Grunwald-Giemsa staining, CD133+ cells were profoundly resistant to apoptosis compared to the CD133- cells. However, the exact mechanism conferring resistance to apoptosis was unknown.

Two major apoptotic signalling pathways include the extrinsic pathway, which acts via death receptors, and the intrinsic pathway, which acts via release of mitochondrial proteins. Deregulation in both pathways has been demonstrated as mechanisms of death evasion in CSCs. The project focused on the intrinsic pathway of apoptosis. Activation of intrinsic pathway can be stimulated by anticancer agents, growth factor withdrawal, hypoxia, or by induction of oncogenes [298]. The pathway is regulated by the release of apoptogenic factors such as cytochrome c from the mitochondrial inter-membrane space into the cytosol. Once released, cytochrome c forms a complex with Apaf-1/caspase-9-containing apoptosome, triggering caspase-3 activation with subsequent induction of apoptosis. Members of Bcl-2 protein family are essential regulators of mitochondrial integrity. The Bcl-2 family comprises of pro- and anti-apoptotic proteins. The anti-apoptotic members include Bcl-2, Bcl-X_L and Mcl-1, and the pro-apoptotic members include Bax and Bak, as well as BH3 domain only molecules, for example Bid, Bim, Bik, Noxa and Puma. Bcl-2 members induce apoptosis by cleavage of Bid by caspase-8 and Bax-Bak oligomerisation causing mitochondrial permeabilization and release of cytochrome c. Bcl-2 members can inhibit apoptosis by various methods including by binding of Bcl-2 and Bcl-X_L to Bcl-2 and Apaf-1 forming a complex with pro-apoptotic proteins Bax and Bak, thereby inhibiting its function [298]. Imbalances in the ratio of pro- and anti-apoptotic proteins of the Bcl-2 family could skew the balance towards cell survival in the presence of an apoptotic stimulus. Over expression of Bcl-2 survival protein in CSCs has been documented to be associated with their resistance. Increased expression of anti-apoptotic proteins Bcl-2 and Mcl-1 was associated with resistance to ABT-737, a Bcl-2 inhibitor and down regulation of Mcl-1 partially reversed this resistance [299]. In line with these observations, chemoresistance in CD133+ glioblastoma cells was associated with significantly higher expression levels of Bcl-2 and Bcl-X_L compared to the CD133- cells [81]. These data suggest that targeting the mitochondrial death amplification pathways may be critical in reversing the apoptosis resistance phenotype of CSCs.

CSCs can also escape apoptosis by preferential activation of AKT pathway. Akt also known as protein kinase B (PKB), is a well-characterized downstream target of the

PI3K-Akt-mTOR pathway, and are mediators of cell survival in response to a number of stimuli. Preferential activation of this pathway by CSCs in various cancers not only augments survival advantage in serum-free and anchorage-independent conditions but also, orchestrates evasion of induced apoptosis [80, 300]. Upregulated constitutive activity of PI3k/Akt pathway is stimulated by autocrine and paracrine growth loops in SCLC cells via β1 integrin mediated interaction with ECM [230, 231, 246]. Akt/PKB through multiple mechanisms inhibits apoptosis. Akt by phosphorylation of pro-apoptotic BAD inhibits this pro-apoptotic member of the Bcl-2 family to form a non-functional heterodimer with survival factor Bcl-X_L, therefore resorting Bcl-X_L's anti-apoptotic function. Additionally Akt, by phosphorylation of caspase-9 inhibits the catalytic activity of this pro-death protease, thereby blocking its function. Finally, Akt by phosphorylation of FKHR, a member of Forkhead family of transcription factors, inhibits activation of its target genes such as BIM and FAS ligand that are pro-apoptotic proteins [301].

Based on the above data, Akt and Bcl-2 were selected as possible proteins deregulated in CD133+ SCLC cells mediating their chemoresistance phenotype. Therefore, sorted population of H345 and H69 cells were subject to western blotting to evaluate the endogenous expression of proteins involved in Akt/PKB and Bcl-2 survival signalling pathways. In both cell lines, CD133 expressing cells when compared to their CD133- counterpart, exhibited a marked preferential expression of active Akt (phosphorylated at Ser473) and higher levels of Bcl-2. Elevated expression of phosphoserine-specific Akt in CD133+ SCLC cells was not a result of an increase in total Akt. To my knowledge, this is the first study to demonstrate that CD133+ SCLC cells are resistant to apoptosis induced by chemotherapy and explain the signalling pathway associated with apoptosis resistance in these aggressive cells.

According to the data I have demonstrated in this chapter, SCLC CD133+ cells, exhibited characteristics similar to known CSCs. Therefore, it can be concluded that CD133+ cells are the CSC-like cells in SCLC cell lines and based on their stem cell-like, chemoresistant and tumorigenic nature, they are the possible cause of SCLC development and recurrence after initial chemoresponse. To strengthen this concept

it would be interesting to evaluate the correlation of CD133 expression with SCLC patient survival. In the present study tissue sections taken from SCLC patients demonstrated high levels of CD133 expression. However, no concluding remarks could be made due to lack of additional information about the patients' treatment history.

CHAPTER 5:
CD133+ cells express high levels of GRP-R and V_{1A}-R which mediate their clonal growth in semi-solid medium

5.1 Introduction

SCLCs are neuroendocrine tumours, characterised by the presence of intra-cytoplasmic neurosecretory granules, which secrete a wide range of hormones and neuropeptides [169, 302]. Some of these include gastrin releasing peptide (GRP), arginine vasopressin (AVP), gastrin, neurotensin and cholecystokinin. The finding that neuropeptides stimulate SCLC growth in an autocrine fashion was initially examined by Cuttitta et al., [190] using a monoclonal antibody to [Lys3]-bombesin (2A11). In the absence of serum, the antibody inhibited SCLC cell line colony formation and abolished the growth of SCLC xenografts in nude mice. Subsequently, it was shown that multiple neuropeptides through autocrine and paracrine interactions fuel SCLC growth and proliferation [169]. Treatment of SCLC xenografts (NCI-H69) with broad spectrum antagonists such as SP-G, that inhibits the growth stimulatory effect of multiple neuropeptides, abolished tumour growth [220, 303]. The growth stimulatory effect of neuropeptides has also been documented in other cancers including breast, colon, pancreatic and prostate cancers [304-307]. Therefore, targeting neuropeptides or their receptors could be an interesting strategy for not only SCLC but also other malignancies with neuroendocrine phenotype.

Much of the studies on SCLC treatment were focused on the mitogenic roles of GRP and AVP. GRP receptor (GRP-R) expression has been detected in various neuroendocrine tumours including breast, prostate, colon and lung, conferring survival advantage in these cells [65]. Expression of GRP-R is associated with malignant transformation of human kidney tissue into renal carcinoma [308]. In SCLC patients, detection of GRP-R in peripheral blood has been proposed as a useful early diagnostic marker [309]. Likewise, vasopressin and its receptor V_{1A} is a well studied neuropeptide associated with SCLC, breast and pancreatic cancer survival and proliferation [169, 310]. Similar to GRP, vasopressin mediates SCLC

growth through an autocrine and paracrine circuit. In line with previous data documented [311], in my laboratory, the expression of V_{1A} receptor was detected in four out of four SCLC cell lines [65]. Taken together, overexpression of these neuropeptide receptors is shown to be associated with malignant status of neoplastic cells.

Waters et al., [65] demonstrated that acquired resistance in SCLC patients was associated with increased expression of neuropeptide receptors on the drug resistance cells. This was evaluated by quantifying the expression levels of GRP-R by semi-quantitative RT–PCR in three human SCLC cell lines (GLC14, 16 and 19) established from a single patient during longitudinal follow-up [65, 228]. During this period, the initial chemosensitive tumour became increasingly chemoresistant. Increased expression of GRP-R on the drug resistant cells (GLC16 exhibited 6 fold and GLC19 exhibited 11 fold increased GRP-R expression compared to GLC14) was associated with increased proliferation and colony formation in the presence of neuropeptides [65]. This indicated the neuropeptide dependent growth of resistant SCLC cells. Thus, neuropeptide growth factors and their receptors could serve as prospective targets for intervention in chemoresistant candidates.

Multiple studies have demonstrated CSCs as resilient cells that are enriched following chemotherapy [80, 82, 141, 312]. In line with this concept, Levina et al., [82] demonstrated that chemotherapy enriched lung CSCs. The author argued that the aggressive phenotype of drug surviving lung CSCs was associated with increased expression of various growth factors with survival and proliferation advantage. Recently, preliminary data by Flores et al, [172] suggested the involvement of GRP-R in ex-vivo expansion of brain CSCs. Based on this data combined with the knowledge that chemoresistance in SCLC cell lines is associated with increased expression of neuropeptide receptors, it was hypothesised that the aggressive phenotype of CD133+ SCLC is due to greater expression of GRP-R and V_{1A}-R. Understanding the mechanism promoting the growth of these aggressive cells is warranted for designing novel therapies.

5.2 Results

5.2.1 CD133+ cells express higher levels of GRP and V_{1A}-receptors in H345 and H69, respectively than their corresponding CD133- cells

H345 cells have relatively high GRP-R expression [313] and H69 cells were previously shown in my laboratory to express V_{1A}-R [225]. Therefore, the expression levels of GRP-R in isolated H345 cells and V_{1A}-R in isolated H69 cells were quantified using q-PCR. Q-PCR provides valuable information regarding the relative expression of transcripts in a cell. RNA was extracted from the isolated cells and was reverse transcribed to cDNA and subsequently the expression levels of GRP-R and V_{1A}-R were quantified by the TaqMan® gene expression assay kit (Applied Biosystems, USA). 18S mRNA was used as internal control. CD133+ H345 cells expressed significantly higher mRNA levels of GRP-R than the CD133- H345 (fold increase in CD133+, 3.4 ± 0.3, and CD133-, 0.84 ± 0.22, P=0.0026) and parent cells (1.5 ± 0.18, P=0.0043) (Figure 43A1). Similarly, H69 CD133+ cells demonstrated significant higher mRNA levels of V_{1A}-R compared to its corresponding negative population (fold increase in CD133+, 4.97 ± 0.15, and CD133-, 0.66 ± 0.38, P=0.0005) and parent (unsorted) cells (2 ± 0.24, P=0.0005) (Figure 43A2). Therefore, CD133+ cells retained higher mRNA levels of neuropeptide receptors compared to their negative counterpart.

The expression of GRP-R in H345 sorted cells and V_{1A}-R in H69 isolated cells were further evaluated for the protein levels by western blotting and data was quantified using ImagJ. As illustrated in Figure 43B1, a band of ~65 kDa was indicative of GRP-P protein expression. CD133+ H345 cells exhibited 1.58 ± 0.012 times (P<0.001) higher GRP-R protein expression compared to the CD133- cells. Lysates of G6A cells (CHO cells transfected with GRP-R [171]) was used as a positive control. Similar observations were made in H69 sorted cells (Figure 1B2). A band of ~48 kDa was indicative of V_{1A}-R expression. CD133+ H69 cells exhibited 1.77 ± 0.01 times (P<0.001) higher V_{1A}-R protein expression compared to the CD133- cells. Lysates of V3B cells (CHO cells transfected with V_{1A}-R [171]) was used as positive control. Protein expression levels were normalised relative to β-actin levels.

Therefore, neuropeptide receptor expression in CD133+ cells was not only transcriptionally but also translationally enhanced compared to CD133- cells.

Figure 43

5.2.2 Exogenous GRP and AVP enhance the colony formation of CD133+ H345 and CD133+ H69 cells, respectively

Multiple Ca^{2+} mobilising neuropeptides augment SCLC cell lines to form colonies in semi-solid medium indicating SCLC growth is regulated by various autocrine and paracrine circuits. Therefore, the effects of exogenous GRP and AVP on the clonogenicity of the corresponding CD133+ were examined. Sorted CD133+ cells were cultured in semi-solid SITA medium in the presence of three different concentrations (1, 10, and 100 nM) of GRP for sorted H345 cells and AVP for sorted H69 cells. The number of colonies formed was evaluated after 21 days by light microscopy. Untreated cells were used as control, representing basal clonogenicity. The effect of neuropeptide on CD133+ colony formation was compared with that of their corresponding parent cells (unsorted cells). The effect of neuropeptide on CD133- H345 and H69 cells could not be evaluated as CD133- cells, despite low levels of GRP-R or V_{1A}-R expression, did not respond to the growth stimulatory effect of neuropeptides in the semi-solid medium and appeared apoptotic within 3-5 days post-culture. As shown in Figure 44A increased colony formation in the CD133+ H345 cells was observed in a dose-dependent manner in the presence of GRP (cloning efficiency at 1 nM, 8.81 ± 1%, at 10 nM, 16.43 ± 0.74% and at 100 nM, 18.34 ± 1.17%) compared to control (basal cloning efficiency 4.84 ± 1.08%). Similar observations were made in the parent H345 cells (cloning efficiency at 1 nM, 2.67 ± 0.56%, at 10 nM, 6.7 ± 0.83%, at 100 nM, 10.4 ± 1.38%, and control 2 ± 0.34%). Although a concentration dependent colony growth was also observed in the parent cells in the presence of GRP, the effect of this neuropeptide on the clonogenicity of CD133+ cells was significantly enhanced. This effect was apparent at low concentration of GRP where 1 nM GRP doubled (P=0.048) the clonal growth of CD133+ cells whereas the same concentration of GRP did not significantly change the clonal growth of parent cells.

The addition of AVP to CD133+ H69 cells enhanced their clonal growth in semi-solid medium (Figure 44B). Like the effects of GRP on the clonal growth of CD133+ H345 cells, the CD133+ H69 cells responded to AVP in a dose-dependent manner with significant enhancement of their cloning efficiency (cloning efficiency at 1 nM,

11.06 ± 0.93%, at 10 nM, 16.44 ± 1.8% and at 100 nM, 14.50 ± 2.07%) compared to untreated cells (basal cloning efficiency 6.51 ± 0.53%). Similar observations were made in the parent cells (cloning efficiency at 1 nM 4.06 ± 0.55%, at 10 nM, 8.47 ± 1.48%, at 100 nM, 5.40 ± 0.6%, and untreated control, 3.40 ± 0.43%). The significant effect of AVP on the colony formation of CD133+ cells compared to that of parent cells was apparent at low concentration of this neuropeptide where 1 nM AVP enhanced the clonogenic efficiency of the CD133+ cells by 2.5 fold (P=0.012) whereas the same concentration of this neuropeptide did not significantly effect the clonogenicity of parent cells. In both CD133+ and parent H69 cells, 10 nM was the maximum concentration of AVP to stimulate colony formation and higher concentration of AVP (100 nM) reduced colony formation. Similar observations were previously made in my laboratory, demonstrating high concentrations of neuropeptide had decreased stimulatory effects [169]. This phenomenon presumably could be associated with homologous desensitisation in this long-term assay. Time-dependent growth desensitisation has also been reported in other cellular systems [314, 315]. Therefore, exogenous neuropeptides significantly stimulate clonal growth of CD133+ cells indicative of autocrine growth signalling mediating their growth.

Figure 44

5.3 Discussion

The data in this chapter demonstrates that CD133+ SCLC cells transcriptionally and translationally express higher levels of neuropeptide receptors, GRP-R and V_{1A}-R. Addition of exogenous neuropeptides significantly enhanced the colony formation of CD133+ cells, indicating for the first time, the critical role of neuropeptides in mediating the autocrine growth of these aggressive cells.

CSCs are the proposed cause underpinning tumour initiation progression and chemoresistance due to their aggressive phenotype. In line with this theory, the present study demonstrated that CD133+ SCLC cells are proliferative cells with higher clonogenicity *in vitro* compared to the CD133- cells. However, the mechanism mediating CD133+ SCLC growth remains unknown.

Levina et al., [82] documented that drug resistant CSCs exhibited significant higher expression levels of angiogenic and growth factors (VEGF, bFGF, IL-6, IL-8, HGF, PDGF-BB, G-CSF, and SCGF-beta) compared to non-CSC population. The author concluded that elevated levels of these factors are associated with high growth profile, tumorigenic and metastatic potentials of CSCs. Similar observation was made in colorectal cancer cells where in CD133+ cells expressed elevated gastrin precursors [316]. Analysis of sixty primary colorectal tumours revealed, increased expression of these peptides on the CD133+ cells through activation of Akt signalling pathways mediate their proliferation, colony formation and chemoresistance. Down-regulation of gastrin peptides in colorectal CD133+ cells was associated with loss of tumour initiation *in vivo*, further supporting the role of this peptide in the survival and growth of CSCs [316]. These data indicate the importance of growth factors in the regulation of CSCs expansion making them promising targets for CSC therapies.

Waters et al., [65] working on GLC cell lines, demonstrated that resistance in SCLC cells is in line with increased expression of neuropeptide receptor, GRP-R which subsequently was associated with their growth in liquid culture and colony formation

in semi-solid medium. This would be similar to the generation of autocrine and paracrine growth loops in cancer development *in vivo*, with malignant cells becoming more dependent on neuropeptide growth factors for survival and resistance. To further emphasise the importance of growth stimulatory effect of neuropeptides, MacKinnon et al., [171], investigated the effect of neuropeptide receptors on the growth of CHO cells. Introduction of GRP-R and V_{1A}-R in CHO cells led to cellular transformation and was associated with enhanced proliferation, colony formation and resistance to etoposide.

Based on the knowledge that drug resistant CSCs express higher levels of growth factors and that neuropeptides and their receptors are essential mediators for SCLC survival, growth and chemoresistance, in the present study I hypothesise that the aggressive phenotype of CD133+ SCLC cells could be associated with their increased expression of neuropeptide receptors. The expression of these receptors was evaluated transcriptionally and translationally on CD133+ cells using q-PCR and western blotting, respectively. As shown in Figure 43, CD133+ H345 cells expressed significantly higher levels of GRP-R and CD133+ H69 cells expressed significantly higher levels of V_{1A}-R compared to corresponding CD133- and parent cells, indicating their greater neuropeptide dependence. Therefore, based on the data obtained in this section and in line with previous observations [82, 316], CD133+ cells express higher levels of growth factors as a possible mechanism mediating their growth and potential tumour initiating capacity.

CD133+ cells in both cell lines demonstrated significant elevated basal colony formation compared to their parent cells (Figure 44). This may be explained by higher neuropeptide receptor expression on the CD133+ cells. Ferris et al., [317] demonstrated that GRP-R is oncogenic when transfected into non-malignant NCM460 colon cancer cell line. Since transfected colon cancer cells lines do not secrete GRP and in the presence of ligand specific antagonist their growth was not influenced, the author concluded that enhanced proliferation in GRP-R transfected cells was associated with constitutive activation of its receptors. Despite no evidence documented of such constitutive activation for V_{1A}-R, it may be suggested that

higher basal clonogenic efficiency observed in the CD133+ cells compared to parent cells could be due to constitutive activation of these receptors triggering the growth signals. In both cell lines, cloning efficiency in response to neuropeptide was increased in the CD133+ population. The observation not only supports the earlier data in this chapter (Figure 43) that CD133+ cells express higher levels of these receptors, but additionally indicated that they are fully functional and mediate SCLC growth through autocrine signalling. However, to confirm the autocrine growth loops in CD133+ SCLC cells, it would be interesting to measure GRP or AVP levels in cultures.

The finding that CD133+ CSCs express significant amount of neuropeptide receptors and that their growth is dependent on their expression would allow us to design therapies that would preferentially eliminate these aggressive cells without significant side effects.

CHAPTER 6:
Peptide-1, therapy for CD133+ SCLC cells?

6.1 Introduction

Multiple intracellular calcium mobilising neuropeptides and their receptors are the proposed prime regulators of SCLC cell growth. Drugs targeting single mitogenic neuropeptides such as the monoclonal antibody 2All which specifically inhibits the binding of GRP to its receptor produced a poor clinical outcome [318]. Thus, analogues that inhibit the mitogenic effect of multiple neuropeptides are warranted to curtain the lethal disease that is fuelled by an extensive neuropeptide network.

Previously, a series of modified substance-P analogues were shown to inhibit the effects of a range of neuropeptides on SCLC cells and have demonstrated efficacy in animal models [64, 220]. These peptide analogues, termed "broad spectrum antagonists" include SP-A and SP-G, via neuropeptide receptors including GRP and V_{1A} receptors, act as "biased agonists" [64, 65, 171, 221, 223, 224]. At the receptor, they display antagonist activity blocking the neuropeptide induced Ca^{2+} mobilisation and agonist activity inducing sustained activation of JNK and ERK. Inhibition of Ca^{2+} release along with prolonged activation of ERK and JNK pathways attenuates cellular proliferation and augments apoptosis. SP-G has completed a phase 1 clinical trial where therapeutic plasma concentrations were achieved with no dose limiting toxicity [66].

Development of resistance to conventional chemotherapy in SCLC cells was accompanied by an increase in neuropeptide receptor expression as investigated on GLC14, 16 and 19, three SCLC cell lines established from one patient during clinical follow-up (see chapter 1 for more details on the GLC cell lines) [65, 227, 228]. This was accompanied by enhanced response to SP-G where this analogue inhibited the growth and colony formation of all three SCLC cell lines but was more effective in the most chemoresistant line GLC19 which expressed higher neuropeptide receptor compared to the more chemosensitive cell lines GLC14 and GLC16 (Figure 45) [65], making SP-G an ideal analogue for treatment of resistant disease. In chapter 5, I have

shown that chemoresistant CD133+ SCLC cells exhibit greater expression of neuropeptide receptors compared to CD133- cells. SP-G may therefore be more effective in CD133+ cells.

Figure 45

A limiting factor in the effectiveness of SP-G is its short half life (25 minutes) in plasma when administered systemically [66]. This is the major factor that has resulted in the suspension of further clinical development of the compound. The short half life is due to rapid metabolism of this analogue investigated *in vitro* using whole mouse liver homogenates and *in vivo* after intra-peritoneal injection in mice [319, 320]. The hexapeptide structure of SP-G includes D-amino acids and N-methylated amino acids located at the N-terminus leaving the C-terminal unmodified where degradation has shown to occur [321, 322]. The enzyme responsible for SP-G degradation is a serine carboxypeptidase with generation two metabolites via initially deamidation of the C-terminus to produce Metabolite I (NH_2-Arg-DTrp-MePhe-DTrp-Leu-Met-OH), and subsequently carboxylation producing Metabolite II (NH_2-Arg-DTrp-MePhe-DTrp-Leu-OH) [319]. Identification of more stable analogues of SP-G with maintained efficacy may lead to the identification of a new clinical candidate for SCLC treatment.

In collaboration with Professor Mark Bradley (Department of Chemistry, Kings Building, Edinburgh), a series of analogues were synthesised based on the structure of SP-G and SP-A, with the aim to enhance stability and possibly potency. Substitution with D-amino acids and N-methylation are well-known devices to aid stability [323, 324]. Dimers have inherent advantages as binding is enhanced due to entropic considerations. The dimers were based on SP-G structure with various linking strategies: Cyclo (Arg-DTrp-NMePhe-DTrp-Leu-Asp), Arg-DTrp-NMePhe-DTrp-Leu-Linker-Arg-DTrp-NMePhe-DTrp-Leu (Linker = Gly or GABA) and O=C (Arg-DTrp-NMePhe-DTrp-Leu)$_2$. The eight analogues are listed below:

1) DArg-Pro-Lys-Pro-DTrp-Gln-DTrp-Phe-DTrp-DLeu-Leu
2) DArg-Pro-Lys-Pro-DTrp-Gln-DTrp-Phe-DTrp-Leu-GABA
3) DArg-Pro-Lys-Pro-DTrp-Gln-DTrp-Phe-DTrp-Leu-Gly
4) DArg-Pro-Lys-Pro-DTrp-Gln-DTrp-Phe-DTrp-Leu-1,2 Ethylenediamine
5) Arg-DTrp-NMePhe-DTrp-DLeu-Met
6) Arg-DTrp-NMePhe-DTrp-Leu-GABA
7) Arg-DTrp-NMePhe-DTrp-Leu-Gly
8) Arg-DTrp-NMePhe-DTrp-Leu-1,2 Ethylenediamine

It is the aim of this chapter to evaluate the efficacy of this new panel of peptides on SCLC cell lines and to establish the efficiency of these analogues on CD133+ cells.

6.2 Results

6.2.1 SCLC cell lines are sensitive to peptide-1

The inhibitory effect of the newly designed peptides was evaluated in H345 and H69 cell lines. Cytotoxicity was determined by MTT accumulation after 72 hours. Untreated cells served as control and data is represented as percentage of control. The potency of the analogues was compared with that of SP-G. The IC_{50} values (concentration of drug required to reduce cell viability by 50%) of the new analogues and SP-G in H345 and H69 are illustrated in Table 9. In both cell lines, peptide-1 proved to be the most potent analogue compared to SP-G and the newly synthesised peptides in inhibiting cell viability. As shown in Figure 46A and B, the efficiency of peptide-1 was significantly higher than that of SP-G in H345 cells (IC_{50} value of peptide-1, 3.06 ± 0.41 μM and SP-G, 11.87 ± 1.04 μM, P=0.0014) and in H69 cells (IC_{50} value of peptide-1, 4.96 ± 0.64 μM and SP-G, 15.53 ± 1.99 μM, P=0.011). Peptide-1 demonstrated ~4 fold increased potency in H345 cells and ~3 fold augmented potency in H69 cells compared to SP-G. Thus, this analogue was selected for further analysis. Peptides 2, 3, 4, 6, 7, and 8, all less potent than SP-G with IC_{50} values above 100 μM were excluded from further analysis. Although peptide-5 demonstrated an IC_{50} value less than 100 μM (IC_{50} value of peptide-5 in H345 cells, 44.34 ± 3.29 μM and in H69 cells, 46.63 ± 2.63 μM), the efficiency of this analogue in inhibiting cell viability compared to SP-G was lower therefore, it was excluded from further studies.

table 9

Figure 46

6.2.2 Peptide-1 inhibits intracellular calcium mobilisation

The mobilisation of $[Ca^{2+}]_i$ stores is one of the earliest events triggered by binding of neuropeptides to their receptors and activation of $G_{\alpha q}$ subunit of G-proteins leading to PLC signalling with subsequent production of IP_3 (Figure 5) [195, 196]. SP-G blocks the Ca^{2+} mobilisation induced by various neuropeptides [171, 224]. In this study, the effect of peptide-1 on GRP- and AVP-induced calcium mobilisation was examined on cell lines transfected with the human GRP and V_{1A} receptors (G6A and V3B cells, respectively [171]). Quiescent G6A and V3B cells were incubated with FURA-2AM at 37°C for 20 minutes and the ratiometric fluorescence was monitored at 37°C. Figure 47, demonstrates a representative trace of intracellular calcium mobilisation in G6A treated with GRP or a combination of GRP and peptide-1.

Initially, the effect of GRP and AVP on the $[Ca^{2+}]_i$ mobilisation in G6A and V3B cells were evaluated in the absence of peptide-1. As shown in Figure 48A, in G6A cells, GRP produced a concentration-dependent increase in $[Ca^{2+}]_i$ (EC_{50} = 1.34 ± 0.12 nM). Similarly, in V3B cells (Figure 48B) an elevation in $[Ca^{2+}]_i$ was observed in a dose-dependent manner (EC_{50} = 1.4 ± 0.24 nM). To evaluate the antagonist effect of peptide-1 on $[Ca^{2+}]_i$ mobilisation induced by neuropeptides, samples were initially treated with various concentrations of peptide-1 (1-100 µM) for 2 minutes at 37°C before adding 10 nM GRP for G6A cells or AVP for V3B cells (Figure 48C, and D). In G6A and V3B cells, 10 nM neuropeptide produced the maximum intracellular calcium mobilisation, thus this concentration was selected for further evaluations. In both cell lines, peptide-1 inhibited the response to GRP and AVP in a dose-dependent manner with resultant IC_{50} values of 0.36 ± 0.12 µM in G6A (Figure 48C) and 1.7 ± 0.34 µM in V3B cells (Figure 48D). Peptide-1 was more efficacious in inhibiting the GRP response than the AVP response. Together, these data suggest that peptide-1 inhibits $[Ca^{2+}]_i$ mobilisation induced by GRP as well as AVP with greater selectivity for GRP.

Figure 47

Figure 48

6.2.3 Peptide-1 inhibits SCLC cell proliferation

SP-G inhibits SCLC growth by blocking neuropeptide-induced $[Ca^{2+}]_i$ mobilisation [214]. It was hypothesised that peptide-1 would similarly attenuate SCLC proliferation in liquid culture. To evaluate this hypothesis, SCLC cells were cultured in serum-free SITA medium, in the presence of SP-G or peptide-1. Untreated samples were used as control. Cell number was determined by NucleoCounter NC-100 for 24 days and data is presented as percentage of control on day 24. As illustrated in Figure 49, peptide-1 inhibited H345 and H69 proliferation in a dose-dependent manner, IC_{50} in H345 was 3.62 ± 0.66 µM (Figure 49A) and in H69 cells was 4.09 ± 0.55 µM (Figure 49B). The efficacy of peptide-1 was significantly greater than SP-G (IC_{50} in H345 cells treated with SP-G was 9.73 ± 1.1 µM and in H69 cells treated with SP-G was 10.33 ± 0.81 µM). Thus, peptide-1 was more potent growth inhibitor than SP-G in H345 (P=0.01) and H69 cells (P=0.003).

Figure 49

6.2.4 Peptide-1 inhibits basal and neuropeptide stimulated colony formation

As described in chapter 5, GRP and AVP stimulate clonal growth of H345 and H69 cells. Previously, at my laboratory, it was demonstrated that SP-G inhibited neuropeptide mediated growth with dramatic decrease in clonogenicity of SCLC cells in the absence and the presence of exogenously added neuropeptide [64]. The present study evaluated the effect of 10 µM peptide-1 on the clonal growth of SCLC cells in the absence and the presence of 10 nM GRP and AVP (Figure 50). The concentration of peptide-1 and GRP and AVP was selected based on the observation that, 10 µM peptide-1 had shown maximum growth inhibitory effect on SCLC cells and 10 nM GRP and AVP displayed maximum stimulatory effect on H345 and H69 cells, respectively.

Peptide-1 inhibited the colony formation of both H345 and H69 cells in the absence as well as in the presence of neuropeptides (Figure 50A and B). This analogue significantly inhibited the basal colony growth of H345 (cloning efficiency of control cells, 2.23 ± 0.27%, and 10 µM peptide-1 treated cells, 1.01 ± 0.12%, P=0.01) and H69 cells (cloning efficiency of control cells, 3.35 ± 0.52%, and 10 µM peptide-1 treated cells, 1.68 ± 0.12%, P=0.01). Additionally, peptide-1 abolished the growth stimulatory effect of exogenously added neuropeptides in H345 (cloning efficiency of 10 nM GRP, 7.30 ± 1.04%, and 10 nM GRP + 10 µM peptide-1, 3.63 ± 0.26%, P=0.02) and H69 cells (cloning efficiency of 10 nM AVP, 9.09 ± 0.39%, and 10 nM AVP + 10 µM peptide-1, 4.18 ± 0.67%, P=0.003). Evidently, peptide-1 inhibited the basal and stimulated clonal growth of SCLC cells in semi-solid medium.

Figure 50

6.2.5 Peptide-1 induces apoptosis

SP-G induces apoptosis in SCLC cells [224]. To determine if the cytotoxicity induced by peptide-1 was due to apoptosis, H345 and H69 were treated with two different concentrations of SP-G or peptide-1 (1 μM and 10 μM) and after 72 hours, apoptosis was determined by cytocentrifuging cells on to glass cover slips and staining with May-Grunwald-Giemsa.

Apoptotic cells appeared as shrunken cells with dense nuclei and were quantified by light microscopy (Figure 51A). Similar to SP-G, peptide-1 induced apoptosis but with greater efficiency than SP-G in both H345 (Figure 51B) and H69 cells (Figure 51C). 1 μM SP-G did not significantly induce apoptosis in the treated cells compared to corresponding controls, whereas the same concentration of peptide-1 significantly increased the percentage of apoptotic cells in H345 (percentage of apoptosis in control, 13.98 ± 0.8%, and in 1 μM peptide-1 treated cells, 36.73 ± 3.35%, P=0.002) and in H69 cells (percentage of apoptosis in control, 17.93 ± 1.52%, and in 1 μM peptide-1 treated cells, 34.06 ± 2.61%, P=0.005). At 10 μM, both peptide analogues induced apoptosis in treated H345 (percentage of apoptosis in cells treated with 10 μM SP-G 40.78 ± 3.4% and peptide-1, 68.90 ± 2.53%) and H69 cells (percentage of apoptosis in cells treated with 10 μM SP-G 33.60 ± 2.62% and peptide-1, 55.86 ± 2.4%) cells. However, the efficiency of peptide-1 was significantly greater than SP-G in H345 (P=0.003) and H69 cells (P=0.003). Therefore, peptide-1 induces apoptosis in H345 and H69 cell lines and it is a significantly more potent than SP-G.

Figure 51

6.2.6 Peptide-1 is more stable than SP-G

Stability of peptide-1 and SP-G was studied *in vivo* using S9 mouse liver preparation. Drug metabolism was investigated over a 130 minute time course and aliquots were removed at appropriate time points for HPLC analysis. HPLC analysis was kindly conducted by Doctor Nikolaos Avlonitis in Professor Mark Bradley's laboratory, Institute of Chemistry, Edinburgh University. Figure 52 demonstrates representative Figures of HPLC traces at different time points. Over time, gradual disappearance of full length peptide which was accompanied by the appearance of two metabolites was observed. By measuring the area under each peak, the amount of non-metabolised peptide-1 or its metabolites produced were calculated. Data is presented as the percentage of non-metabolised analogues present in the sample with time compared to time 0. As illustrated in Figure 53, peptide-1 was found to be approximately 4.5 fold more metabolically stable than SP-G (P=0.03). The t1/2 (the time point when 50% of the analogue is degraded) of SP-G and peptide-1 were 9.32 ± 1.37 and 41.50 ± 2. 56 minutes, respectively.

Figure 52

Figure 53

6.2.7 Peptide-1 inhibits H345 xenografts

SP-G inhibits SCLC cell growth *in vitro*, as well as *in vivo* [64]. To examine the effect of peptide-1 on SCLC xenografts, 15×10^6 H345 cells suspended in growth factor reduced Matrigel (1:1 volume of cells:Matrigel mixed at 4°C, total volume of 100 µl) were implanted subcutaneously in the right flank of *nude/nude* mice. Tumours were palpable 3 days post-injection. Drug exposure was initiated on day 7 and was continued once daily for 5 consecutive days. Peptide-1 was dissolved in sterile distilled H_2O and administered by subcutaneous injection at a dose of 25 mg/kg. Etoposide dissolved in sterile distilled H_2O and was administered by subcutaneous injection at 15 mg/kg. Controls received the same dose schedule of vehicle (H_2O). Tumours were measured using callipers every 3-4 days for a total of 33 days.

As illustrated in Figure 54, until day 15 no significant difference between control animals (treated with vehicle) and animals receiving peptide-1, etoposide, or combination of both drugs was observed. However, from day 20 onwards, a significant reduction in tumour volume was observed in animals receiving treatment(s) compared to controls (tumour volumes on day 20 for controls were, 335.21 ± 43.57 mm^3, for peptide-1 treated animals were, 149.37 ± 47.70 mm^3, for etoposide treated animals were, 187.66 ± 38.68 mm^3, and for peptide-1 + etoposide treated animals were, 160.95 ± 21.46 mm^3, ANOVA, P=0.026) (tumour volumes on day 24 for controls were, 506.65 ± 80.85 mm^3, for peptide-1 treated animals were, 204.41 ± 60.79 mm^3, for etoposide treated animals were, 259.63 ± 71.41 mm^3, and for peptide-1 + etoposide treated animals were, 262.15 ± 34.72 mm^3, ANOVA, P=0.025) (tumour volumes on day 27 for controls were, 875.83 ± 114.59 mm^3, for peptide-1 treated animals were, 228.01 ± 113.61 mm^3, for etoposide treated animals were, 269.85 ± 95.79 mm^3, and for peptide-1 + etoposide treated animals were, 343.11 ± 68.86 mm^3, ANOVA, P=0.003). The inhibitory effect of all three treatments was maintained beyond the duration of administration. To be noted, the tumour volume of the control animals had reached the maximum permissible size authorised by the Home Office license, and were terminated on day 27. Therefore,

the administration of peptide-1 alone produced a significant reduction in tumour volume for the duration of the study and was as efficacious as etoposide alone. These observations indicated that peptide-1 not only attenuated SCLC growth *in vitro* but also profoundly inhibited SCLC xenografts.

Figure 54

6.2.8 Peptide-1 is more effective in CD133+ cells than CD133- cells

As shown above, peptide-1 is a more potent inhibitor of SCLC growth *in vitro* and *in vivo* and also more stable than SP-G, making it an ideal neuropeptide analogue for the treatment of chemoresistant SCLC cells. The inhibitory effect of this analogue was evaluated on the CD133+ and CD133- H345 cells and parent cells (Figure 55) by MTT assay. CD133+ cells were more responsive to peptide-1 compared to their corresponding negative counterpart and parent cells in H345 cell line (IC_{50} values of CD133+, 1.83 ± 0.61 μM, CD133-, 24.71 ± 2.09 μM, and parent 5.85 ± 0.90 μM, P=0.0003, ANOVA).

Figure 55

6.3 Discussion

Data in this chapter revealed that the newly designed peptide-1 is a potent inhibitor of intracellular calcium mobilisation stimulated by neuropeptides in SCLC cell lines. The analogue profoundly inhibited the growth of SCLC cells in liquid and semi-solid medium and induced apoptosis. Peptide-1 was ~4 fold and ~3 fold more potent inhibitor of H345 an H69 cell viability, respectively and ~3 fold more potent inhibitor of SCLC cell growth in both cell lines in liquid culture compared to SP-G. Peptide-1 inhibited basal and neuropeptide stimulated colony formation. In addition to improved potency of peptide-1, the analogue also showed ~4 fold enhanced stability *in vitro* compared to SP-G. In vitro results suggested that, the analogue would also abolish SCLC growth *in vivo*. In line with the hypothesis, peptide-1 profoundly inhibited H345 growth in *nude*/*nude* mice and was as efficacious as etoposide. The knowledge that SP-G is more effective in cells with higher neuropeptide receptor expression prompted the speculation that peptide-1 would be more effective in the chemoresistant CD133+ cells that over express neuropeptide receptors. Supporting this hypothesis, CD133+ SCLC cells exhibited significant increased sensitivity to peptide-1 compared to the CD133- sub-population, making it an interesting analogue for treatment of chemoresistant SCLC patients.

Despite numerous studies and advances in cytotoxic drug development, SCLC still remains as an incurable disease. Recurrence with intractable resistance results in fatality. In the present study it has been proven that, within SCLC cell lines resides a sub-population of CD133 expressing cells with stem cell-like phenotype. These cells are clonogenic and chemoresistant *in vitro*, and are more tumorigenic *in vivo* than the CD133- population and could be the possible cause of SCLC chemoresistance and recurrence. Therefore, structuring drugs that selectively target these aggressive cells could open a new horizon in SCLC management.

SP-G, a broad spectrum neuropeptide antagonist, inhibits the growth stimulatory effect of multiple neuropeptides in SCLC cells *in vitro* and *in vivo* [64, 220, 226]. SP-G, despite novel potential, encounters a major drawback with its instability in

plasma making therapy impracticable [66]. This urged the necessity to design analogues with added stability. Eight novel analogues were modelled based on the structures of either SP-G or SP-A with the aim to increase stability and possible potency compared to SP-G. Peptide-1 was the only analogue that exhibited enhanced inhibitory effect in H345 and H69 cells and was chosen for further evaluations. Peptide-1, DArg-Pro-Lys-Pro-DTrp-Gln-DTrp-Phe-DTrp-DLeu-Leu, consists of 11 amino acids with chemical structure similar to SP-A, DArg-Pro-Lys-Pro-DTrp-Gln-DTrp-Phe-DTrp-Leu-Leu-NH2, but has a D-Leucine substitution at position 10. The efficiency of this novel analogue was compared with SP-G which has successfully completed a phase 1clinical trial [66].

Multiple neuropeptides stimulate $[Ca^{2+}]_i$ mobilisation in SCLC cells [64] and SP-G blocks the Ca^{2+} mobilisation induced by various neuropeptides [171, 223, 224]. The inhibitory effect of peptide-1 on $[Ca^{2+}]_i$ mobilisation induced by neuropeptide was evaluated in CHO cells transfected with GRP and V_{1A} receptors. Previously, in my laboratory the stimulatory effect of GRP and AVP and the inhibitory effect of SP-G on $[Ca^{2+}]_i$ mobilisation was evaluated on transfected CHO cells with GRP and V_{1A} receptors [171], therefore, in the present study these cells were chosen for evaluation of the effect of peptide-1 on $[Ca^{2+}]_i$ mobilisation. In line with previous data obtained from my laboratory [171], GRP and AVP produced a concentration-dependent increase in $[Ca^{2+}]_i$ in the transfected cells. Peptide-1 functioned as an antagonist for Ca^{2+} release and inhibited calcium production in a dose-dependent manner. This observation was in line with the antagonist activity observed by SP-G. AVP and GRP act through distinct receptors, but activate common signal transduction pathways. Peptide-1 inhibited the stimulatory effect of both neuropeptides. This could suggest that peptide-1, similar to SP-G, could function as a broad spectrum antagonist inhibiting the growth stimulatory effect of multiple neuropeptides. However, to confirm this concept the inhibitory affect of peptide-1 on $[Ca^{2+}]_i$ mobilisation stimulated by other neuropeptides including bradykinin, galanin, cholecystokinin, and neurotensin should be evaluated. Peptide-1 demonstrated more selectivity for GRP receptor than V_{1A} receptor. Thus, the compound may be tailored for the treatment of specific tumours with higher GRP-R over expression.

Peptide-1 inhibited the growth of SCLC cell lines in liquid culture. The inhibitory effect of this compound was ~3 fold higher in H345 and in H69 cells compared to SP-G. As expected, peptide-1 also caused a dramatic decrease of the cloning efficiency of these cells in the absence of any exogenously added peptide (basal colony formation) and in the presence of neuropeptide (GRP or AVP) stimulation. These findings suggest that the structural modification of SP-A (substitution of Leu with D-Leu at the position 10 of SP-A) did not disrupt the anti-cancer activity of this compound and that peptide-1 was significantly more efficacious than SP-G.

Similarly, the structural modification of SP-A to design the novel analogue did not effect the pro-apoptotic action of this compound on SCLC cell lines. Similar to SP-G, peptide-1 induced apoptosis in H345 and H69 cells, with peptide-1 efficacy significantly higher than SP-G. Although, mechanism of action of peptide-1 was not evaluated in the present study, cytotoxic effects on SCLC cells with a similar mechanism as SP-G are speculated.

The most outstanding feature of SP-G is its augmented efficacy in chemoresistant SCLC cells due to their higher neuropeptide dependent growth. In the present study it was demonstrated that chemoresistant CD133+ sub-population express higher levels of GRP-R and V_{1A}-R. Therefore, it was hypothesised that these cells would respond better to peptide-1 compared to the CD133- sub-population. In H345 cell lines, CD133+ cells were significantly more sensitive to peptide-1 than CD133- cells. Increased sensitivity could be associated with enhanced expression of neuropeptide receptors. Parent cells displayed a moderate response to peptide-1 this could be explained by presence of both CD133+ and CD133- cells, therefore the response to peptide-1 would be a value between each single population.

The inhibitory effect of peptide-1 on SCLC growth was also evaluated *in vivo*. Peptide-1 profoundly inhibited the tumour growth, and was as efficacious as etoposide, the most commonly employed cytotoxic agent for the treatment of SCLC patients. Combined therapy of etoposide and peptide-1 had similar inhibitory effect. I have shown that CD133+ population is more resistant to etoposide compared to the

CD133- sub-population and are enriched after etoposide exposure however, these resistant cells are more sensitive to peptide-1 in contrast to CD133- cells. Therefore, hypothetically, treatment of SCLC xenografts with combined therapy of etoposide and peptide-1 would eradicate the CD133- as well as CD133+ cells. This would serve as a model to demonstrate that elimination of CD133+ cells may be essential to prevent tumour recurrence in SCLC patients. In this study, despite inhibitory effect of the combined therapy on the SCLC xenograft, it was not possible to draw conclusions due to time limitation. The study would need to be continued for a longer period so that the inhibitory effect of the combined therapy on tumour recurrence could be compared to monotherapies.

The hexapeptide structure of SP-G includes D-amino acid and an N-methylated amino acid at the N-terminus leaving the C-terminus region of SP-G unmodified and susceptible to degradation [322]. Therefore, attempts have been made to design more stable analogues. Peptide-1 was shown to be ~4 fold more stable than SP-G. Therefore, the findings in this chapter demonstrate that the newly designed analogue is more potent with added stability than SP-G making the compound a promising analogue for SCLC clinical trials.

Concluding, peptide-1 is an exciting compound for SCLC therapy. Together, it can be proposed that peptide-1 in conjugation with first line therapy or as a second line therapy could be beneficial in SCLC patients. Suggested combined therapy with both drugs is speculated to not only eradicate the CD133- cells but also SCLC roots, the CD133+ cells therefore inhibit tumour recurrence after therapy.

CHAPTER 7:
Final conclusions and future directions

SCLC is an aggressive, highly metastatic and fatal malignancy. Despite improvements in conventional cytotoxic regimes, cure has remained elusive for most SCLC candidates. With the advent of the CSC hypothesis, the pathogenesis of SCLC should be revised. This section will include final conclusions of findings of this thesis and future aims for the study of CSCs in SCLC.

7.1 Do CSCs exist in SCLC cell lines?

In this study the presence of CSCs was investigated in H345 and H69 human SCLC cell lines. Established from metastatic sites of patients that had undergone chemotherapy [239, 325], both cell lines displayed resistance to etoposide *in vitro* in accordance with their clinical presentation. Upregulated Bcl-2 and PI3K activation, commonly observed in SCLCs, are known causes of chemoresistance and survival advantage in these cells [58, 231, 246, 326]. However, the presence of CSCs, underpinning resistance was speculated. This was based on the observation that not all SCLC cells cultured in semi-solid medium were able to form colonies, reflecting tumour cell heterogeneity, and indicating that cells within the neoplasm differ in their tumorigenic capacities.

Markers including CD133, Oct-4, and ALDH have been employed for the detection of CSCs in pulmonary malignancies [79, 152, 158]. Both SCLC cell lines demonstrated CD133 and Oct-4 expression and ALDH enzyme activity suggesting that the SCLC cell lines retain a sub-population which expresses CSC makers. CD133, the most commonly used marker, has consistently identified the stem cell-like, chemoresistant and tumorigenic lung cancer cells [79, 82, 84], and was therefore chosen for the identification of prospective SCLC CSCs.

CD133+ SCLC cells were proliferative and displayed augmented anchorage-independent growth. These cells maintained the expression of CD133 antigen and clonogenic potentials over prolonged periods in serum-free SITA medium suggesting

their possible self-renewing potential. In the presence of serum, they differentiated resulting in reduction of CD133 expression and loss of stem like features. Additionally, CD133+ cells expressed Oct-4, a well know regulator of stemness [158], whereas CD133- cells were devoid of the protein. Implantation of 1×10^5 CD133+ cells consistently resulted in growth of tumour xenografts, in contrast to higher numbers of CD133- cells that were not tumorigenic in *nude/nude* mice. The histological features of tumours formed by implantation of CD133+ cells closely resembled those developed by parent cells (unsorted cells) as shown by hematoxylin and eosin staining, indicating that CD133+ cells could effectively reproduce the disease generated by parent cells, further emphasising on its stem cell-like nature. These data clearly indicate that CD133 selects for clonogenic, stem cell-like, and tumorigenic SCLC cells.

CD133+ cells were enriched upon exposure to etoposide, demonstrating their chemoresistant phenotype. Insensitivity to etoposide in CD133+ cells was associated with enhanced apoptosis resistance in these cells compared to their negative counterpart. Deregulation in Akt and Bcl-2 expression assist cancer cells to evade apoptosis. Activated Akt in CD133+ H345 and H69 cells was significantly upregulated. Likewise, the anti-apoptotic Bcl-2 showed greater expression in this sub-population in the SCLC cell lines. To my knowledge, both proteins were for the first time demonstrated to have higher expression in CD133+ SCLC cells, promoting chemoresistance. Therefore, CD133 selects for chemoresistant cells in SCLC cell lines.

Data obtained from this thesis clearly demonstrates that H345 and H69 cells consist of a heterogeneous population of cells with different clonogenic, sensitivity to treatment, and tumorigenic capacities. CD133, a well-known CSC marker, selects the aggressive SCLC cells from the non-aggressive cells and that CD133 expressing population fulfils the CSC criteria. Therefore it can be concluded that human SCLC cell lines do retain a sub-population of cells that exhibit CSC-like characteristics and that these cells may be the possible SCLC initiators, promoting treatment resistance and disease recurrence.

7.2 CSC, a myth or a reality?

Despite multiple studies in the last decade which have supported the concept of CSCs in leukaemia and solid tumours, some groups disagree with the CSC concept and consider these cells as an artifact produced by inductions of an artificial environment presented to cells. In the present study, I have illustrated that CD133+ cells are clonogenic, chemoresistant, and tumorigenic cells with stem cell-like phenotype. Based on the literature, cells expressing CD133 marker with above mentioned criteria are considered as CSC-like cells. Ignoring the term cancer stem cell and its origin, CD133 as a marker has facilitated the selection of an aggressive population of cells within SCLC cell lines, explaining the possible cause of SCLC treatment resistance and recurrence. Therefore, the focus of the CSC theory should not be on the term "cancer stem cell" but on the fact that this concept has unveiled that tumours consist of a heterogeneous population of cells and that not all cells within the tumour may exhibit a similar response to therapy. CD133 in the present study has shown to be an ideal marker for selecting SCLC aggressive cells which could be a great step in better understanding SCLC.

7.3 Animal models and mouse lung CSCs in translational medicine

Animal models serve as a front line for predicting efficacy and monitoring toxicity of experimental and conventional drugs. Subcutaneous injections of lung cancer cell suspension in the immune-deficient mice were employed in the present study. Subcutaneous implants are easy to monitor tumour growth and therapy results however, do not mimic the pulmonary environment for the lung cancer cells [327]. Additionally, immune-deficient mice are not representative of the human body. An immune-competent mouse with an intact immune system may better mimic the internal milieu in human. A sporadic mouse SCLC (mSCLC) model has been introduced by Meuwissen et al. [103]. To my knowledge, no study has investigated the potency of SCLC CSCs in an immune-competent mouse. Characterisation of mSCLC CSCs in a syngenic mouse may better reflect their potentials.

Mutations commonly found in pathogenesis of human SCLCs are, inactivation of *Rb1* and *Trp53* [18]. MSCLC was obtained by somatic application of Cre-loxP to lung epithelial cells leading to deletion of *Rb1* and *Trp53* genes and the development of multiple tumours with histological morphology and clinical features closely resembling human SCLC [103]. These cells were highly invasive and expressed markers for neuroendocrine differentiation including NCAM, calcitonin-gene related peptide, GRP and GRP-R, further supporting its similarity to human SCLC. Furthermore, mSCLC cells exhibited high levels of L-myc, N-myc. Amplification of *Myc* gene, *N-myc*, *L-myc* or *C-myc* has been documented in 18-31% of SCLCs [328-330]. Thus, mSCLC cells not only mimic histological and pathological characteristics of human SCLC, but also resemble these cells in their genetic aberration.

MSCLC JC9569 and JC9574 cell lines (kind donation by professor Anton Berns) were obtained with the aim to evaluate the presence of putative CSCs in these cell lines for their *in vivo* characterisation. Primary data demonstrated that in both mSCLC cell lines, cells expressing CD133 and Oct-4 exist, confirmed by western blot (Figure 56). Therefore, within JC9569 and JC9574 cells reside a population of cells expressing CSCs marker. Characterising CD133+ mSCLC cells, including evaluating their clonogenicity, chemosensitivity, and self-renewal and differentiation potentials compared to CD133- will allow determining if these cells similar to human CD133+ SCLC cells represent the CSC-like sub-population. Additionally, intra-thoracic pulmonary implants of CD133+ cells from mSCLC cell lines in the immune-competent mice will allow studying the tumorigenic potential of the prospective mSCLC CSCs in a pathophysiological environment and in the presence of an intact immune system. Such study would serve as an ideal preclinical model for translation from bench to beside studies.

Figure 56

7.4 Therapy for SCLC with the aim of eradication of CD133+ cells

If CD133+ cells are the possible cause of SCLC development, understanding the mechanisms which regulate their growth and survival is critical. This would help designing drugs that would specifically target the aggressive cells with minimal effect on the non-cancerous cells. Characterisation of isolated cells demonstrated that CD133+ H345 and H69 cells transcriptionally and translationally expressed higher GRP and V_{1A} receptors, respectively than their corresponding CD133- counterparts. Addition of exogenous GRP and AVP enhanced clonogenic efficiency of the CD133+ cells indicating for the first time, the autocrine mediated neuropeptide dependent growth of CD133+ SCLC cells, making these growth factor receptors an interesting target for therapy.

As multiple neuropeptides mediate SCLC growth, it is essential to evaluate the expression of other neuropeptide receptors, including bradykinin, galanin, neurotensin, and gastrin, transcriptionally and translationally by qPCR and western blotting, respectively on the CD133+ sub-population. This is critical since developing analogues which would inhibit the mitogenic effect of single growth factor would not provide satisfactory results as seen with monoclonal antibody 2A11. If CD133+ SCLC cells demonstrate elevated levels of multiple neuropeptide receptor expression, broad spectrum antagonists, such as substance P analogues that inhibit the mitogenic effect of multiple neuropeptides would be suitable for the elimination of these aggressive cells.

In this thesis, I demonstrated that CD133+ cells despite being resistant to chemotherapy were in fact more sensitive to treatment with the new peptide analogue peptide-1 that was designed based on the known structure of SP-G. SP-G has shown benefit in animal models and in early clinical trials. Increased sensitivity to peptide-1 was possibly due to increased expression of neuropeptide receptors by the CD133+ cells. The identification of the new analogue that was more potent and more stable *in vitro* and efficacious *in vivo* than SP-G is an exciting step forward in the identification of a potential new therapy for resistant disease. It would also be

interesting to evaluate if peptide-1 has anti-tumour effects in other neuroendocrine cancers such as prostate, pancreatic, and breast cancers.

The CSC theory states that, cytotoxic agents target tumour bulk leaving behind chemoresistant CSCs which are the speculated cause of chemoresistance and disease recurrence. Peptide-1 may serve as drug of choice for the treatment of SCLC with its ability to target the aggressive CD133+ cells. Co-administration of conventional agents along with peptide-1 is expected to eradicate tumour bulk and tumour roots, the CD133+ cells. To confirm this concept, it would be interesting to evaluate in xenografts models whether the new analogue could prevent the recurrence of resistant tumours after chemotherapy.

A major challenge of drug development is the introduction of an analogue with minimal potentially undesirable off target effects. CSCs and cells of their origin share similar characteristics. Pulmonary neuroendocrine cells (PNECs), subject to oncogenic mutations are suggested forerunners of SCLC [103, 104]. Peptide-1 is a neuropeptide antagonist as shown by its ability to inhibit intracellular calcium mobilisation induced by neuropeptides. The question that rises is will this analogue exhibit undesirable inhibitory effect on PNEC? In a normal lung, GRP is produced by PNECs with highest number of GRP observed in fetal lung [331]. Normally, GRP expressing PNEC are infrequent after birth. Therefore, it can be speculated that in patients exposed to peptide-1, CD133+ SCLC cells will be the main target of this analogue. Thus, peptide-1 fulfils the essential criteria of an ideal drug for the treatment of SCLC including efficiency on the aggressive, stem cell-like CD133+ cells without affecting the PNEC cells.

7.5 Future studies to strengthen the concept of CSC-like cells within SCLC cell lines

1. In the present study, CD133+ cells maintained colony forming ability in prolonged periods of culturing, indicating their possible self-renewing potential. However, the self-renewing capacity of these cells was not confirmed. A gold-standard assay reflecting CD133+ self-renewal and differentiation potential is serial transplantation of these cells in animal models. A cancer cell which is able to retain its cancer initiating potential over serial transplantation probably possesses self-renewing capacity to be able to proliferate indefinitely without differentiating. This assay could be performed by subcutaneously implanting CD133+ cells (1×10^5 cells) in *nude/nude* mice. After tumour development, CD133+ cells within the developed tumour would be isolated using FACS and transplanted in another *nude/nude* mice with matching age and sex. This procedure should be continued in 4-5 animals to confirm the self-renewing potential of CD133+ SCLC cells.

2. Knockdown studies have revealed the importance of CD133 expression on cells with stem cell-like phenotype [77, 127]. Knockdown of this gene in neuroblastoma has been associated with loss of clonogenicity and tumorigenicity and in colorectal cancer led to increased sensitivity of CD133+ cells to chemotherapy. It would be interesting to evaluate knockdown of CD133 using shRNA in CD133+ isolated SCLC cells and its effect on clonogenicity, sensitivity to etoposide, and tumorigenicity. This would confirm if CD133 truly selects the aggressive SCLC cells.

3. CSC theory states that only a small subset of cells are the cause of tumour development [289], however, in the present study a relatively high percentage of H345 (~18%) and H69 (~20%) cells were positive for CD133 antigen. SCLC cell lines utilised in the present study were established from patients exposed to chemotherapy. Therefore, a high percentage of CD133 expression

could be due to the enrichment of this chemoresistant population within the SCLC cell lines. Additionally, I have also shown that not all CD133+ cells are clonogenic, indicative of heterogeneity within CD133 expressing cells. Therefore, a combination of CD133 with another stem cell marker such as ALDH may be a more accurate method for detection of pure CSCs in SCLC cells. To confirm this concept the characteristics of cells expressing either CD133 or ALDH could be compared with that of cells positive for both marker (CD133+ ALDH+).

4. Stem cells and CSCs share various similar signalling pathways including Notch and Wnt which are important regulatory factors in both cell types. The main aim of CSC studies is to develop effective therapeutic strategies that selectively target human malignancies. The challenge is to identify the differences between stem cells and CSCs. Microarray and genome wide techniques could be utilised to detect possible genetic and epigenetic differences between these two cell types. Additionally, these techniques would familiarise us with trends in genetic and epigenetic "blueprints" for CSCs to better understand the true signature of these cells.

5. Studies have implicated the importance of CD133 as a prognostic maker for NSCLC [85, 118]. Evaluation of CD133 expression in tissue section of SCLC patients by IHC would allow determining the potential prognostic value of CD133 expression in SCLC patients.

Chemotherapy forms the cornerstone for SCLC management. However, advances in chemo-radiation have reached a plateau. Findings in this study that SCLC cells contain a sub-population of aggressive cells that evade apoptosis and are tumorigenic in animals, distinct from other cancer cells implicates that therapeutic strategies should consider tumours as a heterogeneous cellular mass initiated and propagated selectively by these cancer stem cell-like cells. From this view, targeted therapy of CSCs should be the focus for cancer management. In this regards, peptide-1 which

demonstrated greater efficacy to CD133+ SCLC cells may be provital in the management of SCLC.

References:

1. Ginsberg, M.S., R.K. Grewal, and R.T. Heelan, *Lung cancer.* Radiol Clin North Am, 2007. **45**(1): p. 21-43.
2. Harkness, E.F., et al., *Changing trends in incidence of lung cancer by histologic type in Scotland.* Int J Cancer, 2002. **102**(2): p. 179-83.
3. Janssen-Heijnen, M.L. and J.W. Coebergh, *The changing epidemiology of lung cancer in Europe.* Lung Cancer, 2003. **41**(3): p. 245-58.
4. Ettinger, D.S., *Overview and state of the art in the management of lung cancer.* Oncology (Williston Park), 2004. **18**(7 Suppl 4): p. 3-9.
5. Franceschi, S. and E. Bidoli, *The epidemiology of lung cancer.* Ann Oncol, 1999. **10 Suppl 5**: p. S3-6.
6. Murray, N. and A.T. Turrisi, 3rd, *A review of first-line treatment for small-cell lung cancer.* J Thorac Oncol, 2006. **1**(3): p. 270-8.
7. Hann, C.L. and C.M. Rudin, *Management of small-cell lung cancer: incremental changes but hope for the future.* Oncology (Williston Park), 2008. **22**(13): p. 1486-92.
8. Govindan, R., et al., *Changing epidemiology of small-cell lung cancer in the United States over the last 30 years: analysis of the surveillance, epidemiologic, and end results database.* J Clin Oncol, 2006. **24**(28): p. 4539-44.
9. Puglisi, M., et al., *Treatment options for small cell lung cancer - do we have more choice?* Br J Cancer. **102**(4): p. 629-38.
10. Ferlay, J., D.M. Parkin, and E. Steliarova-Foucher, *Estimates of cancer incidence and mortality in Europe in 2008.* Eur J Cancer. **46**(4): p. 765-81.
11. Ettinger, D.S. and J. Aisner, *Changing face of small-cell lung cancer: real and artifact.* J Clin Oncol, 2006. **24**(28): p. 4526-7.
12. Riaz, S.P., et al., *Trends in incidence of small cell lung cancer and all lung cancer.* Lung Cancer. **75**(3): p. 280-4.
13. Toh, C.-K., et al., *Differences between small-cell lung cancer and non-small-cell lung cancer among tobacco smokers.* Lung cancer (Amsterdam, Netherlands), 2007. **56**(2): p. 161-166.
14. Karim-Kos, H.E., et al., *Recent trends of cancer in Europe: a combined approach of incidence, survival and mortality for 17 cancer sites since the 1990s.* Eur J Cancer, 2008. **44**(10): p. 1345-89.
15. Alberg, A.J. and J.M. Samet, *Epidemiology of lung cancer.* Chest, 2003. **123**(1 Suppl): p. 21S-49S.
16. Hibi, K., et al., *Three distinct regions involved in 3p deletion in human lung cancer.* Oncogene, 1992. **7**(3): p. 445-9.
17. Kok, K., S.L. Naylor, and C.H. Buys, *Deletions of the short arm of chromosome 3 in solid tumors and the search for suppressor genes.* Adv Cancer Res, 1997. **71**: p. 27-92.
18. Miura, I., et al., *Chromosome alterations in human small cell lung cancer: frequent involvement of 5q.* Cancer Res, 1992. **52**(5): p. 1322-8.
19. D'Amico, D., et al., *High frequency of somatically acquired p53 mutations in small-cell lung cancer cell lines and tumors.* Oncogene, 1992. **7**(2): p. 339-46.

20. Harbour, J.W., et al., *Abnormalities in structure and expression of the human retinoblastoma gene in SCLC.* Science, 1988. **241**(4863): p. 353-7.
21. Travis, W.D., *Advances in neuroendocrine lung tumors.* Ann Oncol. **21 Suppl 7**: p. vii65-71.
22. Chong, S., et al., *Neuroendocrine tumors of the lung: clinical, pathologic, and imaging findings.* Radiographics, 2006. **26**(1): p. 41-57; discussion 57-8.
23. Gandhi, L. and B.E. Johnson, *Paraneoplastic syndromes associated with small cell lung cancer.* J Natl Compr Canc Netw, 2006. **4**(6): p. 631-8.
24. Dalmau, J. and M.R. Rosenfeld, *Paraneoplastic syndromes of the CNS.* Lancet Neurol, 2008. **7**(4): p. 327-40.
25. Zelen, M., *Keynote address on biostatistics and data retrieval.* Cancer Chemother Rep 3, 1973. **4**(2): p. 31-42.
26. Suzuki, S., *[Lambert-Eaton myasthenic syndrome (LEMS)]*. Brain Nerve. **62**(4): p. 419-26.
27. Laurent, F., M. Montaudon, and O. Corneloup, *CT and MRI of Lung Cancer.* Respiration, 2006. **73**(2): p. 133-42.
28. Gustafsson, B.I., et al., *Bronchopulmonary neuroendocrine tumors.* Cancer, 2008. **113**(1): p. 5-21.
29. Argiris, A. and J.R. Murren, *Staging and clinical prognostic factors for small-cell lung cancer.* Cancer J, 2001. **7**(5): p. 437-47.
30. Haddadin, S. and M.C. Perry, *History of small-cell lung cancer.* Clin Lung Cancer. **12**(2): p. 87-93.
31. Shepherd, F.A., et al., *The International Association for the Study of Lung Cancer lung cancer staging project: proposals regarding the clinical staging of small cell lung cancer in the forthcoming (seventh) edition of the tumor, node, metastasis classification for lung cancer.* J Thorac Oncol, 2007. **2**(12): p. 1067-77.
32. Carmichael, J., et al., *Chemosensitivity testing of human lung cancer cell lines using the MTT assay.* Br J Cancer, 1988. **57**(6): p. 540-7.
33. Green, R.A., et al., *Alkylating agents in bronchogenic carcinoma.* Am J Med, 1969. **46**(4): p. 516-25.
34. Lowenbraun, S., et al., *The superiority of combination chemotherapy over single agent chemotherapy in small cell lung carcinoma.* Cancer, 1979. **44**(2): p. 406-13.
35. Roth, B.J., et al., *Randomized study of cyclophosphamide, doxorubicin, and vincristine versus etoposide and cisplatin versus alternation of these two regimens in extensive small-cell lung cancer: a phase III trial of the Southeastern Cancer Study Group.* J Clin Oncol, 1992. **10**(2): p. 282-91.
36. Sundstrom, S., et al., *Cisplatin and etoposide regimen is superior to cyclophosphamide, epirubicin, and vincristine regimen in small-cell lung cancer: results from a randomized phase III trial with 5 years' follow-up.* J Clin Oncol, 2002. **20**(24): p. 4665-72.
37. Mavroudis, D., et al., *A multicenter randomized clinical trial comparing paclitaxel-cisplatin-etoposide versus cisplatin-etoposide as first-line treatment in patients with small-cell lung cancer.* Ann Oncol, 2001. **12**(4): p. 463-70.

38. Clark, R. and D.C. Ihde, *Small-cell lung cancer: treatment progress and prospects.* Oncology (Williston Park), 1998. **12**(5): p. 647-58; discussion 661-3.
39. von Pawel, J., et al., *Topotecan versus cyclophosphamide, doxorubicin, and vincristine for the treatment of recurrent small-cell lung cancer.* J Clin Oncol, 1999. **17**(2): p. 658-67.
40. Albain, K.S., et al., *Predictors of survival following relapse or progression of small cell lung cancer. Southwest Oncology Group Study 8605 report and analysis of recurrent disease data base.* Cancer, 1993. **72**(4): p. 1184-91.
41. Kim, Y.H. and M. Mishima, *Second-line chemotherapy for small-cell lung cancer (SCLC).* Cancer Treat Rev. **37**(2): p. 143-50.
42. Kollmannsberger, C., et al., *Topotecan - A novel topoisomerase I inhibitor: pharmacology and clinical experience.* Oncology, 1999. **56**(1): p. 1-12.
43. Sugimoto, Y., et al., *Decreased expression of DNA topoisomerase I in camptothecin-resistant tumor cell lines as determined by a monoclonal antibody.* Cancer Res, 1990. **50**(21): p. 6925-30.
44. Noda, K., et al., *Irinotecan plus cisplatin compared with etoposide plus cisplatin for extensive small-cell lung cancer.* N Engl J Med, 2002. **346**(2): p. 85-91.
45. Crossin, K.L. and D.H. Carney, *Microtubule stabilization by taxol inhibits initiation of DNA synthesis by thrombin and by epidermal growth factor.* Cell, 1981. **27**(2 Pt 1): p. 341-50.
46. Kirschling, R.J., et al., *Paclitaxel and G-CSF in previously untreated patients with extensive stage small-cell lung cancer: a phase II study of the North Central Cancer Treatment Group.* Am J Clin Oncol, 1999. **22**(5): p. 517-22.
47. Onoda, S., et al., *Phase II trial of amrubicin for treatment of refractory or relapsed small-cell lung cancer: Thoracic Oncology Research Group Study 0301.* J Clin Oncol, 2006. **24**(34): p. 5448-53.
48. Kaira, K., et al., *A phase II study of amrubicin, a synthetic 9-aminoanthracycline, in patients with previously treated lung cancer.* Lung Cancer. **69**(1): p. 99-104.
49. Pignon, J.P., et al., *A meta-analysis of thoracic radiotherapy for small-cell lung cancer.* N Engl J Med, 1992. **327**(23): p. 1618-24.
50. Warde, P. and D. Payne, *Does thoracic irradiation improve survival and local control in limited-stage small-cell carcinoma of the lung? A meta-analysis.* J Clin Oncol, 1992. **10**(6): p. 890-5.
51. Paumier, A. and C. Le Pechoux, *Radiotherapy in small-cell lung cancer: where should it go?* Lung Cancer. **69**(2): p. 133-40.
52. Takada, M., et al., *Phase III study of concurrent versus sequential thoracic radiotherapy in combination with cisplatin and etoposide for limited-stage small-cell lung cancer: results of the Japan Clinical Oncology Group Study 9104.* J Clin Oncol, 2002. **20**(14): p. 3054-60.
53. Turrisi, A.T., 3rd, et al., *Twice-daily compared with once-daily thoracic radiotherapy in limited small-cell lung cancer treated concurrently with cisplatin and etoposide.* N Engl J Med, 1999. **340**(4): p. 265-71.
54. Jeremic, B., et al., *Role of radiation therapy in the combined-modality treatment of patients with extensive disease small-cell lung cancer: A randomized study.* J Clin Oncol, 1999. **17**(7): p. 2092-9.

55. Arriagada, R., et al., *Prophylactic cranial irradiation for patients with small-cell lung cancer in complete remission.* J Natl Cancer Inst, 1995. **87**(3): p. 183-90.
56. Auperin, A., et al., *Prophylactic cranial irradiation for patients with small-cell lung cancer in complete remission. Prophylactic Cranial Irradiation Overview Collaborative Group.* N Engl J Med, 1999. **341**(7): p. 476-84.
57. Slotman, B., et al., *Prophylactic cranial irradiation in extensive small-cell lung cancer.* N Engl J Med, 2007. **357**(7): p. 664-72.
58. Jiang, S.X., et al., *Expression of bcl-2 oncogene protein is prevalent in small cell lung carcinomas.* J Pathol, 1995. **177**(2): p. 135-8.
59. Shoemaker, A.R., et al., *Activity of the Bcl-2 family inhibitor ABT-263 in a panel of small cell lung cancer xenograft models.* Clin Cancer Res, 2008. **14**(11): p. 3268-77.
60. Stauffer, S.R., *Small molecule inhibition of the Bcl-X(L)-BH3 protein-protein interaction: proof-of-concept of an in vivo chemopotentiator ABT-737.* Curr Top Med Chem, 2007. **7**(10): p. 961-5.
61. Gandhi, L., et al., *Phase I study of Navitoclax (ABT-263), a novel Bcl-2 family inhibitor, in patients with small-cell lung cancer and other solid tumors.* J Clin Oncol. **29**(7): p. 909-16.
62. Tarhini, A., et al., *Phase II Study of Everolimus (RAD001) in Previously Treated Small Cell Lung Cancer.* Clinical Cancer Research. **16**(23): p. 5900-5907.
63. Pandya, K.J., et al., *A randomized, phase II trial of two dose levels of temsirolimus (CCI-779) in patients with extensive-stage small-cell lung cancer who have responding or stable disease after induction chemotherapy: a trial of the Eastern Cooperative Oncology Group (E1500).* J Thorac Oncol, 2007. **2**(11): p. 1036-41.
64. Sethi, T., et al., *Growth of small cell lung cancer cells: stimulation by multiple neuropeptides and inhibition by broad spectrum antagonists in vitro and in vivo.* Cancer Res, 1992. **52**(9 Suppl): p. 2737s-2742s.
65. Waters, C.M., et al., *Increased gastrin-releasing peptide (GRP) receptor expression in tumour cells confers sensitivity to [Arg6,D-Trp7,9,NmePhe8]-substance P (6-11)-induced growth inhibition.* Br J Cancer, 2003. **88**(11): p. 1808-16.
66. Clive, S., et al., *Forearm blood flow and local responses to peptide vasodilators: a novel pharmacodynamic measure in the phase I trial of antagonist G, a neuropeptide growth factor antagonist.* Clin Cancer Res, 2001. **7**(10): p. 3071-8.
67. Murray, N., R. Salgia, and F.V. Fossella, *Targeted molecules in small cell lung cancer.* Semin Oncol, 2004. **31**(1 Suppl 1): p. 106-11.
68. Dy, G.K., et al., *A phase II trial of imatinib (ST1571) in patients with c-kit expressing relapsed small-cell lung cancer: a CALGB and NCCTG study.* Ann Oncol, 2005. **16**(11): p. 1811-6.
69. Krug, L.M., et al., *Imatinib mesylate lacks activity in small cell lung carcinoma expressing c-kit protein: a phase II clinical trial.* Cancer, 2005. **103**(10): p. 2128-31.

70. Peck, R.A., et al., *Phase I and pharmacokinetic study of the novel MDR1 and MRP1 inhibitor biricodar administered alone and in combination with doxorubicin.* J Clin Oncol, 2001. **19**(12): p. 3130-41.
71. Heppner, G.H. and B.E. Miller, *Tumor heterogeneity: biological implications and therapeutic consequences.* Cancer Metastasis Rev, 1983. **2**(1): p. 5-23.
72. Southam, C.M. and A. Brunschwig, *Quantitative studies of autotransplantation of human cancer. Preliminary report.* Cancer, 1961. **14**(5): p. 971-978.
73. Visvader, J.E. and G.J. Lindeman, *Cancer stem cells in solid tumours: accumulating evidence and unresolved questions.* Nat Rev Cancer, 2008. **8**(10): p. 755-68.
74. Bonnet, D. and J.E. Dick, *Human acute myeloid leukemia is organized as a hierarchy that originates from a primitive hematopoietic cell.* Nat Med, 1997. **3**(7): p. 730-7.
75. Al-Hajj, M., et al., *Prospective identification of tumorigenic breast cancer cells.* Proc Natl Acad Sci U S A, 2003. **100**(7): p. 3983-8.
76. O/'Brien, C.A., et al., *A human colon cancer cell capable of initiating tumour growth in immunodeficient mice.* Nature, 2007. **445**(7123): p. 106-110.
77. Ricci-Vitiani, L., et al., *Identification and expansion of human colon-cancer-initiating cells.* Nature, 2007. **445**(7123): p. 111-5.
78. Singh, S.K., et al., *Identification of a cancer stem cell in human brain tumors.* Cancer Res, 2003. **63**(18): p. 5821-8.
79. Eramo, A., et al., *Identification and expansion of the tumorigenic lung cancer stem cell population.* Cell Death Differ, 2008. **15**(3): p. 504-14.
80. Ma, S., et al., *CD133+ HCC cancer stem cells confer chemoresistance by preferential expression of the Akt/PKB survival pathway.* Oncogene, 2008. **27**(12): p. 1749-58.
81. Liu, G., et al., *Analysis of gene expression and chemoresistance of CD133+ cancer stem cells in glioblastoma.* Mol Cancer, 2006. **5**: p. 67.
82. Levina, V., et al., *Drug-selected human lung cancer stem cells: cytokine network, tumorigenic and metastatic properties.* PLoS One, 2008. **3**(8): p. e3077.
83. Ginestier, C., et al., *ALDH1 is a marker of normal and malignant human mammary stem cells and a predictor of poor clinical outcome.* Cell Stem Cell, 2007. **1**(5): p. 555-67.
84. Bertolini, G., et al., *Highly tumorigenic lung cancer CD133+ cells display stem-like features and are spared by cisplatin treatment.* Proc Natl Acad Sci U S A, 2009. **106**(38): p. 16281-6.
85. Shien, K., et al., *Prognostic impact of cancer stem cell-related markers in non-small cell lung cancer patients treated with induction chemoradiotherapy.* Lung Cancer, (0).
86. Baker, S.J., et al., *Suppression of human colorectal carcinoma cell growth by wild-type p53.* Science, 1990. **249**(4971): p. 912-5.
87. Iwasaki, H. and K. Akashi, *Myeloid lineage commitment from the hematopoietic stem cell.* Immunity, 2007. **26**(6): p. 726-40.
88. Kotton, D.N. and A. Fine, *Lung stem cells.* Cell Tissue Res, 2008. **331**(1): p. 145-56.

89. Giangreco, A., et al., *Stem cells are dispensable for lung homeostasis but restore airways after injury.* Proc Natl Acad Sci U S A, 2009. **106**(23): p. 9286-91.
90. Rawlins, E.L., *Lung epithelial progenitor cells: lessons from development.* Proc Am Thorac Soc, 2008. **5**(6): p. 675-81.
91. Knight, D.A. and S.T. Holgate, *The airway epithelium: structural and functional properties in health and disease.* Respirology, 2003. **8**(4): p. 432-46.
92. Stripp, B.R. and S.D. Reynolds, *Maintenance and repair of the bronchiolar epithelium.* Proc Am Thorac Soc, 2008. **5**(3): p. 328-33.
93. Van Winkle, L.S., et al., *Cellular response in naphthalene-induced Clara cell injury and bronchiolar epithelial repair in mice.* Am J Physiol, 1995. **269**(6 Pt 1): p. L800-18.
94. Hong, K.U., et al., *In vivo differentiation potential of tracheal basal cells: evidence for multipotent and unipotent subpopulations.* Am J Physiol Lung Cell Mol Physiol, 2004. **286**(4): p. L643-9.
95. Reynolds, S.D., et al., *Neuroepithelial bodies of pulmonary airways serve as a reservoir of progenitor cells capable of epithelial regeneration.* Am J Pathol, 2000. **156**(1): p. 269-78.
96. Rawlins, E.L. and B.L. Hogan, *Epithelial stem cells of the lung: privileged few or opportunities for many?* Development, 2006. **133**(13): p. 2455-65.
97. Giangreco, A., S.D. Reynolds, and B.R. Stripp, *Terminal bronchioles harbor a unique airway stem cell population that localizes to the bronchoalveolar duct junction.* Am J Pathol, 2002. **161**(1): p. 173-82.
98. Kim, C.F., et al., *Identification of bronchioalveolar stem cells in normal lung and lung cancer.* Cell, 2005. **121**(6): p. 823-35.
99. Rawlins, E.L., et al., *The role of Scgb1a1+ Clara cells in the long-term maintenance and repair of lung airway, but not alveolar, epithelium.* Cell Stem Cell, 2009. **4**(6): p. 525-34.
100. Malkinson, A.M., *Molecular comparison of human and mouse pulmonary adenocarcinomas.* Exp Lung Res, 1998. **24**(4): p. 541-55.
101. Jackson, E.L., et al., *Analysis of lung tumor initiation and progression using conditional expression of oncogenic K-ras.* Genes Dev, 2001. **15**(24): p. 3243-8.
102. Ventura, J.J., et al., *p38alpha MAP kinase is essential in lung stem and progenitor cell proliferation and differentiation.* Nat Genet, 2007. **39**(6): p. 750-8.
103. Meuwissen, R., et al., *Induction of small cell lung cancer by somatic inactivation of both Trp53 and Rb1 in a conditional mouse model.* Cancer Cell, 2003. **4**(3): p. 181-9.
104. Wistuba, II, A.F. Gazdar, and J.D. Minna, *Molecular genetics of small cell lung carcinoma.* Semin Oncol, 2001. **28**(2 Suppl 4): p. 3-13.
105. Minna, J.D., J.M. Kurie, and T. Jacks, *A big step in the study of small cell lung cancer.* Cancer Cell, 2003. **4**(3): p. 163-6.
106. Wikenheiser-Brokamp, K.A., *Rb family proteins differentially regulate distinct cell lineages during epithelial development.* Development, 2004. **131**(17): p. 4299-310.

107. Watkins, D.N., et al., *Hedgehog signalling within airway epithelial progenitors and in small-cell lung cancer.* Nature, 2003. **422**(6929): p. 313-7.
108. Ericson, J., et al., *Two critical periods of Sonic Hedgehog signaling required for the specification of motor neuron identity.* Cell, 1996. **87**(4): p. 661-73.
109. Ball, D.W., *Achaete-scute homolog-1 and Notch in lung neuroendocrine development and cancer.* Cancer Lett, 2004. **204**(2): p. 159-69.
110. Yin, A.H., et al., *AC133, a novel marker for human hematopoietic stem and progenitor cells.* Blood, 1997. **90**(12): p. 5002-12.
111. Corbeil, D., et al., *The human AC133 hematopoietic stem cell antigen is also expressed in epithelial cells and targeted to plasma membrane protrusions.* J Biol Chem, 2000. **275**(8): p. 5512-20.
112. Corbeil, D., et al., *Selective localization of the polytopic membrane protein prominin in microvilli of epithelial cells - a combination of apical sorting and retention in plasma membrane protrusions.* J Cell Sci, 1999. **112 (Pt 7)**: p. 1023-33.
113. Piechaczek, C., *Cd133.* J Biol Regul Homeost Agents, 2001. **15**(1): p. 101-2.
114. Miraglia, S., et al., *A novel five-transmembrane hematopoietic stem cell antigen: isolation, characterization, and molecular cloning.* Blood, 1997. **90**(12): p. 5013-21.
115. Potgens, A.J., et al., *Monoclonal antibody CD133-2 (AC141) against hematopoietic stem cell antigen CD133 shows crossreactivity with cytokeratin 18.* J Histochem Cytochem, 2002. **50**(8): p. 1131-4.
116. Gordon, P.R., et al., *Large-scale isolation of CD133+ progenitor cells from G-CSF mobilized peripheral blood stem cells.* Bone Marrow Transplant, 2003. **31**(1): p. 17-22.
117. Alessandri, G., et al., *Isolation and culture of human muscle-derived stem cells able to differentiate into myogenic and neurogenic cell lineages.* Lancet, 2004. **364**(9448): p. 1872-83.
118. Woo, T., et al., *Prognostic value of CD133 expression in stage I lung adenocarcinomas.* Int J Clin Exp Pathol. **4**(1): p. 32-42.
119. Horst, D., et al., *Prognostic significance of the cancer stem cell markers CD133, CD44, and CD166 in colorectal cancer.* Cancer Invest, 2009. **27**(8): p. 844-50.
120. Zeppernick, F., et al., *Stem cell marker CD133 affects clinical outcome in glioma patients.* Clin Cancer Res, 2008. **14**(1): p. 123-9.
121. Yu, J.W., et al., *Expressions and clinical significances of CD133 protein and CD133 mRNA in primary lesion of gastric adenocacinoma.* J Exp Clin Cancer Res. **29**: p. 141.
122. Fargeas, C.A., et al., *Prominin-1 (CD133): from progenitor cells to human diseases.* Future Lipidology, 2006. **1**(2): p. 213-225.
123. Bauer, N., et al., *New insights into the cell biology of hematopoietic progenitors by studying prominin-1 (CD133).* Cells Tissues Organs, 2008. **188**(1-2): p. 127-38.
124. Freund, D., et al., *Polarization of human hematopoietic progenitors during contact with multipotent mesenchymal stromal cells: effects on proliferation and clonogenicity.* Stem Cells Dev, 2006. **15**(6): p. 815-29.
125. Pine, S.R., et al., *Microenvironmental modulation of asymmetric cell division in human lung cancer cells.* Proc Natl Acad Sci U S A. **107**(5): p. 2195-200.

126. Marzesco, A.M., et al., *Release of extracellular membrane particles carrying the stem cell marker prominin-1 (CD133) from neural progenitors and other epithelial cells.* J Cell Sci, 2005. **118**(Pt 13): p. 2849-58.
127. Takenobu, H., et al., *CD133 suppresses neuroblastoma cell differentiation via signal pathway modification.* Oncogene. **30**(1): p. 97-105.
128. de Wynter, E.A., et al., *CD34+AC133+ cells isolated from cord blood are highly enriched in long-term culture-initiating cells, NOD/SCID-repopulating cells and dendritic cell progenitors.* Stem Cells, 1998. **16**(6): p. 387-96.
129. Gehling, U.M., et al., *In vitro differentiation of endothelial cells from AC133-positive progenitor cells.* Blood, 2000. **95**(10): p. 3106-3112.
130. Padovan, C.S., et al., *Expression of neuronal markers in differentiated marrow stromal cells and CD133+ stem-like cells.* Cell Transplant, 2003. **12**(8): p. 839-48.
131. Koehl, U., et al., *Autologous transplantation of CD133 selected hematopoietic progenitor cells in a pediatric patient with relapsed leukemia.* Bone Marrow Transplant, 2002. **29**(11): p. 927-30.
132. Bussolati, B., et al., *Isolation of renal progenitor cells from adult human kidney.* Am J Pathol, 2005. **166**(2): p. 545-55.
133. Belicchi, M., et al., *Human skin-derived stem cells migrate throughout forebrain and differentiate into astrocytes after injection into adult mouse brain.* J Neurosci Res, 2004. **77**(4): p. 475-86.
134. Richardson, G.D., et al., *CD133, a novel marker for human prostatic epithelial stem cells.* J Cell Sci, 2004. **117**(Pt 16): p. 3539-45.
135. Collins, A.T., et al., *Prospective identification of tumorigenic prostate cancer stem cells.* Cancer Res, 2005. **65**(23): p. 10946-51.
136. O'Brien, C.A., et al., *A human colon cancer cell capable of initiating tumour growth in immunodeficient mice.* Nature, 2007. **445**(7123): p. 106-10.
137. Elsaba, T.M., et al., *The stem cell marker CD133 associates with enhanced colony formation and cell motility in colorectal cancer.* PLoS One. **5**(5): p. e10714.
138. Li, C.Y., et al., *Higher percentage of CD133+ cells is associated with poor prognosis in colon carcinoma patients with stage IIIB.* J Transl Med, 2009. **7**: p. 56.
139. Bao, S., et al., *Glioma stem cells promote radioresistance by preferential activation of the DNA damage response.* Nature, 2006. **444**(7120): p. 756-60.
140. Ma, S., et al., *Identification and characterization of tumorigenic liver cancer stem/progenitor cells.* Gastroenterology, 2007. **132**(7): p. 2542-56.
141. Tan, S., et al., *Selective enrichment of hepatocellular cancer stem cells by chemotherapy.* J Int Med Res, 2009. **37**(4): p. 1046-56.
142. Yang, Z., et al., *Transient mTOR inhibition facilitates continuous growth of liver tumors by modulating the maintenance of CD133+ cell populations.* PLoS One. **6**(12): p. e28405.
143. Song, W., et al., *Expression and clinical significance of the stem cell marker CD133 in hepatocellular carcinoma.* Int J Clin Pract, 2008. **62**(8): p. 1212-8.
144. Carney, D.N., et al., *Demonstration of the stem cell nature of clonogenic tumor cells from lung cancer patients.* Stem Cells, 1982. **1**(3): p. 149-64.

145. Goodell, M.A., et al., *Isolation and functional properties of murine hematopoietic stem cells that are replicating in vivo.* J Exp Med, 1996. **183**(4): p. 1797-806.
146. Patel, M., et al., *ALDH1A1 and ALDH3A1 expression in lung cancers: correlation with histologic type and potential precursors.* Lung Cancer, 2008. **59**(3): p. 340-9.
147. Marchitti, S.A., et al., *Non-P450 aldehyde oxidizing enzymes: the aldehyde dehydrogenase superfamily.* Expert Opin Drug Metab Toxicol, 2008. **4**(6): p. 697-720.
148. Black, W.J., et al., *Human aldehyde dehydrogenase genes: alternatively spliced transcriptional variants and their suggested nomenclature.* Pharmacogenet Genomics, 2009. **19**(11): p. 893-902.
149. Vasiliou, V. and A. Pappa, *Polymorphisms of human aldehyde dehydrogenases. Consequences for drug metabolism and disease.* Pharmacology, 2000. **61**(3): p. 192-8.
150. Gudas, L.J. and J.A. Wagner, *Retinoids regulate stem cell differentiation.* J Cell Physiol. **226**(2): p. 322-30.
151. Ma, I. and A.L. Allan, *The role of human aldehyde dehydrogenase in normal and cancer stem cells.* Stem Cell Rev. **7**(2): p. 292-306.
152. Jiang, F., et al., *Aldehyde dehydrogenase 1 is a tumor stem cell-associated marker in lung cancer.* Mol Cancer Res, 2009. **7**(3): p. 330-8.
153. Moreb, J.S., et al., *ALDH isozymes downregulation affects cell growth, cell motility and gene expression in lung cancer cells.* Mol Cancer, 2008. **7**: p. 87.
154. Koelling, T.M., et al., *Development and characterization of a cyclophosphamide-resistant subline of acute myeloid leukemia in the Lewis x Brown Norway hybrid rat.* Blood, 1990. **76**(6): p. 1209-13.
155. Niwa, H., J. Miyazaki, and A.G. Smith, *Quantitative expression of Oct-3/4 defines differentiation, dedifferentiation or self-renewal of ES cells.* Nat Genet, 2000. **24**(4): p. 372-6.
156. Gidekel, S., et al., *Oct-3/4 is a dose-dependent oncogenic fate determinant.* Cancer Cell, 2003. **4**(5): p. 361-70.
157. Atlasi, Y., et al., *OCT-4, an embryonic stem cell marker, is highly expressed in bladder cancer.* Int J Cancer, 2007. **120**(7): p. 1598-602.
158. Chen, Y.C., et al., *Oct-4 expression maintained cancer stem-like properties in lung cancer-derived CD133-positive cells.* PLoS One, 2008. **3**(7): p. e2637.
159. Ponti, D., et al., *Isolation and in vitro propagation of tumorigenic breast cancer cells with stem/progenitor cell properties.* Cancer Res, 2005. **65**(13): p. 5506-11.
160. Bar, E.E., et al., *Cyclopamine-mediated hedgehog pathway inhibition depletes stem-like cancer cells in glioblastoma.* Stem Cells, 2007. **25**(10): p. 2524-33.
161. Peacock, C.D., et al., *Hedgehog signaling maintains a tumor stem cell compartment in multiple myeloma.* Proc Natl Acad Sci U S A, 2007. **104**(10): p. 4048-53.
162. Zhao, C., et al., *Hedgehog signalling is essential for maintenance of cancer stem cells in myeloid leukaemia.* Nature, 2009. **458**(7239): p. 776-9.

163. Fan, X., et al., *Notch pathway inhibition depletes stem-like cells and blocks engraftment in embryonal brain tumors.* Cancer Res, 2006. **66**(15): p. 7445-52.
164. Rasheed, Z.A., et al., *Concise review: Emerging concepts in clinical targeting of cancer stem cells.* Stem Cells. **29**(6): p. 883-7.
165. Levina, V., et al., *Elimination of human lung cancer stem cells through targeting of the stem cell factor-c-kit autocrine signaling loop.* Cancer Res. **70**(1): p. 338-46.
166. Todaro, M., et al., *IL-4-mediated drug resistance in colon cancer stem cells.* Cell Cycle, 2008. **7**(3): p. 309-13.
167. Gupta, P.B., et al., *Identification of selective inhibitors of cancer stem cells by high-throughput screening.* Cell, 2009. **138**(4): p. 645-59.
168. Matsui, W., et al., *Anti-tumour activity of interferon-alpha in multiple myeloma: role of interleukin 6 and tumor cell differentiation.* Br J Haematol, 2003. **121**(2): p. 251-8.
169. Sethi, T. and E. Rozengurt, *Multiple neuropeptides stimulate clonal growth of small cell lung cancer: effects of bradykinin, vasopressin, cholecystokinin, galanin, and neurotensin.* Cancer Res, 1991. **51**(13): p. 3621-3.
170. Rozengurt, E., *Neuropeptides as cellular growth factors: role of multiple signalling pathways.* Eur J Clin Invest, 1991. **21**(2): p. 123-34.
171. MacKinnon, A.C., et al., *Expression of V1A and GRP receptors leads to cellular transformation and increased sensitivity to substance-P analogue-induced growth inhibition.* Br J Cancer, 2005. **92**(3): p. 522-31.
172. Flores, D.G., et al., *Cancer stem cells and the biology of brain tumors.* Curr Stem Cell Res Ther, 2009. **4**(4): p. 306-13.
173. Rozengurt, E., *Signal transduction pathways in the mitogenic response to G protein-coupled neuropeptide receptor agonists.* J Cell Physiol, 1998. **177**(4): p. 507-17.
174. Palczewski, K., et al., *Crystal structure of rhodopsin: A G protein-coupled receptor.* Science, 2000. **289**(5480): p. 739-45.
175. Ji, T.H., M. Grossmann, and I. Ji, *G protein-coupled receptors. I. Diversity of receptor-ligand interactions.* J Biol Chem, 1998. **273**(28): p. 17299-302.
176. De Lean, A., J.M. Stadel, and R.J. Lefkowitz, *A ternary complex model explains the agonist-specific binding properties of the adenylate cyclase-coupled beta-adrenergic receptor.* Journal of Biological Chemistry, 1980. **255**(15): p. 7108-7117.
177. Seifert, R. and K. Wenzel-Seifert, *Constitutive activity of G-protein-coupled receptors: cause of disease and common property of wild-type receptors.* Naunyn Schmiedebergs Arch Pharmacol, 2002. **366**(5): p. 381-416.
178. Hermans, E., *Biochemical and pharmacological control of the multiplicity of coupling at G-protein-coupled receptors.* Pharmacol Ther, 2003. **99**(1): p. 25-44.
179. Hepler, J.R. and A.G. Gilman, *G proteins.* Trends Biochem Sci, 1992. **17**(10): p. 383-7.
180. Wettschureck, N. and S. Offermanns, *Mammalian G proteins and their cell type specific functions.* Physiol Rev, 2005. **85**(4): p. 1159-204.
181. Hamm, H.E., *The many faces of G protein signaling.* J Biol Chem, 1998. **273**(2): p. 669-72.

182. Farfel, Z., H.R. Bourne, and T. Iiri, *The expanding spectrum of G protein diseases.* N Engl J Med, 1999. **340**(13): p. 1012-20.
183. Lyons, J., et al., *Two G protein oncogenes in human endocrine tumors.* Science, 1990. **249**(4969): p. 655-9.
184. Chan, A.M., et al., *Expression cDNA cloning of a transforming gene encoding the wild-type G alpha 12 gene product.* Mol Cell Biol, 1993. **13**(2): p. 762-8.
185. Erspamer, V., et al., *Occurrence of bombesin and alytesin in extracts of the skin of three European discoglossid frogs and pharmacological actions of bombesin on extravascular smooth muscle.* Br J Pharmacol, 1972. **45**(2): p. 333-48.
186. Spindel, E.R., et al., *Cloning and characterization of cDNAs encoding human gastrin-releasing peptide.* Proceedings of the National Academy of Sciences, 1984. **81**(18): p. 5699-5703.
187. Kroog, G.S., R.T. Jensen, and J.F. Battey, *Mammalian bombesin receptors.* Med Res Rev, 1995. **15**(5): p. 389-417.
188. Wang, D., H. Yeger, and E. Cutz, *Expression of gastrin-releasing peptide receptor gene in developing lung.* Am J Respir Cell Mol Biol, 1996. **14**(5): p. 409-16.
189. Gudermann, T. and S. Roelle, *Calcium-dependent growth regulation of small cell lung cancer cells by neuropeptides.* Endocr Relat Cancer, 2006. **13**(4): p. 1069-84.
190. Cuttitta, F., et al., *Bombesin-like peptides can function as autocrine growth factors in human small-cell lung cancer.* Nature, 1985. **316**(6031): p. 823-6.
191. Cornelio, D., R. Roesler, and G. Schwartsmann, *Gastrin-releasing peptide receptor as a molecular target in experimental anticancer therapy.* Annals of Oncology, 2007. **18**(9): p. 1457-1466.
192. Thibonnier, M., et al., *Molecular pharmacology of human vasopressin receptors.* Adv Exp Med Biol, 1998. **449**: p. 251-76.
193. Zingg, H.H., *Vasopressin and oxytocin receptors.* Baillieres Clin Endocrinol Metab, 1996. **10**(1): p. 75-96.
194. Wittau, N., et al., *The galanin receptor type 2 initiates multiple signaling pathways in small cell lung cancer cells by coupling to G(q), G(i) and G(12) proteins.* Oncogene, 2000. **19**(37): p. 4199-209.
195. Mikoshiba, K., *The InsP3 receptor and intracellular Ca2+ signaling.* Curr Opin Neurobiol, 1997. **7**(3): p. 339-45.
196. Exton, J.H., *Regulation of phosphoinositide phospholipases by hormones, neurotransmitters, and other agonists linked to G proteins.* Annu Rev Pharmacol Toxicol, 1996. **36**: p. 481-509.
197. Noh, D.Y., S.H. Shin, and S.G. Rhee, *Phosphoinositide-specific phospholipase C and mitogenic signaling.* Biochim Biophys Acta, 1995. **1242**(2): p. 99-113.
198. Paolucci, L. and E. Rozengurt, *Protein kinase D in small cell lung cancer cells: rapid activation through protein kinase C.* Cancer Res, 1999. **59**(3): p. 572-7.
199. Hedin, K.E., et al., *Gi proteins use a novel beta gamma- and Ras-independent pathway to activate extracellular signal-regulated kinase and mobilize AP-1*

transcription factors in Jurkat T lymphocytes. J Biol Chem, 1999. **274**(28): p. 19992-20001.
200. Jaffe, A.B. and A. Hall, *Rho GTPases in transformation and metastasis.* Adv Cancer Res, 2002. **84**: p. 57-80.
201. Woll, P.J. and E. Rozengurt, *Multiple neuropeptides mobilise calcium in small cell lung cancer: effects of vasopressin, bradykinin, cholecystokinin, galanin and neurotensin.* Biochem Biophys Res Commun, 1989. **164**(1): p. 66-73.
202. Schuller, H.M., M. Orloff, and G.K. Reznik, *Antiproliferative effects of the Ca2+/calmodulin antagonist B859-35 and the Ca(2+)-channel blocker verapamil on human lung cancer cell lines.* Carcinogenesis, 1991. **12**(12): p. 2301-3.
203. Schuller, H.M., *Carbon dioxide potentiates the mitogenic effects of nicotine and its carcinogenic derivative, NNK, in normal and neoplastic neuroendocrine lung cells via stimulation of autocrine and protein kinase C-dependent mitogenic pathways.* Neurotoxicology, 1994. **15**(4): p. 877-86.
204. Carney, D.N., *Clinical implications of the biology of small cell lung cancer.* Eur J Respir Dis Suppl, 1987. **149**: p. 5-9.
205. Weber, S., et al., *Gastrin releasing peptide is a selective mitogen for small cell lung carcinoma in vitro.* J Clin Invest, 1985. **75**(1): p. 306-9.
206. Alexander, R.W., et al., *Effects of bombesin on growth of human small cell lung carcinoma in vivo.* Cancer Res, 1988. **48**(6): p. 1439-41.
207. North, W.G., et al., *Human neurophysins as potential tumor markers for small cell carcinoma of the lung: application of specific radioimmunoassays.* J Clin Endocrinol Metab, 1980. **51**(4): p. 892-6.
208. North, W.G., et al., *Expression of all known vasopressin receptor subtypes by small cell tumors implies a multifaceted role for this neuropeptide.* Cancer Res, 1998. **58**(9): p. 1866-71.
209. Coulson, J.M., et al., *Detection of small cell lung cancer by RT-PCR for neuropeptides, neuropeptide receptors, or a splice variant of the neuron restrictive silencer factor.* Methods Mol Med, 2003. **75**: p. 335-52.
210. Chaudhry, A., et al., *Phase I and Imaging Trial of a Monoclonal Antibody Directed against Gastrin-releasing Peptide in Patients with Lung Cancer.* Clinical Cancer Research, 1999. **5**(11): p. 3385-3393.
211. Mahmoud, S., et al., *[Psi 13,14] bombesin analogues inhibit growth of small cell lung cancerin vitro and in vivo.* Cancer Res, 1991. **51**(7): p. 1798-802.
212. Datar, P., et al., *Substance P: structure, function, and therapeutics.* Curr Top Med Chem, 2004. **4**(1): p. 75-103.
213. Woll, P.J. and E. Rozengurt, *A neuropeptide antagonist that inhibits the growth of small cell lung cancer in vitro.* Cancer Res, 1990. **50**(13): p. 3968-73.
214. Woll, P.J. and E. Rozengurt, *[D-Arg1,D-Phe5,D-Trp7,9,Leu11]substance P, a potent bombesin antagonist in murine Swiss 3T3 cells, inhibits the growth of human small cell lung cancer cells in vitro.* Proc Natl Acad Sci U S A, 1988. **85**(6): p. 1859-63.
215. Hruby, V.J., F. al-Obeidi, and W. Kazmierski, *Emerging approaches in the molecular design of receptor-selective peptide ligands: conformational,*

topographical and dynamic considerations. Biochem J, 1990. **268**(2): p. 249-62.
216. Keire, D.A., et al., *The lipid-associated 3D structure of SPA, a broad-spectrum neuropeptide antagonist with anticancer properties.* Biophys J, 2006. **91**(12): p. 4478-89.
217. Seckl, M.J., T. Higgins, and E. Rozengurt, *[D-Arg1,D-Trp5,7,9,Leu11]Substance P coordinately and reversibly inhibits bombesin- and vasopressin-induced signal transduction pathways in Swiss 3T3 cells.* J Biol Chem, 1996. **271**(46): p. 29453-60.
218. Woll, P.J. and E. Rozengurt, *Two classes of antagonist interact with receptors for the mitogenic neuropeptides bombesin, bradykinin, and vasopressin.* Growth Factors, 1988. **1**(1): p. 75-83.
219. Sethi, T. and E. Rozengurt, *Galanin stimulates Ca2+ mobilization, inositol phosphate accumulation, and clonal growth in small cell lung cancer cells.* Cancer Res, 1991. **51**(6): p. 1674-9.
220. Langdon, S., et al., *Broad spectrum neuropeptide antagonists inhibit the growth of small cell lung cancer in vivo.* Cancer Res, 1992. **52**(16): p. 4554-7.
221. MacKinnon, A.C., et al., *[Arg6,D-Trp7,9,NmePhe8]-substance P (6-11) activates JNK and induces apoptosis in small cell lung cancer cells via an oxidant-dependent mechanism.* Br J Cancer, 1999. **80**(7): p. 1026-34.
222. Mousli, M., et al., *G protein activation: a receptor-independent mode of action for cationic amphiphilic neuropeptides and venom peptides.* Trends in Pharmacological Sciences, 1990. **11**(9): p. 358-362.
223. Jarpe, M.B., et al., *[D-Arg1,D-Phe5,D-Trp7,9,Leu11]Substance P acts as a biased agonist toward neuropeptide and chemokine receptors.* J Biol Chem, 1998. **273**(5): p. 3097-104.
224. MacKinnon, A.C., et al., *Bombesin and substance P analogues differentially regulate G-protein coupling to the bombesin receptor. Direct evidence for biased agonism.* J Biol Chem, 2001. **276**(30): p. 28083-91.
225. MacKinnon, A.C., et al., *Targeting V1A-vasopressin receptors with [Arg6, D-Trp7,9, NmePhe8]-substance P (6-11) identifies a strategy to develop novel anti-cancer therapies.* Br J Pharmacol, 2009. **156**(1): p. 36-47.
226. MacKinnon, A.C., et al., *[Arg(6), D-Trp(7,9), N(me)Phe(8)]-substance P (6-11) (antagonist G) induces AP-1 transcription and sensitizes cells to chemotherapy.* Br J Cancer, 2000. **83**(7): p. 941-8.
227. Berendsen, H.H., et al., *Characterization of Three Small Cell Lung Cancer Cell Lines Established from One Patient during Longitudinal Follow-up.* Cancer Research, 1988. **48**(23): p. 6891-6899.
228. de Vries, E.G.E., et al., *Resistance Mechanisms in Three Human Small Cell Lung Cancer Cell Lines Established from One Patient during Clinical Follow-up.* Cancer Research, 1989. **49**(15): p. 4175-4178.
229. Ricci-Vitiani, L., et al., *Influence of local environment on the differentiation of neural stem cells engrafted onto the injured spinal cord.* Neurol Res, 2006. **28**(5): p. 488-92.
230. Hodkinson, P.S., et al., *ECM overrides DNA damage-induced cell cycle arrest and apoptosis in small-cell lung cancer cells through beta1 integrin-*

dependent activation of PI3-kinase. Cell Death Differ, 2006. **13**(10): p. 1776-88.
231. Moore, S.M., et al., *The presence of a constitutively active phosphoinositide 3-kinase in small cell lung cancer cells mediates anchorage-independent proliferation via a protein kinase B and p70s6k-dependent pathway.* Cancer Res, 1998. **58**(22): p. 5239-47.
232. Spatzenegger, M. and W. Jaeger, *Clinical importance of hepatic cytochrome P450 in drug metabolism.* Drug Metab Rev, 1995. **27**(3): p. 397-417.
233. Wiegand, H.J., et al., *Toxicology of engineered nanomaterials - introduction.* Toxicol Lett, 2009. **186**(3): p. 147.
234. Grynkiewicz, G., M. Poenie, and R.Y. Tsien, *A new generation of Ca2+ indicators with greatly improved fluorescence properties.* J Biol Chem, 1985. **260**(6): p. 3440-50.
235. Takahashi, A., et al., *Measurement of intracellular calcium.* Physiol Rev, 1999. **79**(4): p. 1089-125.
236. Jiang, T., et al., *Achaete-scute complex homologue 1 regulates tumor-initiating capacity in human small cell lung cancer.* Cancer Res, 2009. **69**(3): p. 845-54.
237. Yu, X., et al., *CD133, Stem Cells, and Cancer Stem Cells: Myth or Reality?* Curr Colorectal Cancer Rep. **7**(4): p. 253-259.
238. Greve, B., et al., *Flow cytometry in cancer stem cell analysis and separation.* Cytometry A.
239. Carney, D.N., et al., *Establishment and identification of small cell lung cancer cell lines having classic and variant features.* Cancer Res, 1985. **45**(6): p. 2913-23.
240. Franken, N.A., et al., *Clonogenic assay of cells in vitro.* Nat Protoc, 2006. **1**(5): p. 2315-9.
241. Carney, D.N., A.F. Gazdar, and J.D. Minna, *Positive correlation between histological tumor involvement and generation of tumor cell colonies in agarose in specimens taken directly from patients with small-cell carcinoma of the lung.* Cancer Res, 1980. **40**(6): p. 1820-3.
242. Freedman, V.H. and S.I. Shin, *Cellular tumorigenicity in nude mice: correlation with cell growth in semi-solid medium.* Cell, 1974. **3**(4): p. 355-9.
243. Herman, I.M., *Actin isoforms.* Curr Opin Cell Biol, 1993. **5**(1): p. 48-55.
244. Salnikov, A.V., et al., *CD133 is indicative for a resistance phenotype but does not represent a prognostic marker for survival of non-small cell lung cancer patients.* Int J Cancer. **126**(4): p. 950-8.
245. Lucas, J.N. and D. Pinkel, *Orientation measurements of microsphere doublets and metaphase chromosomes in flow.* Cytometry, 1986. **7**(6): p. 575-81.
246. Hodkinson, P.S., A.C. Mackinnon, and T. Sethi, *Extracellular matrix regulation of drug resistance in small-cell lung cancer.* Int J Radiat Biol, 2007. **83**(11-12): p. 733-41.
247. Sartorius, U.A. and P.H. Krammer, *Upregulation of Bcl-2 is involved in the mediation of chemotherapy resistance in human small cell lung cancer cell lines.* Int J Cancer, 2002. **97**(5): p. 584-92.
248. Luo, J., B.D. Manning, and L.C. Cantley, *Targeting the PI3K-Akt pathway in human cancer: rationale and promise.* Cancer Cell, 2003. **4**(4): p. 257-62.

249. Hsia, T.C., et al., *Relationship between chemotherapy response of small cell lung cancer and P-glycoprotein or multidrug resistance-related protein expression.* Lung, 2002. **180**(3): p. 173-9.
250. Jain, N., et al., *Mechanisms of resistance of human small cell lung cancer lines selected in VP-16 and cisplatin.* Cancer, 1996. **77**(9): p. 1797-808.
251. Wojtalla, A. and A. Arcaro, *Targeting phosphoinositide 3-kinase signalling in lung cancer.* Crit Rev Oncol Hematol. **80**(2): p. 278-90.
252. Keely, P.J., et al., *Cdc42 and Rac1 induce integrin-mediated cell motility and invasiveness through PI(3)K.* Nature, 1997. **390**(6660): p. 632-6.
253. Chen, W., et al., *Anti-human CD133 monoclonal antibody that could inhibit the proliferation of colorectal cancer cells.* Hybridoma (Larchmt). **29**(4): p. 305-10.
254. Cortes-Dericks, L., et al., *High expression of octamer-binding transcription factor 4A, prominin-1 and aldehyde dehydrogenase strongly indicates involvement in the initiation of lung adenocarcinoma resulting in shorter disease-free intervals.* Eur J Cardiothorac Surg. **41**(6): p. e173-81.
255. Pan, G.J., et al., *Stem cell pluripotency and transcription factor Oct4.* Cell Res, 2002. **12**(5-6): p. 321-9.
256. Kennedy, J.A., et al., *Comment on "Tumor growth need not be driven by rare cancer stem cells".* Science, 2007. **318**(5857): p. 1722; author reply 1722.
257. Eyler, C.E. and J.N. Rich, *Survival of the fittest: cancer stem cells in therapeutic resistance and angiogenesis.* J Clin Oncol, 2008. **26**(17): p. 2839-45.
258. Lee, H.E., et al., *An increase in cancer stem cell population after primary systemic therapy is a poor prognostic factor in breast cancer.* Br J Cancer. **104**(11): p. 1730-1738.
259. Corti, S., et al., *Isolation and characterization of murine neural stem/progenitor cells based on Prominin-1 expression.* Exp Neurol, 2007. **205**(2): p. 547-62.
260. Clement, V., et al., *Limits of CD133 as a marker of glioma self-renewing cells.* Int J Cancer, 2009. **125**(1): p. 244-8.
261. Dean, M., T. Fojo, and S. Bates, *Tumour stem cells and drug resistance.* Nat Rev Cancer, 2005. **5**(4): p. 275-84.
262. Vermeulen, L., et al., *Cancer stem cells--old concepts, new insights.* Cell Death Differ, 2008. **15**(6): p. 947-58.
263. Neuzil, J., et al., *Tumour-initiating cells vs. cancer 'stem' cells and CD133: what's in the name?* Biochem Biophys Res Commun, 2007. **355**(4): p. 855-9.
264. Pallini, R., et al., *Cancer stem cell analysis and clinical outcome in patients with glioblastoma multiforme.* Clin Cancer Res, 2008. **14**(24): p. 8205-12.
265. Nichols, J., et al., *Formation of pluripotent stem cells in the mammalian embryo depends on the POU transcription factor Oct4.* Cell, 1998. **95**(3): p. 379-91.
266. Graham, S.M., et al., *Primitive, quiescent, Philadelphia-positive stem cells from patients with chronic myeloid leukemia are insensitive to STI571 in vitro.* Blood, 2002. **99**(1): p. 319-25.
267. Dean, M., *ABC transporters, drug resistance, and cancer stem cells.* J Mammary Gland Biol Neoplasia, 2009. **14**(1): p. 3-9.

268. Bepler, G., et al., *Establishment, growth properties, and morphological characteristics of permanent human small cell lung cancer cell lines.* J Cancer Res Clin Oncol, 1987. **113**(1): p. 31-40.
269. Yokoyama, M., et al., *Influence of fetal calf serum on differentiation of mesenchymal stem cells to chondrocytes during expansion.* J Biosci Bioeng, 2008. **106**(1): p. 46-50.
270. Ke, C.-C., et al., *High pluripotent status and metastatic ability of CD133 positive cells in primary papillary thyroid cancer.* J NUCL MED MEETING ABSTRACTS. **51**(2_MeetingAbstracts): p. 1128-.
271. Maeda, S., et al., *CD133 expression is correlated with lymph node metastasis and vascular endothelial growth factor-C expression in pancreatic cancer.* Br J Cancer, 2008. **98**(8): p. 1389-97.
272. Dalerba, P. and M.F. Clarke, *Cancer stem cells and tumor metastasis: first steps into uncharted territory.* Cell Stem Cell, 2007. **1**(3): p. 241-2.
273. Rygaard, K., et al., *Expression of cadherin and NCAM in human small cell lung cancer cell lines and xenografts.* Br J Cancer, 1992. **65**(4): p. 573-7.
274. Hanahan, D. and R.A. Weinberg, *The hallmarks of cancer.* Cell, 2000. **100**(1): p. 57-70.
275. Fischer, B., M. Marinov, and A. Arcaro, *Targeting receptor tyrosine kinase signalling in small cell lung cancer (SCLC): what have we learned so far?* Cancer Treat Rev, 2007. **33**(4): p. 391-406.
276. Nicholson, K.M. and N.G. Anderson, *The protein kinase B/Akt signalling pathway in human malignancy.* Cell Signal, 2002. **14**(5): p. 381-95.
277. Gao, M.Q., et al., *CD24+ cells from hierarchically organized ovarian cancer are enriched in cancer stem cells.* Oncogene. **29**(18): p. 2672-80.
278. Fillmore, C.M. and C. Kuperwasser, *Human breast cancer cell lines contain stem-like cells that self-renew, give rise to phenotypically diverse progeny and survive chemotherapy.* Breast Cancer Res, 2008. **10**(2): p. R25.
279. Coller, H.A., L. Sang, and J.M. Roberts, *A new description of cellular quiescence.* PLoS Biol, 2006. **4**(3): p. e83.
280. Potten, C.S., *Stem cells in gastrointestinal epithelium: numbers, characteristics and death.* Philos Trans R Soc Lond B Biol Sci, 1998. **353**(1370): p. 821-30.
281. Fuchs, E., T. Tumbar, and G. Guasch, *Socializing with the neighbors: stem cells and their niche.* Cell, 2004. **116**(6): p. 769-78.
282. Borovski, T., et al., *Cancer stem cell niche: the place to be.* Cancer Res. **71**(3): p. 634-9.
283. Boral, D. and D. Nie, *Cancer stem cells and niche mircoenvironments.* Front Biosci (Elite Ed). **4**: p. 2502-14.
284. Sethi, T., et al., *Extracellular matrix proteins protect small cell lung cancer cells against apoptosis: a mechanism for small cell lung cancer growth and drug resistance in vivo.* Nat Med, 1999. **5**(6): p. 662-8.
285. Garcia Campelo, M.R., et al., *Stem cell and lung cancer development: blaming the Wnt, Hh and Notch signalling pathway.* Clin Transl Oncol. **13**(2): p. 77-83.
286. Collins, B.J., W. Kleeberger, and D.W. Ball, *Notch in lung development and lung cancer.* Semin Cancer Biol, 2004. **14**(5): p. 357-64.

287. Sullivan, J.P., et al., *Aldehyde dehydrogenase activity selects for lung adenocarcinoma stem cells dependent on notch signaling.* Cancer Res. **70**(23): p. 9937-48.
288. Clement, V., et al., *HEDGEHOG-GLI1 signaling regulates human glioma growth, cancer stem cell self-renewal, and tumorigenicity.* Curr Biol, 2007. **17**(2): p. 165-72.
289. Clarke, M.F., et al., *Cancer stem cells--perspectives on current status and future directions: AACR Workshop on cancer stem cells.* Cancer Res, 2006. **66**(19): p. 9339-44.
290. Quintana, E., et al., *Efficient tumour formation by single human melanoma cells.* Nature, 2008. **456**(7222): p. 593-8.
291. Wolf, C., et al., *Metastasis to the appendix: sonographic appearance and review of the literature.* J Ultrasound Med, 1999. **18**(1): p. 23-5.
292. Pol, M., et al., *MRI in detection of brain metastases at initial staging of small-cell lung cancer.* Neuroradiology, 1996. **38**(3): p. 207-210.
293. Komaki, R., J.D. Cox, and W. Whitson, *Risk of brain metastasis from small cell carcinoma of the lung related to length of survival and prophylactic irradiation.* Cancer Treat Rep, 1981. **65**(9-10): p. 811-4.
294. Brabletz, T., et al., *Opinion: migrating cancer stem cells - an integrated concept of malignant tumour progression.* Nat Rev Cancer, 2005. **5**(9): p. 744-9.
295. Gilchrist, A.J., et al., *Cell adhesion-mediated transformation of a human SCLC cell line is associated with the development of a normal phenotype.* Exp Cell Res, 2002. **276**(1): p. 63-78.
296. Pirozzi, G., et al., *Epithelial to mesenchymal transition by TGFbeta-1 induction increases stemness characteristics in primary non small cell lung cancer cell line.* PLoS One. **6**(6): p. e21548.
297. Hermann, P.C., et al., *Distinct populations of cancer stem cells determine tumor growth and metastatic activity in human pancreatic cancer.* Cell Stem Cell, 2007. **1**(3): p. 313-23.
298. Fulda, S. and S. Pervaiz, *Apoptosis signaling in cancer stem cells.* Int J Biochem Cell Biol. **42**(1): p. 31-8.
299. Tagscherer, K.E., et al., *Apoptosis-based treatment of glioblastomas with ABT-737, a novel small molecule inhibitor of Bcl-2 family proteins.* Oncogene, 2008. **27**(52): p. 6646-56.
300. Wang, Y.K., et al., *Activation of Akt and MAPK pathways enhances the tumorigenicity of CD133+ primary colon cancer cells.* Carcinogenesis. **31**(8): p. 1376-80.
301. Vivanco, I. and C.L. Sawyers, *The phosphatidylinositol 3-Kinase AKT pathway in human cancer.* Nat Rev Cancer, 2002. **2**(7): p. 489-501.
302. Sorenson, G.D., et al., *Hormone production by cultures of small-cell carcinoma of the lung.* Cancer, 1981. **47**(6): p. 1289-96.
303. Seckl, M. and E. Rozengurt, *Substance P analogues act as broad-spectrum neuropeptide antagonists.* Letters in Peptide Science, 1998. **5**(2): p. 199-204.
304. Reubi, J.C., et al., *Y(1)-mediated effect of neuropeptide Y in cancer: breast carcinomas as targets.* Cancer Res, 2001. **61**(11): p. 4636-41.
305. Rozengurt, E. and J.H. Walsh, *Gastrin, CCK, signaling, and cancer.* Annu Rev Physiol, 2001. **63**: p. 49-76.

306. Ryder, N.M., et al., *G protein-coupled receptor signaling in human ductal pancreatic cancer cells: neurotensin responsiveness and mitogenic stimulation.* J Cell Physiol, 2001. **186**(1): p. 53-64.
307. Rozengurt, E., *Neuropeptides as growth factors for normal and cancerous cells.* Trends Endocrinol Metab, 2002. **13**(3): p. 128-34.
308. Pansky, A., et al., *Gastrin releasing peptide-preferring bombesin receptors mediate growth of human renal cell carcinoma.* J Am Soc Nephrol, 2000. **11**(8): p. 1409-18.
309. Taneja, T.K. and S.K. Sharma, *Markers of small cell lung cancer.* World J Surg Oncol, 2004. **2**: p. 10.
310. Folny, V., et al., *Pancreatic vasopressin V1b receptors: characterization in In-R1-G9 cells and localization in human pancreas.* Am J Physiol Endocrinol Metab, 2003. **285**(3): p. E566-76.
311. Ocejo-Garcia, M., et al., *Use of RT-PCR to detect co-expression of neuropeptides and their receptors in lung cancer.* Lung Cancer, 2001. **33**(1): p. 1-9.
312. Kim, J.J. and I.F. Tannock, *Repopulation of cancer cells during therapy: an important cause of treatment failure.* Nat Rev Cancer, 2005. **5**(7): p. 516-25.
313. Corjay, M.H., et al., *Two distinct bombesin receptor subtypes are expressed and functional in human lung carcinoma cells.* J Biol Chem, 1991. **266**(28): p. 18771-9.
314. Millar, J.B. and E. Rozengurt, *Heterologous desensitization of bombesin-induced mitogenesis by prolonged exposure to vasopressin: a post-receptor signal transduction block.* Proc Natl Acad Sci U S A, 1989. **86**(9): p. 3204-8.
315. Millar, J.B. and E. Rozengurt, *Chronic desensitization to bombesin by progressive down-regulation of bombesin receptors in Swiss 3T3 cells. Distinction from acute desensitization.* J Biol Chem, 1990. **265**(20): p. 12052-8.
316. Ferrand, A., et al., *Expression of gastrin precursors by CD133-positive colorectal cancer cells is crucial for tumour growth.* Biochim Biophys Acta, 2009. **1793**(3): p. 477-88.
317. Ferris, H.A., et al., *Constitutive activation of the gastrin-releasing peptide receptor expressed by the nonmalignant human colon epithelial cell line NCM460.* J Clin Invest, 1997. **100**(10): p. 2530-7.
318. Chaudhry, A., et al., *Phase I and imaging trial of a monoclonal antibody directed against gastrin-releasing peptide in patients with lung cancer.* Clin Cancer Res, 1999. **5**(11): p. 3385-93.
319. Jones, D.A., et al., *Metabolism of the anticancer peptide H-Arg-D-Trp-NmePhe-D-Trp-Leu-Met-NH2.* Peptides, 1995. **16**(5): p. 777-83.
320. Cummings, J., et al., *Pharmacokinetics, metabolism and tumour disposition of 8-chloroadenosine 3',5'-monophosphate in breast cancer patients and xenograft bearing mice.* Ann Oncol, 1996. **7**(3): p. 291-6.
321. Sandberg, B.E., et al., *Synthesis and biological properties of enzyme-resistant analogues of substance P.* Eur J Biochem, 1981. **114**(2): p. 329-37.
322. Cummings, J., et al., *Stability and in vitro metabolism of the mitogenic neuropeptide antagonists [D-Arg1,D-Phe5, D-Trp7,9, Leu11]-substance P and [Arg6, D-Trp7,9, MePhe8]-substance P (6-11) characterized by high-*

performance liquid chromatography. J Pharm Biomed Anal, 1994. **12**(6): p. 811-9.
323. Powell, M.F., et al., *Peptide stability in drug development. II. Effect of single amino acid substitution and glycosylation on peptide reactivity in human serum.* Pharm Res, 1993. **10**(9): p. 1268-73.
324. Chatterjee, J., et al., *N-methylation of peptides: a new perspective in medicinal chemistry.* Acc Chem Res, 2008. **41**(10): p. 1331-42.
325. Gazdar, A.F., et al., *Characterization of variant subclasses of cell lines derived from small cell lung cancer having distinctive biochemical, morphological, and growth properties.* Cancer Res, 1985. **45**(6): p. 2924-30.
326. Krystal, G.W., G. Sulanke, and J. Litz, *Inhibition of phosphatidylinositol 3-kinase-Akt signaling blocks growth, promotes apoptosis, and enhances sensitivity of small cell lung cancer cells to chemotherapy.* Mol Cancer Ther, 2002. **1**(11): p. 913-22.
327. Hoffman, R.M., *Orthotopic metastatic mouse models for anticancer drug discovery and evaluation: a bridge to the clinic.* Invest New Drugs, 1999. **17**(4): p. 343-59.
328. Krystal, G., et al., *Multiple mechanisms for transcriptional regulation of the myc gene family in small-cell lung cancer.* Mol Cell Biol, 1988. **8**(8): p. 3373-81.
329. Richardson, G.E. and B.E. Johnson, *The biology of lung cancer.* Semin Oncol, 1993. **20**(2): p. 105-27.
330. Funa, K., et al., *Increased expression of N-myc in human small cell lung cancer biopsies predicts lack of response to chemotherapy and poor prognosis.* Am J Clin Pathol, 1987. **88**(2): p. 216-20.
331. Degan, S., et al., *Gastrin-releasing peptide, immune responses, and lung disease.* Ann N Y Acad Sci, 2008. **1144**: p. 136-47.